GENERATION AND CHARACTERIZATION OF 4-VINYLPHENOL AND 1,2-DIARYL ENOL RADICAL CATIONS IN SOLUTION

by

Yan Rodríguez-Evora

Submitted in partial fulfillment of the requirements
for the degree of Doctor of Philosophy

at

Dalhousie University
Halifax, Nova Scotia
March 2006

Canada

DALHOUSIE UNIVERSITY

TABLE OF CONTENTS

LIST OF FIGURES

x

LIST OF TABLES

ABSTRACT

Naturally occurring compounds containing a 4-vinylphenol fragment are important components in several biological systems. Specifically, these classes of organic molecules are building blocks for the biosynthesis of natural products such as lignin, the second most abundant biopolymer on earth, and plant lignans, which frequently possess important therapeutic properties. 4-Vinylphenol radical cations are supposed to be involved in the biosynthesis of lignin and lignans, however practically nothing is known about these reactive species.

This thesis therefore focuses on the generation and characterization of 4-vinylphenol radical cations. Special attention is devoted to explore the viability of radical cation mediated dimerization of 4-vinylphenol substrates. The radical cations of coniferyl alcohol, isoeugenol and 2-methoxy-4-vinylphenol were generated by direct laser flash photolysis or by photoinduced electron-transfer. The lifetime of the radical cations in acidic acetonitrile were found to increase due to a shift in the radical cation - vinylphenoxyl radical acid-base equilibrium to the side of the radical cation. Additionally the reaction of 2-methoxy-4-vinylphenol radical cation with its neutral precursor has been found to proceed with a second order rate constant of 8.6×10^8 $M^{-1}s^{-1}$, indicating a possible [2+1] cycloaddition reaction. The radical cation of 2-methoxy-4-vinylphenol also reacts with non-phenolic substituted styrenes with second-order rate constants in the order of $ca. 10^8$ $M^{-1}s^{-1}$.

The thesis also focuses on the chemistry of enol radical cations in solution. These species have been widely studied in the gas phase, however the information concerning the chemistry of these reactive species in solution is limited to enol radical cations generated from stable enols. The thesis describes the generation of five short-lived 1,2-diaryl enol radical cations in acidic acetonitrile. The generation of these species was achieved by protonation of α-carbonyl radicals initially formed by laser irradiation of α-bromoketones. The acid dissociation constants as well as the deprotonation rate constants for these species are highly influenced by the nature of the substituents on the aromatic rings. Theoretical optimization of the structures of the radical cations shows that these species are twisted, which compromises the conjugation between the charge and the substituents.

LIST OF ABBREVIATIONS AND SYMBOLS USED

A	acceptor
Abs	absorption
AdoCBl	3,4-anhydroadenosyl cobalamin
Ado-CH_3	5'-deoxyadenosine
BET	back electron transfer
BP	biphenyl
Cbl^{II}	cobalamin
Chl	chloranil (tetrachloro-p-benzoquinone)
D	donor
DCA	9,10-dicyanoanthracene
DCE	1,2-dichloroethane
DiP	dirigent protein
DMSO	dimethyl sulfoxide
DNA	deoxyribonucleic acid
ΔO.D.	changes in optical density
EA	electron affinity
E^{ox}	oxidation potential
e.p.r.	electron paramagnetic resonance
ET	electron transfer
EtOH	ethanol
eV	electron volt
ε	extinction coefficient
FePHEN	iron (III) phenanthroline
GC	gas chromatography
HIV	human immunodeficiency virus
HOMO	highest occupied molecular orbital
HRP	horseradish peroxidase
ISC	intersystem crossing
i-PrOH	iso-propanol
K	equilibrium constant
k	rate constant
λ	wavelength
LiP	lignin peroxidase
LUMO	lowest occupied molecular orbital
μs	microsecond
MeCA	3-(3,4-dimethoxyphenyl)prop-2-en-1-ol
MeCN	acetonitrile
MeOH	methanol
MS	mass spectrometry
nm	nanometers

NHE	normal hydrogen electrode
Nu	nucleophile
NVC	N-vinylcarbazole
PET	photoinduced electron transfer
Porp	porphyrin
SCE	standard calomel electrode
SOMO	single occupied molecular orbital
tert-BuOH	*tert*-butanol
TFE	2,2,2-trifluoroethanol
THF	tetrahydrofuran
UV	ultraviolet
4-VP	4-vinylphenol

ACKNOWLEDGMENTS

Chapter I. Introduction to Radical Cations

Radical cations have been extensively studied by virtue of their potential use as intermediates in organic synthesis[1] as well as by their applications in optoelectronics as molecular switches, in electrochromic materials, in organic magnets and in delignification.[2] In addition, recent studies have demonstrated that radical cations are involved as intermediates in the interaction of carcinogens and DNA.[2, 3] For instance polycyclic aromatic hydrocarbons (PHAs), the most widespread environmental carcinogens, are not active on their own. Instead, they are activated by one electron oxidation resulting in the formation of the corresponding radical cations, which then react with DNA.[2]

Even though radical cations are involved in biological processes and despite the potential use of these species in synthesis or material science, the information concerning the chemical and physical properties of various types of radical cations is very scarce or nonexistent. Specifically, 4-vinylphenol radical cations might be involved in the biosynthesis of lignins and lignans; however no information is available concerning these species. Similarly, enol radical cations are implicated as intermediates in enzymatic processes like the diol dehydrase cycle; nevertheless, the information concerning the chemistry of these species in solution is extremely limited.

The intent of the work in this thesis is to fill these gaps in our knowledge of the chemistry of radical cations by studying the generation and properties of 4-vinylphenol and enol radical cations. The results of these studies are given in Chapters 2 and 3. In the present chapter, basic information concerning the chemistry of radical cations is reviewed.

the present chapter, basic information concerning the chemistry of radical cations is
reviewed.

1.1 Radical Cations

Radical cations or cation radicals are open-shell species formed by the removal of
an electron – usually from the HOMO – of a neutral molecule, Scheme 1.1.

Scheme 1.1
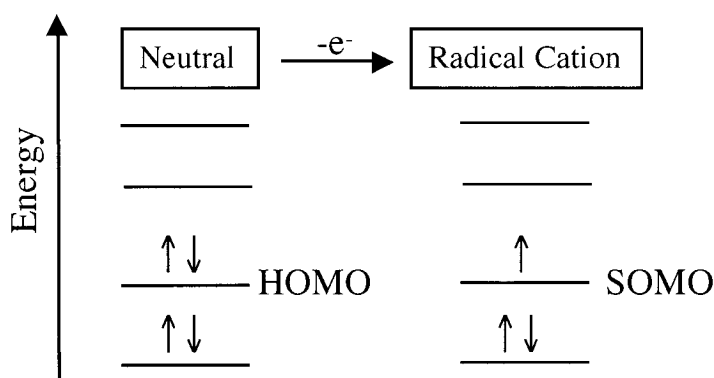
Generally, radical cations are classified as atomic radical cations which are
produced by abstraction of an electron from an atom with an even number of electrons, or
as molecular radical cations, generated by ionization of an electron from a neutral
molecule. Molecular radical cations are divided in two subtypes,[4] namely (i) the *π-type*
characterized by the fact that the SOMO is a π molecular orbital, and (ii) the *σ-type*, in
which the SOMO is a σ-type molecular orbital or an n (non-bonding) atomic orbital
located in the σ -plane of a π-bond containing system, Scheme 1.2. In cases where the
positive charge and the spin are uncoupled, the radical cation is referred to as "distonic".

Scheme 1.2

π-type Radical Cation   σ-type Radical Cation   Distonic Radical Cation
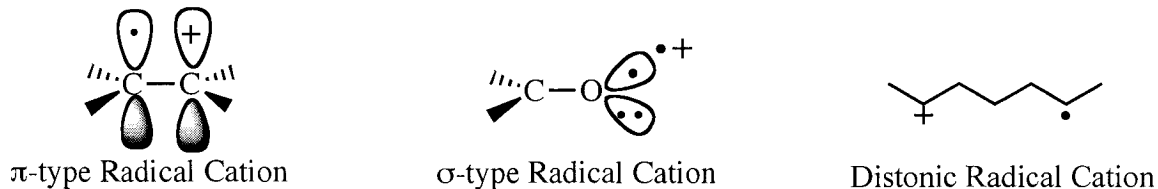
Radical cations can also be classified as localized or delocalized depending on whether the SOMO is concentrated in a bond between two atoms – or even on a single atom – or whether it is delocalized over more than two atoms. Thus, simple alkene radical cations are localized radical cations, while the SOMO in styrene radical cations can be extensively delocalized, Scheme 1.3.

Scheme 1.3
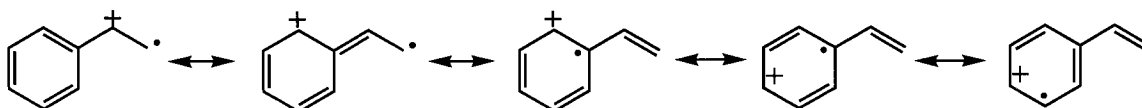
As a result of the extensive delocalization of the SOMO in styrene radical cations, these species are typically represented as shown in Scheme 1.4. The dot represents the unpaired electron and the positive sign represents the positive charge of the radical cation. Note that this terminology is not limited to styrene radical cations but to any radical cation in which the SOMO is extensively delocalized through the molecular framework.

Scheme 1.4

(styrene radical cation)   (naphthalene radical cation)   (biphenyl radical cation)

3
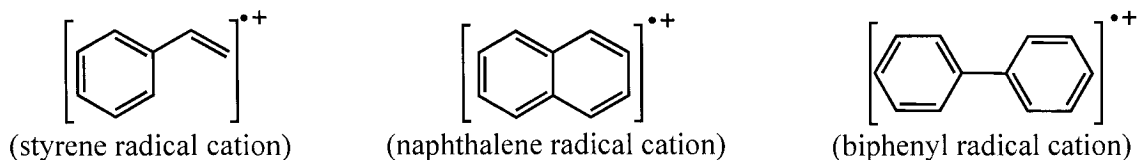
1.1.1 Generation of Radical Cations

1.1.1.1 Chemical Method for the Generation of Radical Cations

The chemical method of generation of radical cations involves the use of chemical oxidants that accept an electron from the precursor of the radical cation to give the desired radical cation and the reduced form of the oxidant. Radical cations can be generated by a wide variety of chemical oxidants like Bronsted and Lewis acids,[5, 6] metallic ions,[7] dioxygenyl ions,[8] certain zeolites,[9] Scheme 1.5, and stable organic cations,[1, 4] Scheme 1.6.

Noticeably, some of the oxidants shown in Scheme 1.5 are not practical for synthetic purposes. For instance, oxidation with dioxygenyl ions is a particularly attractive approach because the reduction product is molecular oxygen which is a gas and is potentially easy to remove. However, the preparation of this oxidant is difficult and the reaction requires extreme conditions.

Scheme 1.5

4
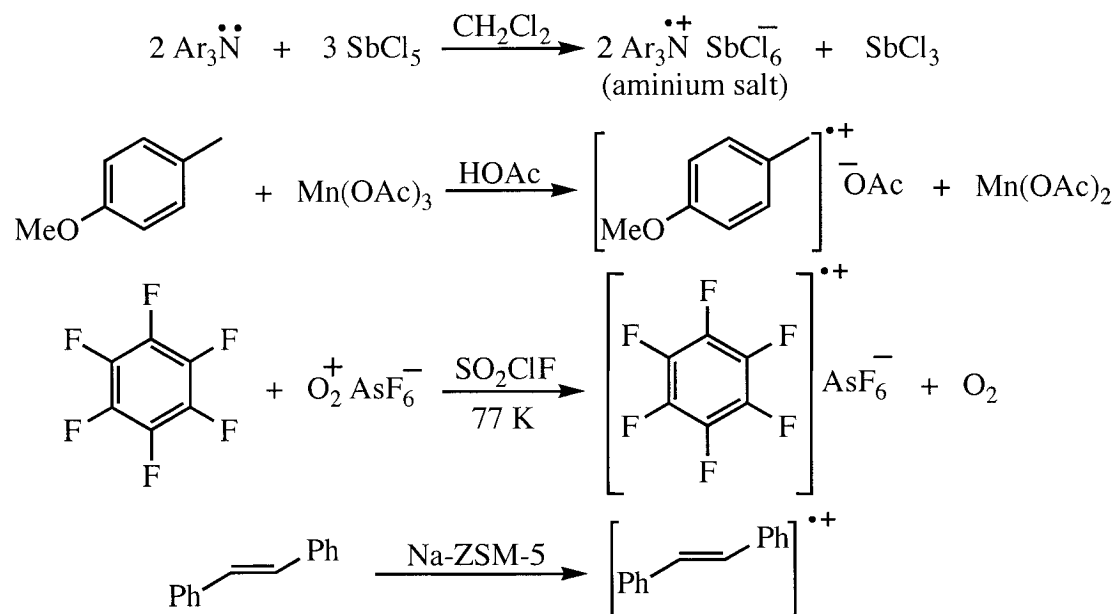
Triarylaminium salts are among the most useful agents for the generation of organic radical cations.[10-13] These salts can be easily prepared as shown in Scheme 1.5,[6] and are also commercially available. In addition, as shown in Scheme 1.6, their relatively high oxidation potentials makes them suitable to oxidize a variety of other substrates.[4]

Scheme 1.6

$E^{ox} = 1.06$ V vs SCE in MeCN

$E^{ox} = 1.50$ V vs SCE in MeCN
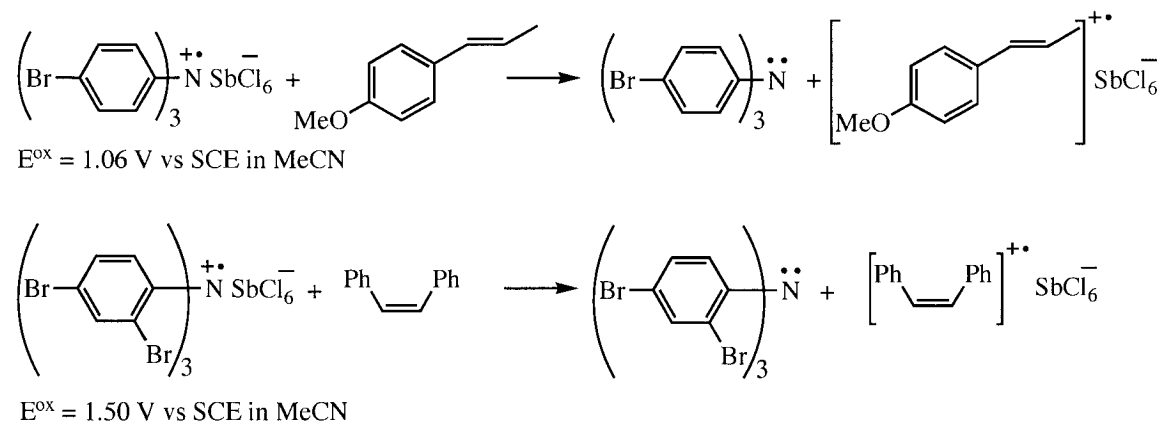
1.1.1.2 Biological Generation of Radical Cations

Biological generation of radical cations constitutes a special case of chemical oxidations whereby the oxidizing agents are enzymes or other biological molecules involved in metabolism.

Cytochromes and peroxidases are among the most important oxidizing enzymes. They are involved in the oxidation of a broad range of drugs, pesticides, carcinogens, steroids, and fat-soluble vitamins.[2] Peroxidases typically catalyze one-electron oxidations of a wide variety of organic molecules, with peroxide being needed to activate the enzyme.[14] Most of these enzymes contain iron (III) protoporphyrin IX or heme group in the active site. This group possesses two axial coordination sites, Scheme 1.7. One of these sites, the proximal site, is usually involved in a coordinated bond between the iron

(III) and the nitrogen or sulfur atom of histidine or cysteine, depending on the specific enzyme. The other axial site, the distal site, is usually vacant in the resting, or native, form of the enzyme.

Scheme 1.7
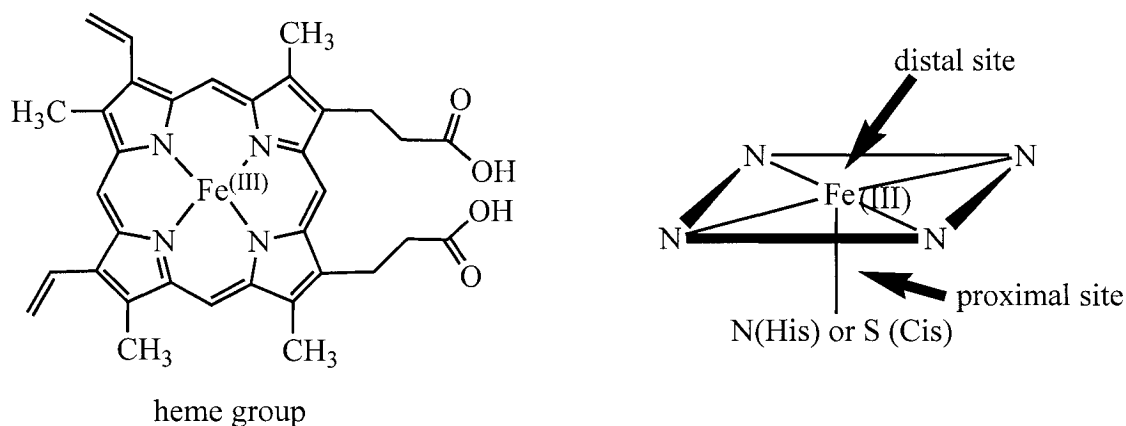
heme group

The iron center can coordinate to hydrogen peroxide at the distal coordination site to ultimately yield compound I, a low spin oxoferryl species with a π-radical cation located on the heme group, Figure 1.1. Compound I then accepts an electron from an adequate substrate (S) to give the corresponding radical cation and compound II, which is also a low-spin oxoferryl species but is one oxidation state equivalent below compound I. One-electron oxidation of the substrate by compound II finally regenerates the native enzyme, Figure 1.1.

Formation of Compound I

native enzyme   hydroperoxide complex   transition state   compound I
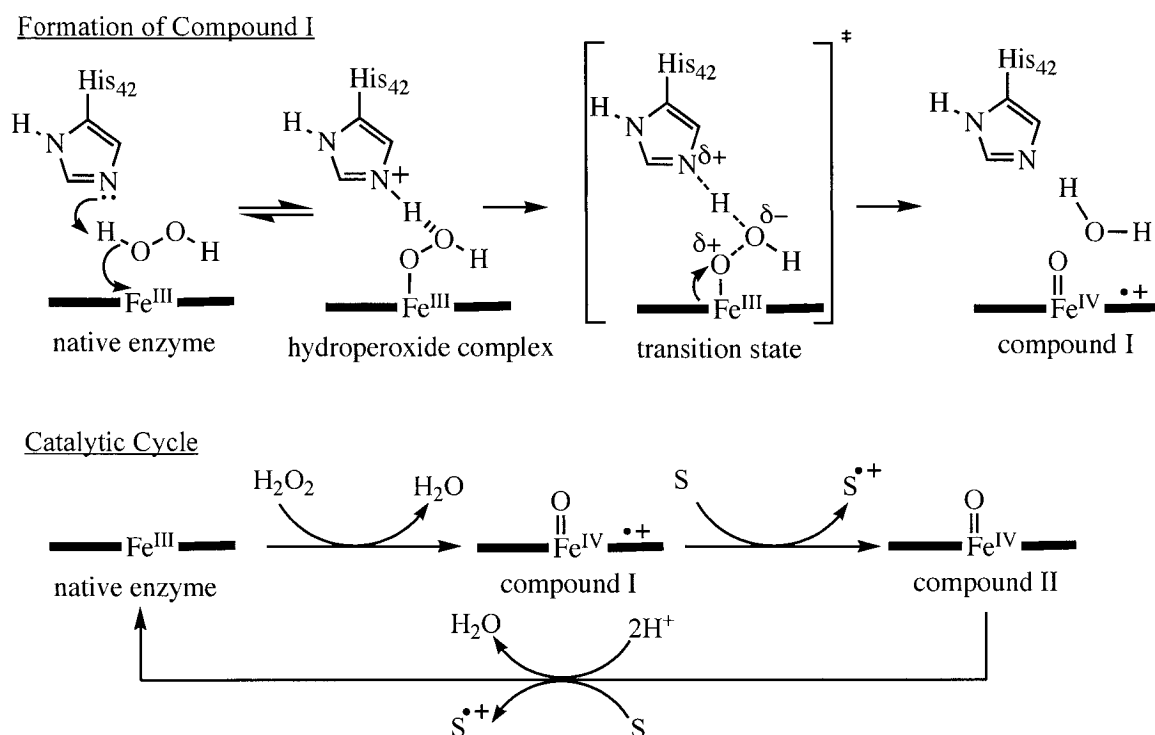
Catalytic Cycle

Figure 1.1 Proposed[15] mechanism for generation of compound I in HRP and catalytic cycle for enzymatic oxidation of an hypothetical substrate (S).

Despite the high efficiency of biological processes, enzymatic generation of radical cations has not been widely exploited to generate and study these reactive intermediates. The relatively small number of substrates that can be oxidized due to the high specificity of enzymes, as well as the low solubility of most organic compounds in water limit the number of substrates that can be enzymatically oxidized. Nonetheless, a few studies involving the enzymatic generation of organic radical cations have been reported[16-18]. For instance, lignin peroxidase is involved in the natural degradation of lignin by catalyzing the oxidation of this macromolecule to generate radical cation sites within the macromolecule. These radical cations then undergo a series of bond-cleavages that result in the conversion of lignin, a biopolymer, into low molecular weight aromatic compounds. In order to gain more insights into this process Baciocchi et al.[17] studied the

enzymatic oxidation of small systems with structural similarities to lignin. Interaction of these small systems with hydrogen peroxide/lignin peroxidase (LiP) led to the same products that the one electron oxidation of the systems with $K_5[Co^{III}W_{12}O_{40}]$. Based on these observations the authors concluded that LiP oxidizes the substrates to the corresponding radical cations as shown in Scheme 1.8.

Scheme 1.8
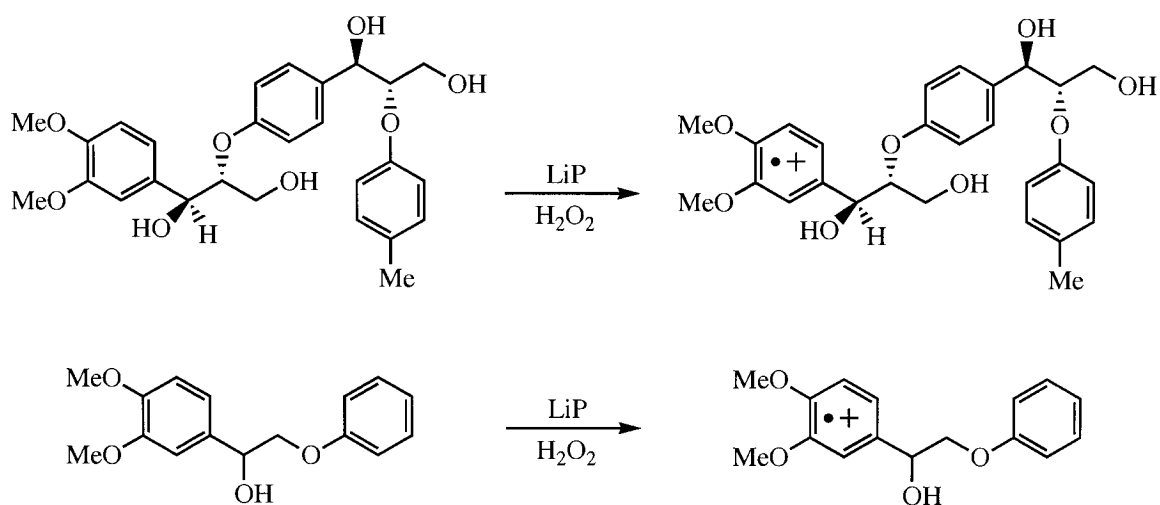
A different study has confirmed that LiP also oxidizes methoxybenzene derivatives to the corresponding radical cations.[18] In this case, the enzymatically generated radical cations were detected by e.p.r. spectroscopy. In addition, the products derived from the enzymatic oxidation – benzoquinone and methanol, Scheme 1.9 - were the same as those obtained by voltametric oxidation, providing further evidence of the biological generation of the radical cations.

Scheme 1.9

8
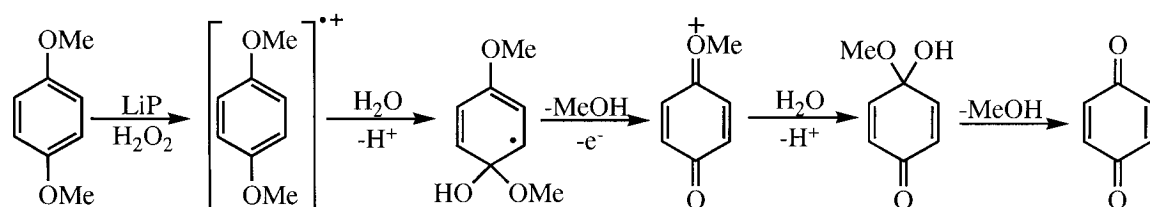
1.1.1.3 Physical Methods for the Generation of Radical Cations

The generation of radical cations can also be accomplished using physical methods such as electrochemical oxidation, γ radiation, pulse radiolysis, laser excitation and photosensitized electron transfer.[4, 5] The last three have the advantage of being a rapid source of radical cations, which makes these methods very useful for kinetic studies. As laser excitation and photosensitized electron transfer were the techniques employed in this thesis, this section will be limited to the presentation of these methods.

1.1.1.3.1 Photoinduced Electron Transfer

Photoinduced electron transfer is based on the enhancement of the oxidative power of an electron acceptor and the reductive power of an electron donor upon photoexcitation. As illustrated in Scheme 1.10 photoexcitation of a given molecule results in a decrease in its ionization energy (EI) as well as in an increase of its electron affinity (EA).

Scheme 1.10
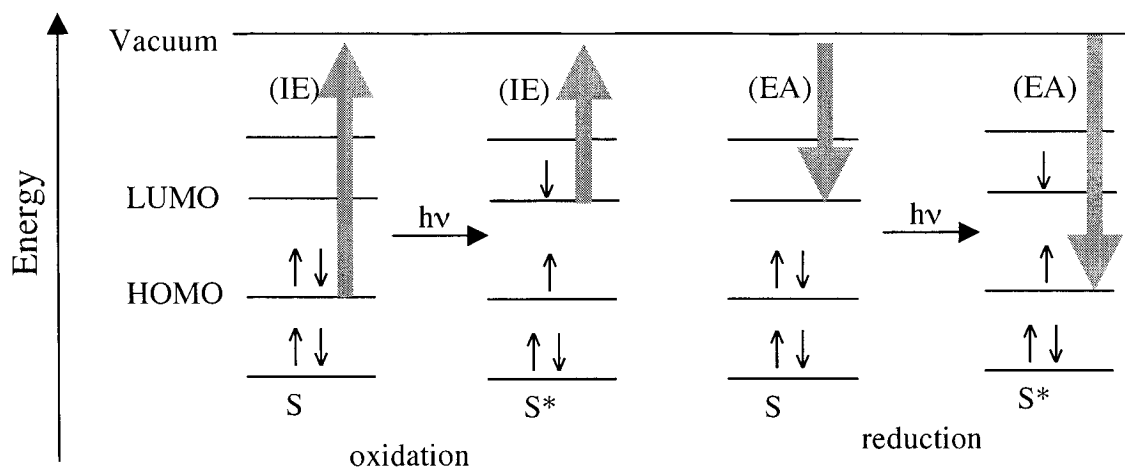
The essence of photoinduced electron transfer is illustrated in Scheme 1.11. That is, excitation of the photosensitizer (acceptor) makes it a stronger oxidant that accepts an

9

electron from a precursor (donor), generating a radical cation/radical anion pair. The same radical ion pair may be generated by excitation of the donor (D) and further electron transfer from the excited donor to the acceptor (A).

Scheme 1.11

$$hv \searrow$$
$$hv \nearrow$$

$$D + A \longrightarrow D + A^{*1} \longrightarrow [D^{+\cdot}/A^{-\cdot}] \longleftarrow D^{*1} + A \longleftarrow D + A$$
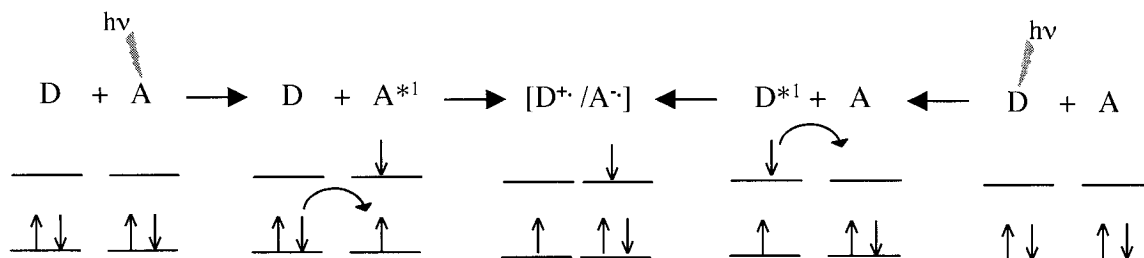
Once the radical ion pair is formed, two processes will compete: (*i*) back electron transfer (BET), which regenerates the neutral acceptor and donor; and (*ii*) cage escape or separation, which yields the free radical ions, Scheme 1.12. The yield of formation of radical cations is closely related to the back electron transfer process. The yield of radical cation will be high if the back electron transfer is slow compared to the cage escape process. In singlet radical ion pairs back electron transfer usually takes place with rate constants around $\sim 5 \times 10^8$ s^{-1},[19] competing efficiently with cage escape. On the other hand, the use of triplet sensitizers generates triplet radical ion pairs, in which the back electron transfer is spin forbidden. Therefore, the triplet radical ion pair must undergo intersystem crossing to the singlet state prior to the back electron transfer, making this process much slower than in the case of the singlet ion pair, Scheme 1.12. The most common triplet sensitizers are ketones and quinones. On the other hand, aromatic hydrocarbons, often substituted with one or more cyano groups, are the most frequently used singlet sensitizers.[1]

Scheme 1.12

(singlet sensitizer)   (triplet sensitizer)

$A^{*1} + D$ — ET → $[D^{+\cdot}/A^{-\cdot}]^1$ —sep→ $D^{+\cdot} + A^{-\cdot}$

hv, BET, $k_{BET} \sim 5 \times 10^8 \text{ s}^{-1}$, A + D

$A^{*3} + D$ — ET → $[D^{+\cdot}/A^{-\cdot}]^1$ —ISC→ $[D^{+\cdot}/A^{-\cdot}]^3$ —sep→ $D^{+\cdot} + A^{-\cdot}$

hv, BET, A + D
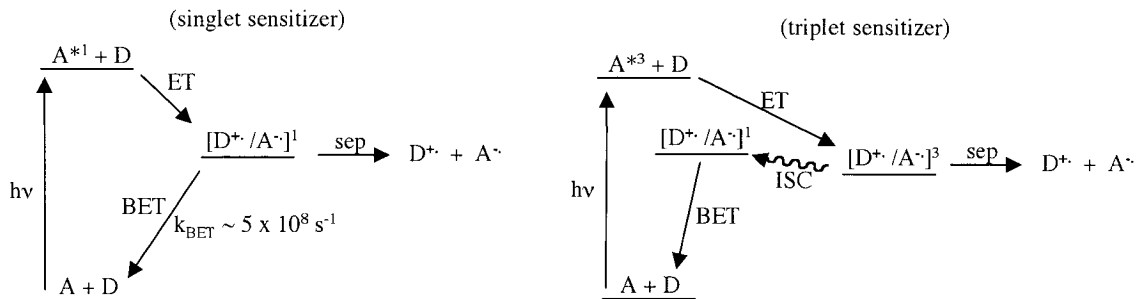
A different approach to reduce the efficiency of the back electron transfer is the use of cosensitization. That is, in addition to the substrate of interest, a second donor (co-donor or cosensitizer) is used, with the cosensitizer having a higher oxidation potential than the "precursor donor", i.e. the precursor of the radical cation of interest. Scheme 1.13 shows the energy diagram for cosensitization mechanism as well as for direct sensitization using a singlet sensitizer. Selective excitation of the acceptor (A) in presence of the donor (D) and the co-donor (C) is followed by electron transfer from both species to give singlet radical ions pairs $[C^+/A^-]$ and $[D^+/A^-]$. However, using much larger concentrations of co-donor with respect to the donor guarantees that most of the excited acceptor is reduced by the co-donor. Thus, the formation of the donor-acceptor radical ion pair $[D^+/A^-]$ is negligible under these conditions. The singlet radical ion pair $[C^+/A^-]$ can either undergo separation giving the free ions or back electron transfer to regenerate the neutral acceptor and co-donor. However, even when the radical ion pair is in its singlet state, the free energy associated with the back electron transfer is more negative than that associated with the back electron transfer in the radical ion pair $[D^+/A^-]$. As a result of this energetic difference, and in accordance with Marcus theory, the back electron transfer is slower in the $[C^+/A^-]$ ion pair than in $[D^+/A^-]$. Consequently, the cage escape is more efficient resulting in a higher yield of free co-donor radical cation.

Given that the oxidation potential of the co-donor radical cation is higher than that of the donor radical cation, the former can accept an electron from the donor to give the free radical cation of this species.

Scheme 1.13

$$A^{*1} + C \qquad\qquad\qquad\qquad\qquad\qquad\qquad A^{*1} + D$$

$$[A^{-\cdot}/C^{+\cdot}]^1 \longrightarrow A^{-\cdot} + C^{+\cdot} \quad\overset{D}{\searrow}$$

$$D^{+\cdot} + A^{-\cdot} \longleftarrow [D^{+\cdot}/A^{-\cdot}]^1$$

$$h\nu \qquad\qquad\qquad\qquad\qquad\qquad\qquad\qquad h\nu$$

$$A + C \qquad\qquad\qquad\qquad\qquad\qquad\qquad A + D$$
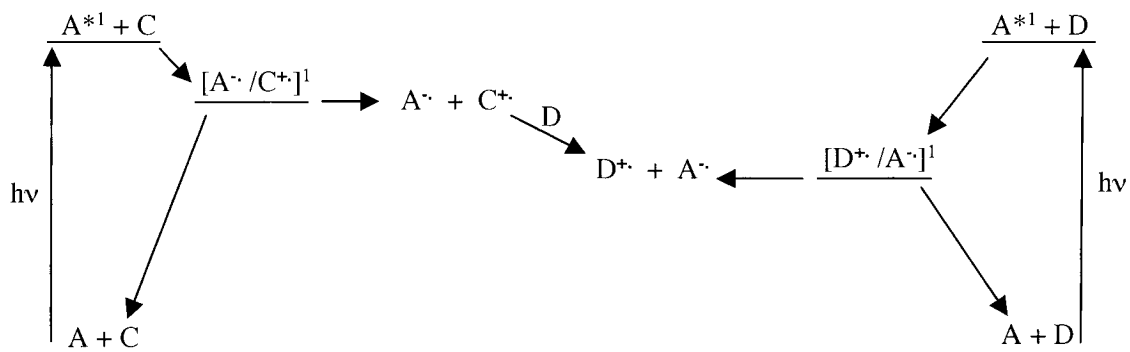
A typical co-donor widely used in cosensitization is biphenyl, while cyano-substituted aromatic compounds are commonly used as acceptors.[20] For instance, selective irradiation of 9,10-dicyanoanthracene (DCA) in presence of biphenyl (0.15 M) and 4-methoxystilbene (5 x 10^{-4} M) in acetonitrile gives 4-methoxystilbene radical cation in much higher quantum yield than excitation of DCA in presence of neutral 4-methoxystilbene, Scheme 1.14.[21] As mentioned before this is a direct consequence of the larger efficiency of cage escape due to an increase in the exergonicity of the back electron transfer process. The free energy for back electron transfer in the radical ion pair [trans-4-methoxystilbene$^+$/DCA$^-$] in acetonitrile is -1.96 eV while that for the pair [biphenyl$^+$/DCA$^-$] is -2.87 eV. Consequently, the quantum yield for ion pair separation or cage escape in the former pair ($\phi = 0.052$) is almost 15 times smaller than that for cage escape in the [biphenyl$^+$/DCA$^-$] radical ion pair ($\phi = 0.75$).[21]

Scheme 1.14

Co-sensitization

$$DCA + BP \xrightarrow{\ h\nu\ } DCA*^1 + BP \longrightarrow DCA^{\bullet-} / BP^{\bullet+} \xrightarrow{\ \phi = 0.75\ } DCA^{\bullet-} + BP^{\bullet+}$$

$$\Delta G_{BET} = -2.87\ eV$$

$$\downarrow 4MS$$

$$DCA^{\bullet-} + BP + 4MS^{\bullet+}$$

Direct sensitization

$$DCA + 4MS \xrightarrow{\ h\nu\ } DCA*^1 + 4MS \longrightarrow DCA^{\bullet-} / 4MS^{\bullet+} \xrightarrow{\ \phi = 0.052\ } DCA^{\bullet-} + 4MS^{\bullet+}$$

$$\Delta G_{BET} = -1.96\ eV$$

DCA =   BP =   4MS =
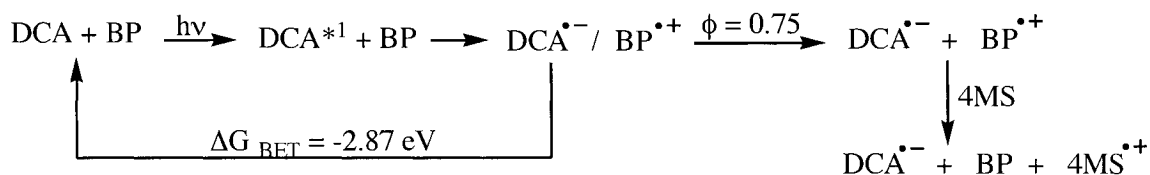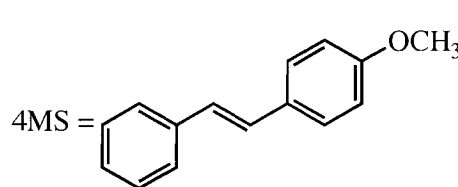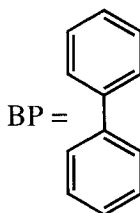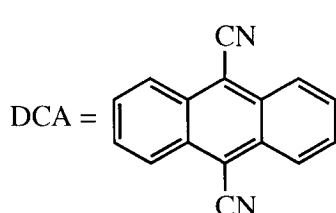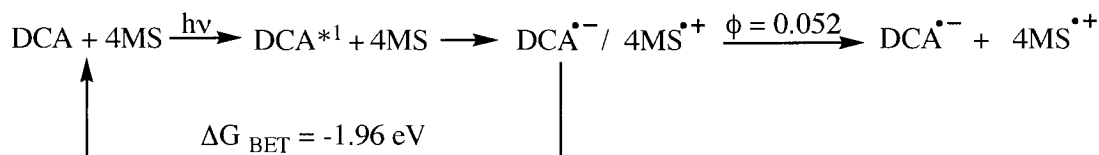
1.1.1.3.2 Laser Excitation or Photoionization

Photoionization involves direct irradiation of the substrate by a laser pulse, which causes ejection of an electron from the substrate, resulting in the formation of a radical cation and a solvated electron, Eq. 1.1.[22-26]

$$Substrate + n\ h\nu \longrightarrow [Substrate]^{+\bullet} + e^-_{(solv)} \qquad (Eq.\ 1.1)$$
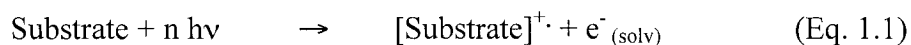
Generally, photoionization takes place from an upper excited state produced either by absorption of a single high-energy photon or by sequential two-photon absorption. The bi-photonic process is usually called Resonant Two-Photon Ionization.[27] Initially the substrate (S) is excited to its first singlet excited ($^1S^*$) state by absorption of one photon. Absorption of a second photon gives S in a higher singlet excited state ($^1S^{**}$). If the energy of $^1S^{**}$ is higher than the ionization energy of the substrate (S), then electron

detachment from $^1S^{**}$ takes place resulting in the formation of $S^{+\cdot}$ and one electron,

Scheme 1.15.

Scheme 1.15
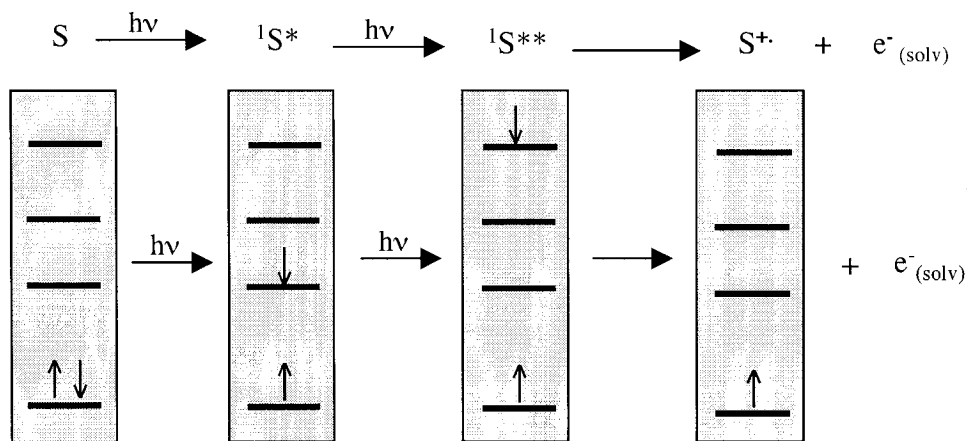
Sequential two-photon ionization is more frequently observed when using lasers as the irradiation source and not at all common with steady-state irradiation. The light emitted by lasers is more intense than that coming from steady-state irradiation sources. That is, the number of photons per unit of time is very large compared to steady-state irradiation, allowing the sequential absorption of two photons. Bi-photonic processes are usually identified by measuring the intensity of the signal due to the transient generated by irradiation as a function of the intensity of the laser beam. A linear relationship between the intensity of the signal and the square of the intensity of the irradiation source will indicate a bi-photonic process while a linear relationship of the intensity of the signal and the intensity of the light is indicative of a mono-photonic process.

Laser excitation has some advantages compared with the photoinduced electron transfer method. For instance, photoionization of the substrate gives a transient spectrum without any absorption characteristic of the reduced sensitizer, simplifying the analysis of the spectrum. Moreover, the laser excitation method allows the use of lower substrate

concentrations, which minimizes reactions between the radical cation and its neutral parent.

Conversely the photoionization method is restricted to relatively easily oxidized substrates. Given that electron detachment will only occur if the ionization energy of the substrate is smaller than the energy of the substrate in its upper excited state, only easily oxidized molecules will undergo photoinduced electron ejection. Another limitation of this method is that it requires polar solvents to stabilize both the radical cation and the ejected electron. In addition, when photoionization is bi-photonic, both the lifetime and the excitation coefficient of the substrate first singlet excited state ($^1S^*$) at the excitation wavelength must have proper values to permit the absorption of the second photon.

1.1.2 Reactivity of Radical Cations

Radical cations are much more reactive than the corresponding neutral precursors as a result of the structure-weakening and destabilization associated with the loss of one electron. Given the dual character of these species – radical and ionic – the reactivity of radical cations is comparable to that of radicals or of carbocations. Like radicals, radical cations can undergo coupling reactions to give dications[4] and like carbocations they act as electrophiles easily reacting with nucleophiles.[23, 28] In addition, radical cations undergo a wide variety of other reactions like electron transfer,[20, 25] rearrangements,[4, 29] deprotonation,[7] mesolytic cleavage[4, 30] and cycloaddition reactions to neutral unsaturated systems[24, 31]. Examples of some of these reactions are shown in Scheme 1.16. Nucleophilic addition, deprotonation and cycloaddition are the main reactions of the radical cations studied in the present work. A detailed description of these reactions is given in Chapters 2 and 3.

Scheme 1.16

$$2 \, Ph_3\overset{\bullet+}{N} \quad \xrightarrow{\text{radical coupling}} \quad Ph_2N-\!\!\!\!\!\underset{H}{\overset{H}{\diagdown}}\!\!\!\!\!-NPh_2$$

$$\left[\underset{Ph}{\overset{Ph}{\diagup}}\!\!=\!\! \right]^{\bullet+} + \, MeOH \xrightarrow[\text{addition}]{\text{nucleophilic}} \underset{Ph \; H}{\overset{Ph \quad OMe}{\diagup\!\!\diagdown}}H + H^+$$

$$\left[MeO-\!\!\!\bigcirc\!\!\!- \right]^{\bullet+} + \, AcO^- \xrightarrow{\text{deprotonation}} MeO-\!\!\!\bigcirc\!\!\!-\overset{\bullet}{CH_2} + AcOH$$

$$Me_2\overset{\bullet+}{N}-\!\!\!\bigcirc\!\!\!-\!\!\!\bigcirc \xrightarrow[\text{cleavage}]{\text{mesolytic}} Me_2N-\!\!\!\bigcirc\!\!\!-\!\!\!\diagdown^+ \quad + \quad \diagdown\!\!\!\!-\!\!\!\bigcirc$$

$$\left[\diagup\!\!\diagdown\!\!\diagup \right]^{\bullet+} + \diagup\!\!\diagdown\!\!\diagup \xrightarrow{\text{cycloaddition}}$$
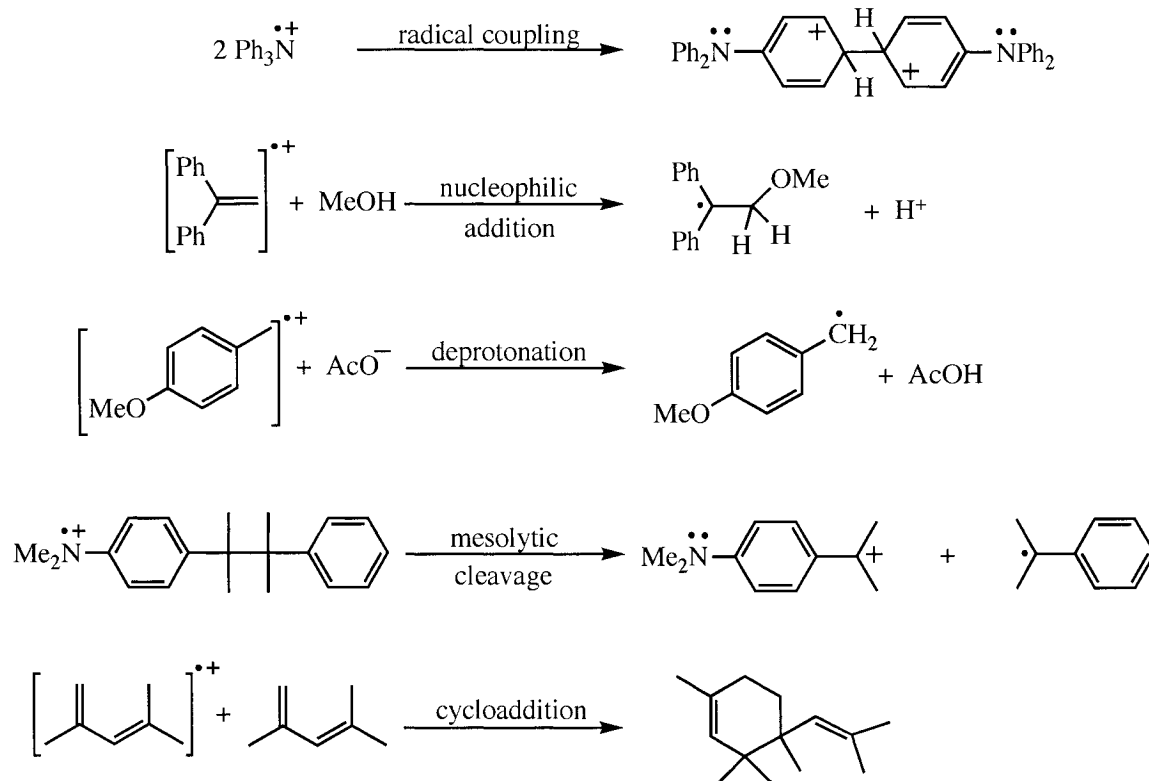
1.1.3 Characterization of Radical Cations

Radical cations are frequently identified by their characteristic UV-visible absorptions and by comparison of their spectra to those obtained in matrices at low temperature. These species typically show two absorption bands, one associated with an electronic transition from the SOMO to the LUMO and a second band associated with a transition from the HOMO-1 orbital to the SOMO, Scheme 1.17.[5] The positions of these absorption bands depend on the structure of the radical cations. For instance, the radical cations of substituted styrenes typically show one strong absorption band centered between 350 and 400 nm, and a second weaker absorption band centered around 600 nm. On the other hand, the radical cations of substituted stilbenes show a strong band between 470 and 520 nm, and a second band in the region between 700 and 800 nm.[32] Table 1.1 summarizes the absorption maxima of several π-type radical cations.

Scheme 1.17
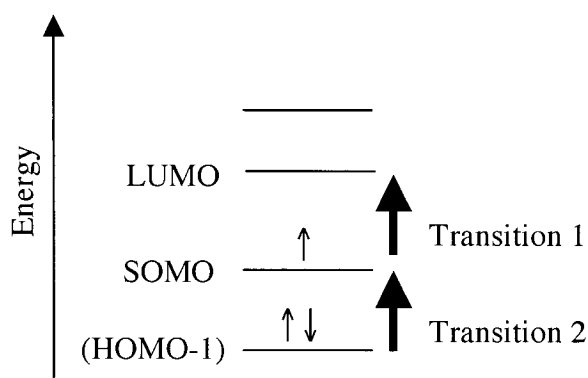
Table 1.1 Absorption maxima of alkene and arylalkene radical cations.[32]

Alkene	λ_{max} (nm)	Solvent
butadiene	315, 570	s-BuCl
all-*trans*-1,3,5-hexatriene	400, 650	s-BuCl
trans-stilbene	480, 758	i-BuCl
trans-α,β-dimethylstilbene	447, 750	s-BuCl
trans-4-methylstilbene	496, 795	s-BuCl
styrene	350, 620	cyclohexane
4-methoxystyrene	350, 600	TFE
trans-β-methyl-4-methoxystyrene	380, 600	MeCN

The detection of transient spectra similar to those of radical cations is not enough evidence to identify the transient species as a radical cation. Diagnostic tests are also commonly employed to identify radical cations species. For instance, rapid reaction with nucleophiles strongly indicates that the transient species is positively charged, although it does not discriminate between a radical cation and a carbocation intermediate. However, generation of the same transient species by photoinduced electron transfer (PET) will eliminate the possibility of a carbocation since PET does not generally lead to the formation of carbocations. Similarly, reaction of the observed transient with a more

easily oxidized substrate to give a well-characterized radical cation provides strong evidence for the identification of a radical cation. Radical cations are easily distinguished from radicals and triplet species by their reactions with molecular oxygen. Radicals and triplet species are rapidly quenched in presence of oxygen ($k_{O2} > 10^9$ M^{-1} s^{-1}), whereas the reaction of radical cations with oxygen is very slow ($k_{O2} < 10^8$ M^{-1} s^{-1}).[33]

Therefore, radical cation species are generally recognized by their characteristic absorption spectra as well as by their reactivity towards nucleophiles and their lack of reactivity to oxygen. Electron transfer reactions with more easily oxidized donor to give the radical cation of the donor also strongly support a radical cation assignment.

1.2 Scope of Thesis

Despite the amount of available information concerning the chemistry and applications of radical cations, there are still some aspects involving the chemistry of these species that have not been studied. The present thesis focus on the generation and characterization of biologically relevant radical cations by nanosecond laser flash photolysis.

The thesis results are described in two chapters based on the nature of the radical cation studied. Chapter 2 focus on the generation of substituted 4-vinylphenol radical cations. The spectral characteristics, the reactivity of these species towards hydroxylic and anionic species, as well as the influence of the acidity on the lifetimes of these radical cations are thoroughly discussed in this chapter. Special attention is focused on the reactivity of these radical cations towards their neutral precursors and other substituted styrenes.

18

Chapter 3 presents the results involving the generation and study of 1,2-diaryl enol radical cations in solution. The discussion concentrates on the influence of electronic substituent effects on the acidity and lifetimes of these enol radical cations using linear free energy relationships and electronic structure calculations. Chapter 4 provides a detailed description of the fundamentals as well as the procedures used for laser flash photolysis experiments. Finally, Chapter 5 summarizes the results described in this thesis and presents the final conclusions of this research work.

Chapter II. Substituted 4-Vinylphenol Radical Cations

2.1 Introduction

Naturally occurring compounds, like *p*-coumaric acid and coniferyl alcohol, that contain a 4-vinylphenol fragment are important components in several biological systems. Specifically, these classes of organic molecules are building blocks for the biosynthesis of natural products such as lignin, the second most abundant biopolymer on earth, and plant lignans, which frequently possess important therapeutic applications. Even though the biosynthesis of these natural products is subject of active debate,[34, 35] it is commonly accepted that the initial step is the oxidation of the neutral vinylphenolic precursors by oxidizing enzymes like peroxidases and laccases to give resonance stabilized phenoxyl radicals that further undergo coupling reactions to yield oligomeric materials.

While some authors consider the phenoxyl radicals as the direct product of the enzymatic oxidation, others[36, 37] have proposed the intermediacy of a 4-vinylphenol radical cation which then undergoes rapid deprotonation to yield the corresponding 4-vinylphenoxyl radical, Scheme 2.1.

Scheme 2.1
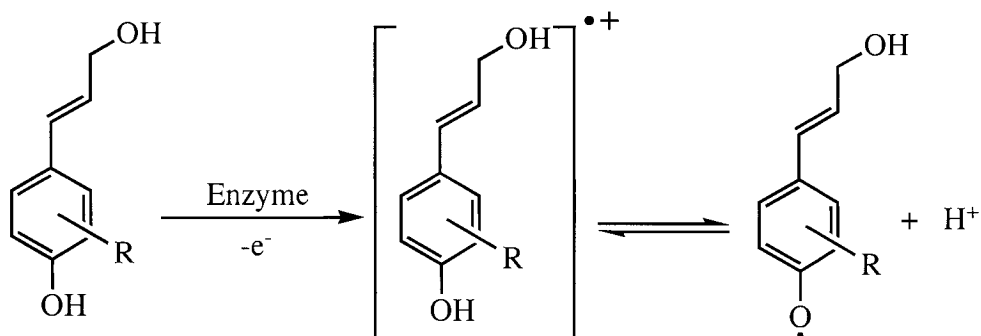
While the chemistry of 4-vinylphenoxyl radical has been studied using several methods like e.p.r. spectroscopy[38] and laser flash photolysis,[39, 40] 4-vinylphenol radical cations have not yet been studied. Thus, given the absence of information with reference to these reactives species, the first goal of my research is to study the spectral and kinetic properties of 4-vinylphenol radical cations in solution.

In addition, as described in detail in Section 2.4.3, the cycloaddition reaction of styrene radical cations with neutral styrenes often gives products with the same structural framework as some lignans. For example, the lignans galbulin and isogalbulin can be prepared by radical cation mediated dimerization, Scheme 2.2, of 1-(3,4-dimethoxyphenyl)propene.[41] These observations open the door to the possibility of a radical cation based mechanism for the biosynthesis of lignans, and the feasibility of radical cation mediated dimerization of 4-vinylphenols is also explored in this chapter.

Scheme 2.2
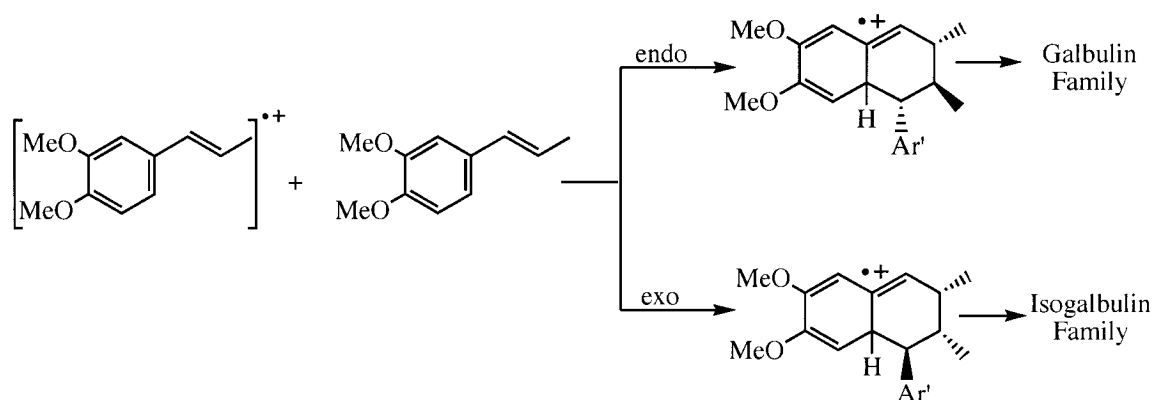
2.1.1 Biosynthesis of Lignin

Lignin is a tridimensional phenolic polymer mainly composed of three phenylpropenoid monomers, namely coniferyl alcohol, p-coumaryl alcohol and sinapyl alcohol, Scheme 2.3. This biopolymer constitutes one of the main structural components

of the cell wall in higher plants. As such, lignin is responsible for the protection of plant

cells, as well as for providing support for the plant against gravity.

Scheme 2.3

coniferyl alcohol   p-coumaryl alcohol   sinapyl alcohol
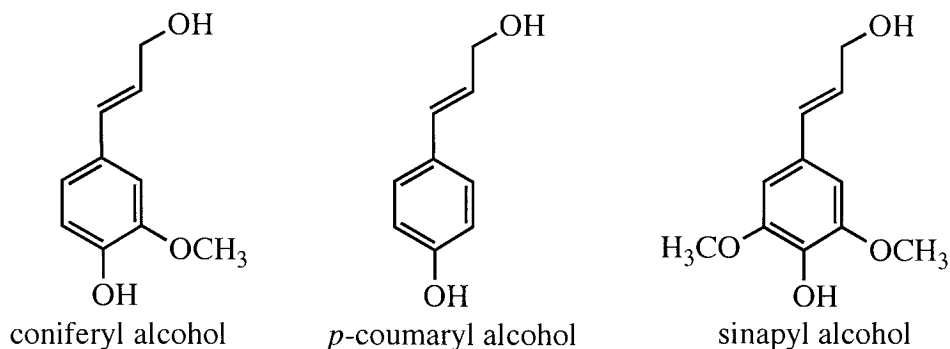
More than forty years ago, Freudenberg and coworkers published a series of reports

accounting for the formation of polymeric structures with some similarities to natural

lignins by *in vitro* oxidation of p-hydroxycinnamyl alcohols with hydrogen peroxide in

presence of peroxidases. Based on these results Freudenberg proposed a mechanism[42] for

the biosynthesis of lignin that is still well accepted, Figure 2.1. Accordingly, the

oxidation of p-hydroxycinnamyl alcohols leads to the formation of resonance stabilized

phenoxyl-like radicals that undergo cross coupling reactions to yield a variety of dimeric

systems. Further growth of these dimers can occur by addition of phenols to the quinone

methides, Figure 2.2, or by further oxidative coupling, resulting in the formation of the

lignin polymer. Interestingly, although the formation of the phenoxyl radicals clearly

implies the participation of the peroxidases, the polymerization is generally viewed as a

non-enzymatic random process.[35, 42, 43]
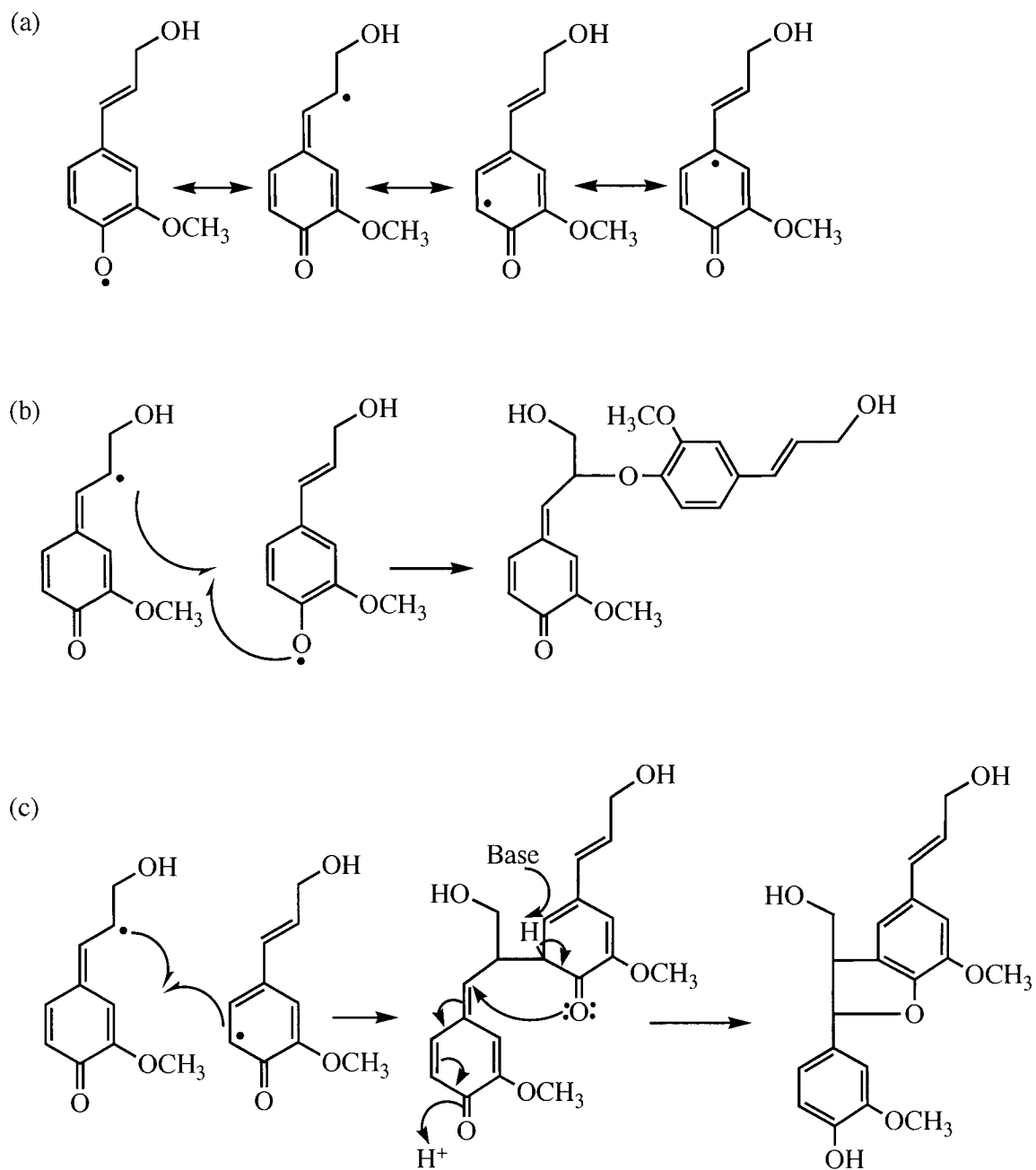
Figure 2.1 (a) Resonance structures of 4-vinylphenoxyl radical. (b) and (c) cross-coupling dimerizations.

23
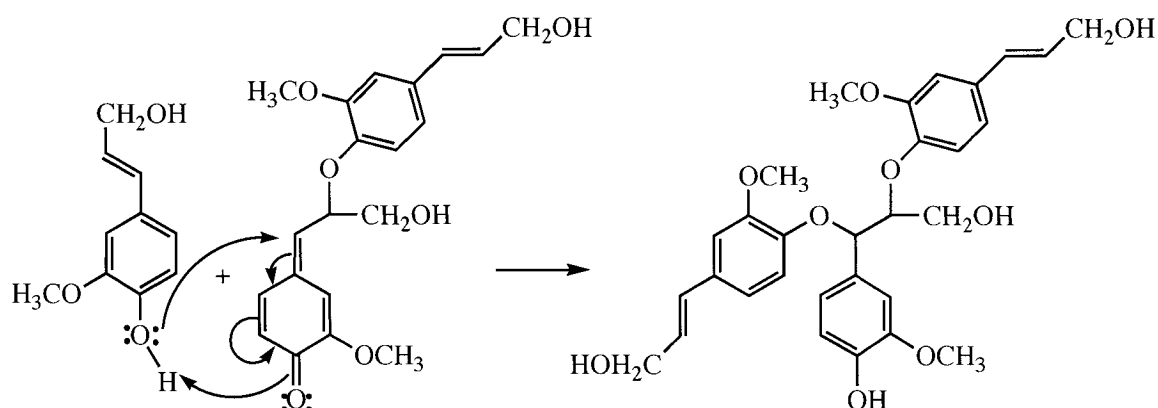
Figure 2.2 Trimerization via phenol addition to quinone methide subunits.

2.1.2 Biosynthesis of Lignans

Lignans are a group of naturally occurring products that have attracted the attention of the scientific community by virtue of their anti-tumor, anti-HIV, anti-fungal and immunosuppressive activities.[44] For instance, the lignan 4'-demethylepipodophyllotoxin is the precursor of etoposide, Scheme 2.4, which is a very efficient anticancer agent used in the treatment of small cell lung cancer, testicular cancer and lymphomas.

Scheme 2.4

4'-demethylepipodophyllotoxin   etoposide
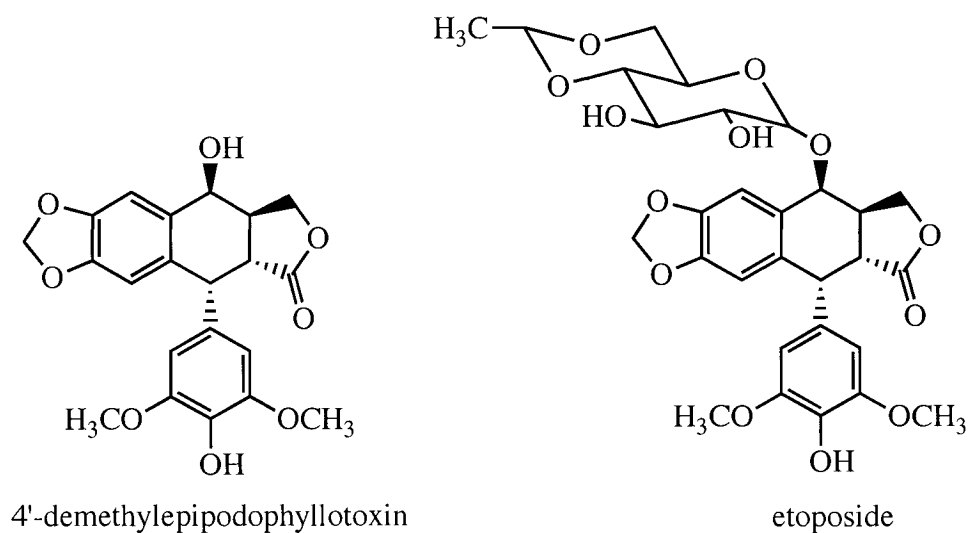
Lignans are composed by two β-β' linked phenylpropanoid subunits, **I** in Scheme 2.5. Based on their general structures, these products are typically divided in six groups:[45] the dibenzylbutanes have the phenylpropanoid subunits linked β-β' only, the lactones, furans and furofurans possess an oxygen bridge in addition to the β-β' bond, and the arylnaphthalenes and bridged biphenyls which have a second C-C bond joining the two subunits, Scheme 2.5.

Scheme 2.5

I

(dibenzylbutanes)　　(lactones)

(furans)

(furofurans)　　(arylnaphthalenes)　　(bridged biphenyls)
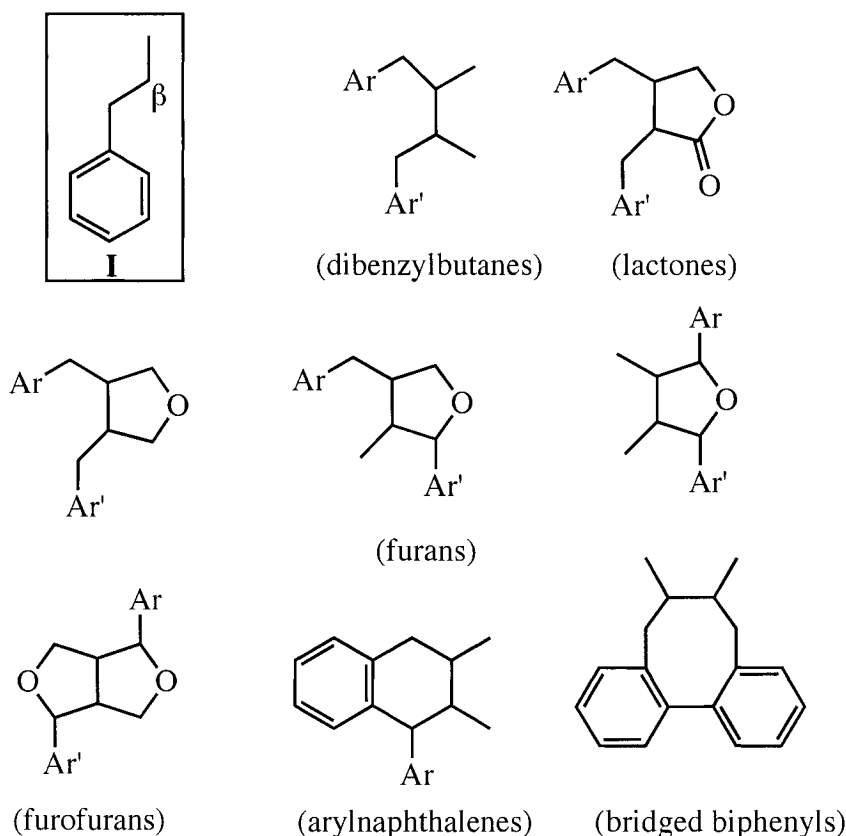
As lignin, lignans are considered to be biosynthesized via bimolecular coupling of phenoxyl radical initially formed by enzymatic oxidation of 4-vinylphenol substrates. For instance, pinoresinol – a lignan of the group of furofurans - is formed by β-β' coupling of two phenoxyl radicals derived from coniferyl alcohol, Scheme 2.6.[46] The initially formed dimeric diquinone then undergoes intramolecular nucleophilic addition

of the aliphatic hydroxyl groups to the C-C double bond of the quinone methide system

to give pinoresinol.

Scheme 2.6
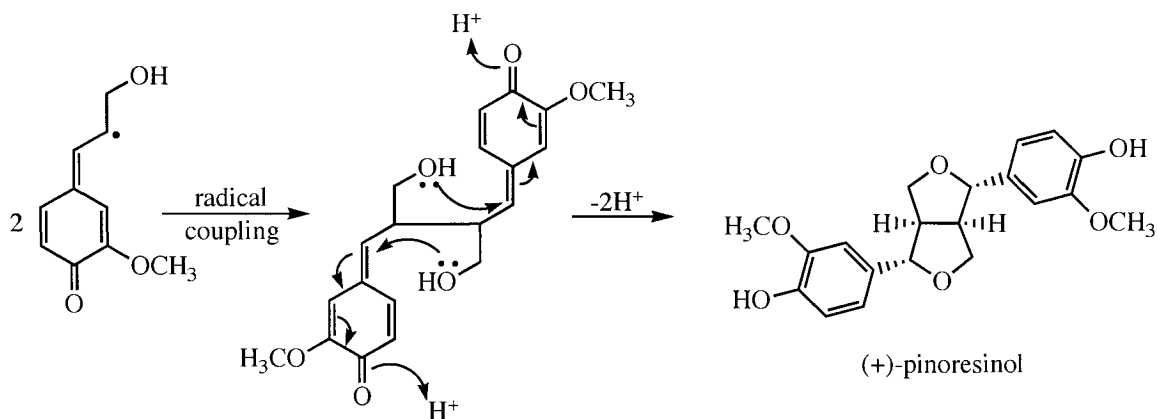
(+)-pinoresinol

Similarly, desoxypodophyllotoxin is derived from pinoresinol, which as shown in

Scheme 2.6, is generated by radical-radical coupling. Initially, pinoresinol undergoes

reductive opening of the furan rings to give secoisolariciresinol, Scheme 2.7. Further

oxidation of one of the primary alcohols to carboxylic acid followed by lactone ring

formation yields the lignan metairesinol. Modification of the aromatic substitution

pattern transform metairesinol into yatein. Deprotonation of this species followed by

intramolecular nucleophilic attack to the quinone methide system finally gives

desoxypodophyllotoxin.[46]

Scheme 2.7

(+)-pinoresinol
secoisolariciresinol
matairesinol

desoxypodophyllotoxin

yatein
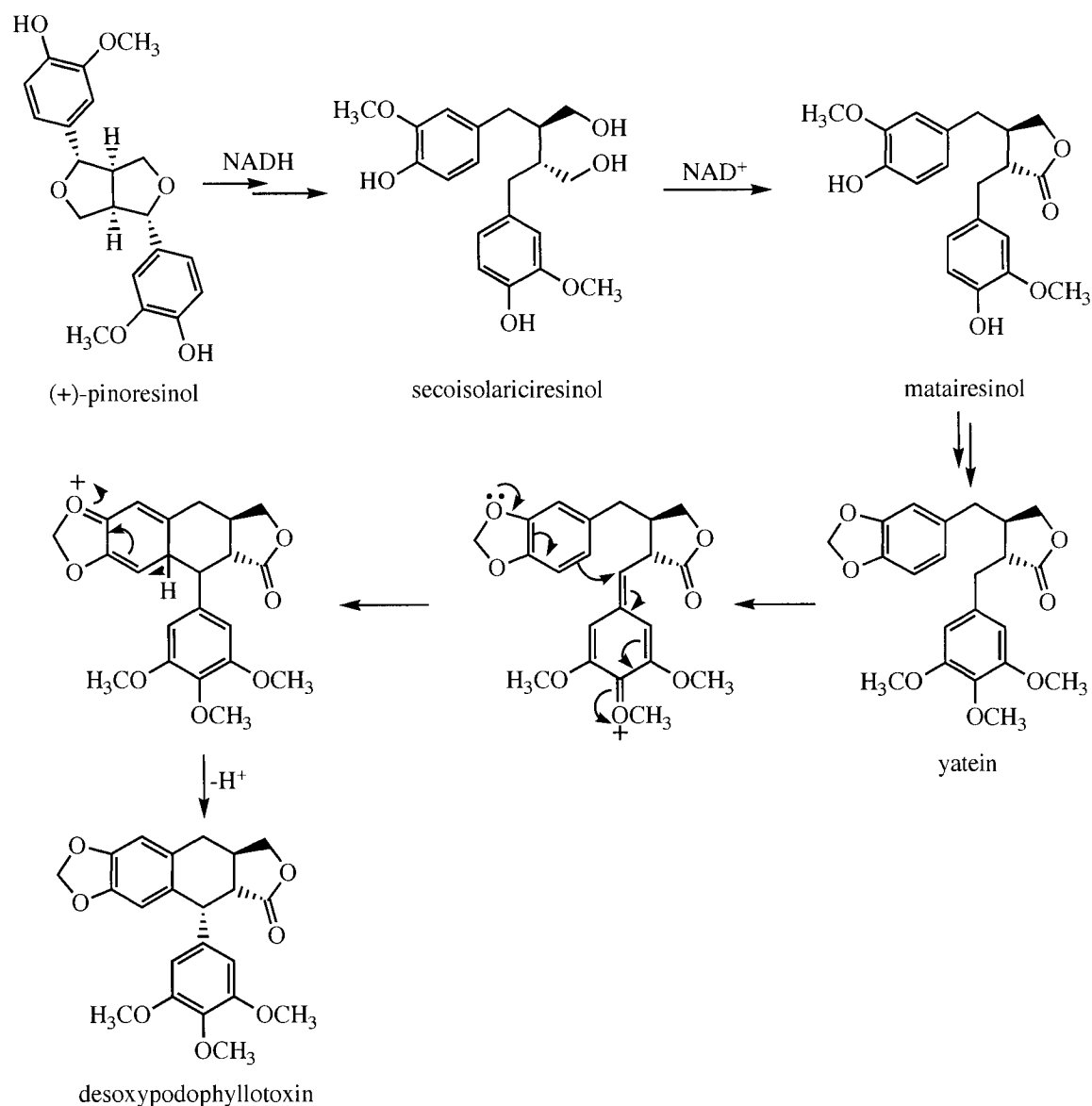
Based on the lack of regio and stereospecificity of phenoxy radical coupling reactions carried out in vitro and on the fact that lignans are optically active, Lewis *et al.*[47] have proposed the participation of an auxiliary 'dirigent' protein (DiP) in the biosynthesis of lignans. This protein does not catalyze the oxidation of substrates but it fixes the orientation of the phenoxyl radicals, defining the stereoselectivity of the dimerization.[47] It is important to note that Lewis *et al.*[47] have also suggested the

participation of an auxiliary protein in the biosynthesis of lignin. Nevertheless, while the involvement of the DiP in the biosynthesis of lignans has been well accepted,[44, 48] the implication of a DiP in the lignification process has encountered some challenges. According to Ralph et al.[49] a DiP-directed lignin should be optically active; however lignin is racemic. Meyermans et al.[50] have stated that the great variety of monolignols that can be incorporated in a functional lignin structure implies a plasticity of lignin biosynthesis that is not consistent with the idea of a controlled process. Moreover, it has been pointed out that as a result of the impossibility of proteins to diffuse through the lignified cell walls, lignin would be expected to possess a large amount of the DiP trapped in its network; however this has not been demonstrated so far.[51]

2.1.3 Photochemistry of 4-Vinylphenols

The production of a lignin like polymer by photolysis of coniferyl alcohol[52] stimulated a great deal of investigation concerning the intermediates produced by the photolysis of coniferyl alcohol and similar compounds. Leary[39] studied the photochemistry of coniferyl alcohol and isoeugenol, Scheme 2.8, in an attempt to detect the corresponding phenoxyl-like radicals. Flash photolysis of both compounds in water or ethanol yielded a long-lived transient species with an absorption maximum near 350 nm that was identified as 4-allylidene-2-methoxy-cyclohexa-2,5-dienone (methide quinone), Scheme 2.8.

Scheme 2.8

HO—⟨benzene ring⟩—CH=CH—CH₃
OMe
isoeugenol

O=⟨cyclohexadienone ring⟩=CH—CH=CH₂
OMe
4-Allylidene-2-methoxy-cyclohexa-2,5-dienone
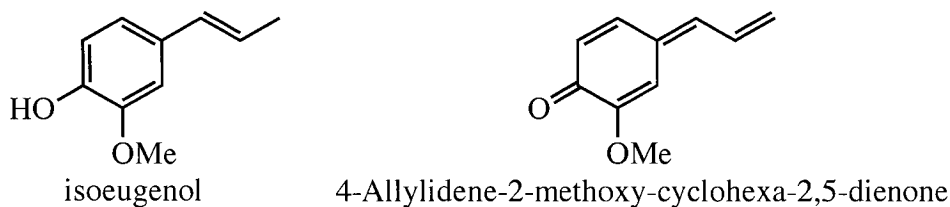
The yield of the quinone methide obtained upon flash photolysis of coniferyl alcohol was at least five times larger when very polar solvents like water and acetic acid were used instead of ethanol. Nevertheless, the transient identified as the quinone methide was also observed upon flash photolysis of coniferyl alcohol in non-polar solvents like tetrachloromethane. Based on these observations Leary[40] proposed two mechanisms for the formation of the quinone methide: (a) a polar mechanism, and (b) a radical mechanism. According to the polar mechanism coniferyl alcohol undergoes deprotonation from an excited state to give a phenoxy anion that is then transformed to the methide quinone by elimination of the aliphatic hydroxy group, Scheme 2.9. The radical mechanism was not detailed in this report;[40] the author only suggested the intermediacy of a phenoxyl radical without giving any other details concerning the mechanism of formation of the quinone methide.

Scheme 2.9
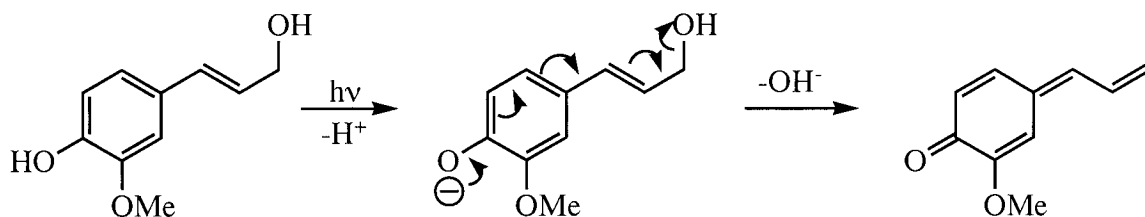
On the other hand, Miller et al.[53] reported that the yield of the quinone methide was substantially reduced when coniferyl alcohol was photolyzed in presence of radical trapping species, strongly suggesting the intermediacy of radical species. Miller et al.[53]

29

also observed that the yield of the quinone methide was increased when coniferyl alcohol was photolyzed in presence of acetic acid or hydrochloric acid. Based on these observations Miller *et al.*[53] proposed that the formation of the quinone methide from coniferyl alcohol involved a radical cation intermediate as shown in Scheme 2.10. Accordingly, irradiation of coniferyl alcohol initially generates the corresponding phenoxyl radical, which undergoes acid-catalyzed elimination of the aliphatic hydroxyl group to yield an intermediate radical cation. Further reduction of this species finally yields the quinone methide.

Scheme 2.10
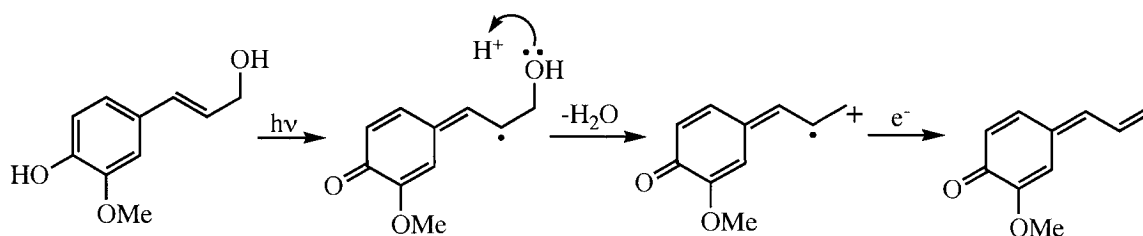
The formation of radical species upon photolysis of coniferyl alcohol has been demonstrated by electron paramagnetic resonance (e.p.r.) spectroscopy. Radical species has been observed by e.p.r. after photolysis of coniferyl alcohol at room temperature or upon photochemical oxidation with *t*-butylperoxide in presence of the spin trapping species 2-methyl-2-nitrosopropane.[38] Since photolysis of coniferyl alcohol results in the formation of quinone methide, the observation of radical species upon photolysis of coniferyl alcohol is consistent with the intermediacy of radical species in the formation of quinone methide. E.p.r. spectra obtained from the free radicals formed by photolysis of coniferyl alcohol in low temperature matrices also support the involvement of radical intermediates in the formation of the quinone methide.[54]

Product studies of the photolysis of coniferyl alcohol[55] and isoeugenol[56] have also been reported. According to these studies polymerization, attributed to phenoxyl radical coupling, together with addition of hydroxylic solvent and isomerization of the double bond appear to be the main processes involved in the photolysis of coniferyl alcohol and isoeugenol, Scheme 2.11.

Scheme 2.11

In contradiction with previous reports, Radotic *et al.*[57] have reported that no radicals were detected by e.p.r. measurements, not even at low temperature (-150 °C) in the presence of the spin-trap N-*tert*-butyl-α-phenylnitrone, when studying the photochemical transformation of coniferyl alcohol in water. It was also found that addition of DMSO and several alcohols suppressed the formation of the transient identified as 4-allylidene-2-methoxy-cyclohexa-2,5-dienone, indicating that protons are needed for this process. Consequently, an ionic mechanism was proposed to explain the conversion of coniferyl alcohol to 4-allylidene-2-methoxy-cyclohexa-2,5-dienone. The mechanism involves the protonation of the γ–OH group in the excited state coniferyl alcohol, followed by elimination of water and a proton to yield the quinone methide, Scheme 2.12. According to this report,[57] the photopolymerization takes place by consecutive additions of the phenols to the 4-allylidene-2-methoxy-cyclohexa-2,5-dienone subunits, as represented in Figure 2.2.

Scheme 2.12

In summary, polymerization, double bond isomerization and solvent addition are the main reactions observed upon irradiation of coniferyl alcohol and isoeugenol. Most of the studies involving the photochemistry of coniferyl alcohol lead to the conclusion that 4-allylidene-2-methoxy-cyclohexa-2,5-dienone is formed upon photolysis of coniferyl alcohol. However, there are several discrepancies regarding the mechanism of formation of the substituted quinone methide. Some authors propose the intermediacy of 4-vinylphenoxyl radicals in the generation of 4-allylidene-2-methoxy-cyclohexa-2,5-dienone while others state that the formation of this species takes place via an ionic mechanism without participation of any radical species.

2.1.4 Styrene Radical Cation Reactions

Given the structural similarity between 4-vinylphenol radical cations and styrene radical cations, both of these species are expected to show similar reactivity. For the same reason, 4-vinylphenol radical cations and phenol radical cations are likely to participate in the same type of reactions. The next sections are devoted to detail the most typical reactions of styrene radical cations and phenol radical cations.

2.1.4.1 Electron Transfer

As mentioned previously, a potential difficulty in the generation of radical cations using the photoinduced electron transfer method is the back electron transfer between the

radical cation and the radical anion within the initially formed radical ion pair. In fact, the acceptance of an electron by the SOMO of a radical cation from another oxidizable substrate to form the neutral form of the radical cation is one of the most characteristic reactions of radical cations, Eq. 2.1.

$$D^{+\cdot} + S \rightarrow D + S^{+\cdot}$$
(Eq. 2.1)

In order for the electron transfer reaction to take place, the reaction must be exergonic, with the radical cation $D^{+\cdot}$ being more easily reduced than the radical cation $S^{+\cdot}$ of the substrate. This is a direct consequence of the relationship between the rate constant for electron transfer reaction and the thermodynamic driving force for the electron transfer, as described by the Marcus equation, shown in its simplest form in Eq. 2.2.[4, 58] According to Marcus, the activation free energy $(\Delta G^{\neq})$ for an electron transfer reaction depends on the free energy change (ΔG°) for the reaction and the intrinsic activation energy $(\Delta G^{\neq}_o)$, which is the activation free energy for a reaction with no thermodynamic driving force $(\Delta G^{\neq}_o = 0)$.

or

$$\Delta G^{\neq} = \Delta G^{\neq}_o \left[1 + \frac{\Delta G^{o}}{4 \Delta G^{\neq}_o} \right]^2$$

$$\Delta G^{\neq} = \Delta G^{\neq}_o + \frac{1}{2} \Delta G^{o} + \frac{\left(\Delta G^{o} \right)^2}{16 \Delta G^{\neq}_o}$$

Eq 2.2

According to this equation, $\Delta G^{\neq}$ is expected to be large when ΔG° is positive, indicating that endergonic electron transfer reactions will be relatively slow. Given that styrene radical cations can undergo rapid reaction with nucleophiles or their neutral precursors, endergonic electron transfer reactions involving styrene radical cations will be too slow to compete with other typical reactions of these species like nucleophilic addition or cycloadditions.

33

The Marcus equation also predicts that the free energy of activation decreases as $\Delta G°$ becomes more negative until the thermodynamic driving force has an absolute value four times that of the intrinsic activation energy ($\Delta G° = -4\Delta G^{\neq}_{o}$), at which point $\Delta G^{\neq} = 0$. Thus, for moderately exergonic electron-transfer reactions, the rate constants for electron transfer reactions involving radical cations will be rapid, and could reasonably be expected to compete with other fast reactions of radical cations.

According to the Marcus equation, the relationship between the activation free energy and the thermodynamic driving force is quadratic. Therefore, when $\Delta G° < -4\Delta G^{\neq}_{o}$ the activation energy ($\Delta G^{\neq}$) begins to increase as the thermodynamic driving force becomes progressively more negative. Thus, the Marcus equation predicts that the electron transfer reaction will become slower for highly exergonic electron transfer processes. When this behavior is observed experimentally, the region where the rate constants decrease with increasing exergonicity of the electron transfer is termed the Marcus inverted region. Typically, the inverted region is not observed. Instead, the most common observation is that the rate constant for electron transfer increases as the free energy becomes more negative. Once the thermodynamic driving force equals $-4\Delta G^{\neq}_{o}$, the electron transfer process becomes diffusion-controlled and no further increase is observed in the rate constant for electron transfer. It must be mentioned however that there are several examples confirming the existence of the inverted region predicted by Marcus. Most commonly, the inverted region is observed for back-electron transfer reactions of ion pairs.[4, 20, 21]

2.1.4.2 Reaction with Nucleophiles

The carbocationic character of styrene radical cations is evidenced in their reactions with nucleophiles. This type of reaction has been found to proceed with different types of nucleophiles, including neutral nucleophiles like water, alcohols and amines, and anionic species such as Cl$^-$, CN$^-$ and CH$_3$COO$^-$. The reaction with anionic species is very rapid, taking place with diffusion-controlled rate constants in solvents such as acetonitrile (MeCN) and 2,2,2-trifluoroethanol (TFE), Scheme 2.13.[23, 26, 33]

Scheme 2.13

Nu	k / M^{-1}s^{-1}
CN$^-$ (MeCN)	2.9 x 10^{10}
N$_3^-$ (TFE)	7.0 x 10^9
(MeCN)	9.9 x 10^8
MeOH (H$_2$O:MeCN) (4 : 1)	3.0 x 10^4
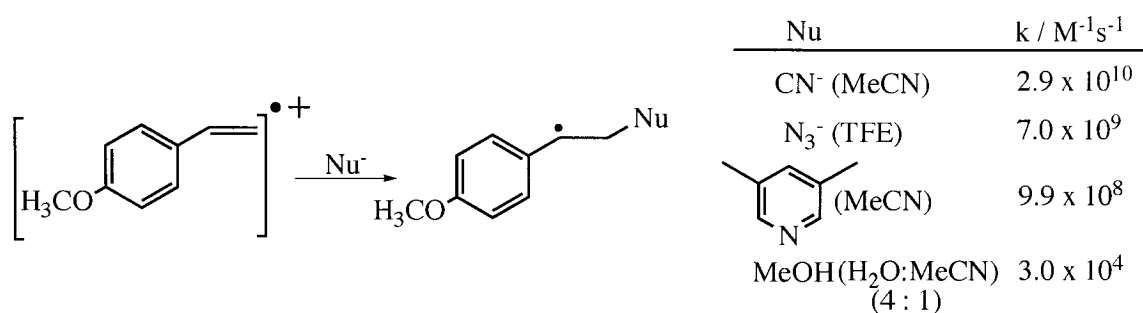
As shown in Scheme 2.13, the addition of the nucleophile occurs at the β-position of the styrene framework, resulting in the formation of benzyl radicals that can sometimes be clearly distinguished by their characteristic absorption band in the 300-340 nm region and by their reactivity towards oxygen (k$_{O2}$ ~ 10^{10} M^{-1}s^{-1} in acetonitrile).[59]

The rate constants for addition of neutral nucleophiles to styrene radical cations are markedly affected by steric and electronic effects associated with substituents on the aromatic ring and the double bond. For example, the second-order rate constants for addition of methanol to *para*-substituted styrene radical cations in TFE increases by almost two orders of magnitude in the order CH$_3$ < F < H, Scheme 2.14.[23] The increase

in reactivity is consistent with the decrease in electron donating power of the substituents, which obviously destabilizes the radical cation.

Incorporation of a methyl group at the β-position of styrene radical cation decreases the rate constant for addition of methanol by one order of magnitude. Addition of a second methyl group in the β-position further decreases the second-order rate constant for the reaction with methanol, Scheme 2.14.[23] Given that alkyl groups are good electron donors, the inclusion of alkyl substituents at the β-position of the styrene radical cations stabilizes these species by electronic effects. In addition, increasing substitution at the β-position increases the steric bulk around this position, impeding the nucleophilic attack and consequently reducing the magnitude of the second-order rate constants.

Scheme 2.14

Radical Cation	k_{MeOH} / $M^{-1}s^{-1}$
R_1 = Me; R_2 = R_3 = H	5.9×10^6
R_1 = F; R_2 = R_3 = H	5.1×10^7
R_1 = R_2 = R_3 = H	1.8×10^8
R_1 = R_2 = H; R_3 = Me	9.7×10^6
R_1 = H; R_2 = R_3 = Me	2.0×10^5
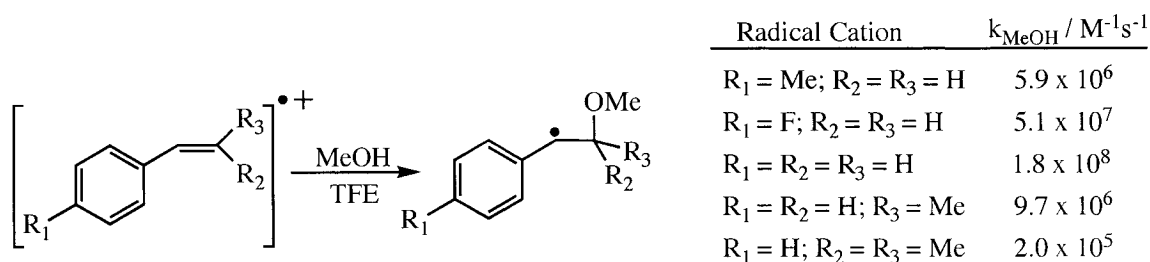
In some cases the addition of the nucleophile competes with electron transfer between the nucleophile and the radical cation. For instance, 4-methoxystyrene radical cation undergoes addition reaction with the azide anion (k_{Nu} = 7.0 x 10^9 $M^{-1}s^{-1}$) in TFE as shown in Eq. 2.3-a. However, when the reaction is carried out in acetonitrile electron transfer takes place instead at diffusion-controlled rate of 3 x 10^{10} $M^{-1}s^{-1}$, Eq. 2.3-b.[60] In MeCN the oxidation potential of the azide ion is *c.a.* 0.6 V lower than that of 4-methoxystyrene, thus the electron transfer reaction can take place with diffusion-controlled rate constant. On the other hand, formation of hydrogen bonds between TFE and the azide ion

stabilizes this species increasing its oxidation potential. As a result, the electron transfer reaction in TFE is not exergonic enough to take place at the diffusion-controlled rate and the addition reaction can compete with the electron transfer.

(Eq 2.3-a)

(Eq 2.3-b)
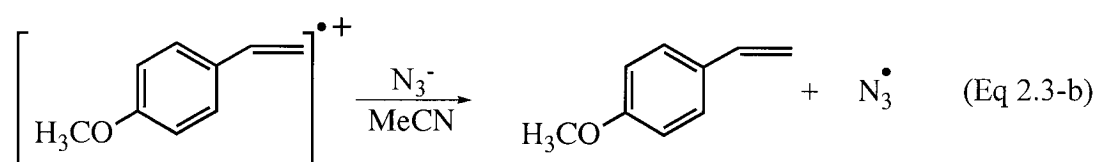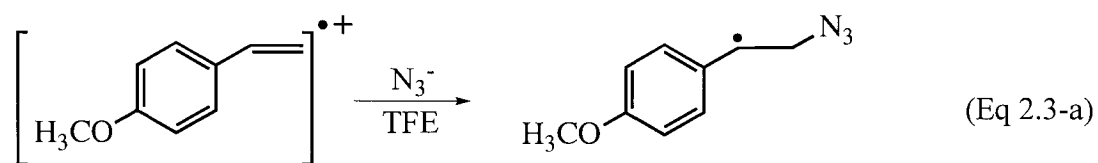
2.1.4.3 Cycloaddition Reactions

Cycloaddition reactions are probably the most interesting and useful reactions of alkene radical cations. These reactions can involve addition of an alkene radical cation to its precursor in a reaction commonly termed a radical cation mediated dimerization, or the radical cation can add to a different unsaturated system in a cross-addition reaction. For example, styrene radical cations undergo [2+1] cycloaddition to their neutral precursor, resulting in the formation of aryl-disubstituted cyclobutane and di- or tetra-hydronaphthalene products, Scheme 2.15.[24, 31, 41, 61, 62]

Scheme 2.15
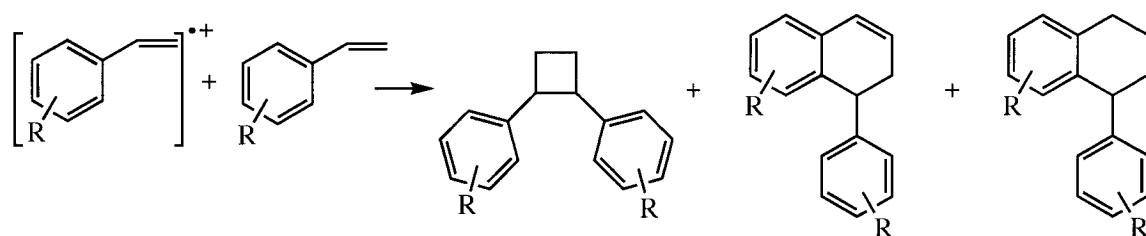
Similarly, arylalkene radical cations can also undergo cross-addition reactions with other alkenes or dienes. As shown in Scheme 2.16, the addition to dienes can follow two pathways, namely cyclobutadimerization [2+1] and Diels-Alder type reactions [4+1]. As exemplified for the nucleophilic addition, electron transfer reactions may compete with the cycloaddition reaction when the oxidation potential of the alkenes or dienes are smaller than those of the styrene like compounds.[25]

Scheme 2.16

An = Anisol
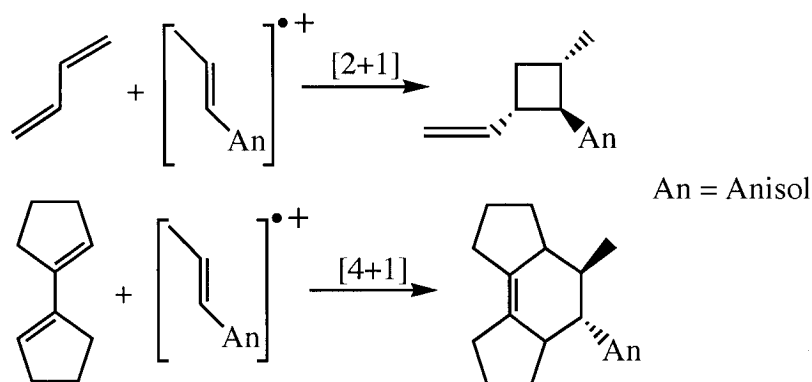
2.1.4.3.1 Mechanism of Radical Cation Cyclodimerization

The mechanism for radical cation mediated dimerization has been studied for more than thirty five years. The earliest studies on the subject were carried out by Ledwith *et al.*[61] in 1970. Based on the work on the radical cation mediated dimerization of N-vinylcarbazole, Ledwith proposed that the cyclobutanation of this system initially involves the reaction of the radical cation with the neutral precursor to give an acyclic distonic radical cation, Scheme 2.17a. Cyclization of this species gives a cyclobutane radical cation that undergoes electron transfer reaction with the precursor resulting in the regeneration of the radical cation and the formation of the cyclobutane derivative. Later studies[63] on the radical cation mediated dimerization of 1,1-diphenylethene led to the

conclusion that the 1,4-distonic radical cation could undergo 1,6-cyclization to give a substituted hexatriene radical cation that leads to dihydro- and tetrahydronaphthalene, Scheme 2.17b.[26, 64]

Scheme 2.17a
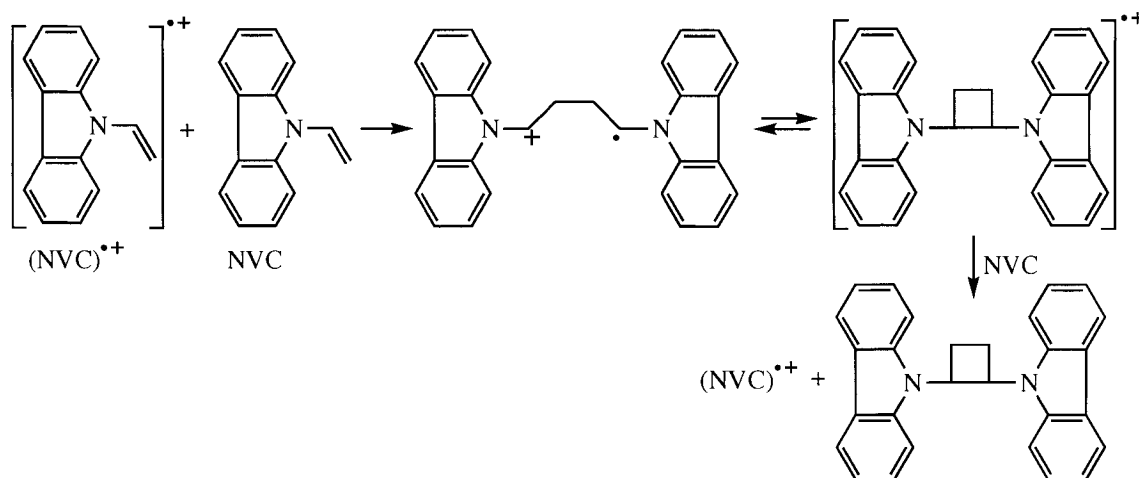
Scheme 2.17b
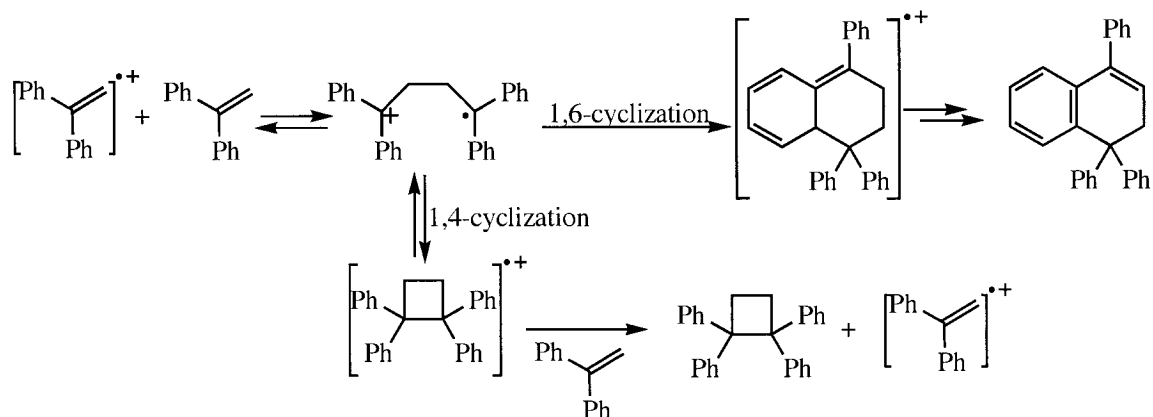
On the other hand, stereochemical studies have shown that the radical cation mediated dimerizations of *trans* and *cis*-anethole are highly stereospecific,[65] which is inconsistent with a distonic radical cation that can freely rotate and hence is expected to

yield a mixture of stereoisomers. Consequently, a mechanism involving a long-bond cyclobutane radical cation[24, 31, 65, 66] as the first intermediate has been proposed, Scheme 2.18 (R=CH$_3$). The long-bond intermediate can either yield the disubstituted cyclobutane by electron transfer with a neutral styrene molecule, or can undergo 1,3-sigmatropic shift to give an hexatriene radical cation which can further yield naphthalene-like derivatives.

Scheme 2.18

An = 4-methoxyphenyl
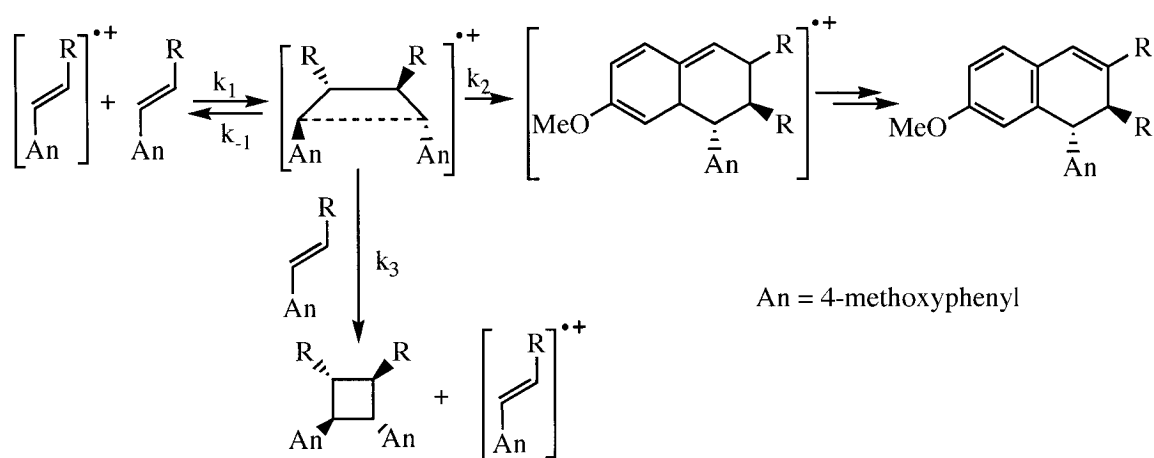
The mechanism shown in Scheme 2.17 have been used to explain radical cation dimerizations of several styrene derivatives.[26, 28, 63] Indeed some authors have reported the detection of the acyclic distonic radical cation formed upon initial coupling of the radical cation with its neutral precursor. Tojo et al.[67] have claimed to have observed the distonic radical cation produced by coupling of 4-methoxystyrene radical cation with the neutral parent in 1,2-dichloroethane. According to this study,[67] the transient spectrum of the distonic radical cation showed a 500-nm absorption band that grew-in with a first-order rate constant (k = 2.6 x 10^7 s^{-1}) that was closely similar to that observed for the decay (k = 1.4 x 10^7 s^{-1}) of the 4-methoxystyrene radical cation. However, the identification of the 500-nm transient as the distonic radical cation has

been challenged.[24] Given the absence of interaction between the radical center and the positive charge in distonic radical cations, these species are expected to show absorption maxima in the region between 300 and 340 nm that correspond to the spectra of the 4-methoxyphenethyl cation (λ_{max} = 340 nm) and the 4-methoxyphenethyl radical (λ_{max} = 310 nm), and not at 500 nm. Brede et al.[26] have also observed the formation of a 500-nm band, identified as the distonic radical cation, simultaneously with the decay of 4-methoxystyrene radical cation in cyclohexane. The authors[26] proposed that the distonic radical cation is folded in such a way that the π-systems of the two aromatic rings interact with each other, therefore explaining the presence of a single absorption band at 500 nm.

The mechanism involving the intermediacy of a long-bond cyclobutane radical cation, Scheme 2.18, has also been used to explain the radical cation mediated dimerization of substituted styrenes.[24, 31, 65, 66] Schepp et al.[24] have clearly established that the radical mediated dimerization of 4-methoxystyrene does take place via a long-bond cyclobutane radical cation. As in previous studies,[26, 67] Schepp et al.[24] observed the formation of a 500-nm transient, previously identified as the distonic radical cation. However kinetics and spectroscopic evidences led to the identification of this transient as the hexatriene radical cation formed by 1,3-sigmatropic shift within the long-bond cyclobutane, Scheme 2.18 (R=H).

2.1.4.3.2 Dynamics of [2+1] Cyclodimerization

Second order rate constants for the addition of substituted styrene radical cations to their neutral precursors have been measured by laser flash photolysis[23, 33] or pulse radiolysis methods.[26] As illustrated in Table 2.1, for styrene radical cations without

substituents on the β-position the dimerization reaction is very rapid, taking place with diffusion-controlled rate constants. The influence of the substituent on the aromatic ring on second-order rate constants is relatively small. On the other hand, the nature of the solvent has a larger impact on the dimerization rate constant. In general, the rate constants in cyclohexane are almost one order of magnitude larger than in polar solvents like TFE or acetonitrile.

Table 2.1 Second-order rate constants for the reaction of substituted styrene radical cation with their neutral precursors.[33]

Substituted Styrene	$k_{dimerization}$ / M^{-1} s^{-1}	Solvent
styrene	8×10^9	cyclohexane
4-chlorostyrene	6×10^9	cyclohexane
α-methylstyrene	1×10^{10}	cyclohexane
β-methylstyrene	$<6 \times 10^7$	cyclohexane
4-methylstyrene	1×10^{10}	cyclohexane
	2.9×10^9	TFE
4-methoxystyrene	1×10^{10}	cyclohexane
	1.1×10^9	TFE
	1.7×10^9	aqueous-acetonitrile
trans-β-methyl-4-methoxystyrene	$<6 \times 10^7$	cyclohexane

Given the complexity of the mechanism of radical cation mediated dimerization, the observed rate constants for these reactions are not simply the rate constants for the

42

coupling of the radical cation with its parent. Instead, the rate constants for the dimerization reactions are a combination of the rate constants corresponding to each of the steps involved in the reaction mechanism. For instance the reaction of 4-methoxystyrene radical cation with its neutral precursor takes place by the mechanism presented in Scheme 2.18 (R = H). According to this mechanism the observed rate constant for the disappearance of 4-methoxystyrene radical cation is given by Eq. 2.4.

$$k_{obs} = \frac{k_1 k_2 [4 - \text{MeOSty}]}{k_{-1} + k_2 + k_3 [4 - \text{MeOSty}]}$$
(Eq. 2.4)

Therefore, the changes in k_{obs} as a function of the concentration of the precursor will depend on the range of concentrations of 4-methoxystyrene. At low concentrations of the 4-methoxystyrene $k_{-1} + k_2 \gg k_3 [4\text{-MeOSty}]$, and under these conditions k_{obs} is given by Eq 2.5.

$$k_{obs} = \frac{k_1 k_2 [4 - \text{MeOSty}]}{k_{-1} + k_2}$$
(Eq. 2.5)

On the other hand, at high concentrations of 4-methoxystyrene, $k_{-1} + k_2 \ll k_3 [4\text{-MeOSty}]$ and k_{obs} is then independent on the concentration of 4-methoxystyrene, Eq 2.6.

$$k_{obs} = \frac{k_1 k_2}{k_3}$$
(Eq. 2.6)

The variations on the relationship between the observed rate constant for the consumption of the radical cation and the concentration of the precursors are clearly observed in the plot of k_{obs} versus the concentration of 4-methoxystyrene, Figure 2.3.
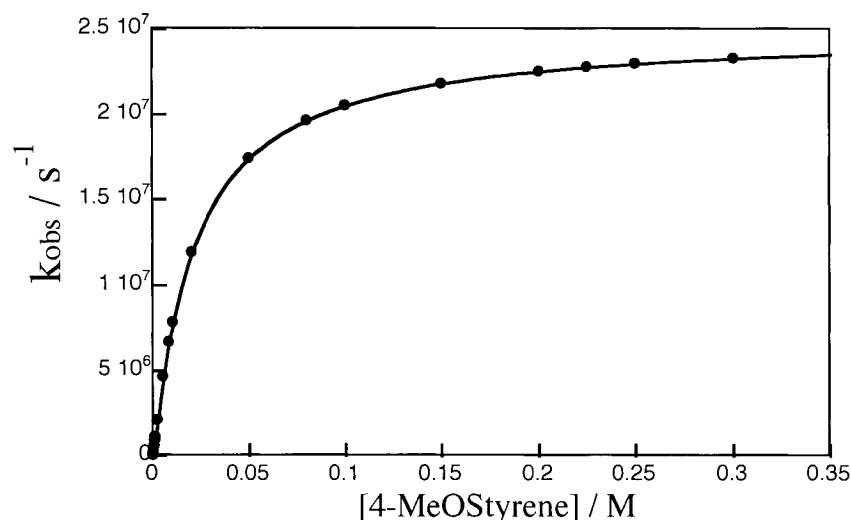
Figure 2.3 Relationship between rate constant observed for the decay of 4-methoxystyrene radical cation and the concentration of 4-methoxystyrene in acetonitrile.[24]

Note that at low concentrations of the styrene, the observed rate constants linearly increase with the concentration. However, at high concentrations of the styrene the k_{obs} no longer depend on the concentration of the precursor and a plateau is reached. The second-order rate constant for the reaction of the radical cation with its neutral precursor can be obtained from the slope of the linear region of the plot. As described in Eq. 2.5, the rate constant depends on the rate constant for the initial coupling of the radical cation with its precursor (k_1), the rate constant for the cleavage of the long bond cyclobutane (k_{-1}) and the rate constant for the electron transfer between the neutral precursor and the long-bond cyclobutane (k_3). Scheme 2.19 summarizes the rate constants estimated for each individual step for the radical cation mediated dimerization of 4-methoxystyrene.

Scheme 2.19

(An = 4-methoxyphenyl)
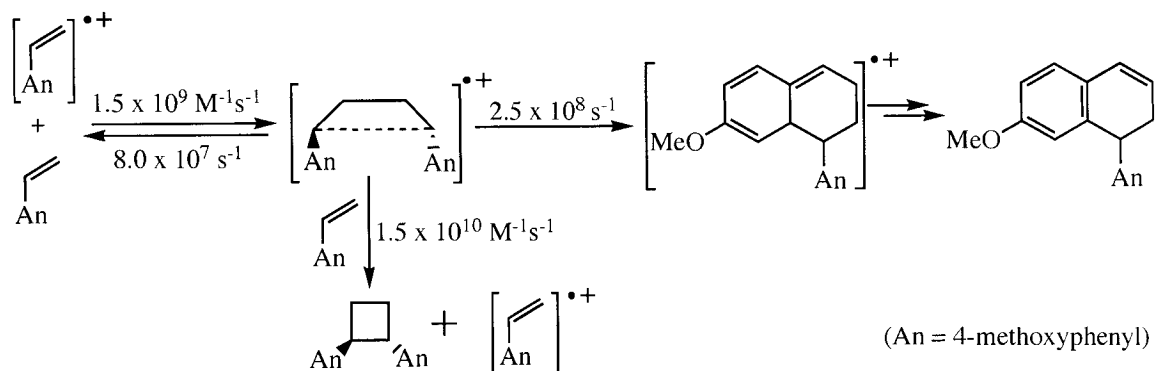
As shown in Table 2.1, the cycloaddition reaction is dramatically slowed down, almost by three orders of magnitude, with the introduction of a methyl group as substituent on the β position. For instance, the radical cation mediated dimerization of 4-methoxystyrene in acetonitrile takes place with a rate constant of 1.7×10^9 $M^{-1}s^{-1}$ while β-methyl-4-methoxystyrene radical cation reacts with its parent with a rate constant smaller than 1×10^6 $M^{-1}s^{-1}$.[24, 68] The slow reactivity of β-alkyl substituted styrene radical cations towards their neutral precursors has been attributed to steric hindrance by the β-substituent, as well as to the stabilization of the radical cation by the electronic inductive effect of the alkyl group.[26] A rapid cleavage of the dimer initially formed by coupling of the radical cation and the neutral parent (k_{-1}) has also been considered as the reason for the small dimerization rate constants observed for β-methyl-4-methoxystyrene.[68] However, the cleavage of 1,2-dianisyl-3,4-dimethylcyclobutane radical cation back to β-methyl-4-methoxystyrene radical cation and neutral β-methyl-4-methoxystyrene takes place with the same rate constant ($k_{-1} = 8.0 \times 10^7$ s^{-1}) that the cleavage of 1,2-dianisylcyclobutane to 4-methoxystyrene radical cation and neutral β-methyl-4-methoxystyrene.[24, 33, 68]

45

2.1.5 Phenol Radical Cation Reactions

Together with electron transfer, deprotonation is the most important type of reaction of phenol radical cations. As a result of its high acidity (see below), phenol radical cations can be rapidly deprotonated even by very weak bases.[69] For instance, the phenol radical cation generated in 1-chlorobutane reacts with weak bases such as acetone and dioxane, Scheme 2.20, with second-order rate constants that range from 2×10^7 to 9×10^{10} $M^{-1}s^{-1}$.[69]

Scheme 2.20

Base	$k / M^{-1}s^{-1}$
1,4-dioxane	2.15×10^7
acetone	1.52×10^9
MeCN	3.67×10^8
EtOH	9.16×10^{10}
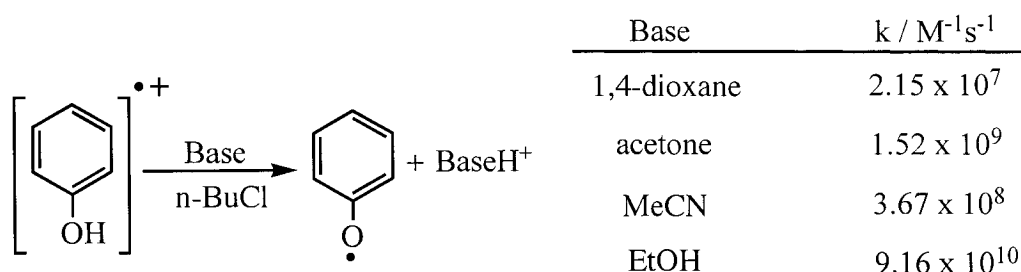
The strong acidity of phenol radical cations is not limited to this particular kind of species; in fact most radical cations are much more acidic than their neutral precursors. The enhancement of acidity is especially remarkable in radical cations of molecules with allylic or benzylic hydrogens and, of course, in systems with hydrogens linked to heteroatoms like in phenols and thiophenols, Table 2.2.

This dramatic change in acidities originates from the fact that the oxidation potentials of the neutral molecules are much greater than those of their conjugate bases. The trend is better understood analyzing the thermodynamic cycle represented in Scheme 2.21.

Table 2.2 Acidity and oxidation potentials (*vs* Ag/AgI) determined in Me$_2$SO. pKa of radical cations were calculated using the formula: $pK_a(HR^{\cdot+})= pK_a(RH)+[E^{OX}(R^-)-E^{OX}(RH)]23.06/1.37$. Note that this table was taken from Ref. [70]

RH	$pK_a(RH)$	$E^{ox}(R^-)$	$E^{ox}(RH)$	$pK_a(HR^{\cdot+})$
PhSH	10.3	0.515	1.82	-12
PhOH	18.0	0.550	2.10	-8.1
PhCH$_2$CN	21.9	-0.034	3.15	-32
Fluorene	22.6	-0.194	2.15	-17

Scheme 2.21
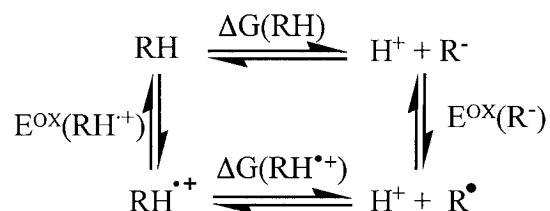
According to this cycle:

$$\Delta G(HR^{\cdot+}) = \Delta G(HR) + [E^{ox}(R^-) - E^{ox}(RH^{\cdot+})]$$

While oxidation of an anionic species will involve the abstraction of an electron from a non-bonding orbital, the oxidation of its conjugated acid involves the ionization of an electron from a bonding orbital. Consequently, the oxidation of the conjugate base (R$^-$) will be easier than that of the conjugate acid (RH). More precisely: $E^{ox}(R^-) < E^{ox}(RH^{\cdot+})$ and $\Delta G(HR^{\cdot+}) < \Delta G(HR)$. Therefore: $pK_a(HR^{\cdot+}) < pK_a(HR)$.

It is important to note that despite the thermodynamic superacidity of radical cations, deprotonation is typically slow especially for radical cations where the acidic

proton is bound to a carbon atom. Given the rapid reaction of styrene radical cations with potential bases (anions, amines and alcohols) via nucleophilic addition or electron transfer, these species are not likely to undergo deprotonation unless very bulky bases with high oxidation potentials are used.[33]

In summary, the most characteristics reactions of styrene radical cations are electron transfer, nucleophilic addition and cycloaddition reactions. Phenol radical cations also undergo electron transfer and nucleophilic addition but the most common reaction of these species is the loss of a proton to generate phenoxyl radicals.

2.2 Results

2.2.1 Laser Irradiation of 4-Vinylphenols in Acetonitrile

2.2.1.1 Coniferyl Alcohol

Laser flash photolysis of coniferyl alcohol in dry acetonitrile generates a transient species with absorption bands at 380 nm and 580 nm, Figure 2.4.[71] The two bands are formed within the laser pulse, and both decay in a first order manner with the same rate constant ($k = 8 \times 10^5$ s^{-1}), which indicates that the two features belong to the same transient species. The decay of this transient is not influenced by the presence of oxygen, indicating that the transient is neither a triplet nor a radical species. However, as described in detail below the decay of the transient is accelerated in presence of anionic reagents such as chloride or bromide and in the presence of hydroxylic solvents like water and ethanol. These observations lead us to identify this transient species as the radical cation of coniferyl alcohol generated by laser induced photoionization of the

neutral coniferyl alcohol, equation 2.7 (R = CH₂OH).[71] In particular, lack of reaction with oxygen together with high reactivity with nucleophiles are features characteristic of other styrene radical cations studied previously.[24, 26] In addition, the absorption bands at 380 and 580 nm match closely those of radical cations generated from other styrene derivatives that typically show two absorption bands, one in the UV region, between 350 and 380 nm and the other in the visible near 600 nm.[23, 24, 26, 32, 33]
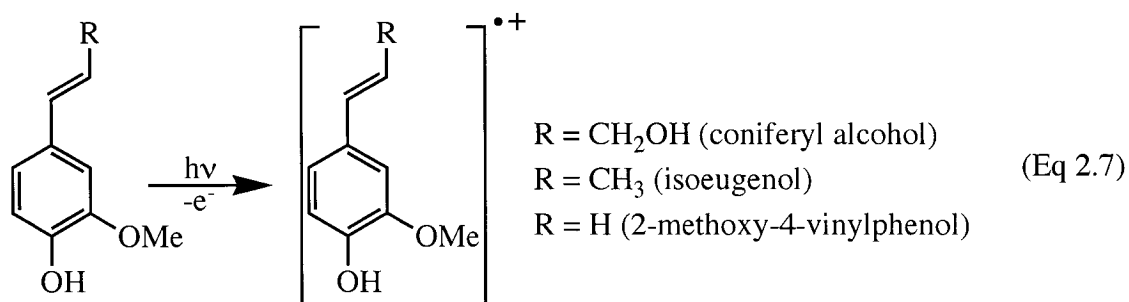
$$R = CH_2OH \text{ (coniferyl alcohol)}$$
$$R = CH_3 \text{ (isoeugenol)}$$
$$R = H \text{ (2-methoxy-4-vinylphenol)}$$

(Eq 2.7)

Generation of the coniferyl alcohol radical cation by photoinduced electron transfer provides further evidence for the identification of the transient species as the radical cation of coniferyl alcohol. Selective irradiation of chloranil with a laser pulse at 355 nm generates triplet chloranil which is well-known to have an absorption maximum at 500 nm.[72] As shown in Figure 2.5, the observed rate constants measured for the decay of triplet chloranil at 500 nm, increase in a linear manner with increasing concentrations of coniferyl alcohol, Figure 3.2. Linear least-square analysis gives a slope of (1.2 ± 0.1) x 10^{10} $M^{-1}s^{-1}$, corresponding to the second-order rate constant for the reaction of coniferyl alcohol with triplet chloranil. After complete quenching of triplet chloranil with coniferyl alcohol, the transient absorption spectra (Figure 2.6) is characterized by a band at 450 nm corresponding to the chloranil radical anion,[72] and by absorption bands at 380 and 580 nm that are closely similar to those generated by laser induced photoionization of coniferyl alcohol. The absorption bands at 450, 380 and 580-nm grow-in with observed

rate constants that are identical to the rate constant observed for the decay of triplet chloranil, $k_o = 1.3 \times 10^7$ s^{-1} at 1.0 mM coniferyl alcohol. These results are consistent with the formation of the coniferyl alcohol radical cation and the chloranil radical anion via a diffusion controlled electron transfer reaction between the coniferyl alcohol and the initially formed chloranil triplet, Eq. 2.8 (R=CH_2OH). Note that the electron transfer reaction between triplet chloranil (E^{ox} = 2.7 V vs SCE in MeCN)[1] and coniferyl alcohol (E^{ox} = 1.2 vs SCE in MeCN)[73] is highly exergonic, hence the large second-order rate constant observed for the electron transfer reaction between both species.

$$
\text{Chl} \xrightarrow[\text{355 nm}]{\text{hv}} \begin{array}{c} [\text{Chl}]^{3*} \\ (500\ \text{nm}) \end{array} + \underset{\substack{\text{OH} \\ (380,\,580\ \text{nm})}}{\overset{R}{\text{(structure)}}} \longrightarrow \left[\underset{\text{OH}}{\overset{R}{\text{(structure)}}} \right]^{\bullet+} + [\text{Chl}]^{\bullet-} \quad (\text{Eq. 2.8})
$$
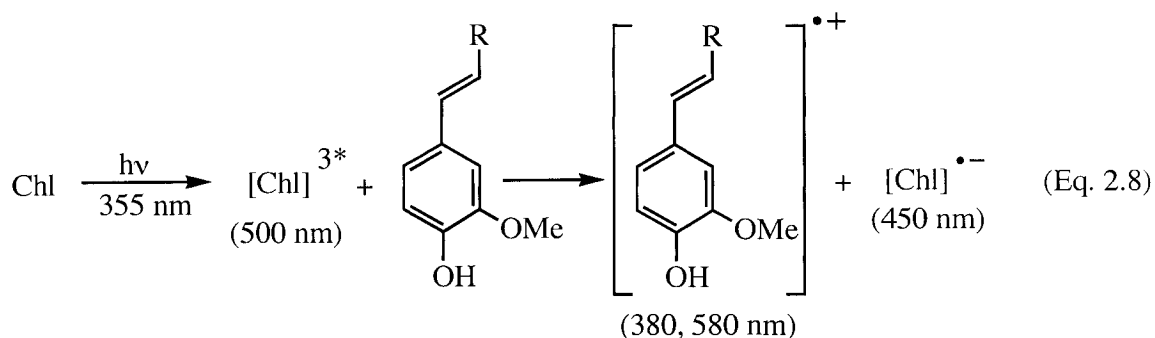
In addition to the absorption bands at 380 and 580 nm shown in Figure 2.4, an additional transient species with a strong absorption band at 340 nm is observed upon the laser irradiation of coniferyl alcohol at 308 nm. Unlike the radical cation bands that appear immediately after the laser pulse, the 340-nm band develops as a function of time after the laser pulse. This transient band was found to grow-in with a rate constant (k = 8 $\times$ 10^5 s^{-1}) identical to that observed for the decay of the radical cation, Figure 2.4 (inset), which indicates that the transient observed at 340 nm is a product of the reaction of the radical cation. The decay of 340-nm transient is not affected by the presence or absence of oxygen. Similarly, the addition of anionic or protic reagents like cyanide or water, respectively do not influence the decay of the 340-nm species. These results, together

50

with the fact that phenol-like radical cations mainly undergo deprotonation reactions to yield phenoxyl radicals,[74] suggest that the 340-nm transient is the 2-methoxy-4-(3-hydroxy-1-propenyl) phenoxyl radical, generated by loss of a proton from the coniferyl alcohol radical cation, Eq. 2.9 (R = CH_2OH).

$$(\text{Eq. 2.9})$$
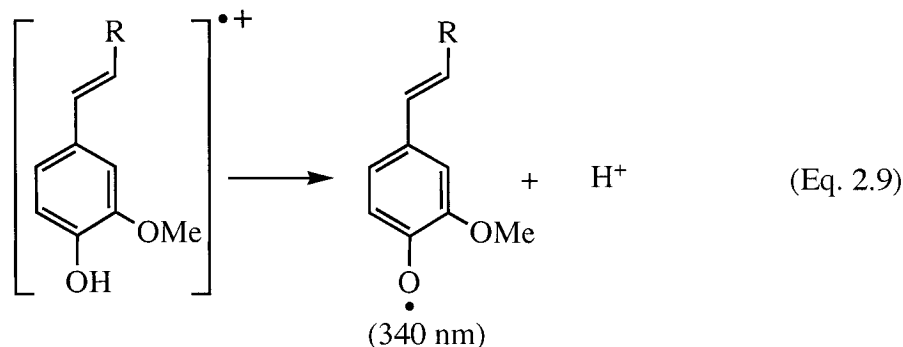
(340 nm)

More evidence confirming the identification of the 340 nm transient as the phenoxyl radical of coniferyl alcohol was obtained upon 355-nm laser irradiation of a solution of di-*tert*-butylperoxide containing small amounts of coniferyl alcohol. Laser irradiation of 10 % di-*tert*-butylperoxide in neat acetonitrile rapidly induces homolytic cleavage of the oxygen-oxygen bond, resulting in the formation of two *tert*-butoxyl radicals (Eq. 2.10a). This radical has little absorption in the 320-700 nm spectral region; therefore no spectral changes are observed after laser photolysis of di-*tert*-butylperoxide alone in acetonitrile. However, a new transient species at 340 nm grows-in after selective laser irradiation of di-*tert*-butylperoxide in acetonitrile containing coniferyl alcohol, Figure 2.7. The observed rate constants for the growth of the 340-nm band increase in a linear manner with increasing concentrations of coniferyl alcohol, Figure 2.7 (inset). This behavior is consistent with a hydrogen atom abstraction reaction in which the *tert*-butoxyl radical removes a hydrogen atom from the phenol hydroxy group of the coniferyl alcohol to give the corresponding phenoxyl radical, Eq. 2.10b. Linear least square

analysis from the relationship between the observed rate constant for the growth of the 340-nm band and the concentration of coniferyl alcohol gives a second-order rate constant for the hydrogen abstraction reaction of 1.7×10^8 $M^{-1}s^{-1}$. The magnitude of the second-order rate constant is consistent with the values reported for hydrogen atom abstraction reaction between *tert*-butoxyl radicals and phenolic groups.[75]

The 340-nm transient species shown in Figure 2.7 is identical to that produced by decay of coniferyl alcohol radical cation, Figure 2.4. Therefore these results provide good evidence that the 340-nm species observed after 308-nm laser irradiation of coniferyl alcohol in acetonitrile is the vinylphenoxyl radical formed by deprotonation of the coniferyl alcohol radical cation as illustrated in Eq 2.9 (R = CH_2OH).

(Eq. 2.10a)

(Eq. 2.10b)

(340 nm)
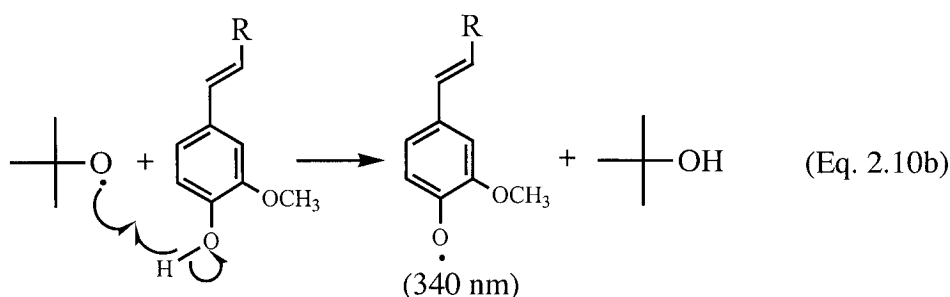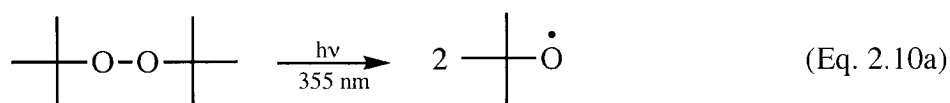
2.2.1.2 Isoeugenol.

Direct laser (308 nm) irradiation of isoeugenol in dry acetonitrile results in the formation of absorption bands centered at 380 and 580 nm, Figure 2.8. These bands decay with an identical rate constant of 9×10^5 s^{-1}, indicating that both bands are due to the same transient species. The decay of this transient is unaffected by the presence of oxygen, but it is rapidly accelerated in presence of anionic species like cyanide and

chloride. These observations as well as the similarity between the transient spectra in Figure 2.8 and the spectrum of the coniferyl alcohol radical cation strongly suggest that the transient with absorption bands at 380 and 580 nm shown in Figure 2.8 is the isoeugenol radical cation generated by photoionization of isoeugenol, Eq 2.7 (R = CH$_3$).

The same transient species is generated by electron transfer between isoeugenol and triplet chloranil initially generated by selective laser irradiation of chloranil at 355-nm, Figure 2.9. As expected from the large difference in oxidation potentials between triplet chloranil (E^{ox} = 2.7 V vs SCE)[1] and isoeugenol (E^{ox} = 1.3 V vs SCE)[73], the electron transfer reaction between these systems is a diffusion controlled process that takes place with a second order rate constant of 1.2 x 10^{10} M^{-1}s^{-1}, Figure 2.9 (inset). These results provides further evidence supporting the identification of the 380, 580-nm transient as the isoeugenol radical cation.

The transient absorption spectra measured upon 308-nm laser irradiation of isoeugenol in neat acetonitrile also shows a 340-nm absorption band, Figure 2.8. This band grows-in in a first-order manner with a rate constant of 9 x 10^5 s^{-1} that is identical to that observed for the decay of isoeugenol radical cation, indicating that the 340-nm transient is a product of the isoeugenol radical cation. The decay of the 340-nm band is not affected by the presence of oxygen or anionic species like chloride and acetate. These results together with the close similarity between the 340-nm band and the absorption maximum of the 2-methoxy-4-(3-hydroxy-1-propenyl)phenoxyl radical, lead to the identification of the 340-nm transient as the 2-methoxy-4-(1-propenyl)phenoxyl radical formed by deprotonation of isoeugenol radical cation, Eq. 2.9 (R = CH$_3$). Generation of the 340-nm transient by hydrogen atom transfer between the phenol

hydroxylic group of isoeugenol and *tert*-butoxyl radical further supports the identification of the 340-nm as the 2-methoxy-4-(1-propenyl)phenoxyl radical. Laser irradiation of di-*tert*-butyl peroxide in presence of isoeugenol results in the formation of a transient species with absorption maxima at 340 nm, Figure 2.10. The rate constant for the growth of this 340-nm band increases in a linear manner with increasing concentration of isoeugenol, Figure 2.10 (inset). Linear least-square analysis of the relationship between the observed rate constant for the growth of the 340-nm transient and the concentration of isoeugenol gives a slope of 2.0 x 10^8 $M^{-1}s^{-1}$, corresponding to the second-order rate constant for the reaction between isoeugenol and *tert*-butoxyl radical, Eq. 2.10b (R = CH_3). The value of the rate constant is in the same order of magnitude as those reported for hydrogen atom transfer reactions between *tert*-butoxyl radicals and phenolic hydroxyl groups.[75]

2.2.1.3 2-Methoxy-4-vinylphenol

Laser irradiation of 2-methoxy-4-vinylphenol, Eq. 2.4 (R=H), leads to the formation of a transient species with absorption maxima at 360 and 560 nm, Figure 2.11. Both absorption bands decay with the same rate constant of 2 x 10^6 s^{-1}, giving rise to a new transient with absorption maxima centered at 330 nm. The rate constant measured for the growth of the 330-nm band is identical (2 x 10^6 s^{-1}) to the rate constant observed for the decay of the absorption bands centered at 360 and 560 nm, indicating that the 330-nm transient is a product of the transient with absorption maxima at 360 and 560 nm. The decay of the 330-nm transient species is not affected by the presence of oxygen or anionic species. On the other hand, the decay of the species with absorption maxima at 360 and 560 nm is accelerated in presence of anions like chloride and bromide; however

the decay of these species is unaffected by the presence of oxygen. The same transients are generated by photoinduced electron transfer using chloranil as photosensitizer, Figure 2.12. These results are very similar to those observed for the coniferyl alcohol and isoeugenol radical cations, and lead to the identification at 360 and 560 nm as the radical cation of 2-methoxy-4-vinylphenol, Eq. 2.4 (R=H), and the transient at 330 nm as the 4-ethenyl-2-methoxyphenoxyl radical, Eq. 2.6 (R=H).

2.2.2 Reaction of Coniferyl Alcohol Radical Cation with Water and Alcohols in Acetonitrile

During the course of the investigation into the generation of the coniferyl alcohol and isoeugenol radical cations, a variation was repeatedly observed in the lifetime of these species as a function of the quality of the acetonitrile used. More precisely, when using acetonitrile from a freshly opened bottle, the radical cation was longer lived, while the lifetime was reduced in acetonitrile previously exposed to air. Since it has been clearly established that the radical cation was insensitive to oxygen, it was suspected that the change in water content on the solvent was the most probable origin of the variability in lifetimes described above. Therefore in order to explain the previous observations the influence of water content was assessed by measuring the decay of the radical cation in the presence of different amounts of water in acetonitrile. As shown in Figure 2.13 (a), the relationship between the observed rate constants for the decay of the coniferyl alcohol radical cation and water concentration is linear. Linear least square analysis of this data gives a second-order rate constant of 6.5×10^7 $M^{-1}s^{-1}$ for the reaction of water with coniferyl alcohol radical cation.

The decay of the coniferyl alcohol radical cation is also accelerated by the presence of methanol, ethanol, 2-propanol and *tert*-butyl alcohol. In each case, the rate constants observed for the decay of the radical cation increase in a linear manner with increasing concentrations of the alcohols, Figure 2.13. Linear least-squares analysis of these data provided the second-order rate constants for the reaction of the coniferyl alcohol radical cation with the alcohols, Table 2.3.[71]

Table 2.3 Second-order rate constants for the reaction of the coniferyl alcohol radical cation with water and alcohols in acetonitrile.

Hydroxylic Reagents	k_{obs} / M^{-1} s^{-1}
H_2O	$(6.5 \pm 0.5) \times 10^7$
MeOH	$(3.1 \pm 0.1) \times 10^7$
EtOH	$(2.0 \pm 0.1) \times 10^7$
iso-PrOH	$(4.7 \pm 0.2) \times 10^7$
tert-BuOH	$(4.9 \pm 0.2) \times 10^7$

As shown in Figure 2.14, in the presence of water the accelerated decay of the radical cation continues to lead to the formation of the 340-nm transient identified as the 2-methoxy-4-(3-hydroxy-1-propenyl) phenoxyl radical. As observed for the study in dry acetonitrile, the rate constant for the growth of the 340-nm band is identical to that observed for the decay of the radical cation. Similar findings were also obtained when alcohols were added instead of water, with the growth of the 340-nm band of the radical accelerating in the same manner as the decay of the radical cation as the alcohol content increased.

2.2.3 Reaction of Coniferyl Alcohol and Isoeugenol Radical Cations with Anionic Species in Acetonitrile

As stated earlier in Section 2.2.1, the bands corresponding to the radical cation species are rapidly quenched by anionic species. To quantify this effect, the reactivities of coniferyl alcohol and isoeugenol radical cations in presence of cyanide, chloride, nitrate and acetate were measured.[71] In all cases a linear relationship between the rate constant for the decay of the radical cation and the concentration of the anion was observed, Figures 2.15 and 2.16. The second order rate constants for the reaction were found to range between 1 and 2 x 10^{10} $M^{-1}s^{-1}$, Table 2.4, indicating that the reactions of these anionic species with the radical cations take place at or near the diffusion-controlled limit.

Table 2.4 Second-order rate constants for decay of the radical cations generated from coniferyl alcohol, isoeugenol and MeCA in presence of different anionic species.

nucleophile	Rate constants / M^{-1} s^{-1}		
	[coniferyl alcohol]$^{+\bullet}$	[isoeugenol]$^{+\bullet}$	[MeCA]$^{+\bullet}$
chloride	$(2.5 \pm 0.4) \times 10^{10}$	$(1.9 \pm 0.3) \times 10^{10}$	$(1.9 \pm 0.1) \times 10^{10}$
cyanide	$(2.0 \pm 0.2) \times 10^{10}$	$(1.4 \pm 0.2) \times 10^{10}$	$(2.0 \pm 0.1) \times 10^{10}$
acetate	$(1.9 \pm 0.2) \times 10^{10}$	$(1.0 \pm 0.1) \times 10^{10}$	$(1.4 \pm 0.1) \times 10^{10}$
nitrate	$(1.2 \pm 0.1) \times 10^{10}$	$(1.4 \pm 0.1) \times 10^{10}$	$< 1 \times 10^{6}$

Figure 2.17 shows the absorption spectrum obtained upon 308-nm laser irradiation of coniferyl alcohol in presence of chloride (0.1 mM) in acetonitrile. At this concentration of chloride, the bands corresponding to the radical cation, at 380 and 580 nm, are almost totally quenched within 240 ns after the laser pulse, and here again a band

at 340 nm grows-in as the radical cation features disappear, Figure 2.17 (inset). The absorption band at 340 nm, which is also insensitive to the presence of oxygen, is analogous to that of the 4-vinylphenoxyl radical generated by deprotonation of the coniferyl alcohol radical cation in dry acetonitrile or in presence of water or alcohols.

Similar spectra to those presented in Figure 2.16 were obtained upon laser irradiation at 308 nm of coniferyl alcohol or isoeugenol in acetonitrile solutions containing acetate or cyanide. In each case, a band a 340 nm, corresponding to the substituted 4-vinylphenoxyl radical, was observed to grow-in with a rate constant identical to that for the decay of the radical cation.

The reactions of the same anions (Cl^-, CH_3COO^-, CN^-, NO_3^-) with 3-(3,4-dimethoxyphenyl)-prop-2-en-1-ol [MeCA] radical cation, Eq. 2.11, were also studied in order to assess the role of the phenolic hydroxyl group of coniferyl alcohol and isoeugenol radical cations on the reaction of these species with anionic systems. The only difference between MeCA and coniferyl alcohol is the fact that MeCA does not have a labile acidic proton. Therefore, nucleophilic addition is anticipated as the main pathway in the reaction of the radical cation generated from MeCA with anionic species. The radical cation of MeCA was generated by 308-nm laser irradiation of 3-(3,4-dimethoxy-phenyl)-prop-2-en-1-ol in neat acetonitrile. As shown in Figure 2.18, the transient spectrum of MeCA radical cation consists of two absorption bands centered at 380 and 580 nm. Both of these bands decay with identical rate constant of 4.1×10^5 s^{-1}. In the presence of chloride, the radical cation of MeCA is rapidly quenched, Figure 2.19, leading to the formation of a new transient with absorption maxima around 300 nm. This transient is quenched by added oxygen and is consistent with the generation of a

phenethyl radical via nucleophilic addition of the chloride to the β-position of the radical

cation, Eq 2.11.

(Eq 2.11)
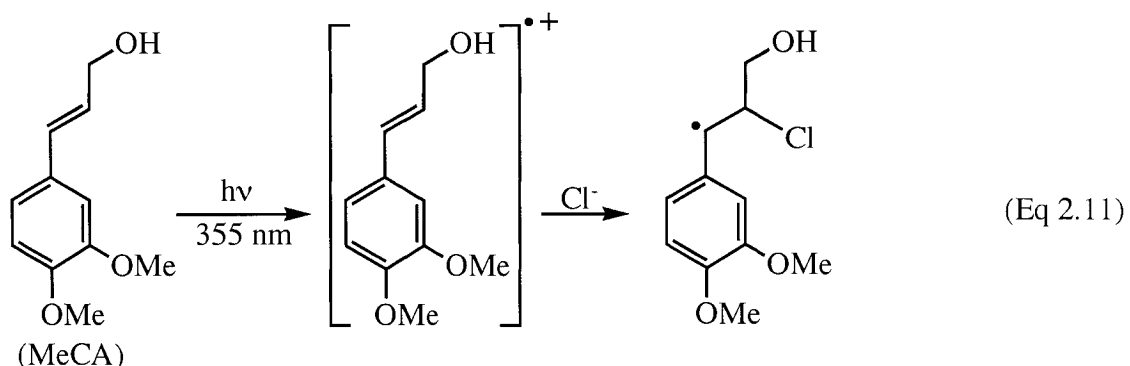
The second-order rate constants for the reaction of MeCA radical cation with

anionic species were obtained from the slopes of the plots of the observed rate constants

for the decay of this radical cation versus the concentration of the anionic species, Figure

2.20. The values of the second-order rate constants for the reaction with chloride,

cyanide and acetate, Table 2.4, range between 1.0 and 2.2 x 10^{10} M^{-1} s^{-1}, indicating that

the reaction of MeCA radical cation with these anions is a diffusion-controlled process.

In contrast, the reaction of the radical cation with nitrate is too slow to be measured with

the nanosecond laser system.

The influence of isotope effects on the reaction of isoeugenol radical cation with

anionic species was studied by comparing the reactivity of the radical cations of

isoeugenol and of isoeugenol having the phenolic hydroxyl group labeled with deuterium

(isoeugenol-OD) with chloride and acetate, Figure 2.21. The second-order rate constants

measured for the reaction of acetate with isoeugenol radical cation and isoeugenol-OD

radical cation were virtually identical, 1.1 x 10^{10} $M^{-1}s^{-1}$ and 1.0 x 10^{10} $M^{-1}s^{-1}$ respectively.

Similarly, the reaction of chloride with isoeugenol radical cation occurred with a second-

order rate constant of 1.3 x 10^{10} $M^{-1}s^{-1}$, almost identical to that measured for the reaction

59

with isoeugenol-OD radical cation, $k_{Cl} = 1.5 \times 10^{10}$ $M^{-1}s^{-1}$. Clearly no isotope effect is observed for these reactions.

2.2.4 Acidity of Isoeugenol Radical Cation in Acetonitrile

The time-resolved transient absorption spectra obtained upon 308-nm laser irradiation of isoeugenol in a solution of $HClO_4$ (0.7 mM) in acetonitrile are presented in Figure 2.22. The radical cation of isoeugenol is still observed. However, while the isoeugenol radical cation in neat acetonitrile completely decays within 6 μs after the laser pulse, Figure 2.8, the absorption bands attributed to this transient persist well beyond the last time scale window taken 6 μs after the laser pulse in acidic acetonitrile, Figure 2.22. Thus, the isoeugenol radical cation is considerably stabilized under acid conditions.

The influence of the concentration of perchloric acid on the decay of the radical cation is illustrated in Figure 2.23. At a concentration of perchloric acid of 0.01 mM, the band at 580 nm corresponding to the radical cation decays with a pseudo-first order rate constant of 1.4×10^6 s^{-1}. However when the concentration of perchloric acid is increased to 0.1 mM, the decay of the radical cation becomes a biphasic process with a fast component occurring with a rate constant of 10^6 s^{-1} and a much slower component which takes place with a rate constant of 2×10^4 s^{-1}. Further increases in the concentration of perchloric acid cause a continuous reduction of the extent of the fast component while the second slower process becomes more dominant. As shown in Figure 2.23-a the fast process is not visible anymore at concentration of $HClO_4$ of 0.7 mM. At this point, the radical cation decays in a single process with a first-order rate constant of around 2×10^4 s^{-1}.

These results imply that, at increasing concentration of acid, the isoeugenol radical cation is no longer completely converted to its conjugate base, the 4-vinylphenoxyl

radical. Instead, the radical cation first decays to an equilibrium state that consists of significant amounts of both species, the phenoxyl radical and the isoeugenol radical cation. The decay of the radical cation to the equilibrium state corresponds to the faster component in the biphasic process described above. The slow process is therefore attributed to the decay of the equilibrium state, which can either occur by reaction of the vinylphenoxyl radical or by reactions of the radical cation.

Figure 2.24 shows the variation of the fraction of radical cation present once the equilibrium state is established with the concentration of perchloric acid. This fraction is expressed as the ratio A_{eq}/A_o, where A_{eq} is the absorption of the radical cation at 580 nm after the equilibrium state is established and A_o is the absorption at 580 nm immediately after the laser pulse. Both, A_o and A_{eq} were obtained from the time-resolved absorption changes observed at 580 nm after laser irradiation of isoeugenol at different concentrations of added acid. The data corresponding to the time-resolved absorption changes at 580 nm were analyzed by fitting to two sequential first-order decays. The analysis of the data was carried out using Kaleidagraph software which provides the rate constants corresponding to the decay processes as well as the absorption values at which each process starts. Further details of the information provided by the Kaleidagraph program is given in Chapter 4. As observed in Figure 2.24, the ratio A_{eq}/A_o is small at low concentrations of acid, which is attributed to the fact that almost all the radical cation is deprotonated to the phenoxyl radical. That is, under these conditions the equilibrium is shifted toward the formation of phenoxyl radical, which is the dominant species in the system. However, the equilibrium is shifted toward the radical cation site as the concentration of acid is increased, resulting in an increase of the ratio of absorptions

61

(A_{eq}/A_o). This ratio reaches a maximum and almost constant value close to one at acid concentrations higher than 0.6 mM.

Mathematically, the ratio of absorptions will change with the concentration of acid according to Eq. 2.12.

$$\frac{A_{eq}}{A_o} = \frac{[H^+]}{[H^+] + K_a}$$

(Eq 2.12)

This equation was deduced assuming that (i) all the phenoxyl radical present in the system is produced only by deprotonation of the radical cation, and (ii) the contribution of protons due to the deprotonation of the radical cation is negligible compared with the amount of protons provided by the perchloric acid (refer to Appendix A). Fitting the data represented in Figure 2.24 to Eq. 2.12 leads to a value for the acid constant of the radical cation equal to $(1.2 \pm 0.2) \times 10^{-4}$ M. Therefore, the pK_a of the isoeugenol radical cation in acetonitrile is 3.9 ± 0.1.[71]

Due to rapid decomposition of coniferyl alcohol in acid acetonitrile, it was not possible to determine the pK_a of coniferyl alcohol as described above. Apparently, coniferyl alcohol undergoes acid-catalyzed elimination of the β-hydroxy group to yield 4-allylidene-2-methoxy-cyclohexa-2,5-dienone, Eq. 2.13, and subsequent products of this intermediate. Attempts to determine the acid dissociation constant of the 2-methoxy-4-vinylphenol radical cation as described above also failed. As shown in Figure 2.25, the lifetime of this radical cation did increase as a function of added acid. For instance, while the 2-methoxy-4-vinylphenol radical cation decays in acidic ($[HClO_4] = 1 \times 10^{-5}$ M) acetonitrile with a first-order rate constant of 2.0×10^6 s^{-1}, the decay of this species in acetonitrile containing 2.0 mM $HClO_4$ takes place with a first-order rate constant of 9.8×10^4 s^{-1}. However, the absorption changes associated with the decay of this radical cation

were too small to determine the required absorption values as a function of acid content, and attempts to quantitatively measure the pK_a of the 2-methoxy-4-vinylphenol radical cation were abandoned.

(Eq. 2.13)
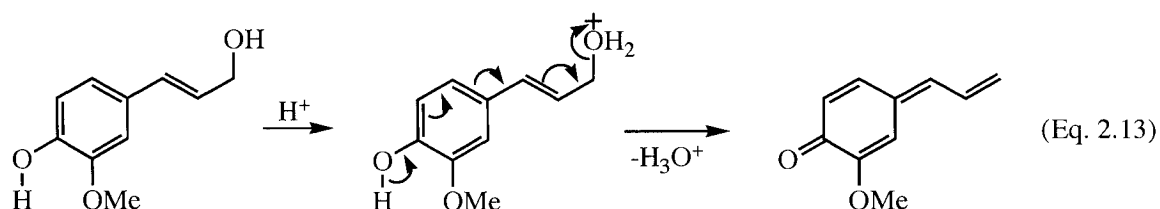
2.2.5 Generation of Isoeugenol Radical Cation by Protonation of 2-Methoxy-4-(1-propenyl)-phenoxyl Radical

As previously described, 2-methoxy-4-(1-propenyl)-phenoxyl radical is generated by hydrogen atom transfer from isoeugenol to tert-butoxyl radical initially formed by 355-nm laser irradiation of 10 % di-tert-butylperoxide, Figure 2.10. The formation of the radical species is readily observed by the growth of the 340-nm transient species, which takes place with a rate constant of 1.2×10^6 s^{-1} in neat acetonitrile containing 6.0 mM isoeugenol.

Laser (355 nm) irradiation of 10 % di-tert-butylperoxide in slightly acidic (1.0 mM $HClO_4$) acetonitrile containing 6.0 mM of isoeugenol also results in the formation of 2-methoxy-4-(1-propenyl)-phenoxyl radical, Figure 2.26a. However, under these conditions two new bands centered at 380 and 580 nm are observed in addition to the 340-nm band corresponding to the phenoxyl radical.[76] The growth of the 340-nm absorption band takes place with a rate constant of 1.2×10^6 s^{-1}, which is identical to that observed for the growth of this species under the same condition, except with no added acid. On the other hand, the 380 and 580-nm bands grow-in more slowly, with a rate

constant of 2.1×10^5 s^{-1}, that is almost six times slower than the growth of the radical. The location and relative intensities of these two bands are very similar to those observed for isoeugenol radical cation generated by photoionization, Figure 2.8, or by photoinduced electron transfer, Figure 2.9. Therefore, the transient responsible for the 380 and 580-nm bands can be identified as the isoeugenol radical cation.

As shown in Figure 2.26-b, increasing the concentration of acid to 10 mM results in an increase of the intensities of the absorption bands at 380 and 580 nm due to the isoeugenol radical cation while the absorption band due to the phenoxyl radical is considerably reduced. The effect of increasing acid concentration is better illustrated in Figure 2.27, which shows the time-resolved absorption changes at 380 and 580 nm at several different acid concentrations. Clearly, the higher the concentration of acid, the higher the yield of isoeugenol radical cation. Additionally, the formation of the radical cation is accelerated with increasing concentration of acid. Figure 2.28 shows the relationship between the rate constant observed for the growth of isoeugenol radical cation and the concentration of perchloric acid. The rate constants increase in a linear manner with the acid content in the range of concentrations between 0 and 6.0 mM. Linear least-squares analysis gives a slope of 2.2×10^8 M^{-1}s^{-1} and an intercept of 1.5×10^5 s^{-1}. At higher acid concentrations, the rate constant for the growth of the isoeugenol radical cation levels off and remains constant at 1.4×10^6 s^{-1}. This rate constant is closely similar to the rate constant ($k_{obs} = 1.2 \times 10^6$ s^{-1}) measured for hydrogen atom transfer from isoeugenol to $tert$-butoxyl radical at the 6.0 mM isoeugenol concentration used in these experiments. Therefore, at acid concentrations higher than 6.0 mM the protonation reaction becomes faster than the initial hydrogen atom transfer step. Consequently, the

generation of the phenoxyl radical becomes the rate limiting step and further increases in acid concentration do not accelerate the growth of the radical cation.

The generation of coniferyl alcohol radical cation by protonation of 2-methoxy-4-(3-hydroxy-1-propenyl) phenoxyl radical was also attempted, however coniferyl alcohol rapidly decomposed in acidic acetonitrile. As previously mentioned, coniferyl alcohol apparently undergoes acid-catalyzed elimination of the β-hydroxy group to yield 4-allylidene-2-methoxy-cyclohexa-2,5-dienone, Eq. 2.13. Irradiation of *tert*-butyl peroxide in presence of 2-methoxy-4-vinylphenol under acidic conditions also failed to produce detectable amounts of the 2-methoxy-4-vinylphenol radical cation. Possible reasons for this are outlined below.

2.2.6 Reactivity of 4-Vinylphenol Radical Cations toward Substituted Styrenes

2.2.6.1 Reactivity Toward Neutral Precursors

As mentioned in the introduction, one goal of the present work was to determine if the radical cations of the 4-vinylphenol derivatives can undergo reactions with their neutral precursors. To examine this reaction kinetically, the decay of the 4-vinylphenol radical cations was measured as a function of the concentration of the precursors to the radical cations. The radical cations were generated by photoinduced electron transfer using chloranil as the sensitizer. Photoinduced electron transfer was used instead of photoionization because it allows the use of larger concentrations of the precursors.

The 2-methoxy-4-vinylphenol radical cation generated by photo-induced electron transfer decays in a first-order manner at all concentrations of 2-methoxy-4-vinylphenol

used. As shown in Figure 2.29, the observed rate constants for the decay of this radical

cation increase in a linear manner as the concentration of 2-methoxy-4-vinylphenol is

increased from 0.5 mM to 20 mM, indicating the presence of a reaction between the

radical cation and its precursor. Linear least squares analysis of the relationship between

observed first-order rate constants and the concentration of the 2-methoxy-4-vinylphenol

over the concentration range of 0.5 mM to 20 mM gives a second-order rate constant of

5.6×10^8 M^{-1} s^{-1}.[76] Attempts were made to obtain data at higher concentrations of 2-

methoxy-4-vinylphenol. However, at these higher concentrations, the solution became

more and more deeply purple colored, and it was not possible to obtain accurate kinetic

data.

Quenching of the radical cation of 2-methoxy-4-vinylphenol using a simple phenol,

4-isopropylphenol, was also examined to determine the importance of a possible reaction

between the radical cation and a phenolic hydroxyl group. No measurable quenching was

observed, even at concentrations as high as 0.05 M 4-isopropylphenol. Given that the 2-

methoxy-4-vinylphenol radical cation decays with a rate constant of 2×10^6 s^{-1} in neat

acetonitrile, the lack of observable quenching at 0.05 M of 4-isopropylphenol indicates

that the potential reactivity of the phenol towards the 2-methoxy-4-vinylphenol radical

cation must be less than 2×10^7 M^{-1} s^{-1}, which is one order of magnitude smaller than the

rate constant measured for the reaction of the same radical cation with 2-methoxy-4-

vinylphenol.

The reactivity of 3,4-dimethoxystyrene radical cation towards its neutral parent was

also studied in order to gain more information regarding the reaction of 2-methoxy-4-

vinylphenol radical cation with its precursor. The radical cation of 3,4-dimethoxystyrene

was generated by direct photoionization, Figure 2.30, and by photoinduced electron transfer using chloranil, Figure 2.31. As observed in these figures, the transient absorption spectrum of the 3,4-dimethoxystyrene radical cation is very similar to that of 2-methoxy-4-vinylphenol radical cation, consisting of absorption bands centered at 360 and 560 nm. Figure 2.32 shows the rate constant observed for the decay of 3,4-dimethoxystyrene radical cation at concentrations of 3,4-dimethoxystyrene ranging from 0.001 to 0.015 M. Note there is a very small increase in the rate constant at concentrations of the precursor smaller than 1.0 mM. However no change in the rate constant is observed at concentrations of 3,4-dimethoxystyrene higher than 2.0 mM.

Figure 2.33 shows the relationship between the observed rate constant for the decay of coniferyl alcohol and isoeugenol radical cations, generated by photoinduced electron transfer with chloranil, and the concentration of the precursors in acetonitrile. The rate constants for the decay of coniferyl alcohol radical cation slightly increase at very low concentrations ranging from 0.1 to 1.0 mM, Figura 2.33-a. However, at higher concentrations the rate constants for the decay of coniferyl alcohol radical cation remain unchanged at $ca.$ 1.6×10^6 s^{-1}. Similarly, the decay of isoeugenol radical cation is slightly accelerated when the concentration of isoeugenol increases from 0.1 up to 2.0 mM. However no further acceleration is observed at concentrations of isoeugenol higher than 2.0 mM, Figure 2.33-b.

2.2.6.2 Product Study

In an attempt to isolate and characterize the products of a potential reaction of isoeugenol radical cation with its neutral parent, a solution of chloranil (1.0 mM) in N_2-saturated acetonitrile containing 0.01 M of isoeugenol was irradiated at 360 nm for six

hours. Since the absorption of isoeugenol at 360 nm is very small compared to the absorption of chloranil at this wavelength, the concentrations used in this experiment guarantee that chloranil absorbs most of the light. Once the sample was irradiated for six hours, the solvent was removed under reduced pressure and the sample was subjected to GC-MS analysis. The gas chromatogram showed the presence of isoeugenol, which was not completely consumed after six hours of irradiation, and a product identified as dehydrodiisoeugenol, Scheme 2.22. The formation of this product has been previously reported,[77, 78] and likely involves the coupling of two 2-methoxy-4-(1-propenyl)-phenoxyl radicals. Presumably, the absence of products directly formed from the reaction of isoeugenol radical cation with its precursor is a consequence of the rapid deprotonation of these species to yield the corresponding phenoxyl radical.

Scheme 2.22

(dehydrodiisoeugenol)
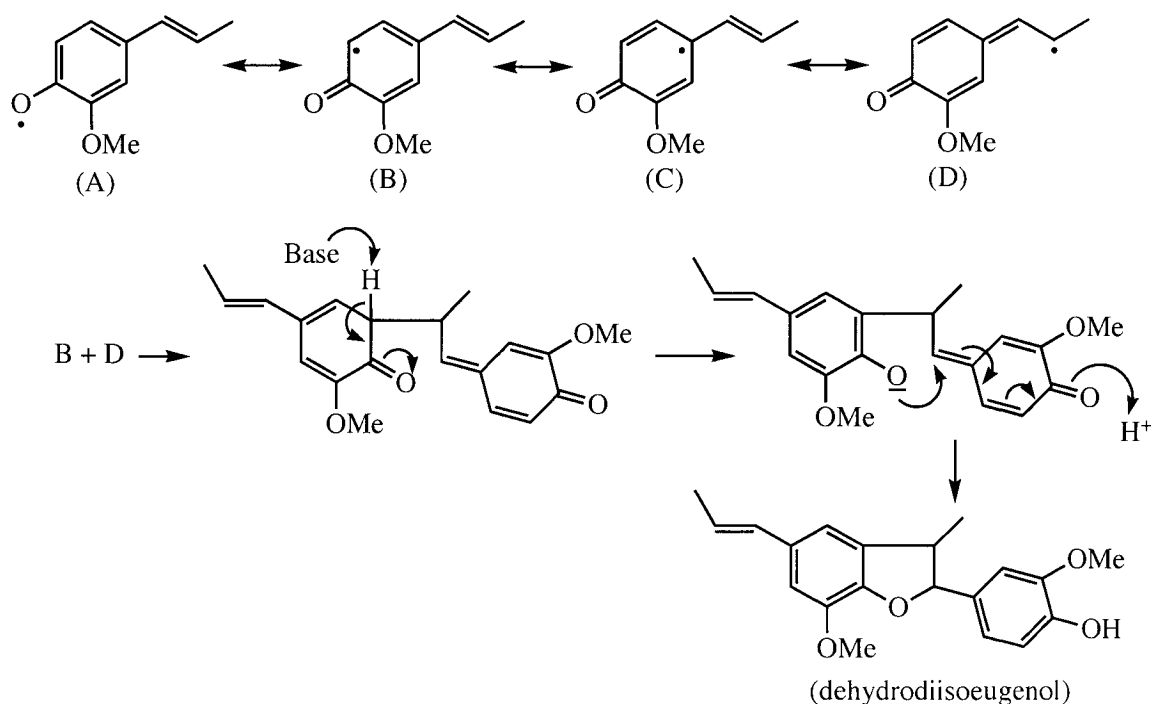
Given that the chloranil radical anion can act as a base to accelerate the deprotonation of the radical cation, the same experiment was repeated using triphenyl pyrilium cation as photosensitizer instead of chloranil. This sensitizer is converted to triphenylpyrilyl radical, which will not act as a base to deprotonate the isoeugenol radical cation. However, in this case as well the only identifiable product was dehydrodiisoeugenol.

Chemical oxidation of isoeugenol using tris(4-bromophenyl)aminium hexachloroantimonate salt was also attempted. However most of the isoeugenol was transformed into diisoeugenol, Scheme 2.23. The same compound is obtained by simply stirring isoeugenol in perchloric or sulfuric acid (1.8 M in acetonitrile) for two hours, which suggests the involvement of carbocationic mechanism in the formation of diisoeugenol. That is, isoeugenol is protonated to generate a carbocation that then reacts with a molecule of isoeugenol to produce a dimer that rearranges to diisoeugenol, Scheme 2.23. Deprotonation of the initially formed isoeugenol radical cation most likely provides the protons involved in the generation of the carbocations. It is worth mentioning there are previous reports involving BrØnsted acid catalyzed dimerizations of arylalkenes in presence of triarylaminium hexachloroantimonate salts.[6, 79] Presumably, $HSbCl_6$ is responsible for the acid catalysis although there is not conclusive proof concerning the nature of the strong acid generated under aminium salt conditions.[4]

Scheme 2.23

(diisoeugenol)
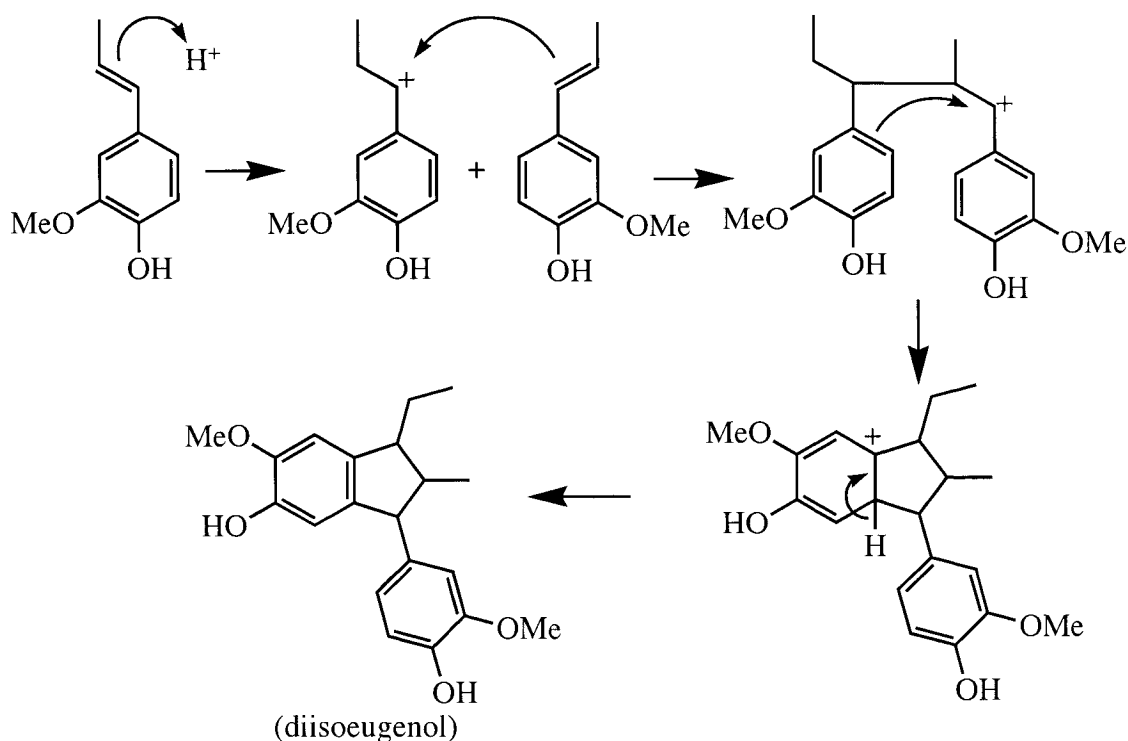
Product studies with 2-methoxy-4-vinylphenol were also carried out using triphenyl pyrilium cation as the photosensitizer or tris(4-bromophenyl)aminium hexachloroantimonate as a chemical oxidant. The photosensitization experiment was carried out by irradiating ($\lambda \geq$ 360 nm) a solution containing 0.01 M 2-methoxy-4-vinylphenol and 0.001 M of triphenyl pyrilium cation. After six hours of irradiation, the resulting solution was analyzed using GC-MS. The gas chromatogram indicated the presence of five new compounds in addition to 2-methoxy-4-vinylphenol which was not completely consumed. According to the chromatogram approximately only two percent of the 2-methoxy-4-vinylphenol had been transformed into products. The mass spectra of the new compounds did not provide enough information to identify these species. Attempts to isolate these compounds by column chromatography were unsuccessful, making impossible the identification of these compounds by NMR spectroscopy.

Chemical oxidation was performed by reaction of 0.15 M 2-methoxy-4-vinyphenol with 0.015 M (4-bromophenyl)aminium hexachloroantimonate. The oxidation was carried out in dichloromethane and, in another experiment, in acetonitrile. In both solvents the reaction time was 21 hours. GC-MS analysis of the resulting material showed the formation of the same compounds observed in the photosensitization experiment. However in this case most of the 2-methoxy-4-vinylphenol was consumed, and the recovered amount of this compound only represented two percent of the total amount of recovered material. The major product formed during chemical oxidation showed an ion at m/z 265 in the GC-MS. According to the gas chromatogram, this product accounts for 94 % of the total mass of material detected. The product was subjected to column chromatographic purification and analyzed by NMR spectroscopy; however the NMR spectra did not provide any useful information to identify this product. It must be mentioned that even when the GC-MS spectrum indicates that the product is 94 % pure the product may contain a large amount of impurities that do not go through the column of the GC instrument and therefore are not detected. According to the NMR spectrum, the material was not pure and showed very wide peaks, probably due to the presence of (4-bromophenyl)aminium salt which is paramagnetic and may cause such broadening of the NMR signals.

2.2.6.3 Reactivity toward other Styrenes

The decay of the 4-vinylphenol radical cations was also measured as a function of the concentration of styrene, 4-methylstyrene and α-methylstyrene.[76] In this case, the radical cations were generated by photoionization using 308-nm laser excitation. This method is useful for these experiments since the substituted styrenes investigated have no

detectable absorption at this wavelength. Thus even at relatively high concentrations of the styrenes (~0.01 M), irradiation with 308-nm laser light selectively excites the 4-vinylphenol derivative.

Figure 2.34-a shows the changes of the observed rate constants for the decay of the 2-methoxy-4-vinylphenol radical cation in acetonitrile as a function of the concentration of 4-methylstyrene. As can be seen, the rate constants increase considerably from 1.6×10^6 s^{-1} to 3.9×10^6 s^{-1} when the concentration of the styrene is increased from 0 to 0.01 M. Linear least squares analysis gives a second-order rate constant of $(2.5 \pm 0.2) \times 10^8$ M^{-1} s^{-1} for the quenching of the radical cation with 4-methylstyrene. α-Methylstyrene and styrene also accelerated the decay of the 2-methoxy-4-vinylphenol radical cation, Figures 2.34-b and 2.34-c. The relationships between the observed rate constants for the decay of the radical cation and concentrations of the substituted styrenes were linear. Linear least-squares analysis of the data give slopes of $(1.4 \pm 0.2) \times 10^8$ M^{-1} s^{-1} for quenching by styrene, and $(1.0 \pm 0.1) \times 10^8$ M^{-1} s^{-1} for quenching by α-methylstyrene.

In acidic acetonitrile the decay of 2-methoxy-4-vinylphenol radical cation is also influenced by the presence of 4-methylstyrene, Figure 2.35. However the magnitude of the quenching is substantially smaller than in non-acidic conditions. Indeed, the second-order rate constant measured for the reaction of the radical cation with 4-methylstyrene in acetonitrile containing 1.0 mM HClO$_4$ is $(8.1 \pm 0.9) \times 10^6$ M^{-1} s^{-1}.

The influence of the concentration of 4-methylstyrene on the decay of 3,4-dimethoxystyrene radical cation was also studied by measuring the changes in the observed rate constants for the decay of this species at concentrations of 4-methylstyrene ranging from 0 to 0.01 M. As shown in Figure 2.35, the rate constant for the decay of the

3,4-dimethoxystyrene radical cation is unaffected by the presence of 4-methylstyrene over this range of concentrations.

Similar experiments were carried out using coniferyl alcohol and isoeugenol radical cations. However, both of these species showed no increase in decay rate constant with an increase in the concentration of any of the three styrenes, Figure 2.37. This result is consistent with the lack of observable quenching for the decay of these transients at increasing concentrations of their neutral precursors.

2.3 Discussion

2.3.1 Generation of 4-Vinylphenol Radical Cations

Transient species observed by direct laser irradiation of 4-vinylphenol derivatives have been identified as the corresponding 4-vinylphenol radical cations generated by photoionization of the neutral precursors, Eq. 2.7. The transient spectra of all the three 4-vinylphenol radical cations consist of two absorption bands centered at 360-380 nm and 560-580 nm. This is consistent with the transient spectra reported for other substituted styrenes radical cations which are characterized by a strong absorption band in the UV region (360-380 nm) and a second weaker absorption band in the region between 560 and 600 nm.[23, 24, 26, 32, 33] Further support for the identification of the 4-vinylphenol radical cations as the transients generated upon direct irradiation of neutral 4-vinylphenol derivatives was provided by generating the same transient species by photoinduced electron transfer using chloranil as photosensitizer. The second-order rate constants (1 x 10^{10} M^{-1} s^{-1}) obtained for the reaction of chloranil triplet with 4-vinylphenol derivatives are consistent with diffusion-controlled electron transfer reactions between these species.

The reactivity of the transient species generated upon 308-nm laser irradiation of 4-vinylphenol derivatives towards hydroxylic and anionic species also agrees with the identification of these transients as the corresponding radical cations.

The decay of the 4-vinylphenol radical cations results in the formation of a 340-nm transient, with the decays and growths taking place with identical first order rate constants. The same 340-nm transient was generated by hydrogen atom transfer between 4-vinylphenol derivatives and $tert$-butoxyl radical. The magnitude of the second-order rate constants ($k_H \sim 1 \times 10^8$ M^{-1} s^{-1}) measured for the reaction between the $tert$-butoxyl radical and the substituted 4-vinylphenols are consistent with second-order rate constants reported for hydrogen atom transfer from substituted phenols to $tert$-butoxyl radicals. For instance, the second-order rate constants for the reaction between $tert$-butoxyl radical and 4-halogen substituted phenols in benzene ranges between 2.4 x 10^8 and 3.8 x 10^8 M^{-1} s^{-1}.[75] Furthermore, the location of the absorption maximum (340 nm) is similar to those reported for other phenoxyl radicals.[74] All of these observations support the identification of the 340-nm transient as the 4-vinylphenoxyl radical generated by loss of a proton from the 4-vinylphenol radical cation. The deprotonation of 4-vinylphenol radical cations to give the corresponding 4-vinylphenoxyl radicals is a reversible process. As shown in experiments involving the generation of isoeugenol radical cation in acidic acetonitrile, the lifetime of this species is strongly influenced by the concentration of added acid. Increasing acid concentration shifts the equilibrium between the radical cation and its conjugate base to the side of the radical cation, increasing the lifetime of the latter species.

As mentioned in the introduction (Section 2.1.3), long-lived species assigned as 4-allylidene-2-methoxy-cyclohexa-2,5-dienone with absorption maximum at 350 nm had previously been observed upon irradiation of coniferyl alcohol. However, identification of the 340-nm transient observed upon 308-nm laser irradiation of coniferyl alcohol, Figure 2.4, as 4-allylidene-2-methoxy-cyclohexa-2,5-dienone is ruled out on the basis of the huge difference in reactivities between the 340-nm transient and the 4-allylidene-2-methoxy-cyclohexa-2,5-dienone. In particular, the lifetime of 4-allylidene-2-methoxy-cyclohexa-2,5-dienone in aqueous solution at room temperature is several minutes,[80] while the absorption band at 340 nm decays completely within 1 ms after the laser pulse, which is in accordance with the reactivity of other phenoxyl radicals.[80]

2.3.1.1 Reactivity of 4-Vinylphenol Radical Cations with Hydroxylic and Anionic Species

One possible pathway for the reaction between the coniferyl alcohol radical cation and water or alcohols is the nucleophilic addition of these reagents to the radical cation. The addition usually occurs at the β position of radical cations, generating phenethyl radicals that are readily observed by their characteristic absorption bands between 300 and 350 nm and by the fact that they are rapidly quenched in the presence of oxygen. In the present work, no spectroscopic evidence was found indicating the generation of a phenethyl radical. Instead, the only observable product resulting from the decay of the coniferyl alcohol radical cation in the presence of hydroxylic species is the 2-methoxy-4-(3-hydroxy-1-propenyl)phenoxyl radical. Therefore, water and alcohols appear to behave as bases rather than nucleophiles in their reaction with the radical cation, Eq. 2.14.

$$[\text{coniferyl alcohol radical cation}]^{\bullet +} + ROH \longrightarrow [\text{coniferyl phenoxyl radical}] + R\overset{+}{O}H_2 \qquad \text{(Eq. 2.14)}$$
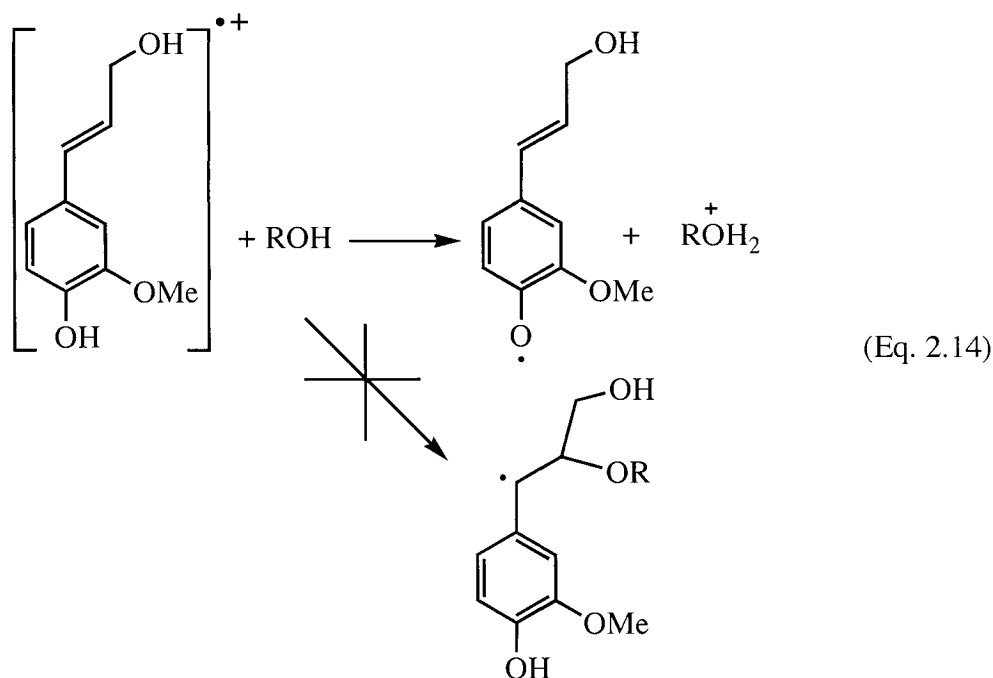
Additional evidence indicating that the alcohols act as bases rather than nucleophiles is the absence of any significant variation in the second-order rate constants for the reaction of coniferyl radical cation with the four alcohols, Table 2.3. If the alcohols reacted as nucleophiles the second-order rate constants for their reaction with coniferyl alcohol radical cation would be expected to decrease as the steric bulk increased. However, such a correlation was not observed, with the rate constant for the reaction with methanol, $k_{MeOH} = 3.1 \times 10^7$ M^{-1} s^{-1}, being slightly smaller than the rate constant for the reaction with $tert$-butanol, $k_{tert\text{-}BuOH} = 4.9 \times 10^7$ M^{-1} s^{-1}. Since the alcohols have similar basicities it is reasonable to expect closely similar second-order rate constants for the deprotonation of coniferyl alcohol radical cation by the alcohols.

Moreover, the second-order rate constants measured for the reaction of coniferyl alcohol radical cation with the alcohols are considerably larger than those reported for the nucleophilic addition of alcohols to substituted styrene radical cations. For example, the addition of methanol to the 4-methoxystyrene radical cation takes place with a rate

constant of 3 x 10^4 $M^{-1}s^{-1}$,[23] that is nearly three orders of magnitude smaller than the second-order rate constants shown in Table 3.1. The rate constant for the nucleophilic addition of methanol to coniferyl alcohol radical cation should be similar to that observed for the addition to the 4-methoxystyrene radical cation, or even slower since the presence of alkyl groups at the β-position slows down the nucleophilic addition.[23] Thus, the presence of a rapid deprotonation reaction appears to be the reason for the much greater measured rate constants compared to those previously reported for nucleophilic addition of alcohols to substituted styrene radical cations.

The rate constants for deprotonation of the coniferyl alcohol radical cation are slighter lower but of the same order of magnitude than the rate constants reported for the deprotonation of methoxy substituted phenols in acetonitrile. For instance, deprotonation of 3,5-dimethoxyphenol radical cation by water and methanol in acetonitrile occur with rate constants of 25 x 10^7 $M^{-1}s^{-1}$ and 8.2 x 10^7 $M^{-1}s^{-1}$,[74] respectively.

As in the reaction of alcohols with coniferyl alcohol radical cation, quenching of coniferyl alcohol and isoeugenol radical cations with anionic nucleophiles also led to the formation of the corresponding 4-vinylphenoxyl radicals. No spectroscopic evidence was found indicating the formation of phenethyl radicals that would be generated by nucleophilic addition of the anions to the β-position of isoeugenol or coniferyl alcohol radical cations. Therefore, even with strong nucleophiles like acetate, cyanide and chloride that normally undergo very fast nucleophilic addition to substituted styrene radical cations,[23, 33] deprotonation appears to be the dominant reaction pathway in the case of the coniferyl alcohol and isoeugenol radical cations due to the presence of their acidic proton, Eq 2.15.

(Eq. 2.15)
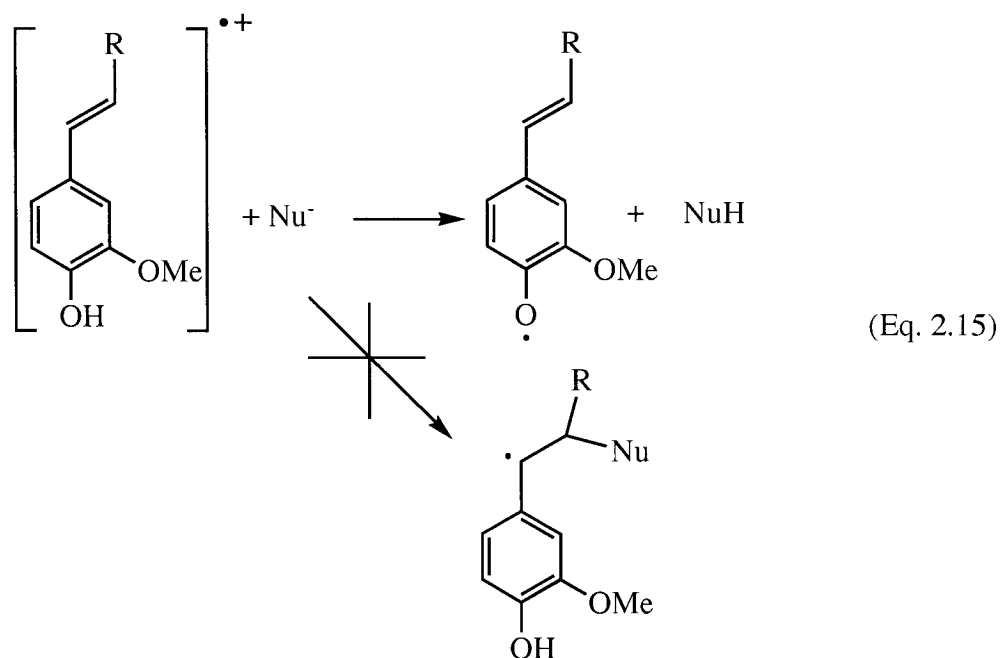
Results from laser experiments involving the quenching of the 3-(3,4-dimethoxy-phenyl)-prop-2-en-1-ol [MeCA] radical cation by acetate, cyanide and chloride show quite clearly that nucleophilic addition is a very rapid process. The decay of this radical cation, which only differs from the radical cation of coniferyl alcohol by the absence of a labile proton, in the presence of chloride, cyanide and acetate led to the formation of a new transient with absorption maximum below 300 nm, which is consistent with the generation of a phenethyl radical via nucleophilic addition of the chloride to the β-position of the radical cation, Eq 2.11. The second-order rate constants measured for the reaction of the radical cation of MeCA with chloride, cyanide and acetate range from 1.0 to 2.2×10^{10} $M^{-1}s^{-1}$ which are consistent with a diffusion-controlled nucleophilic addition to the radical cation.

The reactions of coniferyl alcohol and isoeugenol radical cations with the nitrate anion provide more information concerning the role of anionic species towards 4-vinylphenol radical cations. Nitrate is a poorer nucleophile than chloride, cyanide or

78

acetate. For instance the Swain-Scott nucleophilicity constants of these anions increase in the order: NO_3^- (1.0) < Cl^- (2.7) = CH_3COO^- (2.7) < CN^- (5.1).[81] Therefore the reaction of coniferyl alcohol and isoeugenol radical cation with nitrate may be slower than the reaction with chloride, acetate or cyanide if these anions react as nucleophiles. Indeed, the reaction of nitrate with 3-(3,4-dimethoxyphenyl)prop-2-en-1-ol (MeCA) radical cation in acetonitrile is much slower, taking place with a second-order rate constant less than 10^6 M^{-1} s^{-1}. On the other hand, the second-order rate constants measured for the reaction of the coniferyl alcohol and isoeugenol radical cations with nitrate are diffusion-controlled with values of 1.2 and 1.4 x 10^{10} M^{-1} s^{-1}. Given the absence of a labile hydrogen in the radical cation of MeCA, nitrate can only behave as a nucleophile. This substantial increase in second-order rate constants observed upon substitution of the 4-methoxy group with a OH group strongly suggests that the anionic nitrate behaves as a base rather than a nucleophile towards 4-vinylphenol radical cations, consistent with the conclusion that the other nucleophiles also act as bases towards the acidic radical cations. The basic character of acetate and cyanide is not surprising, given that the acetic acid (pK_a = 4.76) and HCN (pK_a = 9.21) are not strong acids.[81] In contrast, both nitrate and chloride have very strong conjugate acid forms, with pK_a = -7 for HCl and pK_a = -1.64 for HNO_3.[81] However the acidity is markedly affected by the nature of the solvent. For instance, Kolthoff et $al.$[82] have reported that the acid-base equilibrium constants for hydrochloric acid and nitric acid in acetonitrile are both near K_a = 10^{-9} (pK_a = 8.9), which are many orders of magnitude larger than the corresponding dissociation constants in water. Such a large reduction in acidity with the nature of the solvent might be the reason for the behavior of chloride and nitrate as a base in acetonitrile, especially

towards very acidic species like 4-vinylphenol radical cation. In fact, as described later, the pK_a of the radical cation of isoeugenol in acetonitrile is 3.9, which indicates that it is more acidic than the HCl or HNO_3, and further confirms that chloride and nitrate should be effective bases towards the isoeugenol radical cation.

Results from experiments using isoeugenol and isoeugenol-OD did not provide desired evidence for deprotonation as being the main reaction between the 4-vinylphenol radical cations and anionic species, with the second-order rate constants measured for the reaction of acetate and chloride with isoeugenol radical cation remaining unaffected by replacement of the phenolic proton with a deuterium. While this result does not add support for the deprotonation, it does not rule out the possibility that deprotonation is taking place. In particular, diffusion-controlled reactions have such small activation energies that they are frequently unaffected by the change of hydrogen for deuterium. In other words, the Hammond postulate states that the smaller the activation energy the smaller the difference between the transition state and the reactants. So, if the O-H bond strength is similar in the reactants and in the transition state, then the difference in zero-point energies for the reactant and transition state structures will be the same for the ^{1}H and deuterium substituted species, Scheme 2.24. Consequently, change of hydrogen for deuterium will not affect the rate of the deprotonation reaction and no isotope effect will be observed.

Scheme 2.24

$\Delta E^*_o(H) < \Delta E^*_o(D)$ then $k_H/k_D > 1$ $\Delta E^*_o(H) \approx \Delta E^*_o(D)$ then $k_H/k_D \approx 1$
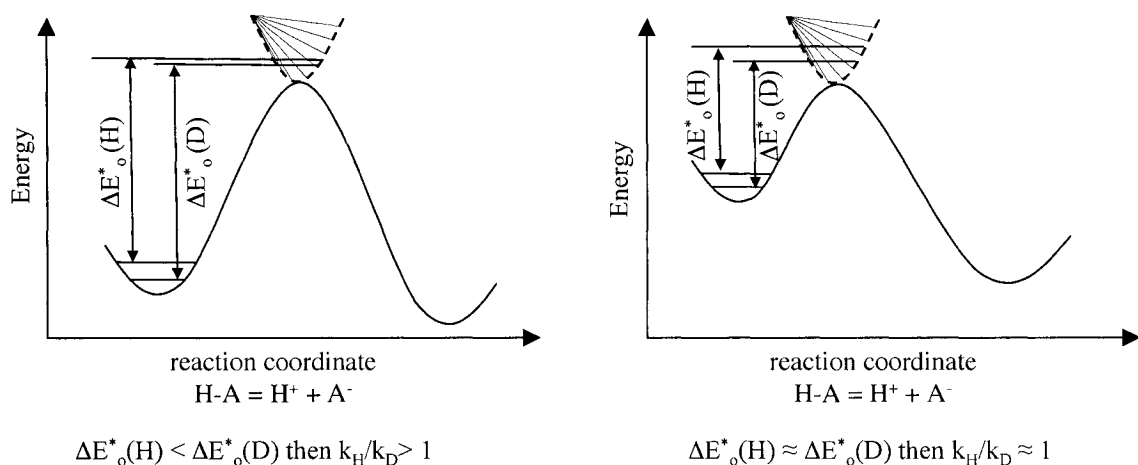
According to Nerbonne et al.,[83] proton transfer between acids and bases is divided into three kinetic steps: (i) the encounter of the reactants, (ii) proton transfer, and (iii) separation of the products, Eq. 2.16.

$$B \;+\; HA \;\xrightleftharpoons{\text{encounter}}\; B\cdot HA \;\xrightleftharpoons{\text{H}^+\ \text{transfer}}\; BH\cdot A \;\xrightleftharpoons{\text{separation}}\; BH \;+\; A \qquad \text{(Eq. 2.16)}$$

The encounter is the rate-determining step when the difference in pK_a between the proton donor and the acceptor is much smaller than zero, i.e. $\Delta pK_a = pK_a(\text{donor})-pK_a(\text{acceptor}) \ll 0$. In this case, the proton transfer is much faster than the rate of diffusion of the two reactants. Consequently, no kinetic isotope effect is observed in this type of situation. Clearly, the reaction of isoeugenol radical cation with anionic species fits well into this case in acetonitrile. That is, the pK_a of the isoeugenol radical cation in acetonitrile is around 4.0 while that of HCl is ca. 9.0, hence $\Delta pK_a \sim -5$. Therefore, according to Nerbonne[83] the rate limiting step should be the diffusion together of chloride and the radical cation and no isotope effect should be observed. Indeed, the reaction between both species is a diffusion-controlled process and no significant isotope effect was detected.

81

The possibility of generation of 4-vinylphenoxyl radical as secondary product via hydrogen abstraction from neutral 4-vinylphenol substrates by phenethyl radicals formed upon nucleophilic addition of the anions to the radical cations was also carefully considered, Scheme 2.25.

Scheme 2.25
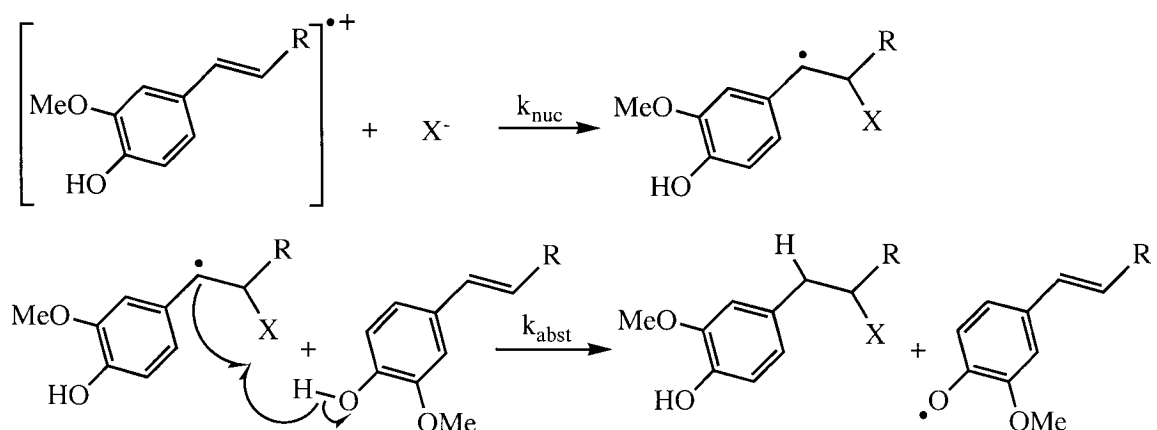
However, this pathway was ruled out by virtue of the large second-order rate constant for the nucleophilic addition. Given that the nucleophilic additions take place with rate constants of *ca.* 1 x 10^{10} $M^{-1}s^{-1}$, hydrogen atom transfer would have to occur with rate constants of the same order of magnitude of that for nucleophilic addition. In other words, if the hydrogen atom transfer step is slower than the nucleophilic addition then it would be possible to detect the intermediate phenethyl radical. However no spectroscopic evidence was found indicating the formation of such phenethyl radical. Therefore, the mechanism shown in Scheme 2.25 would explain the results observed in this work only if the hydrogen atom transfer takes place as fast as the nucleophilic addition step. This is unlikely, as previous studies on hydrogen atom transfer from substituted phenols to alkyl radicals report that these processes take place with rate

constants of the order of 10^5-10^6 M^{-1} s^{-1}.[84] Given the small concentration of coniferyl alcohol and isoeugenol (~0.15 mM) used in laser experiments, a fast reaction between the phenethyl radical and the unreacted coniferyl alcohol or isoeugenol is highly unlikely.

Overall, given the apparent enhanced basicity of anionic species like chloride and nitrate in acetonitrile and the strong spectroscopic evidence for the formation of the vinylphenoxyl radicals it is reasonable to conclude that deprotonation is the major reaction between the 4-vinylphenol radical cations and the anionic reagents. Thus, even though nucleophilic addition to the radical cations is expected to take place with second-order rate constants similar to those measured in the present work for the reaction of the anions with the radical cations, the results show that deprotonation is the dominant reaction, with no evidence for nucleophilic addition. An analogous situation has been reported for the reaction of 4-methoxystyrene radical cation with azide, Section 2.1.4.2.[60] The reaction between these species in TFE takes place via nucleophilic addition, with a second-order rate constant of 7.0 x 10^9 M^{-1}s^{-1}. Conversely, in acetonitrile an electron-transfer reaction takes place with a rate constant of 3.0 x 10^{10} M^{-1} s^{-1}. Since the nucleophilic addition is a diffusion-controlled process in TFE the same reaction would must likely takes place with a diffusion-controlled rate constant in acetonitrile. However no evidence was found indicating the addition of the azide ion to the radical cation in acetonitrile. Thus, despite the fact that both nucleophilic addition and electron transfer reactions should be taking place in acetonitrile with similar second-order rate constants, spectroscopic results indicate that only electron-transfer reaction is occurring in that solvent.

83

2.3.2 Acidity of Isoeugenol Radical Cation and Generation of this Species by Protonation of Phenoxyl Radical

In neat acetonitrile the isoeugenol radical cation completely decays in a first-order manner to yield the 340-nm transient identified as the 2-methoxy-4-(1-propenyl)phenoxyl radical, indicating that in the absence of added acid the radical cation is completely converted into the phenoxyl radical. At increasing concentrations of added acid the decay of the radical cation is no longer a single first-order process but instead consists of two sequential first-order processes with rate constants of 1×10^6 s^{-1} and 2×10^4 s^{-1}, respectively. The magnitude of the change in absorption due to each process is highly influenced by the concentration of acid, with the fast process becoming less important with increasing acid content. These results indicate that in presence of added acid the isoeugenol radical cation is no longer completely transformed into the phenoxyl radical. Instead the radical cation decays to an equilibrium state with significant amounts of both the radical cation and the phenoxyl radical. The equilibrium state then decays by reaction of any of the two species in equilibrium. The decay of the radical cation to the equilibrium state corresponds to the faster of the two processes described above, while the slower process corresponds to the decay of the equilibrium state. Increasing the acid content shifts the acid base equilibrium to the side of the isoeugenol radical cation. That is, the fraction of the radical cation in the equilibrium state will increase with increasing concentration of acid. This is reflected as an increase in the magnitude of the slower process observed for the decay of the radical cation, Figure 2.23-a.

Analysis of the variation of the fraction of isoeugenol radical cation at equilibrium with the concentration of acid led to an estimated dissociation constant for this radical

84

cation of $K_a = (1.2 \pm 0.2) \times 10^{-4}$ M, $pK_a = 3.9 \pm 0.1$ in acetonitrile. According to previous studies concerning the acid-base equilibria of positively charged acids, the K_a of those acids are typically 8 to 9 orders of magnitude larger in water than in acetonitrile.[85] Therefore, assuming this situation is valid for the isoeugenol radical cation, a pK_a value between –4 and –5 is estimated for this species in water. This is consistent with values of pK_a of –4.7 and –6.4 reported for the 4-methoxy- and 2-methoxyphenol radical cations in aqueous solution.[86]

The acid dissociation constant of isoeugenol radical cation was also estimated from the ratio of k_{dep}/k_{prot} obtained from experiments involving the protonation of 2-methoxy-4-(1-propenyl)phenoxyl radical. Given that the formation of isoeugenol radical cation represents the formation of the isoeugenol radical cation/2-methoxy-4-(1-propenyl)phenoxyl radical equilibrium state, Eq. 2.17, the observed rate constant for the growth of isoeugenol radical cation is the sum of the rate constant for protonation (k_{prot}) multiplied by the concentration of acid and the rate constant for deprotonation (k_{dep}), Eq. 2.18.

(Eq. 2.17)
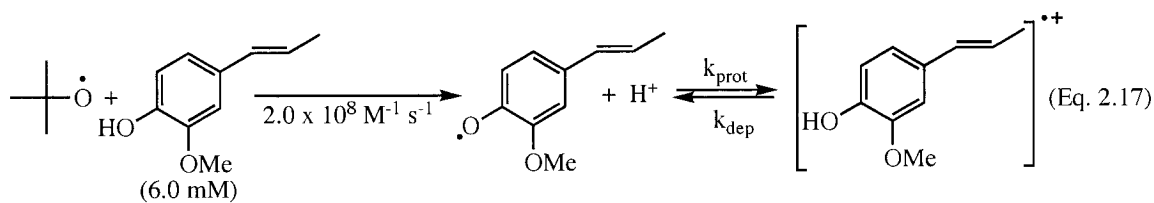
$$k_{obs} = k_{dep} + k_{prot}[H^+] \qquad \text{(Eq 2.18)}$$

According to this expression, the relationship between the observed rate constants and the concentration of acid should be linear, with the slope corresponding to the protonation rate constant and the intercept giving the deprotonation rate constant. As shown in Figure 2.27, the rate constants for the growth of the radical cation did indeed

increase in a linear manner with increasing concentration of added acid but only at concentration of acid less than 6.0 mM. At concentrations of acid higher than 6.0 mM the growth of the isoeugenol radical cation was no longer affected by the concentration of acid. The rate of formation of the phenoxyl radical is limited by the concentration of isoeugenol (6.0 mM) used in this experiment. Given that the reaction between the isoeugenol and the *tert*-butoxyl radical takes place with a second-order rate constant of 2.0×10^8 $M^{-1}s^{-1}$, the generation of the phenoxyl radical will take place with a rate of 1.2×10^6 $s^{-1} = (2.0 \times 10^8$ $M^{-1}s^{-1}) \times 0.006$ M. Therefore at concentrations of acid higher than 6.0 mM, the protonation of the 2-methoxy-4-(1-propenyl)phenoxyl radical becomes faster than its generation. Thus, the growth of isoeugenol radical cation is no longer affected by the concentration of acid and is limited by the rate of formation of the phenoxyl radical.

Linear least square analysis of the linear portion of the plot shown in Figure 2.28 gives a value of $k_{dep} = (1.5 \pm 0.4) \times 10^5$ s^{-1} and a protonation rate constant of $k_{prot} = (2.2 \pm 0.1) \times 10^8$ M^{-1} s^{-1}. The ratio of these constants then gives an acid dissociation constant for isoeugenol radical cation, $K_a = (7 \pm 2) \times 10^{-4}$ M, $pK_a = 3.1 \pm 0.1$. The K_a value is somewhat larger than the K_a value obtained from fitting the fraction of isoeugenol radical cation to Eq. 2.12. Systematic errors in the two different methods might be the cause for such a discrepancy. Solvent effects could be another reason for the difference in the K_a values. While the experiment involving the measurement of the fractions of isoeugenol radical cation was carried out just in acidic acetonitrile, the experiment involving the protonation of 2-methoxy-4-(1-propenyl)phenoxyl radical was carried out in acidic acetonitrile containing 10 % di-*tert*-butylperoxide.

As previously mentioned the generation of coniferyl alcohol radical cation by protonation of its corresponding phenoxyl radical could not be achieved due to the decomposition of coniferyl alcohol in acidic acetonitrile. Most probably, coniferyl alcohol is transformed into quinone methide by acid catalyzed elimination of the aliphatic hydroxylic group as shown in Eq. 2.13.

Failure to detect the formation of the 2-methoxy-4-vinylphenol radical cation by protonation of the corresponding phenoxyl radical most likely originates from the rapid reaction of this radical cation with its neutral precursor. The rate constant for addition of 2-methoxy-4-vinylphenol radical cation to its neutral parent is greater than the rate constant for hydrogen abstraction from 2-methoxy-4-vinylphenol by the *tert*-butoxyl radical. Therefore, the decay of the radical cation would be faster than its formation due to the relatively slow generation of 2-methoxy-4-vinylphenoxyl radical, Scheme 2.26. If the explanation above is correct, the rate constant for the decay of the 2-methoxy-4-vinylphenol radical generated by hydrogen abstraction should increase with increasing concentration of acid, and observing such an increase would have provided evidence that protonation of the radical does indeed take place. However, since our primary goal was to demonstrate that vinylphenol radical cations can be formed in detectable amounts by protonation of vinylphenoxyl radicals, no further experiments, including monitoring the decay of the radical as a function of acid concentration, were carried out once it was determined that the radical cation could not be detected.

Scheme 2.26

$$>\!\!-\!\!\overset{\bullet}{O} + \text{(4-vinyl-2-methoxyphenol, HO-, OMe)} \xrightarrow{1.2 \times 10^8 \text{ M}^{-1}\text{s}^{-1}} \bullet O\text{-(OMe)} + H^+ \underset{k_{dep}}{\overset{k_{prot}}{\rightleftharpoons}} [HO\text{-(OMe)}]^{\bullet +}$$

HO-(OMe)

$4.3 \times 10^8 \text{ M}^{-1}\text{ s}^{-1}$

(Dimerization)
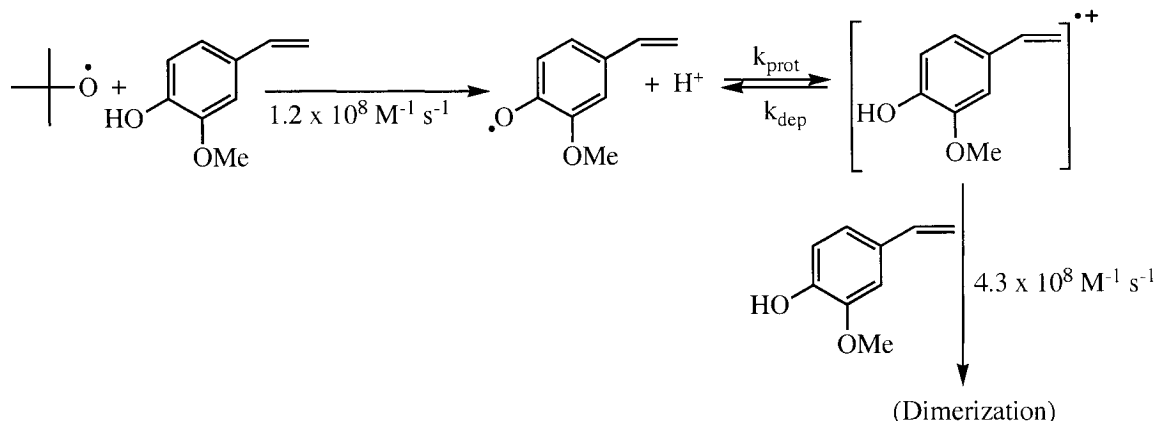
2.3.3 Reactivity of 4-Vinylphenol Radical Cations towards Neutral Precursors and other Substituted Styrenes

Of the three 4-hydroxystyrene derivatives examined in this work, the 2-methoxy-4-vinylphenol radical cation was the only one that clearly reacted with its neutral precursor, 2-methoxy-4-vinylphenol. The second-order rate constant for this reaction was measured to be 4.3×10^8 M^{-1} s^{-1}, which is about one order of magnitude slower than a diffusion controlled process in acetonitrile.

Unlike other styrenes that only contain a nucleophilic vinyl group and typically undergo [2+1] cycloaddition with radical cations, 2-methoxy-4-vinylphenol contains an additional reactive phenolic OH group that could react as a nucleophile or a base with the 2-methoxy-4-vinylphenol radical cation. Direct participation of the phenolic OH can be ruled out upon consideration of the reactivity of 4-vinylphenol radical cations with other hydroxy containing compounds. In particular, rate constants for the reaction of simple alcohols with 4-vinylphenol radical cations in acetonitrile are about one order of magnitude smaller than the second-order rate constant of 4.3×10^8 M^{-1} s^{-1} measured in

this work. Simple phenols are similarly less reactive, as demonstrated by the absence of a noticeable increase in the rate constant for the decay of the 2-methoxy-4-vinylphenol radical cation in the presence of 4-isopropylphenol.

The magnitude of the rate constant for the reaction between the 2-methoxy-4-vinylphenol radical cation and its neutral precursor, $k = 4.3 \times 10^8$ $M^{-1}s^{-1}$, is similar to the rate constant of 1.1×10^9 M^{-1} s^{-1} for the quenching of the 4-methoxystyrene radical cation by neutral 4-methoxystyrene, a reaction which is known to involve addition to give [2+1] cycloaddition products. Thus, on the basis of these comparisons, it is reasonable to conclude that the quenching of the 2-methoxy-4-vinylphenol radical cation with 2-methoxy-4-vinylphenol is also due to a coupling reaction as shown in Eq. 2.19.

(Eq 2.19)
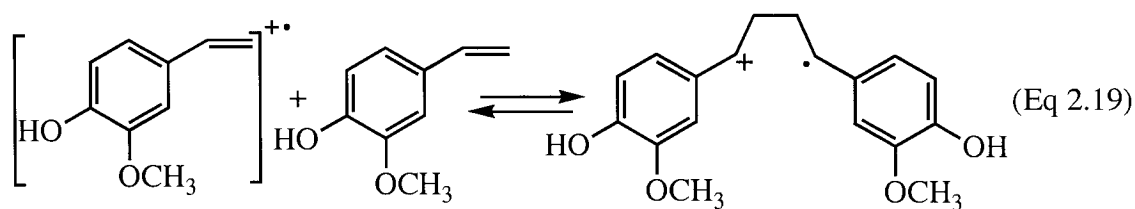
Further evidence indicating that the phenolic hydroxyl group of 2-methoxy-4-vinylphenol is not responsible for the observed quenching of the 2-methoxy-4-vinylphenol radical cation comes from results obtained upon reacting the 2-methoxy-4-vinylphenol radical cation with non-phenolic styrenes. The 2-methoxy-4-vinylphenol radical cation reacted with styrene, 4-methylstyrene and α-methylstyrene with rate constants ranging from 1.0×10^8 M^{-1} s^{-1} to 2.5×10^8 M^{-1} s^{-1}. Since these styrenes contain only the nucleophilic vinyl group, the second-order reaction must involve a dimerization reaction that presumably leads to a β,β'-coupling product.

Table 2.5 shows the rate constants measured for the reaction of the 2-methoxy-4-vinylphenol radical cation and the 4-methoxystyrene radical cations with substituted

styrenes. The reactions of both radical cations with α-methylstyrene and 4-methylstyrene take place with similar second-order rate constants. On the other hand, the reaction of 2-methoxy-4-vinylphenol radical cation with styrene is ten times faster than the reaction of 4-methoxystyrene radical cation with styrene.

Table 2.5 Rate constants for the quenching of the 2-methoxy-4-vinylphenol and 4-methoxystyrene radical cations by substituted styrenes in acetonitrile.

	k / $M^{-1} s^{-1}$	
	2-methoxy-4-vinylphenol radical cation	4-methoxystyrene radical cation
4-methoxystyrene	-----	1.1×10^9
2-methoxy-4-vinylphenol	4.3×10^8	-------
styrene	1.4×10^8	1.3×10^7
4-methylstyrene	2.5×10^8	7.8×10^7
α-methylstyrene	1.0×10^8	1.2×10^8

The dimerization of styrene radical cations with their neutral precursor can be a complex reaction and includes the possibilities that the initially formed radical cation dimer can revert back to the monomer and that the neutral precursor participates as an electron-donor in the product determining step, Schemes 2.17 and 2.18. As a result, the rate constant measured from quenching of the radical cation by its precursor or by another styrene may be a combination of several rate constants rather than simply being the rate constant for the addition reaction. For example, as described in the introduction, the observed second-order rate constant obtained from the reaction of the 4-methoxystyrene radical cation with 4-methoxystyrene contains a term for the addition

step as well as a term for the sigmatropic shift to give the hexatriene radical cation and a term for the revertion of the long-bond cyclobutane radical cation to 4-methoxystyrene radical cation and 4-methoxystyrene. Thus, while the variations observed in Table 2.5 may be the result of structural effects on the addition rate constants, they may also be caused by effects of structural differences on rate constants for other processes that may affect the overall observed rate constant.

The absence of observable quenching of 3,4-dimethoxystyrene radical cation by its neutral precursor or by 4-methylstyrene was very surprising. As illustrated in Table 2.1, the reaction of the radical cations of styrenes not possessing a β-substituent with their neutral precursors typically take place with diffusion-controlled rate constants. As a result, the reaction of the 3,4-dimethoxystyrene radical cation with its parent was anticipated to be a diffusion-controlled process. One possibility for the lack of an observed reaction is that the meta methoxy group stabilizes the radical cation but destabilizes the radical cation dimer that would be generated upon coupling of the 3,4-dimethoxystyrene radical cation with its neutral precursor, Scheme 2.27. As a result, the dimer might rapidly revert to the 3,4-dimethoxystyrene radical cation and its precursor, and no quenching of the radical cation would be observed, Scheme 2.27.

Scheme 2.27
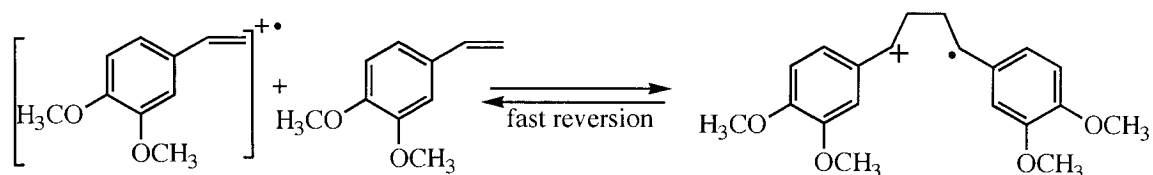
The 2-methoxy-4-vinylphenol radical cation also possesses a methoxy group meta to the vinyl functionality, but in this case the results clearly show that the 2-methoxy-4-

91

vinylphenol radical cation does react with its parent with a rate constant of 4.3 x 10^8 M^{-1} s^{-1}. The only structural difference between 3,4-dimethoxystyrene and 2-methoxy-4-vinylphenol is the presence of a labile hydroxyl group in the latter species. Therefore, the substantial increase in second-order rate constants observed upon substitution of the 4-methoxy group with a OH group strongly suggests that the phenolic OH group is responsible for the large difference in reactivity. Most likely, coupling of 2-methoxy-4-vinylphenol radical cation with its neutral precursor or other styrenes results in the formation of a dimer radical cation that decays either by reverting back to the radical cation and the neutral styrene or by deprotonation, Scheme 2.28. Presumably, the deprotonation step occurs faster than the dissociation of the radical cation which would explain the large difference in reactivity between the 3,4-dimethoxystyrene and 2-methoxy-4-vinylphenol radical cations.

Scheme 2.28
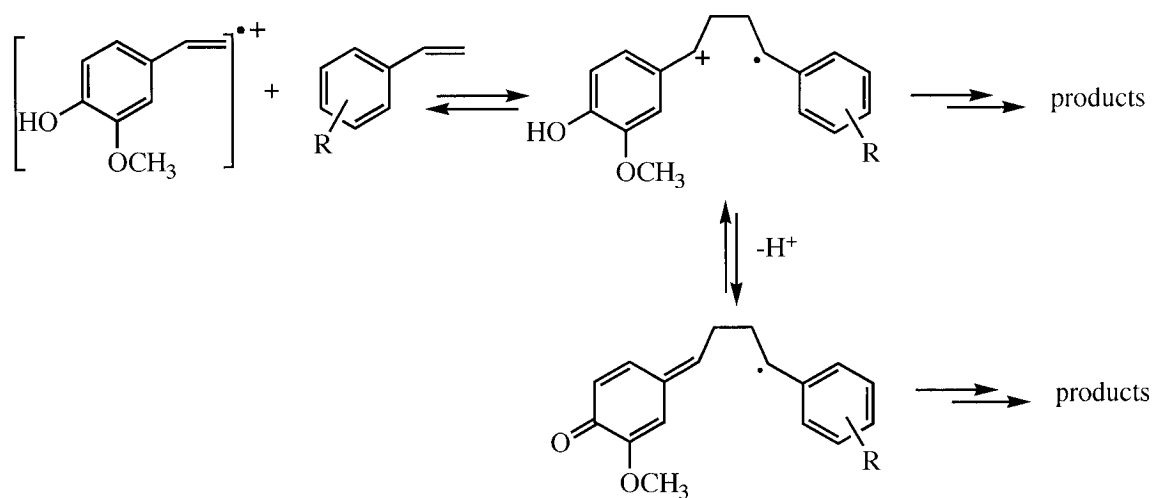
Under acidic conditions (1.0 mM $HClO_4$ in acetonitrile), the reaction of the 2-methoxy-4-vinylphenol radical cation with 4-methylstyrene is almost two orders of magnitude slower than the same reaction in neat acetonitrile, Figure 2.35. Presumably, in

the acidic environment, the 1,4-distonic radical cation dimer would become favoured over its deprotonated form, and revertion back to the starting radical cation would be enhanced. Under these conditions, the observed rate constant for the decay of the radical cation as a function of the concentration of 4-methoxystyrene could be substantially diminished.

Unfortunately, the rate constant for reaction of the 2-methoxy-4-vinylphenol radical cation with its neutral precursor under acidic conditions could not be measured. This measurement would require the use of chloranil as sensitizer, but chloranil decomposes in acidic acetonitrile.

Coniferyl alcohol and isoeugenol contain an additional alkyl substituent at the β-position of the double bond, and the radical cations from these two substrates show no measurable reactivity toward their neutral precursors, or towards the other styrenes used in this study. A similar observation had been made previously for the radical cation of β-methyl-4-methoxystyrene (anethole), which showed no observable reactivity with neutral anethole, even at concentrations as high as 0.10 M.[24] While this result might lead to the conclusion that the anethole radical cation and anethole do not undergo an addition reaction, product studies have provided strong evidence that such a reaction does occur to give 2,3-dimethyl-1,4-bis(4-methoxyphenyl)cyclobutane.[62] However, the addition takes place with a rate constant of 2×10^6 M^{-1} s^{-1} that is relatively slow and difficult to measure directly.[62]

Given the results previously obtained with anethole, it is not surprising that the decays of the radical cations of coniferyl alcohol and isoeugenol, both of which contain β-alkyl groups, show no detectable increase with increasing concentrations of their

93

neutral precursors. At the same time, the results obtained with the anethole radical cation illustrate that an inability to obtain evidence from kinetic studies for radical cation mediated cycloadditions does not rule out that such a reaction still takes place but with a rate constant that is too small to measure.

In the dimerization experiments, the results do show that the decays of coniferyl alcohol, isoeugenol and 3,4-dimethoxystyrene radical cations increase slightly with increasing concentrations of the neutral precursors at concentrations lower than 1.0 mM but then remain unaffected at higher concentrations of the substrates, Figures 2.32 and 2.33. As described in Sections 2.1.4.3.1 and 2.1.4.3.2, somewhat similar results were observed for the reaction between 4-methoxystyrene radical cation and its precursor, Figure 2.3,[24] with the curvature being due to interception of the long-bond cyclobutane dimer radical cation at high concentrations of neutral 4-methoxystrene to regenerate the 4-methoxystyrene radical cation, Scheme 2.18.

However, a major difference between the data obtained for 4-methoxystyrene radical cation, Figure 2.3, and the radical cations of coniferyl alcohol, isoeugenol and 3,4-dimethoxystyrene is the concentration of precursor at which curvature takes place. For the 4-methoxystyrene radical cation curvature begins at ca. 0.05 M 4-methoxystyrene, while for the radical cations of coniferyl alcohol and isoeugenol, curvature begins at precursor concentrations of ca. 0.001 M. As a result, analysis of the data in Figure 2.33 according to the same rate law, Eq. 2.4, used to analyze the data for the 4-methoxystyrene radical cation gives unreasonable values for the rate constants associated with the reactions in Scheme 2.18. In particular, assuming that electron-transfer between the cyclobutane dimer radical cation and the neutral precursor is diffusion controlled, $k_3 = 2 \times$

10^{10} M^{-1} s^{-1}, the data in Figure 2.33 can only fit to Eq. 2.4 if $k_1 > 10^{10}$ M^{-1} s^{-1} and if $k_{-1} + k_2$ < 5 x 10^6 s^{-1}. This value of k_1 is considerably larger than the rate constant for addition of similar radical cations to their neutral precursor; for example, as mentioned previously, the rate constant for addition of the anethole radical cation to anethole is approximately 10^6 M^{-1} s^{-1}. Furthermore, k_{-1} for the anethole radical cation/anethole cyclobutane dimer is 8 x 10^7 s^{-1}, which is two orders of magnitude greater than the upper limit for k_{-1} of 5 x 10^5 s^{-1}. Thus, the changes in rate constants for the decay of the radical cations of coniferyl alcohol, isoeugenol and 3,4-dimethoxystyrene with the concentration of their precursors cannot be explained by a mechanism similar to that established for the radical cation mediated dimerization of 4-methoxystyrene. The small changes in rate constant observed at very low concentrations of the substrates are still to be explained.

Product studies would clearly help to clarify whether or not the isoeugenol or coniferyl alcohol radical cations add to their neutral precursors. However, due to the rapid deprotonation of the radical cations, the only products observed are derived from radical-radical coupling.

2.3.3.1 Implication for the Biosynthesis of Lignans

Despite the fact that definitive information concerning the mode of reaction between 2-methoxy-4-vinylphenol radical cation and neutral styrenes cannot be obtained from kinetic studies alone, the results described in this chapter are consistent with a β,β'-coupling reaction as observed for other styrenes. The results clearly demonstrate that the 2-methoxy-4-vinylphenol radical cation does undergo a rapid reaction with its neutral parent and with other non-phenolic styrenes. The other 4-vinylphenol derivatives, coniferyl alcohol and isoeugenol, showed no observable increase in reactivity in the

presence of neutral styrenes. However, these two systems contain β-alkyl substituents, which are known to reduce the reactivity of styrene radical cations towards neutral styrenes. Indeed, the lack of reactivity of both coniferyl alcohol and isoeugenol radical cations towards neutral styrenes parallels that observed for other β-susbtituted styrenes radical cations. In particular, the anethole radical cation does react with neutral anethole to give a β,β'-coupling product;[62] however, the reaction takes place with a second-order rate constant too slow to measure by laser flash photolysis.[24]

All three 4-vinylphenol radical cations undergo a rapid deprotonation reaction to yield 4-vinylphenoxyl radicals. However, as shown for the isoeugenol phenoxyl radical, rapid reprotonation of these species also takes place under acidic conditions in non-protic, polar solvents. Thus, in a biological system, 4-vinylphenol radical cations need not undergo a dimerization reaction as soon as they are produced by enzymatic oxidation; instead, the radical cations can be 'stored' in their less reactive 4-vinylphenoxyl form, and then regenerated by enzymatic protonation when dimerization is ready to proceed.

Admittedly, there is little biochemical evidence suggesting that the radical cations are involved in the biosynthesis of lignans. Nevertheless, the results obtained in this work indicate that radical cation mediated dimerization of 4-vinylphenols is, in principle, a viable pathway, and that this mechanism may be helpful in understanding results as the mechanism of lignan biosynthesis continues being probed.

2.4 Experimental Section

Materials. Coniferyl alcohol (98 %) and Isoeugenol (98 %) were purchased from Aldrich Chemical Co. and used as received. 2-Methoxy-4-vinylphenol (97%) was acquired from Alfa Aesar and used without further purification. Perchloric acid (60 %

w/w) was purchased from Fisher Scientific Company. Acetonitrile used for laser flash photolysis experiments was spectroscopic grade supplied by Omnisolv, BDH. Tetrabutylammonium salts of chloride, cyanide, acetate and bromide used for quenching of the radical cations were acquired from Aldrich Chemical Co. All the other chemicals used were purchased from Aldrich Chemical Co. Hexanes, ethylacetate and dichloromethane were distilled prior to use.

General Procedures. NMR spectra were recorded on a Brucker AV-500 spectrometer at the Atlantic Region Magnetic Resonance Centre at Dalhousie University. The data were processed with Brucker Xwin-NMR software. Chloroform-d ($CDCl_3$, 0.05 % TMS) was the solvent employed for NMR experiments. Proton chemical shifts were calculated relative to trimethylsilane (TMS) and ^{13}C chemical shifts were determined using the central peak of the $CDCl_3$ carbon signal ($\delta = 77.16$ ppm) as reference. Products formed in product study experiments were identified by GC-MS using a Perkin-Elmer Autosystem XL Turbomass instrument equipped with Supelco MDN-5S 30 m x 0.25 mm x 0.50 μm columns. Parameters setting were as follows: injector temperature = 240 °C, $T_1 = 60$ °C (1 min), $T_2 = 240$ °C (20 min), ramp rate = 20 °C/min. Melting points were measured on a Fisher-Johns apparatus. Absorption spectra of solutions prior to irradiation, and measurement of the absorption of solutions at the appropriate excitation wavelengths were determine using a Cary 100 Bio UV-Visible spectrometer.

Laser experiments. The nanosecond laser system used for laser flash photolysis experiments is thoroughly described on Chapter 4. A Lambda Physiks excimer laser (308 nm, XeCl, 10 ns/pulse, < 100 mJ/pulse) was used for experiments involving direct photoionization of vinylphenol substrates. In experiments using chloranil or di-tert-

butoxyperoxide, a Continuum Nd:YAG NY-61 laser (355 nm, 10 ns/pulse, < 35 mJ/pulse) or a Spectra Physics Quanta Ray INDI-40-10 Nd:YAG laser (355 nm, < 8 ns/pulse, 100 mJ/pulse) was used as the excitation source.

Samples for kinetic experiments were placed in 7 x 7 mm laser cells made out of Suprasil quartz tubing. Solutions were prepared by the addition of a small aliquot (~5 μL) of a stock solution of the appropriate substituted 4-vinylphenol substrate to 1.0 or 2.0 mL of acetonitrile contained in the laser cells. The absorption of the 4-vinylphenol derivatives in the laser cells was approximately 0.4 at 308 nm, corresponding to concentrations of ca. 1 x 10^{-4} M. Solutions to measure rate constants for the reaction of the 4-vinylphenol radical cations with alcohol, water, anions and substituted styrenes were prepared by adding small aliquots (1 to 20 μL) of a stock solution with a known concentration of quencher in acetonitrile directly to laser cells containing 1.0 or 2.0 mL of acetonitrile already containing the appropriate amount of the radical cation precursor. For instance, to measure the rate constant for the reaction of isoeugenol radical cation with chloride, 1 μL of a 0.06 M solution of tetrabutylammonium chloride in acetonitrile was added to 2.0 mL of acetonitrile containing 8.0 x 10^{-5} M of isoeugenol. After obtaining the decay of the radical cation under these conditions, a second 1.0 μL aliquot of the tetrabutylammonium chloride stock solution was added, and the decay of the radical cation under these new conditions was measured again. This process was continued until measurements were made at five to ten different concentrations of chloride. The experiments were repeated three times and the reported rate constants represent the average of these three measurements. The decays of the isoeugenol and

98

coniferyl alcohol radical cations were monitored at 580 and 380 nm. The decay of the 2-methoxy-4-vinylphenol radical cation was monitored at 560 and 360 nm.

The second-order rate constants for the electron transfer reaction of the 4-vinylphenol substrates with triplet chloranil were measured by adding small aliquots (2 to 20 μL) of a 0.05 M solution with known concentrations of the vinylphenol in acetonitrile to laser cells containing 1.0 mL of acetonitrile already containing chloranil. The absorption of the solutions of chloranil contained in the laser cells at 355-nm was 0.4. As described above, increasing amounts of the solution containing the 4-vinylphenol substrates were added directly to the laser cells containing the chloranil solution. The decay of the triplet chloranil was measured at 500 nm after each addition of the stock solution containing the 4-vinylphenol. The procedure was repeated until five to ten concentrations of the 4-vinylphenol had been used. The experiment was repeated three times at each concentration of added 4-vinylphenol. The results obtained by monitoring the decay of the triplet chloranil at 500 nm were identical to those obtained by monitoring the growth of the radical cation at 580 nm.

Measurements involving the reaction of the 4-vinylphenol radical cations with the neutral precursors were carried out by adding small aliquots (2 to 20 μL) of a 0.1 M solution of the 4-vinylphenol substrate to a laser cell containing 1.0 mL of acetonitrile already containing chloranil. The decay of the radical cation, monitored at 580 nm for isoeugenol and coniferyl alcohol or 560 nm for 2-methoxy-4-vinylphenol, was measured after addition of each aliquot of the stock solution containing the 4-vinylphenol. The procedure was repeated until measurements were made at five to ten different

concentrations. The experiment was repeated three times at each concentration of added 4-vinylphenol.

Solutions for experiments carried out under acidic conditions were prepared by making a stock solution ($[HClO_4] = 0.010$ M) of perchoric acid in acetonitrile, and then making the appropriate dilutions with acetonitrile. In order to minimize the possibility of acid-catalyzed decomposition of the 4-vinylphenols, these substrates were added to the acidic solution just prior to performing the laser experiments.

Absorption spectra were measured using a flow cell system to ensure that only fresh solution was subjected to each laser pulse. Most laser experiments were carried out using aerated samples. When oxygen-free solutions were required, the samples were bubbled with a slow stream of dry nitrogen for 20 min prior to laser irradiation. All laser experiments were carried out at room temperature (22 ± 1 °C).

Synthesis

Preparation of 3-(3,4-dimethoxy-phenyl)-prop-2-en-1-ol (MeCA): Coniferyl alcohol (443 mg; 4.26 mmol) was dissolved in 10 mL solution (0.25 M) of NaOH in water. Dimethyl sulfate (232.6 μL; 2.46 mmol) was added dropwise and the mixture was stirred for 3 hours. Then 1 mL of saturated aqueous ammonia was added and the solution was stirred for another 15 minutes. The product was then extracted with H_2O / CH_2Cl_2. The organic fractions were collected and dried over $MgSO_4$. After filtration, the solvent was evaporated under vacuum to yield the product as a yellowish powder in 89 % yield. The ^{1}HNMR spectra measured for this compound agrees with that reported in the literature.[87]

100

mp = 77-78 °C (lit[87] 76-79 °C) ^{1}HNMR (500 MHz, CDCl$_3$): δ = 6.93 (d, 1H, J = 1.8 Hz),

6.91 (dd, 1H, J = 8.2, 1.8 Hz), 6.81 (d, 1H, J = 8.2 Hz), 6.53 (d, 1H, J = 15.5 Hz), 6.23

(td, 1H, J = 15.8, 5.9 Hz), 4.29 (dd, 2H, J = 5.9, 1.3 Hz), 3.88 (s, 3H), 3.87 (s, 3H), 1.88

(s, 1H) ppm. ^{13}CNMR(CDCl$_3$-125.8 MHz): δ = 149.1, 149.9, 131.1, 129.9, 126.687,

119.7, 111.2, 109.0, 63.8, 56.0, 55.9 ppm.

Preparation of isoeugenol-OD: Isoeugenol was stirred overnight in deuterium

oxide at room temperature. The product was extracted with diethyl ether and the organic

fractions were dried over MgSO$_4$. Filtration followed by evaporation of the solvent

afforded the desired product as a colorless oil. The content of isoeugenol was calculated

as the ratio of the intensity of the ^{1}HNMR peak due to the phenolic OH over the intensity

peak due to one the vinyl protons. According to this fraction, the content of isoeugenol-

OD was 80 %.

Product Studies: Product studies using sensitizers were carried out in N$_2$-saturated

acetonitrile containing 0.01 M of the 4-vinylphenol derivative and 1.0 mM of the

sensitizer, either triphenylpyrilium tetrafluoroborate or chloranil. The mixture was

irradiated at λ ≥ 360 nm during six hours. Irradiation was performed by means of a 150

W Xenon lamp and the irradiation wavelength was controlled by an appropriate filter.

The products of these experiments were identified by GC-MS.

Chemical oxidation was carried out at room temperature by adding 1.0 mL of a 2.3 mM

solution of tris(4-bromophenyl)aminium hexachloroantimonate in acetonitrile over a 1.0

mL solution of the 4-vinylphenol substrate (0.179 M in acetonitrile). The combined

solutions suddenly experiments a color change, indicating the reduction of the aminium

salt, which is dark blue. The reaction time for the chemical oxidation was 20 hours.

Both, dehydrodiisoeugenol and diisoeugenol were isolated by column chromatography using silica gel and dichloromethane:methanol (99:1) as solvent system.

Dehydrodiisoeugenol: yellowish solid. ^{1}HNMR is consistent with that reported in the literature.[77, 88]

mp = 130-131 °C (lit[77] 133-135 °C, lit[89] 132-133 °C, lit[88] 128-130 °C) ^{1}HNMR (CDCl$_3$-500 MHz): δ 6.970 (s, 1H), 6.89 (t, 2H, J = 11.4 Hz), 6.77 (d, 2H, J = 11.5 Hz), 6.36 (dd, 1H, J = 15.7, 1.2 Hz), 6.10 (qd, 1H, J = 6.6, 15.6 Hz) , 5.64 (s, 1H), 5.10 (d, 1H, J = 9.0 Hz), 3.90 (s, 3H), 3.87 (s, 3H), 3.44 (qd, 1H, J = 6.9, 9.0 Hz), 1.86 (dd, 3H, J = 6.6, 1.3 Hz), 1.38 (d, 3H, J = 7.0 Hz) ppm. ^{13}CNMR (CDCl$_3$-125.8 MHz): δ 146.8, 145.9, 144.3, 133.4, 132.4, 131.1, 123.6, 120.1, 114.2, 113.5, 109.4, 109.1, 93.9, 56.1, 56.1, 45.8, 18.5, 17.7 ppm. GC-MS m/z: 326.

Diisoeugenol: pink solid, mp = 175-176 °C. ^{1}HNMR (CDCl$_3$-500 MHz): δ 6.84 (d, 1H, J = 8.0 Hz), 6.77 (s, 1H), 6.65 (dd, 1H, J = 8.1, 1.7 Hz), 6.61 (d, 1H, J = 1.6 Hz), 6.48 (s, 1H), 5.53 (s, 1H), 5.49 (s, 1H), 3.89 (s, 3H), 3.81 (s, 3H), 3.73 (d, 1H, J = 9.5 Hz), 2.91 (td, 1H, J = 7.5, 6.8 Hz), 2.46 (m, 1H, J = 7.0, 7.2 Hz), 1.70 (m, 1H, J = 5.8, 6.0 Hz), 1.38 (m, 1H, J = 7.4, 8.8Hz), 1.03 (d, 3H, J = 7.0 Hz), 0.97 (t, 3H, J = 7.4 Hz) ppm. ^{13}CNMR (CDCl$_3$-125.8 MHz): δ 146.6, 145.6, 144.7, 144.3, 139.3, 138.9, 136.0, 121.6, 114.2, 111.2, 110.8, 107.6, 56.9, 56.3, 56.1, 49.4, 48. 7, 22.4, 13.5, 12.4 ppm. GC-MS m/z: 328.
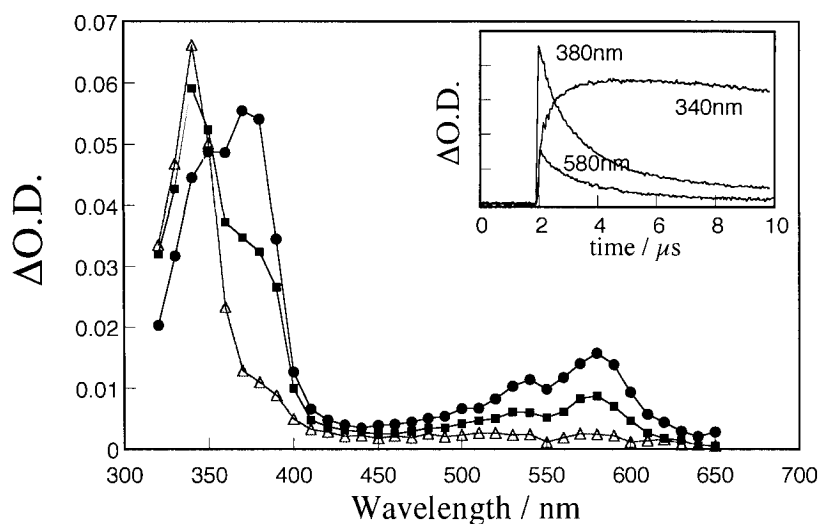
Figure 2.4 Transient absorption spectra recorded (●) 0.24 μs (■) 0.96 μs and (△) 3.58 μs after 308-nm laser irradiation of coniferyl alcohol in air-saturated acetonitrile. Inset shows time resolved absorption changes at 340, 380 and 580 nm.
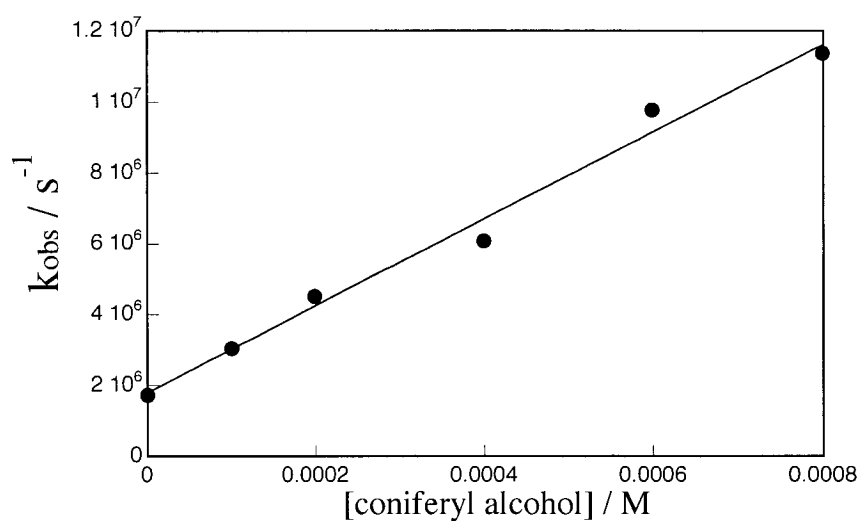
Figure 2.5 Relationship between observed rate constant for the decay of triplet chloranil at 500 nm and the concentration of coniferyl alcohol in N_2-saturated acetonitrile.
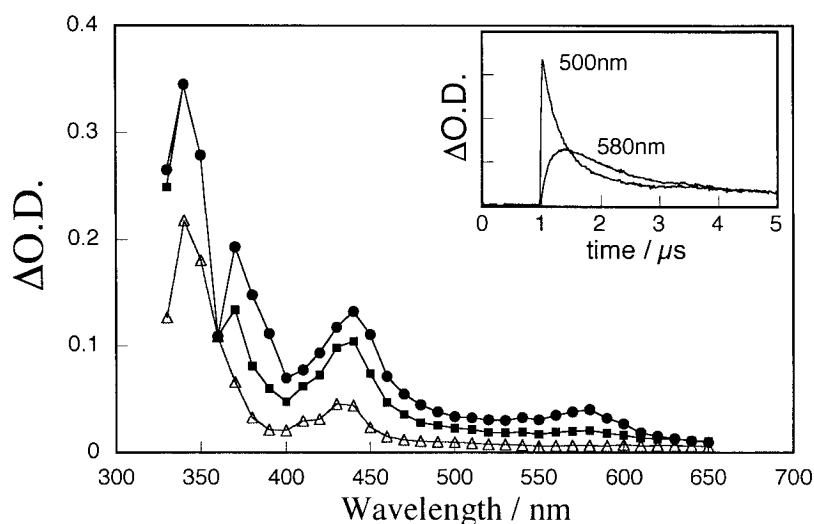
Figure 2.6 Transient absorption spectra recorded (●) 0.36 μs (■) 0.96 μs and (△) 7.16 μs after 355 nm laser irradiation of chloranil in N_2-saturated acetonitrile containing 0.001 M coniferyl alcohol. Inset shows changes in optical density at 500 and 580 nm as a function of time after 355-nm laser irradiation of chloranil in N_2-saturated acetonitrile containing 0.0001 M coniferyl alcohol.
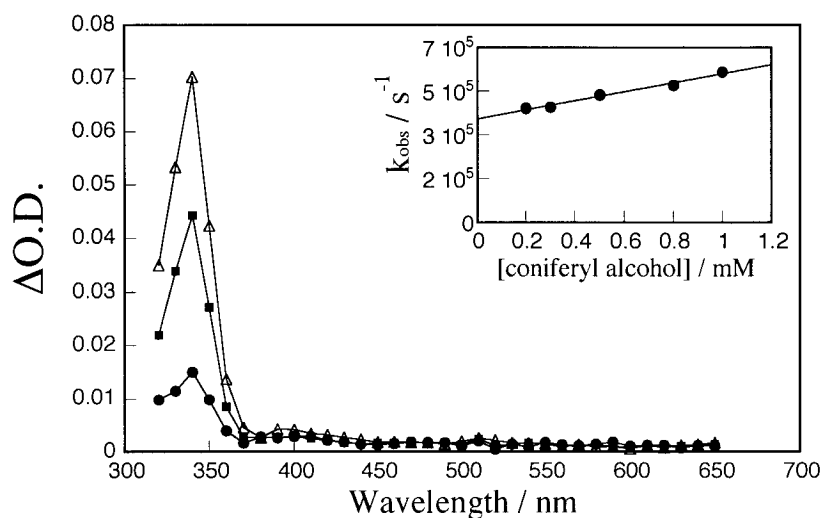
Figure 2.7 Transient absorption spectra recorded (●) 0.48 μs (■) 1.92 μs and (△) 7.24 μs after 355-nm laser irradiation of di-t-butylperoxide (10%) in air-saturated acetonitrile with 0.001 M coniferyl alcohol. Inset shows relationship between the observed rate constants for the growth of 2-methoxy-4-(3-hydroxy-1-propenyl)phenoxyl radical and the concentration of coniferyl alcohol.

104
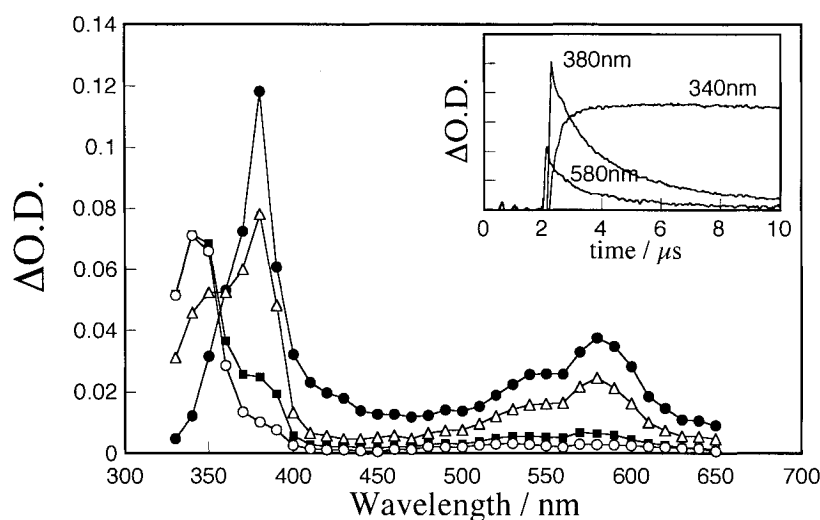
Figure 2.8 Transient absorption spectra recorded (●) 0.14 μs (△) 0.48 μs and (■) 2.98, and (○) 6.32 μs after 308 nm laser irradiation of isoeugenol in air-saturated acetonitrile. Inset shows time resolved absorption changes at 340, 380 and 580 nm.
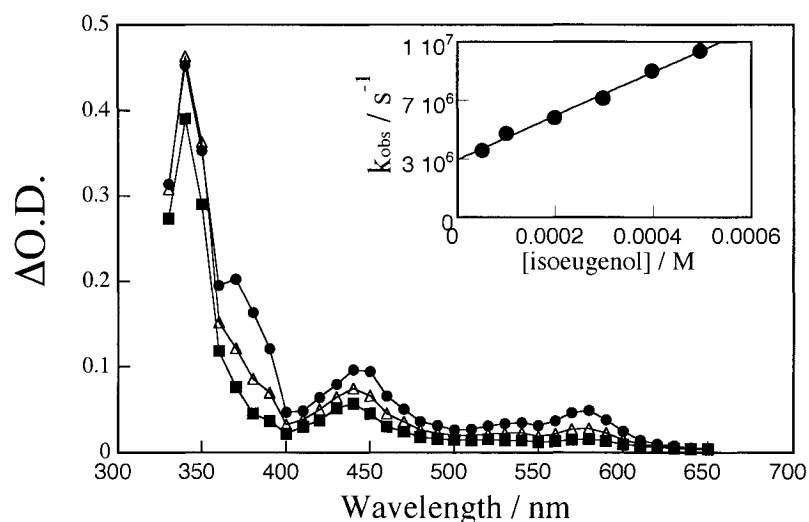
Figure 2.9 Transient absorption spectra recorded (●) 0.12 μs (△) 0.54 μs and (■) 1.32 μs after 355-nm laser irradiation of chloranil in N_2-saturated acetonitrile with 0.006 M isoeugenol. Inset shows relationship between observed rate constant for the decay of triplet chloranil at 500 nm and the concentration of isoeugenol in N_2-saturated acetonitrile.
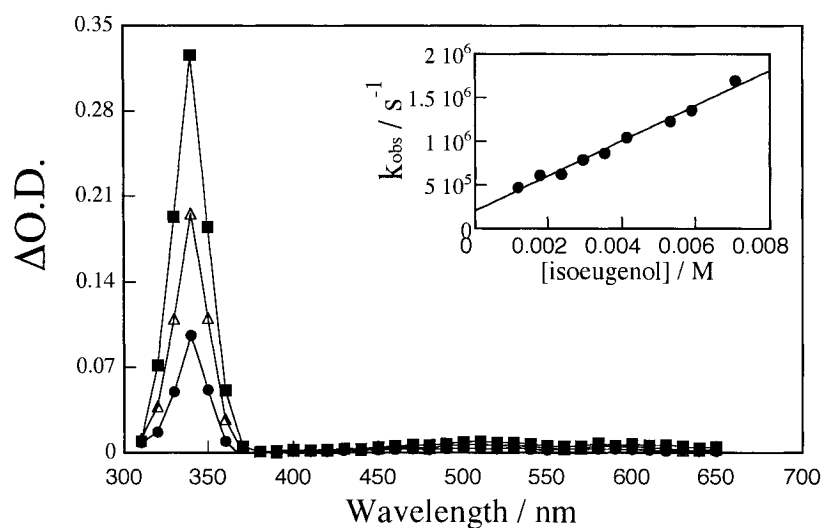
Figure 2.10 Transient absorption spectra recorded (●) 0.18 μs, (△) 0.86 μs and (■) 4.50 μs after 355-nm laser irradiation of di-*tert*-butylperoxide (10%) in air-saturated acetonitrile with 0.006 M isoeugenol. Inset shows relationship between the observed rate constants for the growth of the 340-nm transient species and the concentration of isoeugenol in air-saturated acetonitrile.
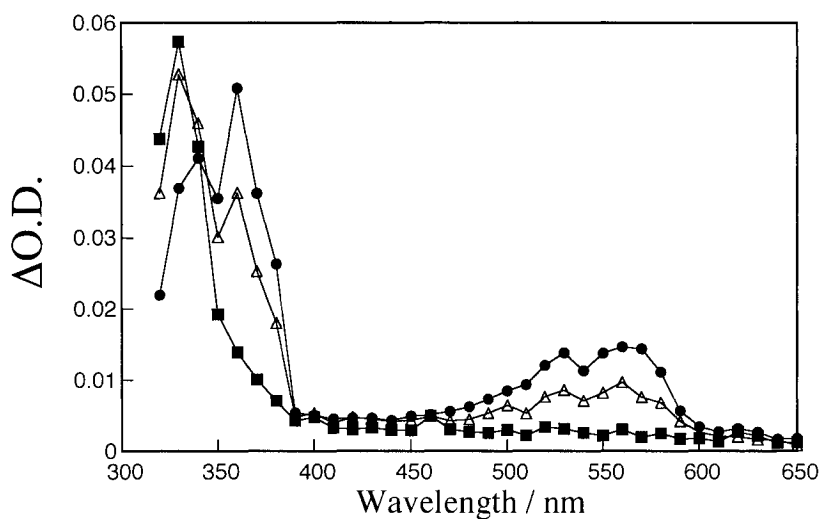
Figure 2.11 Transient absorption spectra recorded (●) 0.14 μs, (△) 0.50 μs and (■) 3.06 μs after 308-nm laser irradiation of 2-methoxy-4-vinylphenol in air-saturated acetonitrile.

106
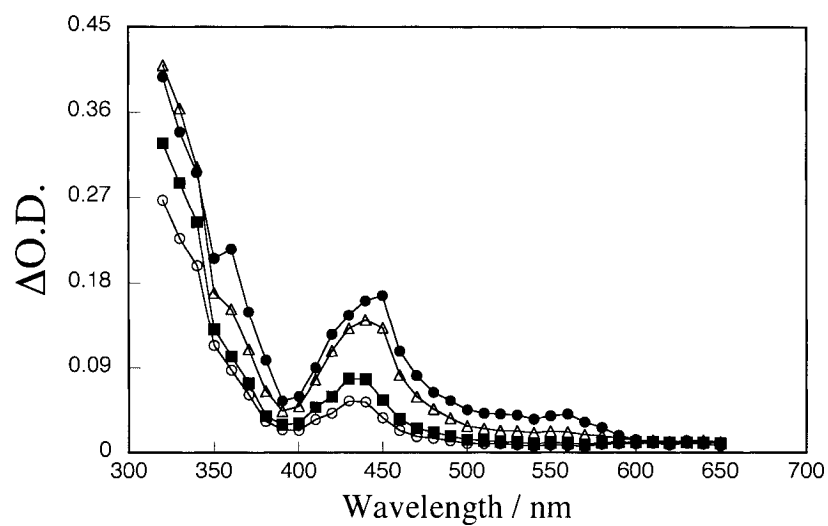
Figure 2.12 Transient absorption spectra recorded (●) 0.18 μs, ($\triangle$) 0.46 μs, (■) 2.98 μs and (○) 6.32 μs after 355-nm laser irradiation of chloranil in air-saturated acetonitrile with 0.004 M 2-methoxy-4-vinylphenol.
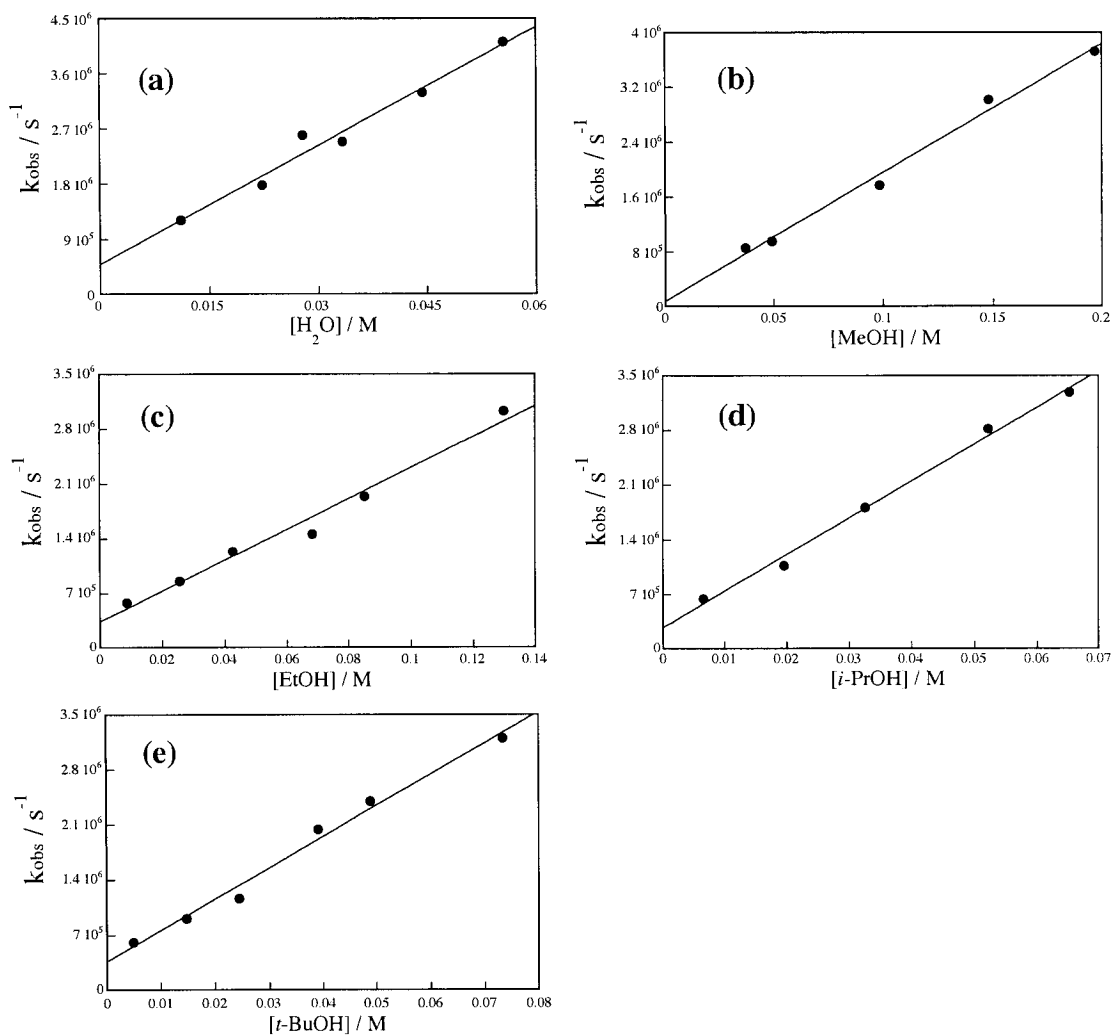
Figure 2.13 Relationship between observed rate constant for the decay of coniferyl alcohol radical cation in air-saturated acetonitrile and the concentration of added (**a**) water, (**b**) methanol, (**c**) ethanol, (**d**) *iso*-propanol, and (**e**) *tert*-butanol.
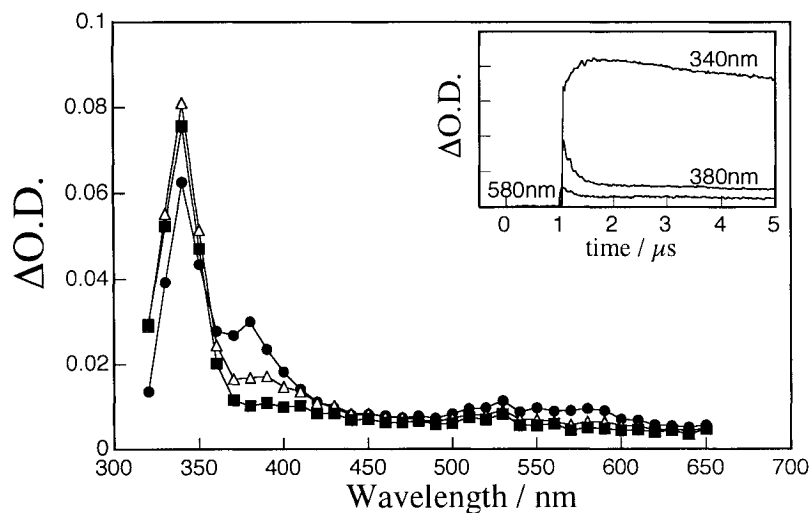
Figure 2.14 Transient absorption spectra recorded (●) 0.07 μs (△) 0.35 μs and (■) 3.16 μs after 308-nm laser irradiation of coniferyl alcohol in air-saturated acetonitrile containing 0.03 M of water. Inset shows time resolved absorption changes at 340, 380 and 580 nm.
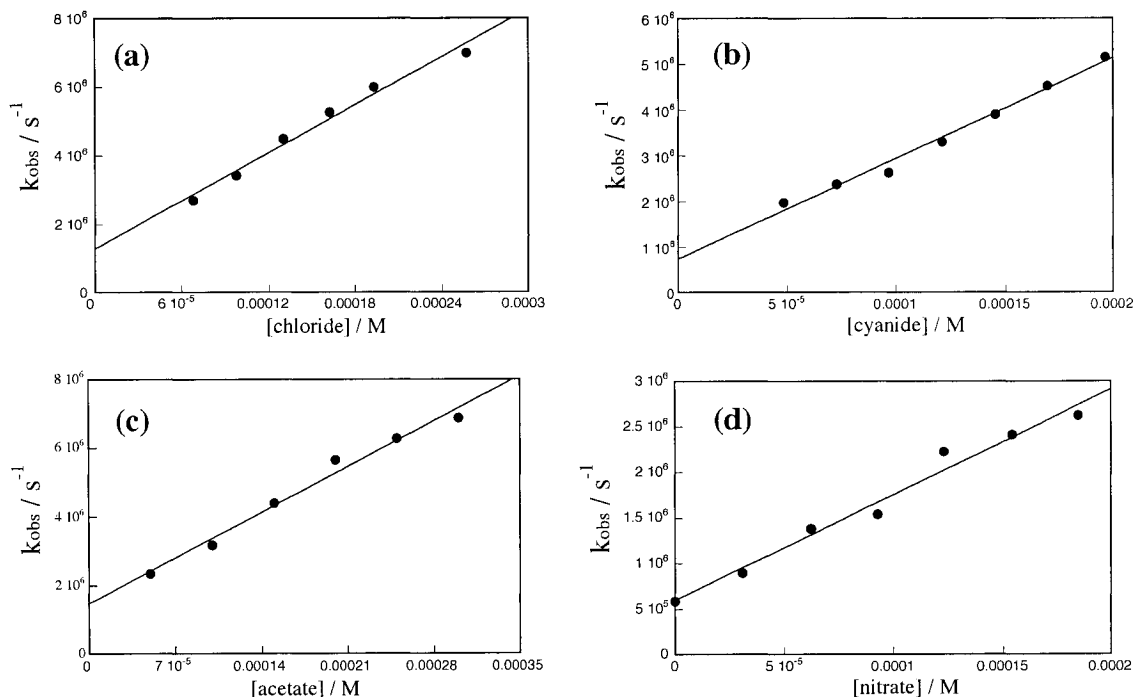
Figure 2.15 Relationship between observed rate constant for the decay of coniferyl alcohol radical cation in air-saturated acetonitrile and the concentration of added (a) chloride, (b) cyanide, (c) acetate, and (d) nitrate.
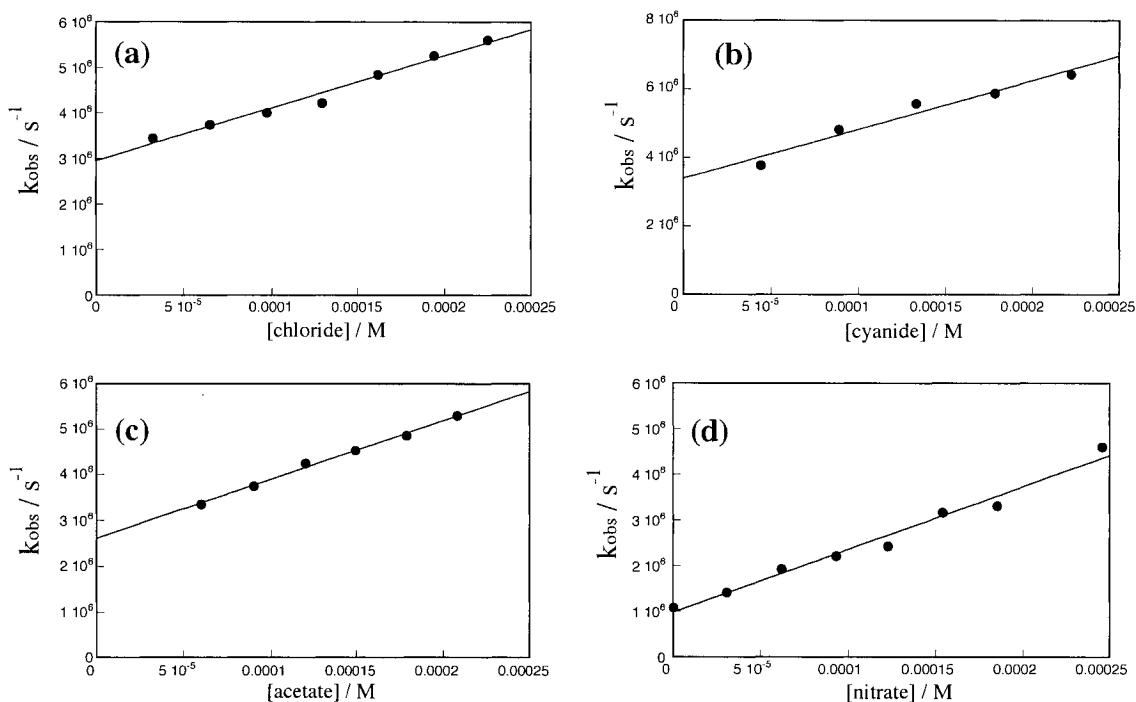
Figure 2.16 Relationship between observed rate constant for the decay of isoeugenol radical cation in air-saturated acetonitrile and the concentration of added (**a**) chloride, (**b**) cyanide, (**c**) acetate, and (**d**) nitrate.
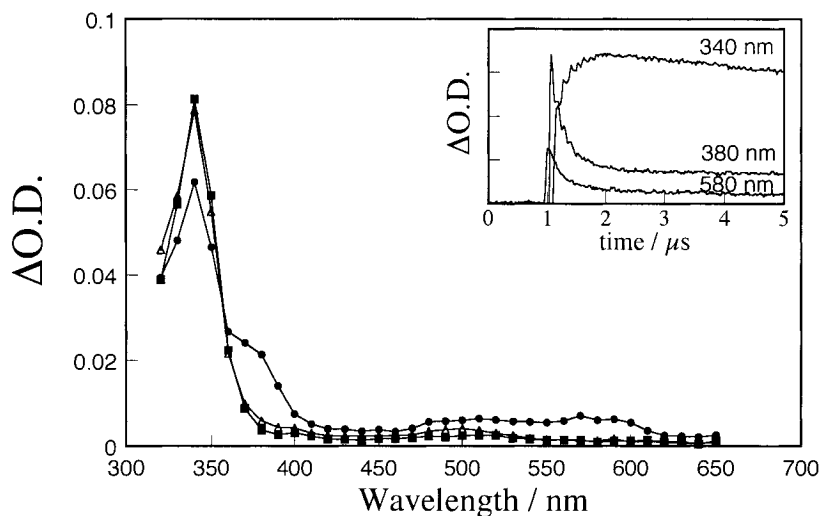
Figure 2.17 Transient absorption spectra recorded (●) 0.24 μs (△) 0.96 μs and (■) 3.58 μs after 308-nm laser irradiation of coniferyl alcohol in air-saturated acetonitrile containing 0.1 mM of tetrabutylamonium chloride. Inset shows time-resolved absorption changes at 340, 380 and 580 nm observed upon 308-nm laser irradiation of coniferyl alcohol in air-saturated acetonitrile containing 0.13 mM of tetrabutylamonium chloride.

110
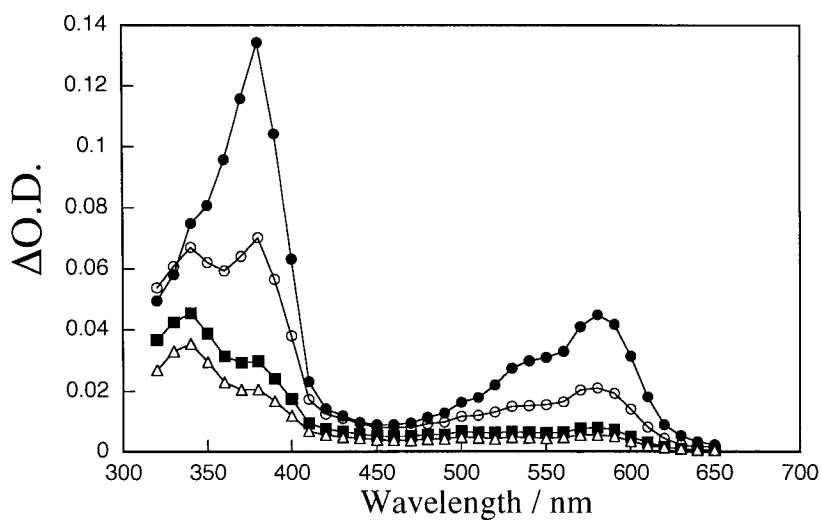
Figure 2.18 Transient absorption spectra recorded (●) 0.40 µs; (O) 1.76 µs; (■) 7.08 µs and (△) 12.8 µs after 308-nm laser irradiation of 3-(3,4-dimethoxy-phenyl)-prop-2-en-1-ol (MeCA) in dry acetonitrile.
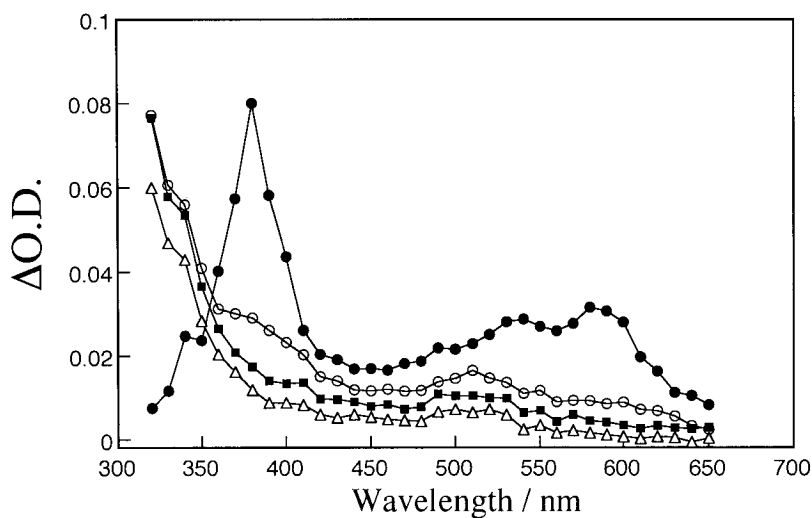
Figure 2.19 Transient absorption spectra recorded (●) 0.10 µs; (O) 0.50 µs; (■) 3.02 µs and (△) 6.36 µs after 308-nm laser irradiation of MeCA in N_2-saturated acetonitrile containing 2.08 x 10^{-4} M of chloride.

111
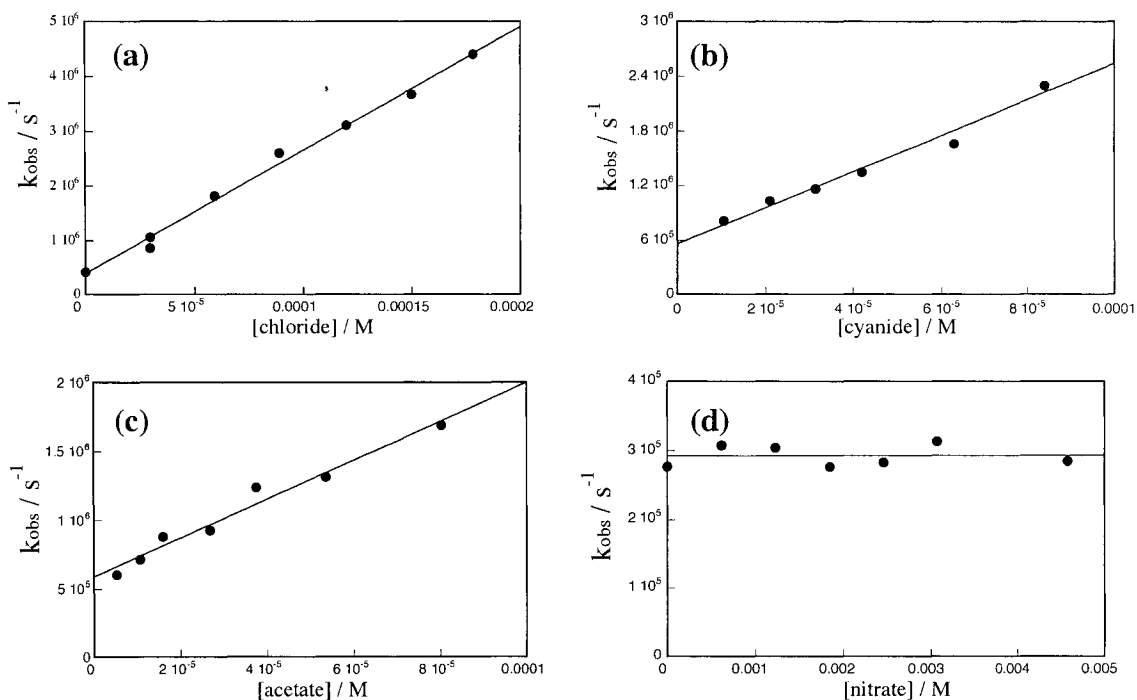
Figure 2.20 Relationship between observed rate constant for the decay of the radical cation of MeCA in air-saturated acetonitrile and the concentration of added (**a**) chloride, (**b**) cyanide, (**c**) acetate, and (**d**) nitrate.
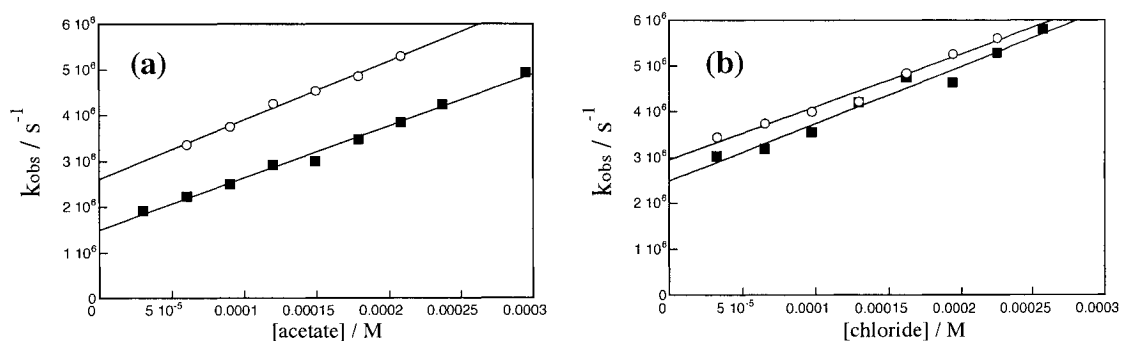
Figure 2.21 Relationship between observed rate constant for the decay of (○) isoeugenol radical cation and (■) deuterated isoeugenol radical cation and the concentration of (**a**) acetate and (**b**) chloride in air-saturated acetonitrile.

112
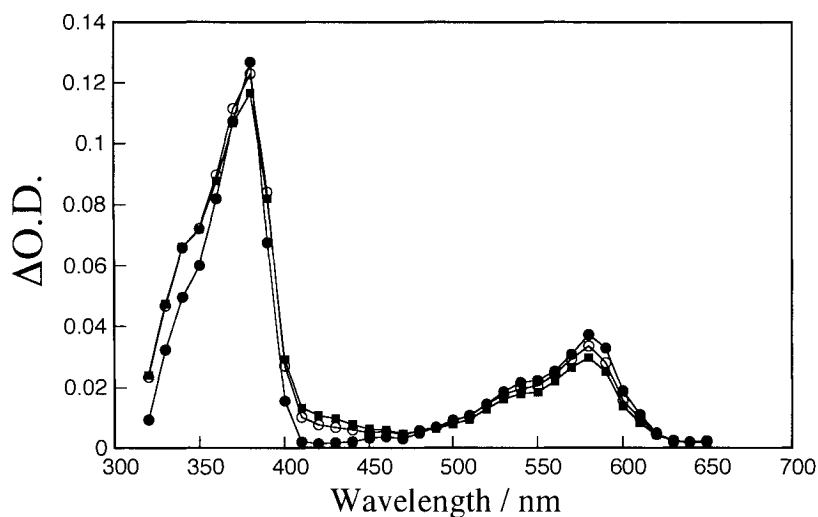
Figure 2.22 Transient absorption spectra recorded (●) 0.48 μs; (O) 2.98 μs and (■) 6.32 μs after 308-nm laser irradiation of isoeugenol in acetonitrile.containing 0.7 mM $HClO_4$.
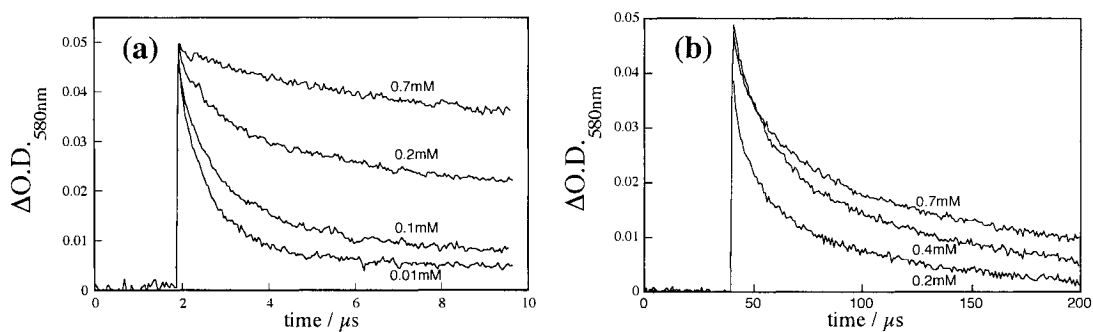
Figure 2.23 Time resolved absorption changes at 580 nm observed along (a) 8 μs, and (b) 160 μs after 308-nm laser irradiation of isoeugenol in acidic acetonitrile containing variable amounts of $HClO_4$.
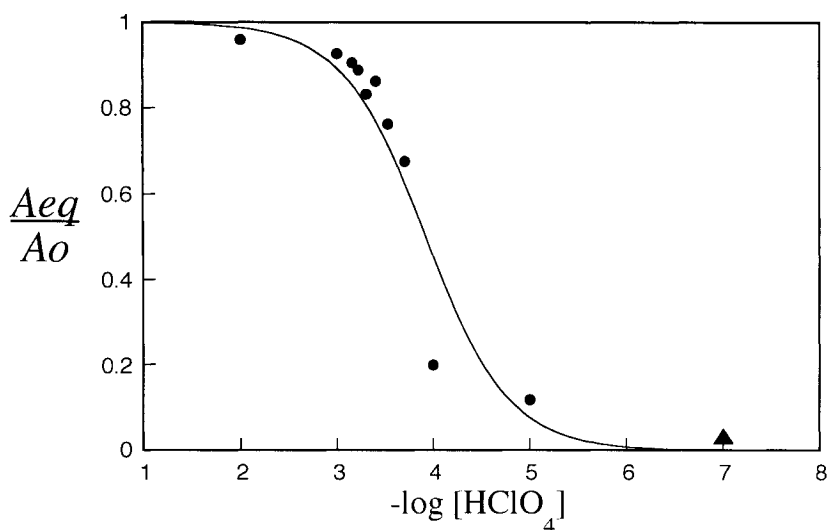
Figure 2.24 Changes in the fraction of isoeugenol radical cation in the equilibrium state with the perchloric acid content in acetonitrile. The point at $-\log[HClO_4] = 7$ corresponds to the fraction measured in neat acetonitrile and was not included in the fitting process to determine the acid constant of the radical cation.
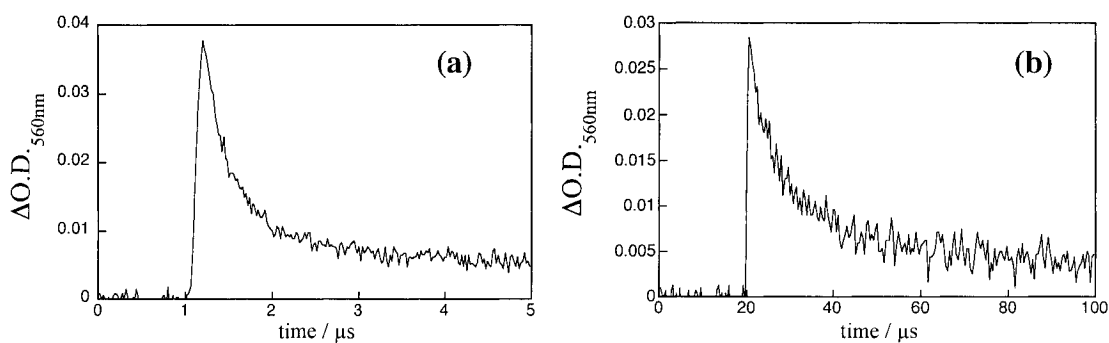
Figure 2.25 Time resolved absorption changes at 560 nm after 308-nm laser irradiation of 2-methoxy-4-vinylphenol in acetonitrile containing (a) 1 x 10^{-5} M of $HClO_4$ and (b) 2 x 10^{-3} M of $HClO_4$.

114
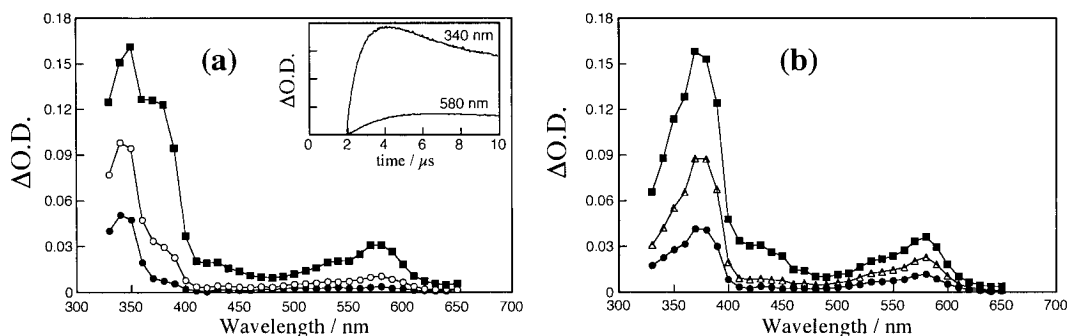
Figure 2.26 Transient absorption spectra recorded (●) 0.18 μs; (○) 0.54 μs and (■) 3.06 μs after 355-nm laser irradiation of 10 % di-*tert*-butylperoxide in acidic acetonitrile containing 6.0 mM isoeugenol and (a) 1.0 mM HClO₄ or (b) 10 mM HClO₄. Inset in (a) shows time-resolved absorption changes at 340 and 580 nm observed after 355-nm laser irradiation of 10 % di-*tert*-butylperoxide in acidic acetonitrile containing 6.0 mM isoeugenol and 1.5 mM HClO₄
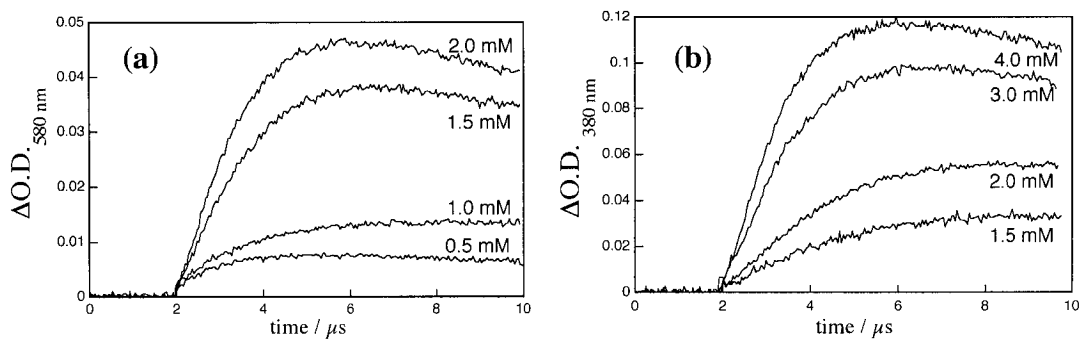
Figure 2.27 Time resolved absorption changes at (a) 580 and (b) 380 nm observed upon 355-nm laser irradiation of 10 % di-*tert*-butylperoxide in acidic acetonitrile containing 6.0 mM isoeugenol and changing amounts of HClO₄.

115
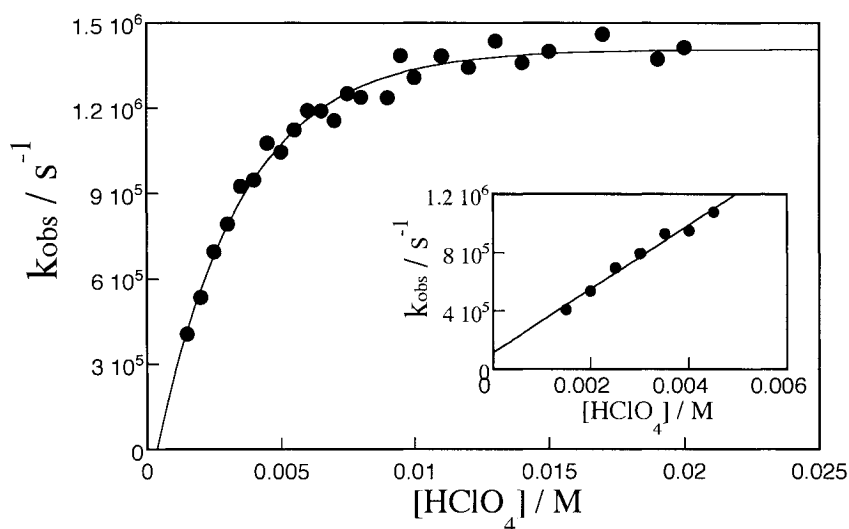
Figure 2.28 Relationship between observed rate constant for the growth isoeugenol radical cation at 580 nm and the concentration of perchloric acid in air-saturated acetonitrile.
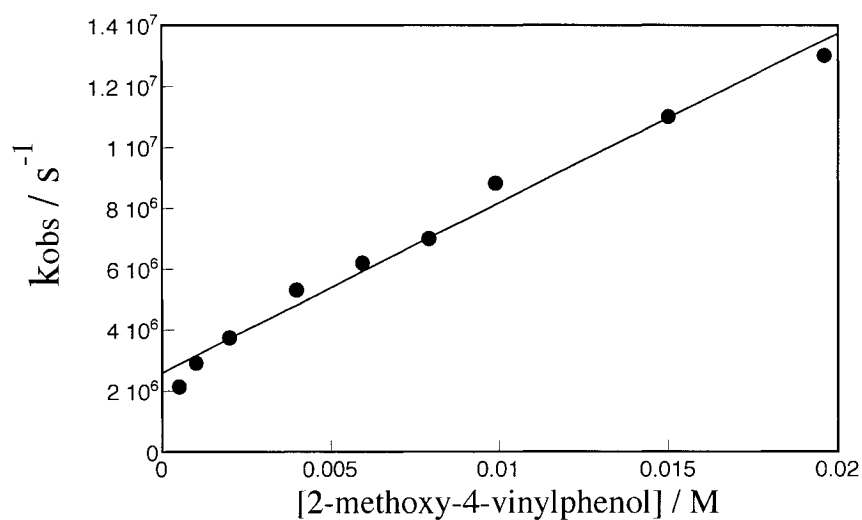
Figure 2.29 Relationship between observed rate constant for the decay of 2-methoxy-4-vinylphenol radical cation at 560 nm, generated by photoinduced electron transfer using chloranil, and the concentration of 2-methoxy-4-vinylphenol in N_2-saturated acetonitrile.
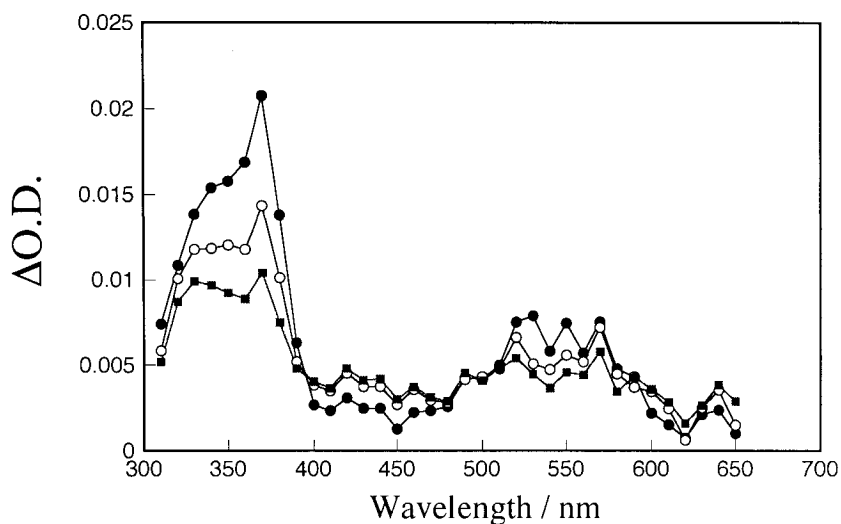
Figure 2.30 Transient absorption spectra recorded (●) 1.8 μs; (O) 6.12 μs and (■) 12.8 μs after 308-nm laser irradiation of 3,4-dimethoxystyrene in N_2-saturated acetonitrile.
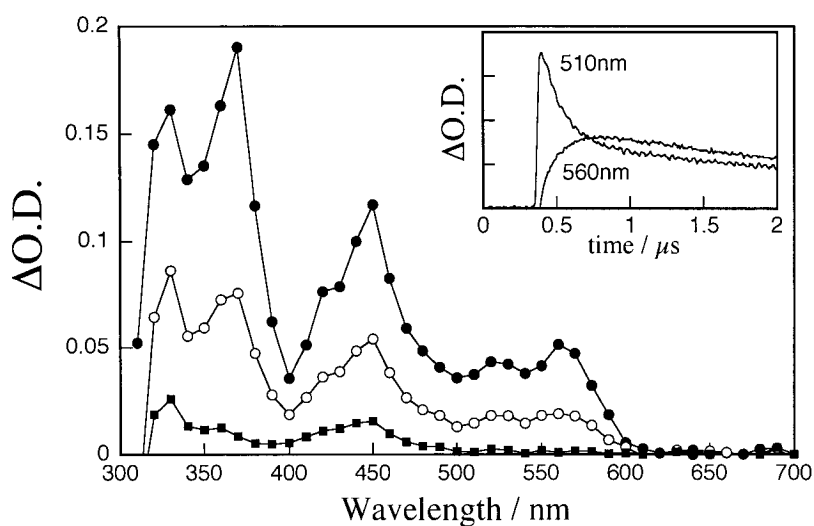
Figure 2.31 Transient absorption spectra recorded (●) 1.40 μs; (O) 5.00 μs and (■) 30.6 μs after 355-nm laser irradiation of chloranil in N_2-saturated acetonitrile containing 1.0 mM 3,4-dimethoxystyrene.

117
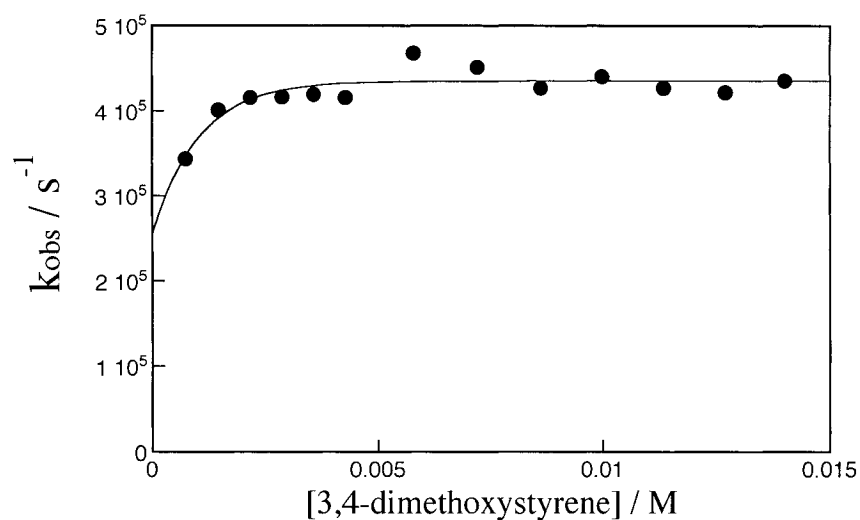
Figure 2.32 Relationship between observed rate constant for the decay of 3,4-dimethoxystyrene radical cation at 560 nm, generated by photoinduced electron transfer using chloranil, and the concentration of 3,4-dimethoxystyrene in N_2-saturated acetonitrile.
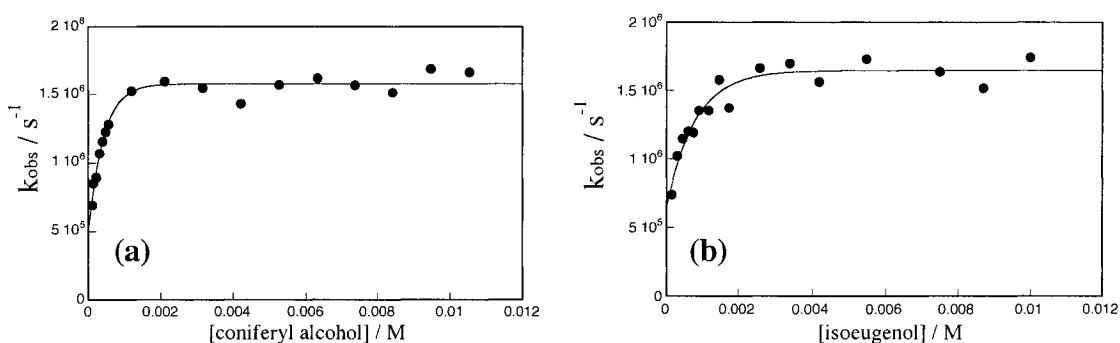
Figure 2.33 Relationship between observed rate constant for the decay of (a) coniferyl alcohol radical cation, and (b) isoeugenol radical cation at 580 nm and the concentration of their neutral precursors in N_2-saturated acetonitrile. Both radical cations were generated by photoinduced electron transfer using chloranil as sensitizer.

118
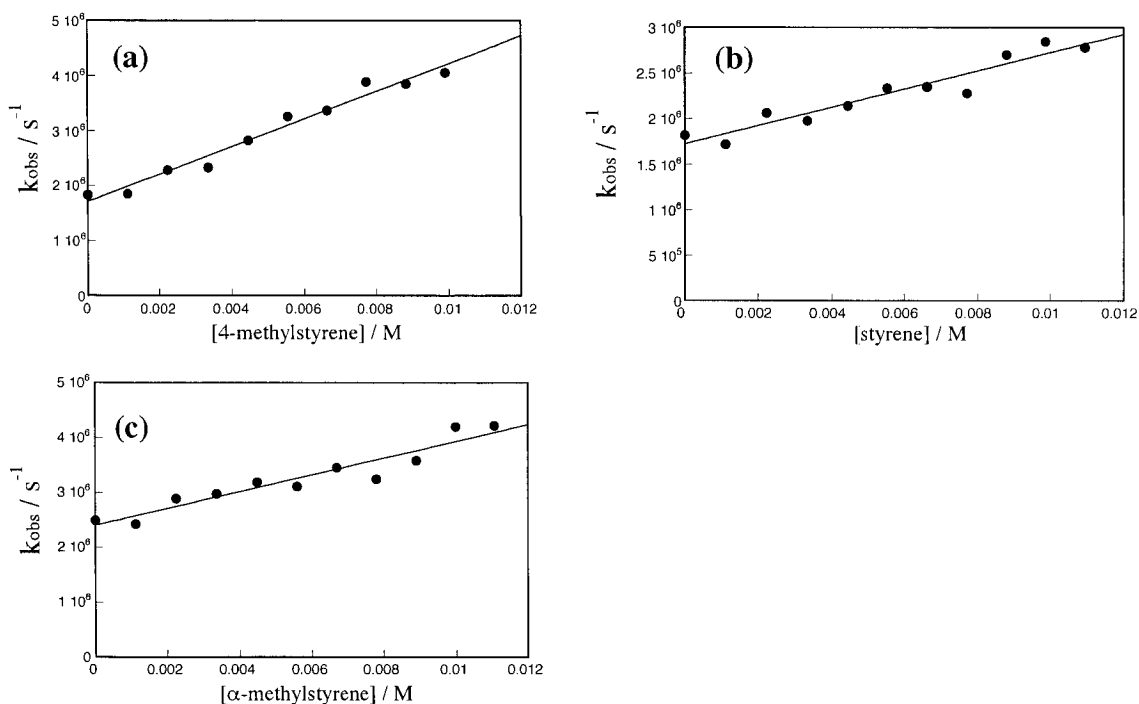
Figure 2.34 Relationship between observed rate constant for the decay of 2-methoxy-4-vinylphenol radical cation at 560 nm and the concentration of (a) 4-methylstyrene, (b) styrene, and (c) α-methylstyrene in N_2-saturated acetonitrile. The generation of the radical cation was carried out by 308-nm laser irradiation of 2-methoxy-4-vinylphenol.
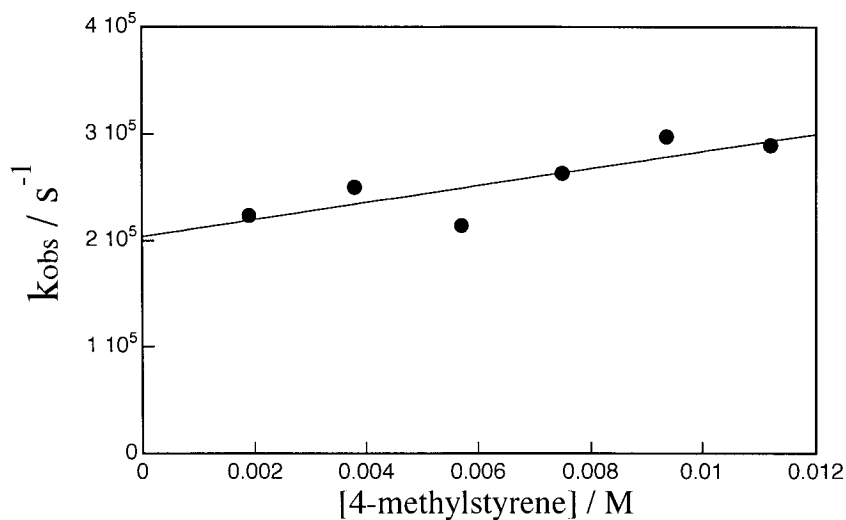
Figure 2.35 Relationship between observed rate constant for the decay of 2-methoxy-4-vinylphenol radical cation at 360 nm and the concentration of 4-methylstyrene in acetonitrile containing 1.0 mM $HClO_4$.

119
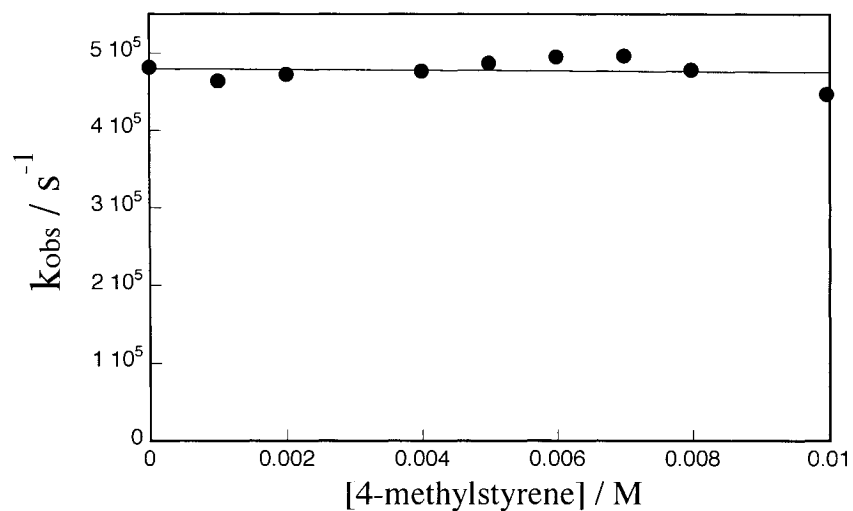
Figure 2.36   Relationship between observed rate constant for the decay of 3,4-dimethoxystyrene radical cation at 560 nm and the concentration of 4-methylstyrene in N$_2$-saturated acetonitrile.   The generation of the radical cation was carried out by 308-nm laser irradiation of 3,4-dimethoxystyrene.
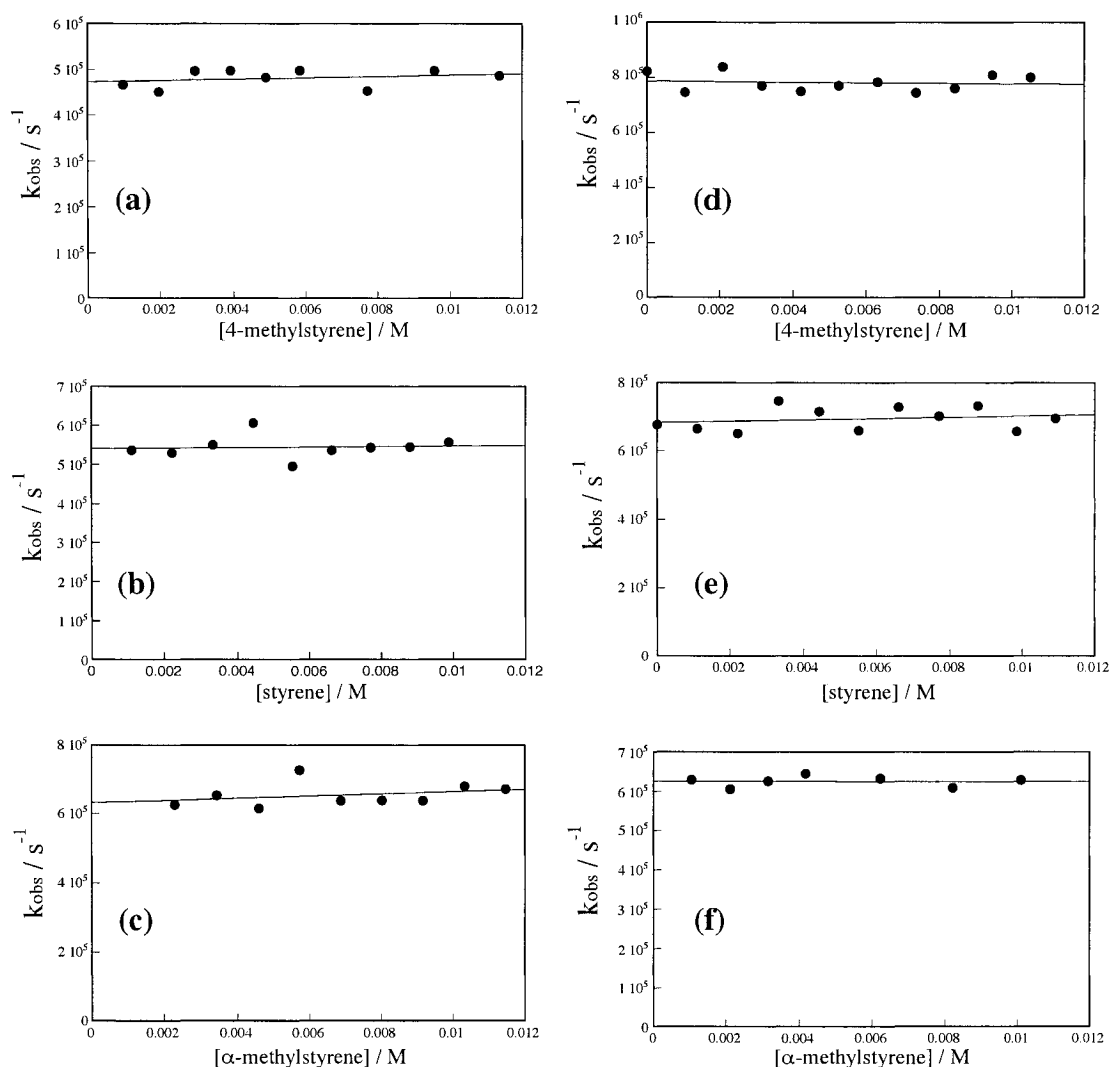
Figure 2.37 Relationship between observed rate constant for the decay of coniferyl alcohol radical cation at 580 nm and the concentration of (a) 4-methylstyrene, (b) styrene, and (c) α-methylstyrene in N_2-saturated acetonitrile. Relationship between observed rate constant for the decay of isoeugenol radical cation at 580 nm and the concentration of (d) 4-methylstyrene, (e) styrene, and (f) α-methylstyrene in N_2-saturated acetonitrile. The generation of the radical cations was carried out by 308-nm laser irradiation of the neutral parent.

121

Chapter III. 1,2-Diaryl Enol Radical Cations in Solution

3.1 Introduction

The 4-vinylphenol radical cations described in the previous section are fundamentally distinct from other styrene radical cations by virtue of the presence of the highly acidic phenolic hydroxy group. Similarly, if the hydroxy group is placed directly on the vinyl group of a styrene as in an enol, the radical cation of that enol would again possess a highly acidic enolic hydroxy group, as suggested by the resonance structures in Scheme 3.1. Thus, while 4-vinylphenol and phenylethenol radical cations may posssess considerably different properties, they are clearly linked by having acidic hydroxyl groups directly attached to the arylethene framework.

Scheme 3.1
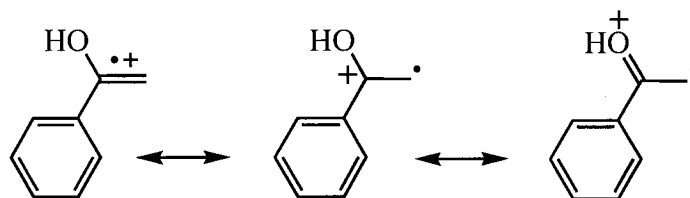
In the present chapter, a review of the known chemistry of enol radical cations is given, followed by a detailed description of results from investigation into the chemistry of some 1,2-diarylethenol radical cations and a discussion of those results. Special attention is focused on utilizing a new photochemical method for generation of the enol radical cations, and on the effect of aryl substituents on the acidity of the radical cations.

3.1.1 Enol Radical Cations in the Gas Phase

Enol radical cations have been of interest to gas phase chemists for several decades, primarily due to unusual features concerning the tautomerization of enol radical cations to keto radical cations. Enol radical cations in the gas phase have been generally studied by mass spectrometry.[90] The preparation of these species has been mostly carried out by McLafferty rearrangement of aldehydes, ketones and carboxylic acids.[91] The McLafferty rearrangement, also called γ-hydrogen rearrangement, is basically the fragmentation of an ionized ketone, aldehyde or carboxylic acid derivative. The rearrangement is formally analogous to the photolytic Norrish II reactions, Scheme 3.2. Initially, the ionized carbonyl system undergoes intramolecular γ-hydrogen atom transfer, to give a distonic radical cation. Cleavage of the C2-C3 bond in the radical cation yields a neutral alkene and the enol radical cation.

Scheme 3.2
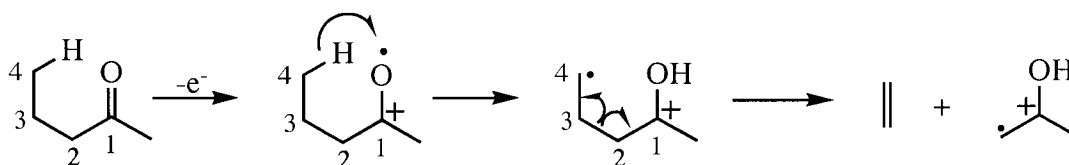
Enols radical cations have also been prepared in gas phase via cycloreversion reactions, which involve the cleavage of ionized cycloalcohols.[91] As shown in Scheme 3.3, the radical cations of cycloalcohols undergo fragmentations to give an enol radical cation and a neutral alkene. Typically, the generation of the cycloalcohol radical cation is carried out by electron impact ionization. The same method is usually employed to ionize the ketones used for McLafferty rearrangements.

Scheme 3.3
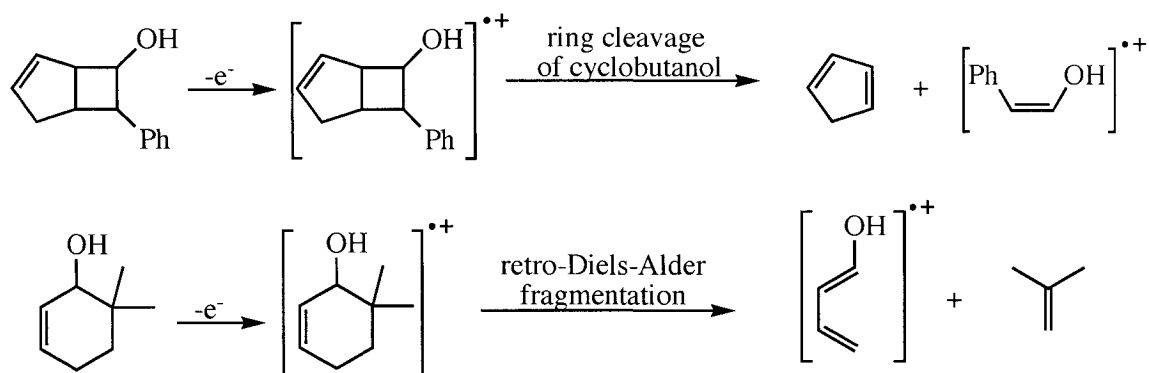
One of the most interesting aspects of the chemistry of keto/enol tautomers is the inversion of the thermodynamic stability of keto/enol forms upon one electron oxidation.[92] Typically, the keto form is more stable than the corresponding enol form; however enol radical cations are more stable than the corresponding keto radical cations. The greater stability of neutral ketones compared to the corresponding enols is mainly due to the stronger bonds involved in ketones compared to those involved in enols, i.e. E[C-H + C-C + C=O] > E[O-H + C-O + C=C]. Specifically the C=O double bond is so strong that it overcomes the fact that the C-O and O-H bonds in the enol form are stronger than the C-C and the C-H bonds in the keto form. On the other hand, the stabilization of enol radical cations over ketone radical cations is a consequence of the amount of energy required to generate these species. Keto radical cations are formed by one electron abstraction from the n-orbital on the oxygen atom of the keto while enol radical cations are produced by removal of one electron from the π-orbital of the enol. The energy needed to remove an electron from the n-orbital of the ketone is much larger than that required to abstract an electron from the π-orbital of the enol. Therefore the generation of an enol radical cation from a neutral enol requires a smaller amount of energy than the generation of a keto radical cation, hence the greater stability of the enol

radical cations compared to ketone radical cations. The inversion of thermodynamic stability upon oxidation has been proved theoretically and experimentally. Figure 3.1 illustrates the energy difference between the enol form and the keto form for several substituted methylcarbonyl substrates, calculated in gas phase.[93] Note the dramatic inversion of stability upon ionization of the tautomers. The diagram included in Figure 3.1 schematically represents the relative energies of neutral and ionized keto/enol pairs.
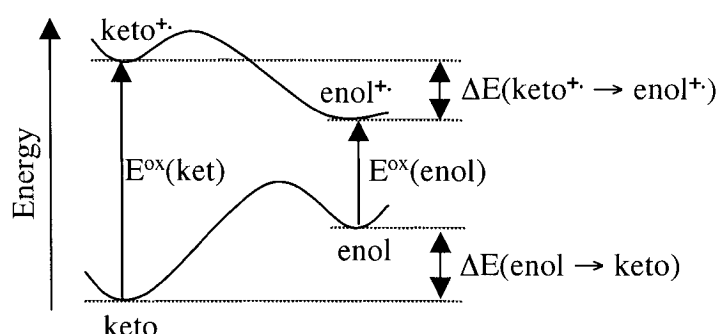
Keto / Enol	ΔE (enol $\rightarrow$ ketone) (kJ / mol)	ΔE (enol$^{+\cdot}$ $\rightarrow$ ketone$^{+\cdot}$) (kJ / mol)
CH_3COF / $CH_2=C(OH)F$	132	-59
CH_3COCH_3 / $CH_2=C(OH)CH_3$	70	-20
CH_3COH / $CH_2=C(OH)H$	68	-33
CH_3COOH / $CH_2=C(OH)OH$	150	-48

Figure 3.1 Relatives and calculated (HF / 6-31G* single point// 3-21 G opt) energy differences of neutral and ionized keto / enol tautomers.[93]

3.1.2 Enol Radical Cations in Biochemistry

Enol radical cations have attracted the attention of the scientific community due to their supposed role in some biological processes like the ribonucleotide reductase process. Stubbe,[94] has hypothesized that enol radical cations are formed by loss of a water molecule from the 3'-ribonucleotide radical, Scheme 3.4. The resulting enol

radical cation would then be reduced by the transfer of two electrons and one proton from the dithiol to give an intermediate 3'-deoxynucleothide radical, which is further reduced to the deoxyribonucleotide, Scheme 3.4.

Scheme 3.4
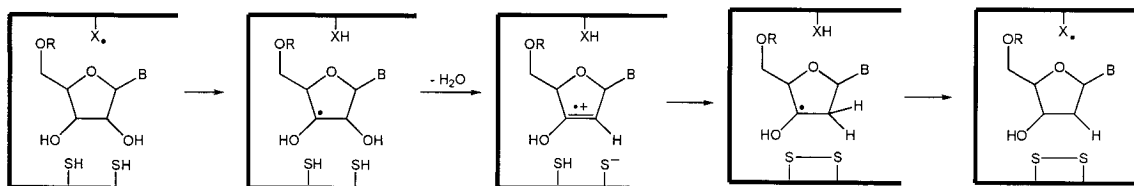
Enol radical cations might also be involved in the cycle of diol dehydrase (DDH),[95] an enzyme that catalyzes the 3,4-anhydroadenosylcobalamin (AdoCbl)-dependent dehydration of vicinal diols to the corresponding aldehydes.[96] Scheme 3.5 illustrates the mechanism of dehydration of 1,2-propanediol. Initially, the diol dehydrase catalyzes the cleavage of the Co-C bond of AdoCbl to generate Cbl^{II} and a 5'-deoxyadenosyl radical. Hydrogen atom abstraction from C_1 of 1,2-propanediol results in the formation of the diol radical and 5'-deoxyadenosine (Ado-CH$_3$). Acid catalyzed water elimination from the diol radical generates an enol radical cation that is transformed to an α-carbonyl radical by loss of a proton. Hydrogen atom transfer from 5'-deoxyadenosine to the α-carbonyl radical, finally gives the aldehyde and the 5'-deoxyadenosyl radical. Recombination of the 5'-deoxyadenosyl radical with Cbl^{II} regenerates the 3,4-anhydroadenosylcobalamin.

Scheme 3.5
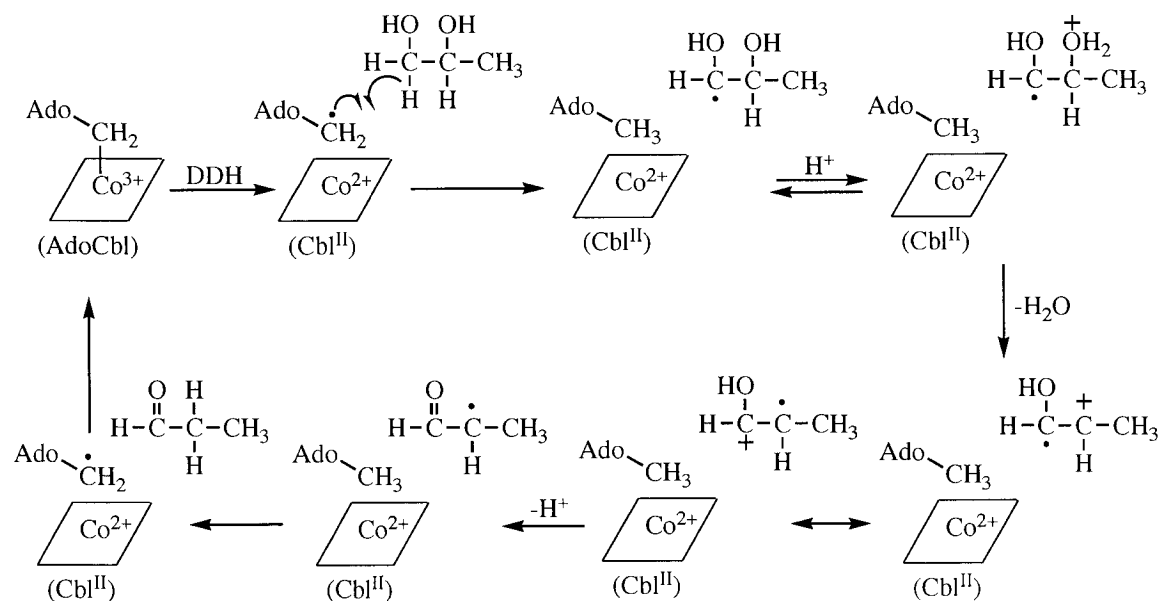
Ado-CH$_3$ = 5-deoxy-adenosyne

It must be mentioned that the mechanism shown in Scheme 3.5 is not the only mechanism proposed to explain the biochemical transformation of vicinal diols to aldehydes. Actually, several authors have proposed a different mechanism that does not involve the intermediacy of enol radical cations.[96, 97] Instead, it has been suggested that the 1,2-diol radical formed upon hydrogen atom transfer from the diol to the 5'-deoxyadenosyl radical undergoes intramolecular hydroxyl radical migration to give a 1,1-diol radical, Scheme 3.6. Further hydrogen abstraction from 5'-deoxyadenosine gives the 1,1-diol, which is finally transformed to the aldehyde by elimination of one molecule of water.

Scheme 3.6

127
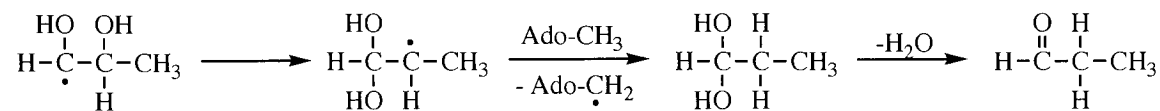
3.1.3 Generation and Reactivity of Enol Radical Cations in Solution

While the chemistry of enol radical cations in gas phase has been considerably explored, only a very small amount of work has been dedicated to study these species in condensed phase. Most simple enols are typically not isolable by virtue of their thermodynamic instability. Thus, the amount of enol in equilibrium with the keto form is typically very small, and ionization of the enol form to generate the enol radical cation is not a generally feasible method to produce detectable amounts of the enol radical cation.

Based on the greater stability of enol radical cations compared to ketone radical cations, it might be expected that the former species could be produced by oxidation of neutral ketones to ketone radical cations followed by tautomerization of the keto radical cations to the enol radical cations. However this approach is not viable for most ketones because the rearrangement of ketone radical cation to enol radical cation is too slow. Calculations involving the isomerization of acetone radical cation to the corresponding enol radical cation have established that the activation barrier for this transformation is much higher than the barriers for other processes like bond dissociation.[98] Therefore, the keto$^{+\cdot}$ → enol$^{+\cdot}$ isomerization will be precluded since other low-energy processes will prevail. For instance, anodic oxidation of 2-hexanone in acetonitrile initially gives the 2-hexanone radical cation. However, this species does not isomerize to the enol radical cation. Instead, the ketone radical cation undergoes γ-hydrogen abstraction to yield a distonic radical cation that is further oxidized to give a carbocation that ultimately yields γ-acetamido-2-hexanone and 2,4,7-trimethyl-4,5-dihydro-1,3-oxazepine, Scheme 3.7.[99]

Scheme 3.7
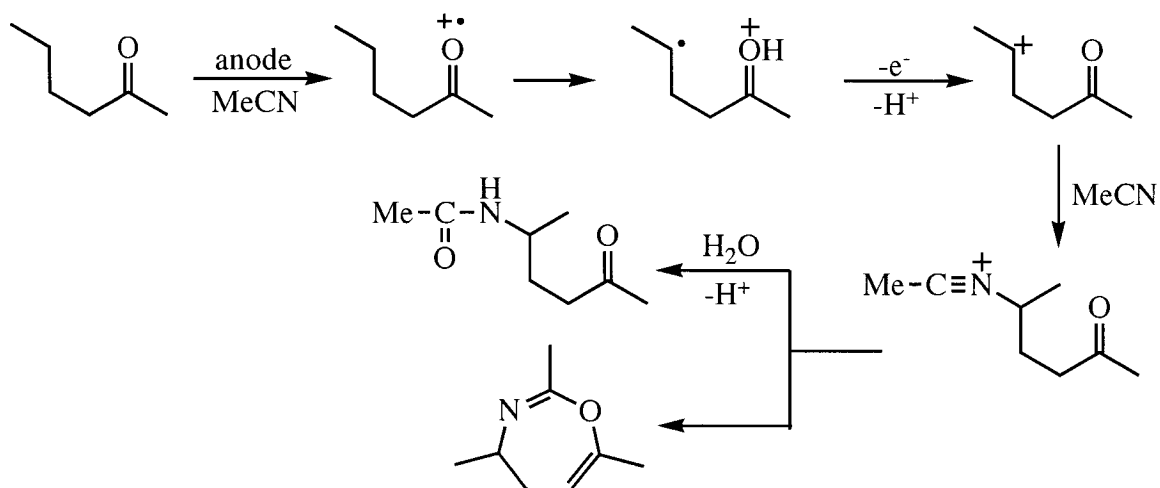
` It must be mentioned that the isomerization of ionized ketones to the corresponding

radical cations has been achieved under cryogenic conditions. Marcineck et al,[100] have

been able to detect the formation of the enol radical cation represented in Scheme 3.8

upon oxidation of o-methylacetophenone and related species in argon matrices. The

ketones were ionized by X-rays and the resulting species were studied by UV-VIS and IR

spectra. According to this study the radical cation of o-methylacetophenone was

transformed to the enol radical cation with first-order rate constant of 454 s^{-1} at 93 K.

Scheme 3.8
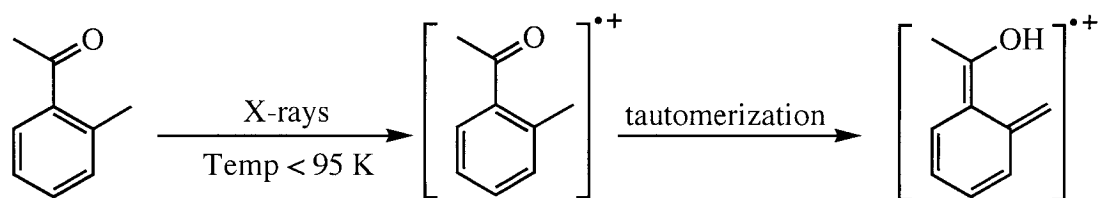
Enol radical cations can be generated by selective oxidation of the neutral enol form

in equilibrium with the keto form. That is, given that the enol form is more easily

oxidized than the keto tautomer it is possible to selectively oxidize the enol form by using

an appropriate oxidant. For instance, Orliac-Le Moing et al.[101] have observed a linear

correlation between the anodic current measured by cyclic voltammetry and the enol content for various α-cyano ketones in acetonitrile, Scheme 3.9.

Scheme 3.9

R$_1$	R$_2$
C$_6$H$_5$	H
C$_6$H$_5$	CH$_3$
4-CH$_3$OC$_6$H$_4$	H
4-CH$_3$OC$_6$H$_4$	CH$_3$
4-CH$_3$OC$_6$H$_4$	CH$_3$C$_6$H$_5$
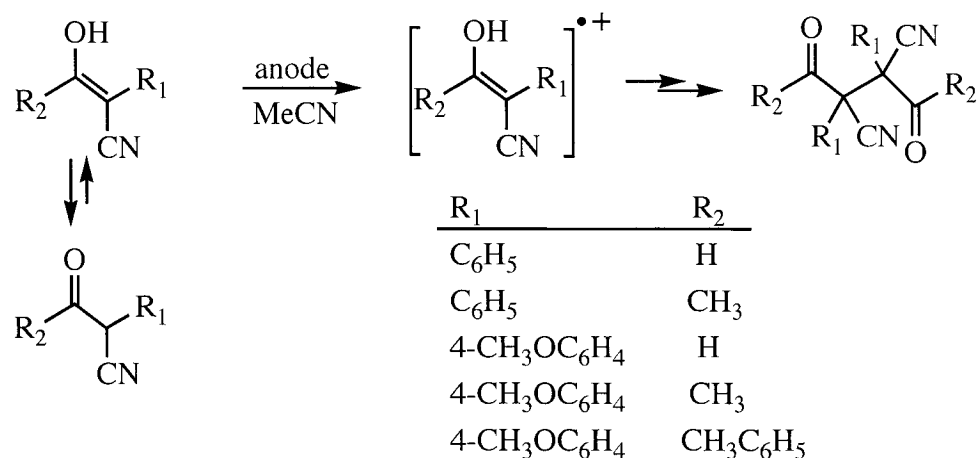
The corresponding 1,4-diketones were generated in about 90% yield upon electrolysis of the α-cyano ketones. According to Orliac-Le Moing et al.,[101] the 1,4-diketones could be formed from the enol radical cation by any of the three different routes shown in Scheme 3.10. The first route involves the deprotonation of the enol radical cation to yield an α-carbonyl radical that then dimerizes to yield the 1,4-diketone. The second route also involves the formation of the α-carbonyl radical by deprotonation of the enol radical cation, but in this case, the radical undergoes a one electron oxidation to form an α-carbonyl carbocation that then reacts with a neutral enol to give the corresponding diketone. The last path involves the generation of a β-hydroxyl radical by a nucleophilic attack to the enol radical cation. This β-hydroxyl radical can either undergo an elimination of HNu to generate an α-carbonyl radical or it can dimerize by a coupling reaction accompanied by elimination of two HNu molecules to yield the corresponding 1,4-diketone. Most of the experiments reported by Orliac-Le Moing et

al.[101] involved the use of water as a nucleophile, although they also used other nucleophiles like cyanide and *tert*-butanol.

Scheme 3.10
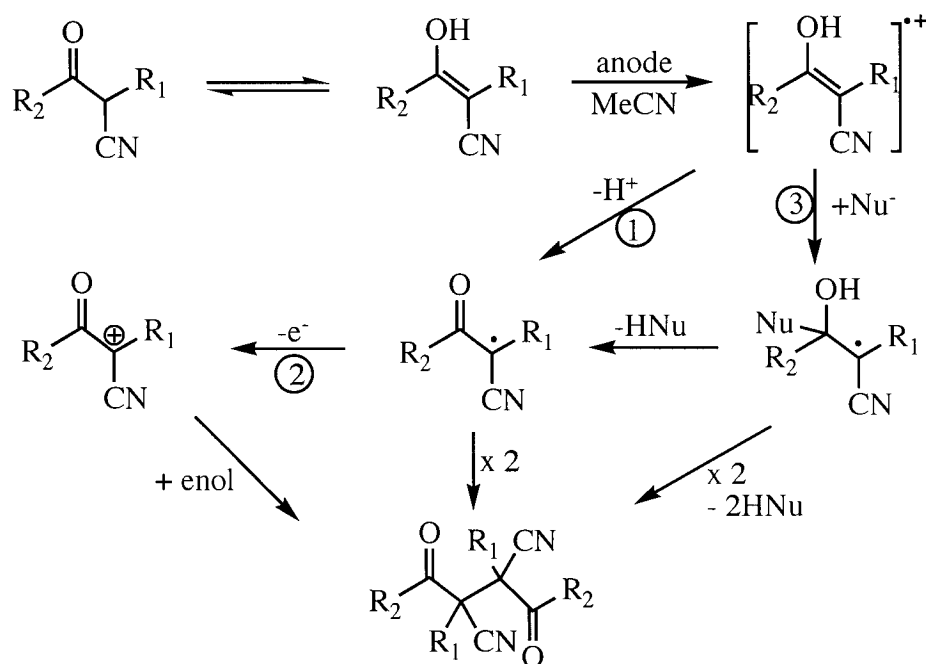
An obvious problem present in these studies is the fact that both the enol and the keto tautomers are simultaneously present during the reactions being studied. However, unambiguous results can be obtained by using stable simple enols which can be isolated from the corresponding keto tautomers. Fuson[102] and Rappoport[103] have shown that sterically hindered enols containing bulky aromatic groups are stabilized and can be obtained pure from their corresponding keto tautomer. Presumably, the reason for such stabilization is the combination of electronic and steric effects. The conjugation of the aromatic groups with the double bond and the OH group in the enol form stabilizes the C=C double bond. Additionally, the presence of steric bulk destabilizes the keto form, specially when two bulky substituents are in the α-carbon. The bonding angle in the enol

131

form is 120 °, which allows both substituents farther apart than in the keto form with bonding angles of 109 °.

The possibility of preparing tautomerically pure simple enols has been exploited to generate the corresponding enol radical cations by simple chemical or electrochemical oxidation of the neutral species. For instance derivatives of 2-mesitylethenol were transformed into the corresponding benzofurans, Scheme 3.11, by treating these enols with chemical oxidants like triarylaminium salts, iron(III) phenanthroline (FePHEN) or thianthrenium perchlorate. Identical products were obtained in cyclic voltammetry studies as well as in electro oxidation experiments, suggesting the intermediacy of the enol radical cations in these reactions.[92]

Scheme 3.11
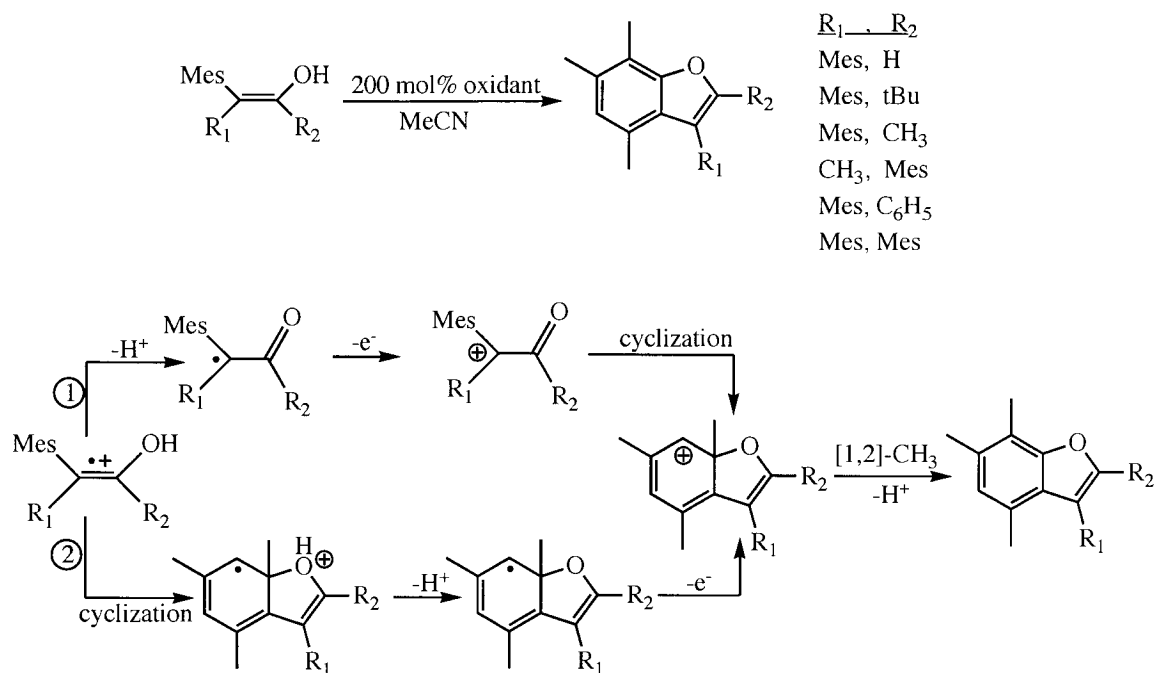
Two mechanisms were proposed to account for the formation of the benzofurans derivative from the enol radical cation, Scheme 3.11. The first mechanism involves the deprotonation of the radical cation to yield an α-carbonyl radical which is then further

oxidized to an α-carbonyl carbocation. Intramolecular cyclization of the carbocation

followed by 1,2 methyl shift and loss of a proton finally yielded the benzofuran

derivative. The second mechanism involves an intramolecular cyclization of the enol

radical cation followed by a rapid loss of a proton to give a cyclic radical species.

Further oxidation of the radical system yielded the same α-carbonyl carbocation

proposed in the first mechanism.

The benzofuran derivatives were the only products obtained from the most

sterically hindered enols, Scheme 3.11 (R_1 = Mes), even in presence of nucleophiles like

methanol. However, when less sterically hindered enols, Scheme 3.11 (R_1 = Ph or Me),

were used, the formation of nucleophile-incorporated compounds was observed, Scheme

3.12.

Scheme 3.12
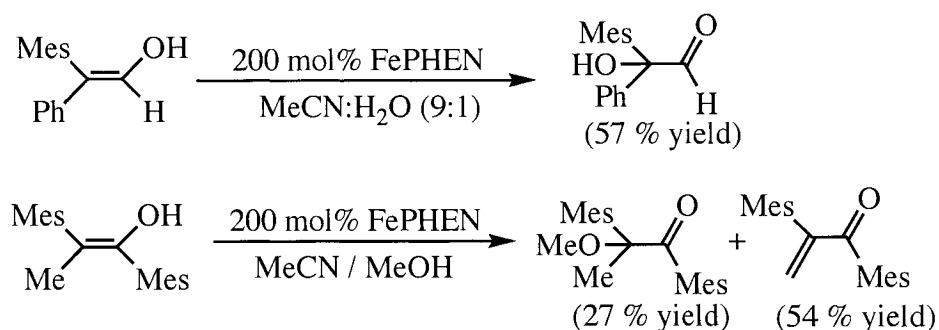
The formation of nucleophile-incorporated systems mentioned above might take

place by three different mechanisms as shown in Scheme 3.13.[92] The first two

mechanisms initially involve a nucleophilic attack to the α or β positions of the enol

radical cation to give radical species. Further oxidation of the radicals generated in the

first step yields the corresponding α or β carbocations which can either get deprotonated

(mechanism 1) to give the final product or incorporate a second molecule of nucleophile

(mechanism 2) to give a disubstituted system which then undergoes an elimination reaction to yield the β-substituted ketone. On the other hand mechanism 3 initially involves a deprotonation of the enol radical cation to give an α-carbonyl radical which is then oxidized to the corresponding α-carbonyl cation. Further addition of the nucleophile to this carbocation finally yields the substituted ketone.

Scheme 3.13
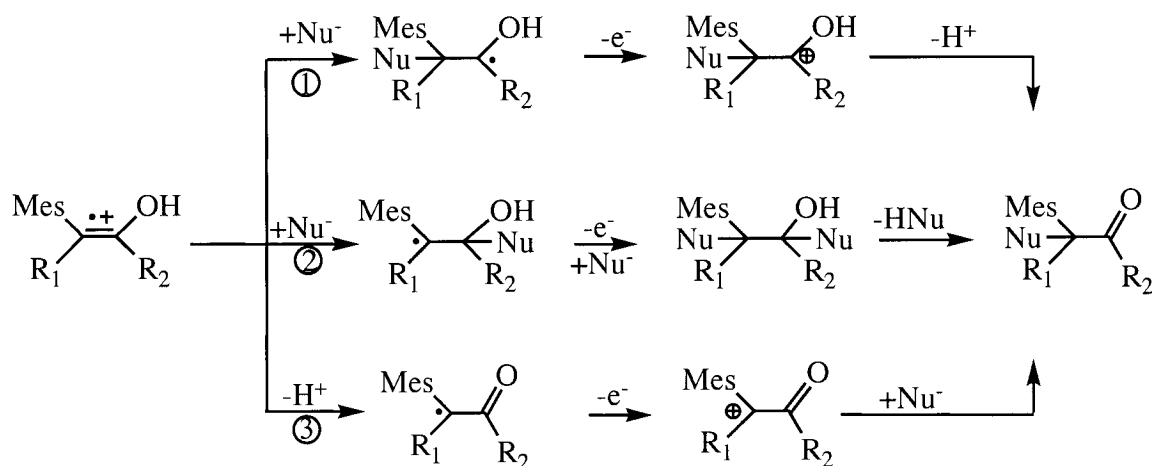
According to mechanisms 1 and 2, the primary reaction of an enol radical cation is a nucleophilic addition at the double bond, while mechanism 3 suggests the major reaction of enol radical cations is deprotonation. It should be mentioned that no direct evidence was obtained to differentiate between mechanism 1, 2, and 3 represented in Scheme 3.13. However, Schmittel[92] and co-workers excluded pathways 1 and 2 as viable mechanisms based on the following results. They showed that the radical cations of 2-mesityl-2-phenylethenol and 1,2-dimesitylprop-1-en-1-ol in acetonitrile are unstable even in the microsecond time scale while the corresponding methyl enol ethers radical cations, Scheme 3.14, have lifetimes in the order of seconds under the same conditions.[92] Therefore, the substitution of the labile enolic proton for a methyl group increases the lifetime of the radical cations more than 10^5 times. This observation clearly suggests that
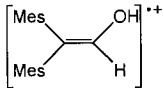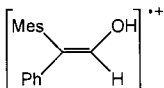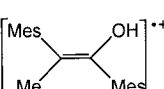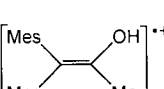
the main reaction of the enol radical cations is deprotonation and not nucleophilic addition. Additionally, the second order rate constants for the reaction of acetonitrile with the methyl enol ether radical cations are below 10 M^{-1} s^{-1}. Assuming that the corresponding enol radical cations also react with acetonitrile with a rate constant of 10 M^{-1} s^{-1} then the enol radical cations should have a lifetime of 5 ms in neat acetonitrile, [MeCN] = 19.1 M, if deprotonation does not take place. That is, the lifetimes of the enol radical cations would be almost 5000 times larger than those observed in the actual experiments. Clearly, the fast deprotonation of enol radical cations is the reason for the short lifetime of these species. It is worth noting that Schmittel[92] reported that the methyl enol ether radical cations shown in Scheme 3.14 have lifetimes of several seconds; however based on second-order rate constants for the reaction of these methyl enol ether radical cations with acetonitrile, the lifetimes of these species in acetonitrile range between 7 ms and 0.5 s. Despite this contradiction, the lifetimes of enol ether radical cations are almost four orders of magnitude longer than the lifetimes of enol radical cations, and it is reasonable to conclude that the primary reaction of enol radical cations is the loss of a proton.

Scheme 3.14

(Z)-2-mesityl-2-phenylethenol

(Z)-2-(2-methoxy-1-phenylvinyl)
-1,3,5-trimethylbenzene

(Z)-1,2-dimesitylprop-1-en-1-ol

(Z)-1,2-dimesityl-1-methoxyprop-1-ene
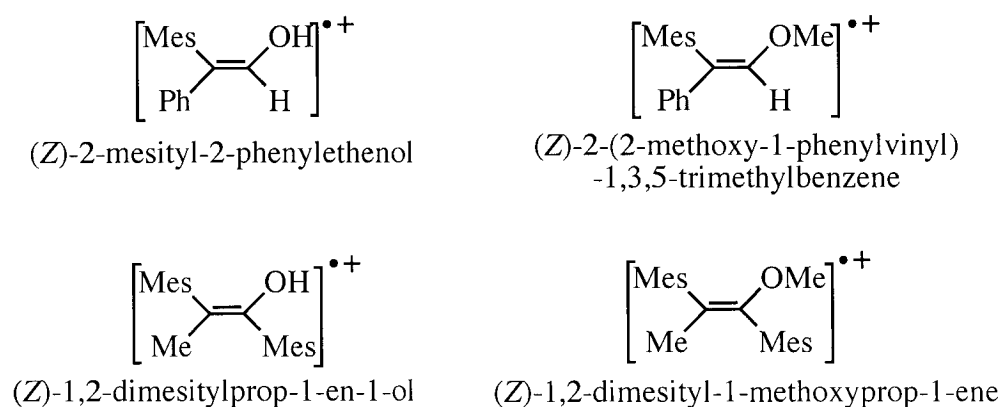
The proposed deprotonation of enol radical cations is consistent with the high acidity estimated for these species. Table 3.1 lists the acid dissociation constants for several enol radical cations in acetonitrile estimated by a thermodynamic cycle.[92] The acid dissociation constants are very sensitive to the nature of the substituents attached to the C-C double bond. For instance, the substitution of one mesityl group for a phenyl group decreases the pK$_a$ from 5.7 to 4.4. Similarly, the position of the substituents on the C-C double bond has a large influence on the acidity of enol radical cations. Exchange between the methyl and mesityl group of 1,1-dimesitylprop-1-en-2-ol to give 1,2-dimesitylprop-1-en-1-ol causes a dramatic increase in acidity, with the pK$_a$ decreasing from 5.6 to 1.3.

Table 3.1 Estimated pK$_a$ values for various enol radical cations in MeCN

Enol Radical Cation	pK$_a$ (in MeCN)
	5.7
	4.4
	1.3
	5.6

Stopped flow studies involving the transformation of β-hydroxyvinyl radicals to α-carbonyl radicals suggest that short-lived enol radical cations might be formed by protonation of β-hydroxyvinyl radicals. According to Gilbert et al.[104] reaction of hydroxyl radicals with but-2-yne-1,4-diol in water leads to the formation of a β-

hydroxyvinyl radical that undergoes acid-catalyzed conversion into an α-carbonyl radical, Scheme 3.15. The authors were able to detect both, the β-hydroxyvinyl and α-carbonyl radical species by epr spectroscopy and based on their observations they suggest the intermediacy of an enol radical cation; however the enol radical cation was not detected.

Scheme 3.15

β-hydroxyvinyl radical   enol radical cation   α-carbonyl radical
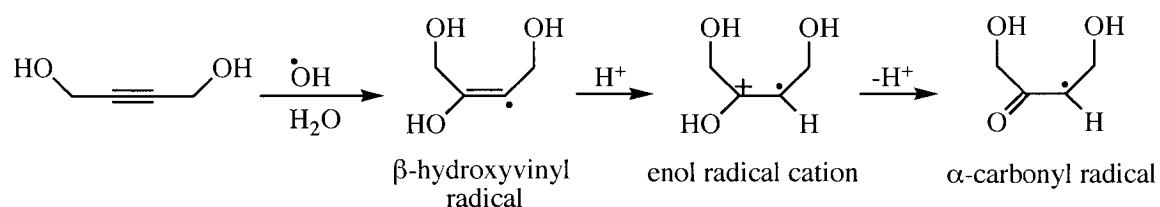
Schepp[105] has recently reported a completely different approach to generate short-lived enol radical cations in solution. Accordingly, 1-(4-methoxyphenyl)prop-1-en-2-ol radical cation is produced by protonation of the corresponding α-carbonyl radical initially generated by laser flash photolysis of 1-bromo-1-(4-methoxyphenyl)propan-2-one, Scheme 3.16.

Scheme 3.16.
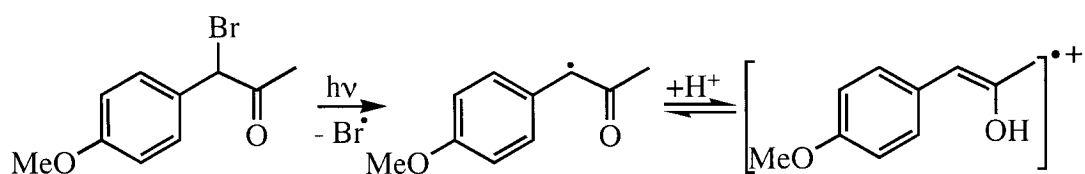
Transient absorption spectroscopy allowed the direct observation of this enol radical cation, which is characterized by strong absorption bands centered at 380 and 600nm. In addition the pK_a of this species was estimated to be 3.2 in acetonitrile, which is consistent with the high acidity characteristic of enol radical cations. The

137

deprotonation of this enol radical cation takes place with a rate constant of 3.9 x 10^6 s^{-1} in acetonitrile, limiting the lifetime of this species to *ca.* 250 ns.

In summary enol radical cations can be generated by three different approaches, namely, (i) selective oxidation of the enol form in equilibrium with the keto tautomer, (ii) oxidation of pure enols, which is obviously limited to very stable enols and (iii) protonation of α-carbonyl radicals, which allows the generation of radical cations of unstable neutral enols. The major reaction pathway for the decay of enol radical cations is the loss of a proton. The deprotonation is generally very fast, which seems to be the reason for the short lifetimes of these species.

3.1.4 Photochemistry of α-Haloketones

Protonation of α-carbonyl radicals produced by photolysis of α-haloketones is the method used in this thesis to generate enol radical cations. A brief review of the photochemistry of α-haloketones is given in this section.

The photochemistry of α-haloketones has been studied in gas phase and in solution. Generally, irradiation of α-haloketones leads to cleavage of the carbon-halogen bond. The cleavage may either be a heterolytic process, giving an α-carbonyl cation and an halogen anion or more frequently, a homolytic process that results in the formation of α-carbonyl radicals and halogen atoms.[106] For instance, irradiation (313 nm) of chloroacetone in vapor phase gives acetone, hydrogen chloride and acetonylacetone as the major products.[107] The mechanism of formation of these compounds involves the coupling or hydrogen atom abstraction by radical species formed upon photohomolysis of the carbon-chloro bond of chloroacetone, Scheme 3.17. The mechanism is supported by

results from studies involving irradiation of chloroacetone and bromoacetone in cyclohexene, that also gives radical-derived products.[108]

Scheme 3.17

$$Cl\text{-}CH_2\text{-}C(=O)\text{-}CH_3 \xrightarrow[313\ nm]{h\nu} \ {}^{\bullet}CH_2\text{-}C(=O)\text{-}CH_3 \ + \ Cl^{\bullet}$$

$$CH_3\text{-}C(=O)\text{-}CH_3 \ + \ Cl^{\bullet} \longrightarrow \ {}^{\bullet}CH_2\text{-}C(=O)\text{-}CH_3 \ + \ HCl$$

$$2\ {}^{\bullet}CH_2\text{-}C(=O)\text{-}CH_3 \longrightarrow CH_3\text{-}C(=O)\text{-}CH_2\text{-}CH_2\text{-}C(=O)\text{-}CH_3$$

(acetonylacetone)
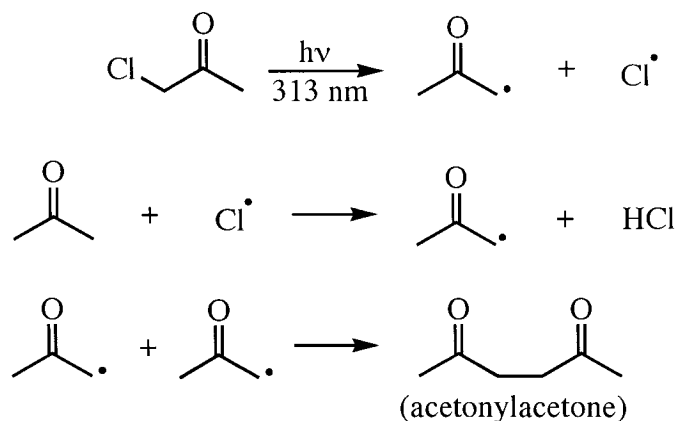
Similarly, laser flash photolysis (266 nm) of 3-bromo-2-coumaranone in cyclohexane results in the homolytic cleavage of the C-Br bond, giving a bromo radical and the 2-coumaranone radical which was detected by transient absorption spectroscopy (λ_{max} = 400 nm).[109] The products obtained upon photolysis of 3-bromo-2-coumaranone at 300 nm in toluene are consistent with a radical mechanism, Scheme 3.18.[109] The initially formed 2-coumaranone radical can either undergo coupling reaction with another 2-coumaranone radical to give a 2-coumaranone dimer, or can abstract an hydrogen atom from toluene to yield 2-coumaranone and a benzyl radical. Coupling of this benzyl radical with a bromo radical gives benzylbromide.

Scheme 3.18

Br

(3-bromo-2-coumaranone) $\xrightarrow[\text{toluene}]{\text{h}\nu \text{ at 300 nm}}$ + Br

+ $\longrightarrow$

+ PhCH$_3$ $\longrightarrow$ + PhCH$_2$

PhCH$_2$ + Br $\longrightarrow$ PhCH$_2$Br
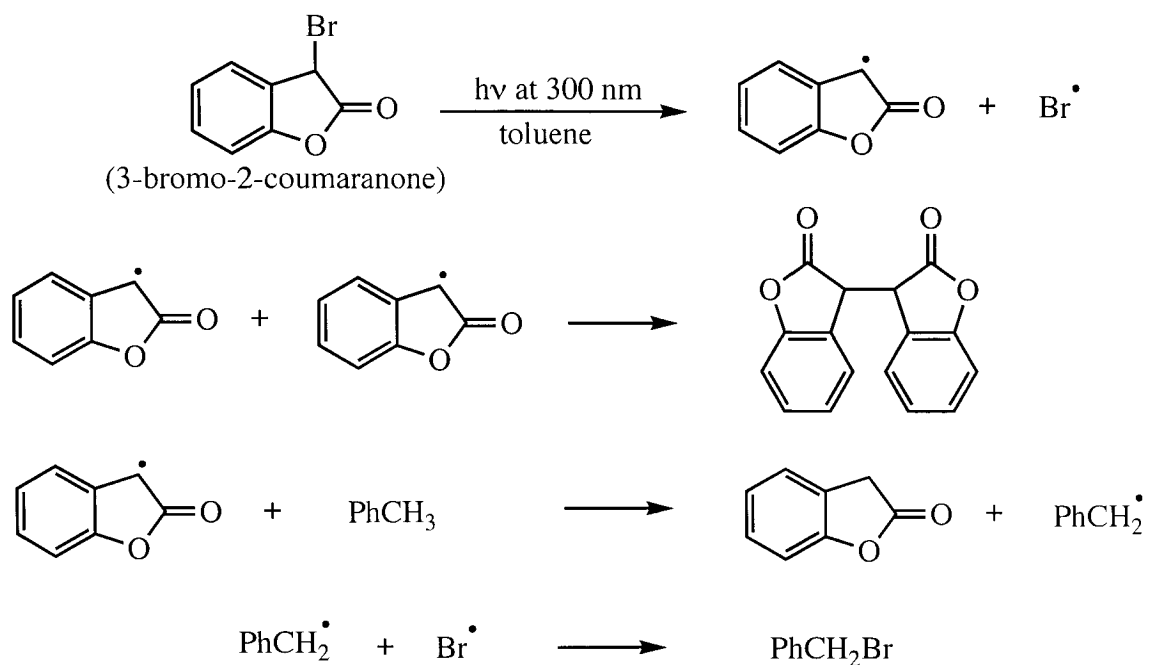
On the other hand, photolysis of α-haloketones can also result in heterolytic cleavage of the carbon-halogen bond. Irradiation of exo-3-chlorobicyclo[2.2.1]hept-5-en-2-one in methanol results in the loss of a chloride anion from the chloroketone. Kaplan et al.,[110] have reported that photolysis of this ketone gives methyl bicyclo[3.1.0]hex-2-ene-6-carboxylate according to the mechanism shown in Scheme 3.19. Experiments under triplet sensitization conditions did not yield any product, indicating that the photolytic process takes place from the singlet excited state. It must be noted that the authors[110] did not provide enough evidence to discard a radical mechanism. Indeed a different study[111] involving irradiation of a closely similar chloroketone reports that the process initially involves a homolytic cleavage. According to Givens et al.,[111] photolysis of 2-chlorobenzobicyclo[2.2.2]octa-5,7-dien-3-one in methanol results in the formation of (1R)-methyl 1a,7b-dihydro-1H-cyclopropa[a]naphthalene-1-carboxylate. Failure to detect carbonium ions led the authors[111] to conclude that the photolysis of this

haloketone results in the formation of a tight radical pair by homolysis of the C-Cl bond. Further rearrangement of the initially formed radical pair led to the formation of the benzonorcaradiene, Scheme 3.20.

Scheme 3.19

3-chlorobicyclo
[2.2.1]hept-5-en-2-one

methyl bicyclo[3.1.0]hex-2-ene-6-
carboxylate

Scheme 3.20

2-chlorobenzobicyclo
[2.2.2]octa-5,7-dien-3-one

methyl 1a,7b-dihydro-1*H*-
cyclopropa[*a*]naphthalene-1-carboxylate
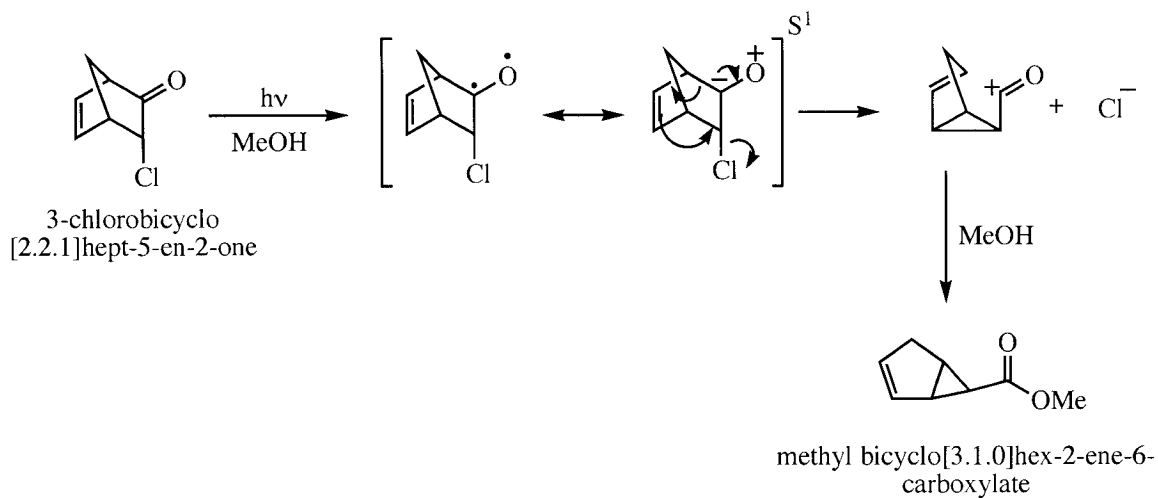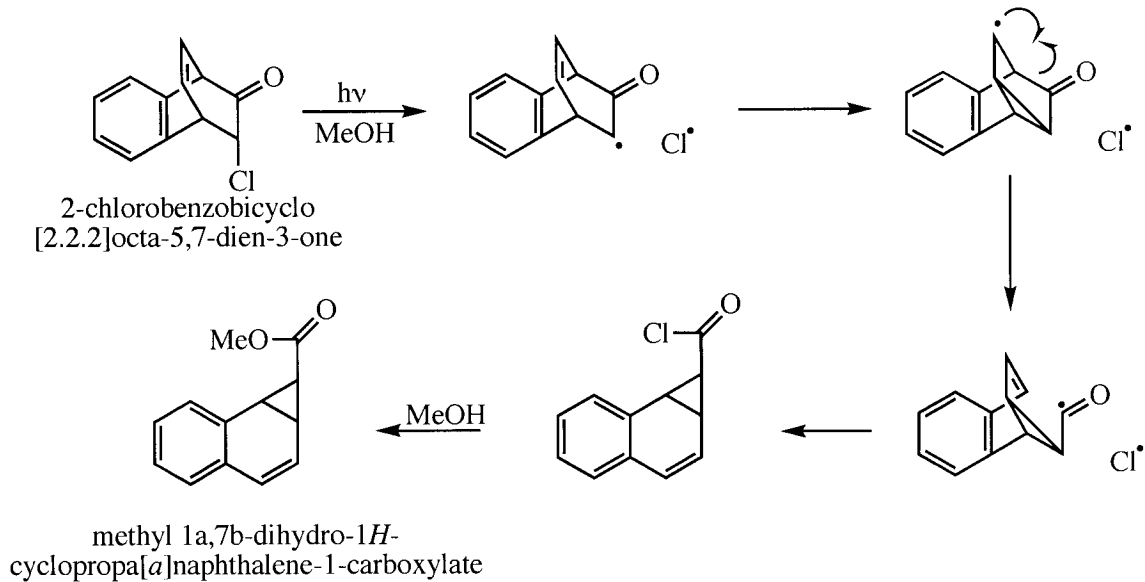
3.1.5 Goal of Chapter III

So far, only the radical cation of the enol of phenylacetaldehyde has been generated using the technique involving protonation of α-ketoradicals.[105] The present work focuses on extending this method to generate a series of 1,2-diarylethenol radical cations as shown in Scheme 3.21. The main goal is to determine if these radical cations can be generated, and to study the effect of substituents on the properties of the enol radical cations.

Scheme 3.21

1a - R_1 = H, R_2 = OMe
2a - R_1 = R_2 = OMe
3a - R_1 = OMe, R_2 = Me
4a - R_1 = OMe, R_2 = H
5a - R_1 = OMe, R_2 = F

1b - 5b

1c - 5c
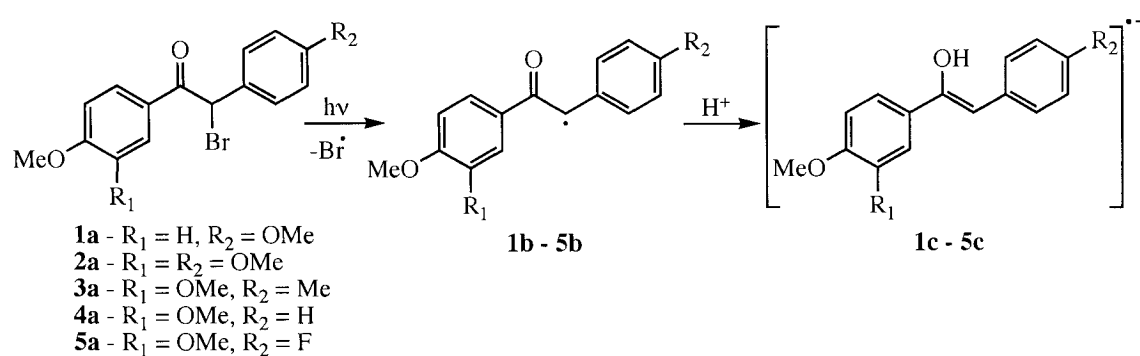
3.2 Results

3.2.1 Generation of Enol Radical Cations in Acidic Acetonitrile

3.2.1.1 1,2-Bis(4-methoxyphenyl)ethenol Radical Cation

Laser flash photolysis of α–bromodeoxyanisoin (**1a**) in N_2–saturated acetonitrile generates a transient species with an absorption band centered at 380 nm and a wide shoulder between 430 and 550 nm, Figure 3.2. This transient species is relatively long-lived decaying in a second order manner over approximately 200 μs. In O_2-saturated acetonitrile ($[O_2] \approx 9.0$ mM)[59] the decay of this transient species is accelerated, Figure 3.2

(inset). Under these conditions, the decay of the 380-nm band takes place with an observed first order rate constant of 7.5 x 10^5 s^{-1}. On the other hand, in the presence of an anionic species like chloride ([Cl$^-$] = 2.0 mM), the decay of the 380-nm band under N_2 is identical to its decay in absence of the anion.

This sensitivity to O_2 and insensitivity to the chloride anion are consistent with the 380-nm transient being a radical species. It is noteworthy that the magnitude of the quenching with oxygen is smaller than that normally observed for carbon-centered radicals. These kinds of radicals typically react with O_2 with second-order rate constants near 10^{10} M^{-1} s^{-1}, and in O_2-saturated acetonitrile where [O_2] is 9 mM, decay with observed rate constants near 10^8 s^{-1}. However, the same is not always true for α-keto radicals which often show reduced reactivity towards oxygen. For example, the 2-coumaranone radical shown in Scheme 3.18 is unreactive toward oxygen.[105, 109] Presumably, the contribution of a resonance structure bearing the unpaired electron on the oxygen atom, Scheme 3.22, is the reason for the low reactivity of α-keto benzyl radicals towards molecular oxygen.

Scheme 3.21
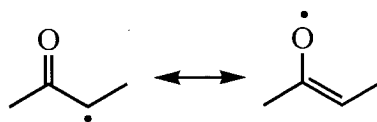
The possibility of the 380-nm transient being the triplet of α-bromodeoxyanisoin (**1a**) was also considered. However, the transient species generated upon 308-nm laser irradiation of deoxyanisoin, Figure 3.3, is clearly different from the species generated upon irradiation of **1a**. The transient generated from deoxyanisoin is short-lived compared with the 380-nm species generated from **1a**. The former transient decays over

143

ca. 20 μs in a first order manner with an observed rate constant of 2.9 x 10^5 s^{-1}, while the transient from **1a** decays slowly in a second-order manner over 200 μs. In addition, the transient produced from deoxyanisoin is much more reactive towards oxygen than the 380-nm transient generated from **1a**, Figure 3.3 (inset). Indeed the decay of the transient generated from deoxyanisoin in O_2-saturated acetonitrile is almost 100 times faster (3.1 x $10^7 s^{-1}$) than the decay of the 380-nm species generated from **1a**.

The possibility that the transient species is a carbocation generated by heterolytic cleavage of the C-Br bond can also be ruled out. Carbocations typically show sensitivity toward nucleophiles like chloride and are insensitive to oxygen concentration, behavior that is opposite to that observed for the 380-nm transient.

Based on the arguments made above, together with previous results showing that homolytic cleavage of carbon-halogen bonds is a typical reaction of α-halo ketones,[107, 109, 111] it can be concluded that the transient generated upon 308-nm irradiation of α-bromodeoxyanisoin (**1a**) is the radical **1b** (1,2-bis(4-methoxyphenyl)-2-oxoethyl radical), formed by photohomolysis of the C-Br bond of **1a**, Scheme 3.23.

Scheme 3.23

1a - R_1 = H, R_2 = OMe
2a - R_1 = R_2 = OMe
3a - R_1 = OMe, R_2 = Me
4a - R_1 = OMe, R_2 = H
5a - R_1 = OMe, R_2 = F

1b - 5b
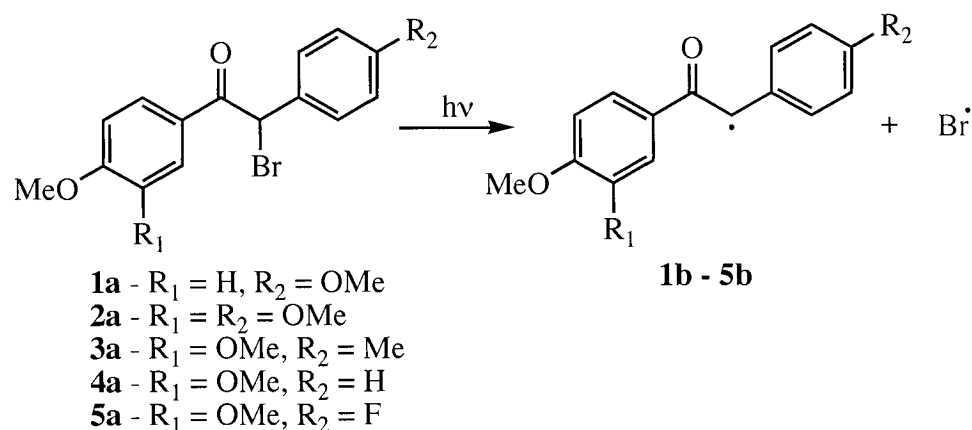
In N_2-saturated acetonitrile containing 0.005 M $HClO_4$, the 380-nm band is still generated and readily observed immediately after the laser pulse. However, as time proceeds the 380-nm band decays and a new transient species grows in, Figure 3.4. As can be observed, the new transient species is characterized by absorption bands at 440, 480 and ca. 740 nm. The growth of each one of these bands takes place with the same first-order rate constant ($k_{obs} = 2.0 \times 10^7$ s^{-1}), indicating that these bands belong to the same transient species. In addition, the rate constant for the growth of the new transient is identical to the rate constant measured for the decay of the 380-nm species ($k_{obs} = 2.2 \times 10^7$ s^{-1}), suggesting that the new transient is a product of the radical species.

From previous studies,[32] it has been shown that the absorption spectra of radical cations of stilbene derivatives typically show two absorption bands, one near 500 nm and a second weaker and broader band above 700nm. The absorption spectra shown in Figure 3.4 contains similar features, and this similarity provides good evidence that the transient generated upon irradiation of α-bromodeoxyanisoin under acidic conditions is the enol radical cation **1c**, Scheme 3.24. In addition, the observation that acidic conditions are required, and that the radical **1b** decay and enol radical cation **1c** growth match is consistent with radical cation formation by protonation of the radical.

Scheme 3.24

(1b)   (1c)
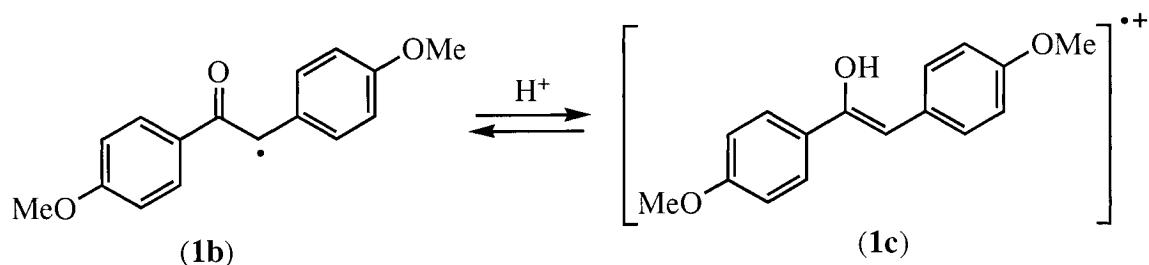
The enol radical cation in Scheme 3.24 is shown in its *trans*-configuration. The absorption spectrum of the transient identified as the enol radical cation in Figure 3.4 is not sufficient to distinguish between the *trans* and *cis* configurations, since both isomers of stilbene radical cations typically have similar absorption spectra.[32] However, due to steric reasons, the *trans* isomer is assumed to be more stable than the *cis* isomer, and it is reasonable to assume that the *trans* enol radical cations will be generated preferentially over the *cis* enol radical cations. Thus, while the results presented in this work do not allow for a definitive conclusion concerning the stereochemistry of the enol radical cations, the assumption will be made throughout that the *trans* enol radical cation is the isomer observed.

One way to test if the transient spectrum in Figure 3.4 does indeed correspond to the enol radical cation is to obtain the spectrum of a similar radical cation that can be generated in a more conventional manner, such as photoionization or photoinduced electron transfer. For enol radical cation **1c**, a reasonable comparison compound would be the radical cation of the corresponding enol ether, 1,2-bis(4-methoxyphenyl)-1-methoxyethene (**6a**).

This radical cation could not be generated by direct photoionization of the 1,2-bis(4-methoxyphenyl)-1-methoxyethene (**6a**), Scheme 3.25. For reasons that are not clear, no transient species was observed upon 308-nm laser irradiation of the enol ether in acetonitrile.

146

Scheme 3.25

(6a)   (6b)
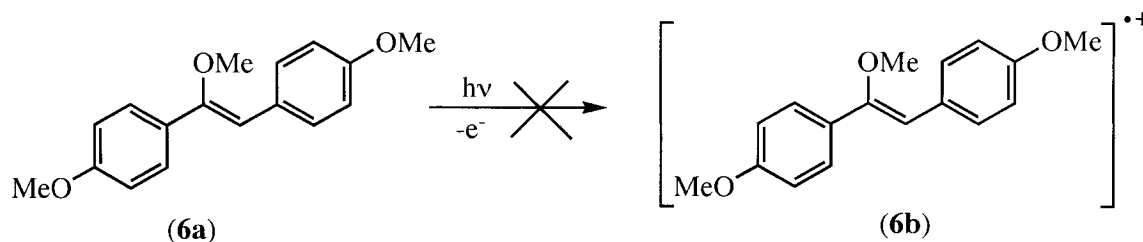
Thus, attempts were made to generate the enol ether radical cation by photoinduced electron transfer using using 2,4,6-triphenylpyrilium tetrafluoroborate as the sensitizer. This sensitizer was chosen instead of chloranil because the chloranil radical anion, expected to be formed in a photoinduced electron transfer reaction, has a characteristic absorption band at 450 nm that would overlap with the bands expected for the enol ether radical cation. Selective irradiation of 2,4,6-triphenylpyrilium tetrafluoroborate with a 355-nm laser pulse generates triplet triphenylpyrilium ion,[112] which is quickly quenched in presence of the neutral enol ether **6a** to give the spectra shown in Figure 3.5. The spectra show the presence of the broad band due to the triphenylpyranyl radical at 550 nm, which indicates that an electron-transfer reaction occurred between the enol ether and the triphenylpyrilium triplet, Scheme 3.26. The spectra also clearly show bands 460, 480 and 750 nm which can be sensibly assigned to the enol ether radical cation **6b**. These bands are very similar to the bands of the transient assigned to the enol radical cation **1c**, and this similarity provides further evidence that the enol radical cation **1c** is generated upon laser irradiation of α-bromodeoxyanisoin in acidic acetonitrile.

Scheme 3.26
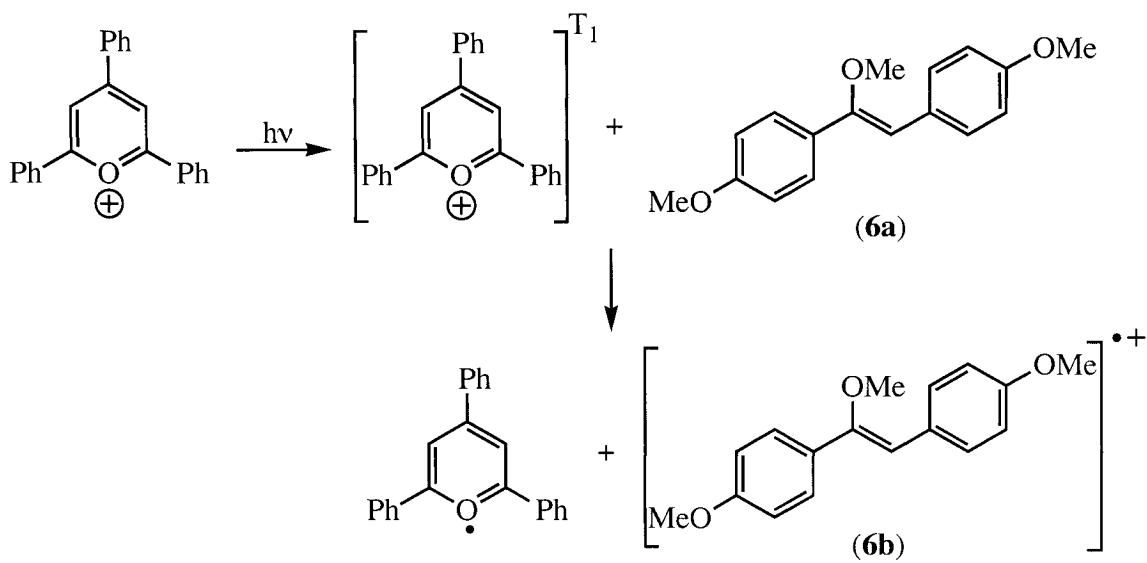
Given the overlap between the absorption band due to the triphenylpyranyl radical and the absorption bands of **6b**, radical cation **6b** was also generated using the co-sensitization method described in Section 1.1.1.3.1. Selective irradiation of 9,10-dicyanoanthracene (DCA) with a 355-nm laser pulse generates the excited singlet DCA, which rapidly undergoes electron transfer with biphenyl to generate biphenyl radical cation (λ_{max} = 380 and 670 nm).[74] The biphenyl radical cation is then reduced in presence of the neutral enol ether **6a** resulting in the formation of radical cation **6b**, Scheme 3.27. The experiment was carried out under O_2-saturated conditions in order to quench the 9,10-dicyanoanthracene radical anion (λ_{max} = 502, 643, 705 nm)[32] formed by electron transfer reaction between the singlet DCA and biphenyl. The transient spectrum measured during this experiment is shown in Figure 3.6. As can be observed, the changes in absorption were very small, and absorption spectra contain significant noise, particularly at the long wavelength region. Nonetheless, as expected, the spectrum immediately after the laser pulse contains bands at 380 and 670 nm corresponding to the

148

biphenyl radical cation. This decays rapidly, and leaves a transient spectrum that clearly contains absorption bands centered at 460, 490 and 760 nm. This spectrum is very similar to the spectrum obtained upon irradiation of **1a** in acidic acetonitrile supporting the conclusion that the enol radical cation **1c** is generated upon laser irradiation of α-bromodeoxyanisoin **1a** in acidic acetonitrile.

Scheme 3.27
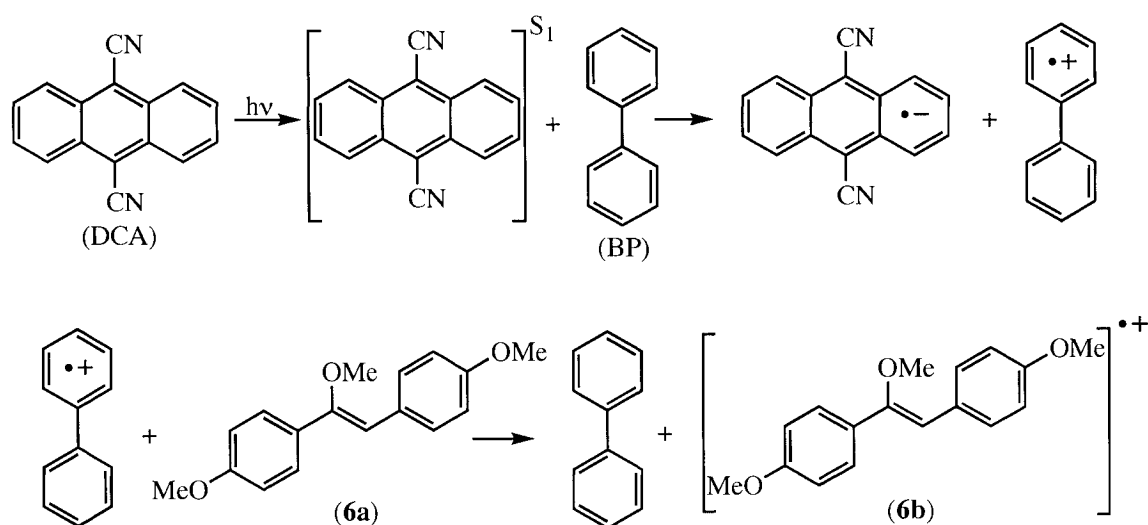
As described in the introduction, it has already been shown that α-keto radicals do undergo protonation under sufficiently acidic conditions to generate enol radical cations. Thus, the observation that the transient with absorption bands at 480 and 700 nm is only observed upon irradiation of α-bromodeoxyanisoin under acidic conditions is also consistent with assignment of that transient as the radical cation of 1,2-bis(4-methoxyphenyl)ethenol **1c**, and that the mechanism for formation of the radical cation is protonation of the radical **1b**, Scheme 3.24.

According to this mechanism, the decay of the radical and the growth of the radical cation should both accelerate with increasing concentrations of acid. Indeed, at acid

concentrations between 0.1 and 0.3 mM HClO$_4$, a distinct time-resolved formation of the radical cation can be observed, Figure 3.7a. Over this range of concentrations, the rate constants for the growth of the radical cation **1c** increase in a linear manner with respect to increasing acid concentrations, Figure 3.7b. Linear least-squares analysis gives a slope of $(4.5 \pm 0.1) \times 10^9$ M^{-1} s^{-1} and an intercept of $(2.5 \pm 0.3) \times 10^6$ s^{-1}.

An increase in the rate constant for the decay of the radical measured at 380 nm as a function of increasing acid concentration is also observed, Figure 3.7c. As shown in Figure 3.7d, the relationship between radical decay and the concentration of HClO$_4$ is linear, and linear least-squares analysis give a slope of $(3.9 \pm 0.1) \times 10^9$ M^{-1} s^{-1} and an intercept of $(8.3 \pm 0.4) \times 10^5$ s^{-1}. Both of these values, particularly the value of the slope, are closely similar to the slope and intercept measured for the growth of the radical cation.

The maximum values of ΔO.D. at 480 and 440 nm were also measured as a function of acid concentration. As shown in Figures 3.8a and 3.8b, the absorption values at these wavelengths are small at low concentrations of acid, and then increase as the acid content increased to 0.02 M. At higher acid concentrations, no further increase in absorbance is observed. This behavior is also consistent with enol radical cation formation by protonation of the α-keto radical, and as discussed later, can be used to estimate the acidity of the enol radical cation.

Figure 3.9 shows the transient absorption spectra obtained upon 308-nm laser irradiation of α-bromodeoxyanisoin at relatively high concentrations of HClO$_4$ (0.01 M) in N$_2$-saturated acetonitrile. The spectrum is clearly dominated by the presence of the enol radical cation, which is consistent with increasing formation of the enol radical

150

cation as the acid content increases. The radical cation is quite stable under these conditions, Figure 3.9 (inset), where it decays over a time period of approximately 100 μs. The decay does not fit well to a first-order exponential, but fits well to a second-order rate law with a rate constant of $\varepsilon(6.0 \times 10^5)$ cm s^{-1}, where ε is the extinction coefficient of the transient at 480 nm.

Normally, a positively charged species like the enol radical cation **1c** would be expected to show high reactivity towards nucleophiles like Cl$^-$ or Br$^-$, and experimental demonstration of such reactivity is often used in studies of radical cations and other electrophilic transients like carbocations as evidence to reinforce transient identification. However, for enol radical cations, the situation is more complicated due to the likelihood of reversible addition of the nucleophile as shown in Scheme 3.28.

Scheme 3.28
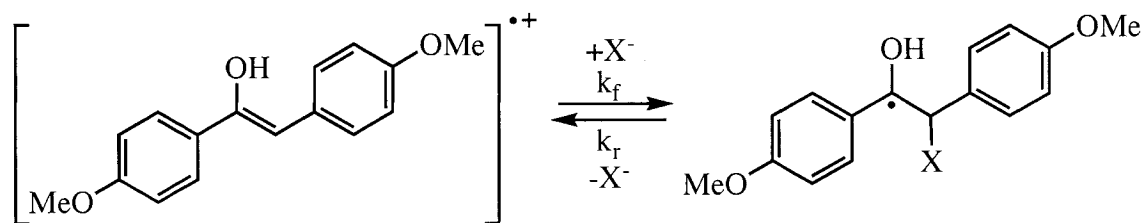
The reversible addition of chloride and bromide to other radical cations has been observed previously,[23, 113] especially for radical cations that are stabilized by electron-donating methyl and methoxy groups. In addition, studies of radicals bearing an adjacent leaving group like chloride or bromide have shown that such β-substituted radicals can undergo rapid heterolytic cleavage of the leaving group to generate the radical cation, with the speed of the heterolysis reaction increasing as the stability of the radical cation increases.[113] The enol radical cation **1c** is strongly stabilized by two 4-methoxyphenyl groups, as well as the enolic OH group. As a result, the absence of quenching by a

nucleophile like Br⁻ or Cl⁻ would not be unexpected, and the utility of such quenching studies as a diagnostic tool to help reinforce identification of the transient as the enol radical cation is limited.

In addition, as discussed in Chapter 2, acids like HCl that are strong acids in aqueous solution appear to be weaker acids in acetonitrile. Thus, since the enol radical cation **1b** is generated in the present work under quite strongly acidic conditions, it is possible that a significant fraction of Cl⁻ added as the tetra-butylammonium salt may be converted to HCl. As a result, the concentration of free chloride ions may be considerably different than expected from the amount of added salt. In addition, the acidity of the solution may also change as the concentration of Cl⁻ changes, which would have an effect on the generation of the enol radical cation.

Attempts were made to study the effect of added tetra-butylammonium chloride on the decay of enol radical cation **1b**, and indeed the results obtained were complicated and difficult to reproduce. Several examples are shown in Figure 3.10, which shows results from different experiments in which the observed rate constants for the decay of the enol radical cation are plotted as a function of the concentration of tetra-butylammonium chloride. As can be seen, weak quenching is observed in two of the three plots, Figure 3.10a and 3.10b, but not in the third, Figure 3.10c. In fact, several other attempts were made to obtain reproducible results, but in each case unacceptable differences like those shown in Figure 3.10 were obtained.

As a result of these complications, attempts to obtain reliable quenching plots for the reaction of the enol radical cation **1c**, and the other transients identified as enol radical cations described later in this section, were abandoned. Instead, qualitative experiments

152

were carried out simply to demonstrate that the transient decay was sensitive to the presence of Br⁻ or Cl⁻. Thus, the decay traces shown in Figure 3.11 show a comparison of the data obtained in the absence of a nucleophile with data obtained in the presence of Br⁻ and Cl⁻. The data clearly show a small, but definite increase in the observed decay. While this kind of data is not ideal, it does show that the transient is electrophilic and is sensitive to the presence of a nucleophile, which is consistent with the transient being an electron deficient species like the enol radical cation.

It is worth noting that the radical cation of 1,2-bis(4-methoxyphenyl)ethenol was also somewhat sensitive to the presence of oxygen. Thus, in O_2-saturated acetonitrile, the radical cation did decay slightly faster than in N_2-saturated acetonitrile, Figure 3.9 inset. While the decays of radical cations are typically insensitive to oxygen concentration, the observed weak quenching of the enol radical cation **1b** by oxygen was not unexpected. Reasons for this are given later in the discussion.

3.2.1.2 1-(3,4-Dimethoxyphenyl)-2-(4-methoxyphenyl)ethenol Radical Cation (2c)

Laser irradiation of 2-bromo-1-(3,4-dimethoxyphenyl)-2-(4-methoxyphenyl) ethanone **(2a)** in N_2-saturated acetonitrile results in the formation of a strong absorption band centered at 390 nm, Figure 3.12. The transient species responsible for this absorption band is quite long-lived, decaying in a second order manner over *c.a.* 200 μs. The decay of this transient is accelerated in O_2-saturated acetonitrile, Figure 3.12 (inset), where it decays with a pseudo first order rate constant of 6.5 x 10^5 s⁻¹. As for the radical species **1b** described above, the magnitude of the quenching by oxygen is less than nomally observed for carbon centered radicals, but it is consistent with that often

observed for α-keto radicals. The decay of the 390-nm species is unaffected by the presence of anionic species like chloride ([Cl⁻] = 2.0 mM). This lack of reactivity toward anionic species as well as the reactivity toward oxygen are consistent with the transient being a radical species. Based on these observations and on the similarity of the transient spectra with that of **1b**, the 390-nm transient was identified as the 1-(3,4-dimethoxyphenyl)-2-(4-methoxyphenyl)-2-oxoethyl radical species **2b**.

As can be observed in Figure 3.13, the decay of **2b** in N_2-saturated acetonitrile containing 2.0 mM $HClO_4$ is accompanied by the growth of new absorption bands centered at 460, 500 and 800 nm. The rate constant for the growth of these bands (k_{obs} = 1.4×10^7 s^{-1}) under these conditions is identical to that measured for the decay (k_{obs} = 1.4 $\times 10^7$ s^{-1}) of the radical species **2b**, indicating that the new transient species is a product of **2b**. In 0.01 M $HClO_4$ the transient absorption spectra is different, Figure 3.14, with the bands at 460, 500 and 800 nm being the dominant feature and forming within the laser pulse. This new transient species is quite stable in acidic (0.02 M $HClO_4$) N_2-saturated acetonitrile, Figure 3.14 (inset), where it decays over a time period of approximately 200 μs. The decay does not fit well to a first-order exponential, but fits well to a second-order rate law with a rate constant of $\varepsilon(1.8 \times 10^5)$ cm s^{-1}, where ε is the extinction coefficient of the transient at 500 nm. In O_2-saturated acetonitrile contaning 0.02 M $HClO_4$ the transient decays slightly faster, Figure 3.14 (inset), and in a first-order manner with a rate constant of 9.4×10^4 s^{-1}. In contrast to the 390-nm transient, the new transient species is sensitive to anionic species like chloride and bromide, Figure 3.15. These observations together with the similarity of the spectra to that observed for **1c**

indicate that the transient species responsible for the absorption bands at 460, 500 and 800 nm is the enol radical cation **2c**.

The enol radical cation **2c** is formed within the laser pulse at concentrations of $HClO_4$ higher than 5.0 mM. However, at lower concentrations of $HClO_4$ (0.1 – 3.0 mM) time-resolved formation of **2c** can be observed, Figure 3.16a. The rate constants for the growth of **2c** increase linearly with increasing concentrations of perchloric acid, Figure 3.16b. Linear least-squares analysis gives a slope of $(6.6 \pm 0.3) \times 10^9$ M^{-1} s^{-1} and an intercept of $(5.0 \pm 0.9) \times 10^5$ s^{-1}.

The maximum values of $\Delta O.D.$ at 500 and 460 nm were also measured as a function of acid concentration, and the shapes of the plots of $\Delta O.D.$ vs $-\log[HClO_4]$ had the same shape, Figure 3.17, as observed for enol radical cation **1c** described above. In particular, the absorption values are small at low acid concentrations, and then increase and finally level off as the acid concentration continues to increase.

As observed in Figures 3.13 and 3.14, in addition to the bands at 460, 500 and 800 nm, assigned to the enol radical cation **2c**, there is another absorption band centered at 350 nm. This absorption band is also present after irradiation in neat acetonitrile but is partially masked by the absorption band at 390 nm due to **2b**. The 350-nm transient species could either be a radical species originated by homolytic cleavage of the (Br)C-C(O) bond or a carbocation species generated by heterolytic cleavage of the C-Br bond, Scheme 3.29.

Scheme 3.29
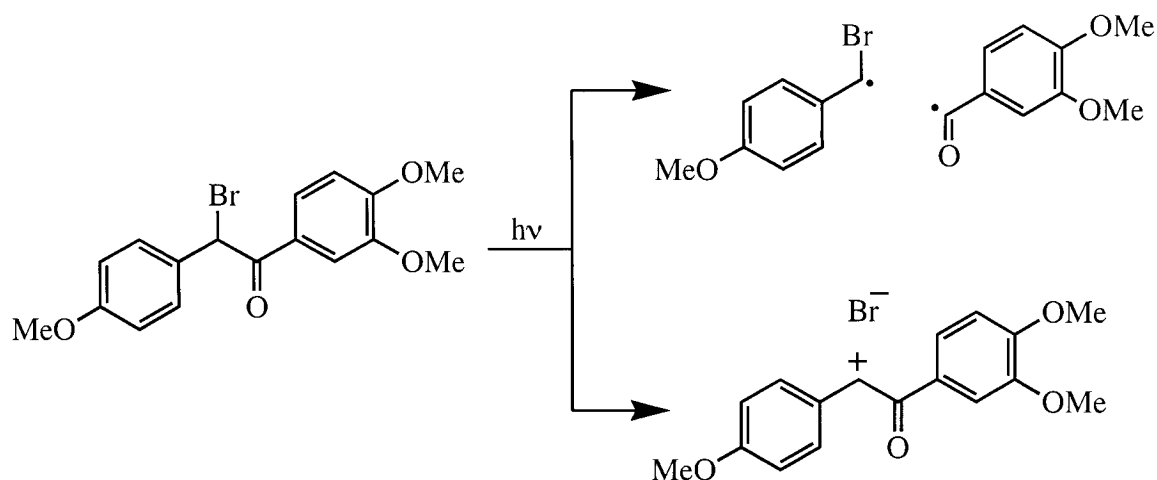
In an attempt to identify the transient species responsible for the 350-nm absorption band the influence of O_2 and chloride on the lifetime of this species was studied under non-acidic conditions. As shown in Figure 3.18, the decay at 350-nm is almost the same in N_2 and O_2-saturated acetonitrile. This transient decays with an observed first order rate constants of 2.7 x 10^5 s^{-1} in N_2-saturated acetonitrile and 3.3 x 10^5 s^{-1} in O_2-saturated conditions. On the other hand, the 350-nm band is rapidly quenched in the presence of anionic species like chloride. As shown in Figure 3.18c, the relationship between the observed rate constants for the decay of the 350 nm transient and the concentration of chloride is linear, giving a diffusion-controlled second-order rate constant of k_{Cl} = 8 x 10^9 M^{-1} s^{-1}. These observations strongly suggest that the 350-nm transient species is the carbocation generated by heterolysis of the C-Br bond as represented above.

3.2.1.3 1-(3,4-Dimethoxyphenyl)-2-(4-methylphenyl)ethenol Radical Cation

Laser irradiation at 308 nm of 2-bromo-1-(3,4-dimethoxyphenyl)-2-(4-methylphenyl)ethanone (**3a**) results in the formation of a transient species characterized by a strong absorption band centered at 370 nm, Figure 3.19. In N_2-saturated acetonitrile

156

the 370-nm transient decays in a second order manner over 200 μs. The decay of this transient is accelerated in O_2-saturated acetonitrile; under these conditions the 370-nm band decays in a first-order manner with a rate constant of k_{obs}= 7.7 x 10^5 s^{-1}. In contrast, the decay of the 370-nm band is insensitive to the presence of anionic species. These observations are consistent with the identification of the 370-nm transient as the 1-(3,4-dimethoxyphenyl)-2-(4-methylphenyl)-2-oxoethyl radical (3b). The identification is further supported by the similarities between the transient spectra of 3b with those of 1b and 2b.

Figure 3.20 shows the transient spectra measured upon laser irradiation of 3a in acidic (2.0 mM $HClO_4$) N_2-saturated acetonitrile. As observed in neat acetonitrile, the radical species 3b is formed within the laser pulse; however as this species disappears a new transient band centered at 450 nm grows in. Both processes, the decay of 3b and the growth of the 450-nm band, take place with identical rate constants (k_{obs} = 1.1 x 10^7 s^{-1}), signifying that the 450-nm transient is a product of 3b. In 0.01 M $HClO_4$, the 450-nm transient is formed within the laser pulse while the band due to the radical species is dramatically reduced, Figure 3.21. The 450-nm transient species is quite stable in acidic (0.02 M $HClO_4$) N_2-saturated acetonitrile, Figure 3.21 (inset), where it decays over a time period of approximately 100 μs. The decay fits well to a second-order rate law with a rate constant of ε(9.0 x 10^5) $cm.s^{-1}$, where ε is the extinction coefficient of the transient at 450 nm. In O_2-saturated acetonitrile the transient decays slightly faster, Figure 3.21 (inset), and in a first order manner with a rate constant of 2.0 x 10^5 s^{-1}. The transient absorption band at 450 nm band is sensitive to anionic species like chloride and bromide, Figure 3.22, indicating that this transient is a positively charged species. These

157

observations strongly suggest that the 450-nm transient is the enol radical cation **3c** generated by protonation of the radical species **3b**.

Further evidence supporting the identification of the 450-nm transient species as the enol radical cation **3c** comes from the sensitivity of this absorption band to the acid content. At concentrations of $HClO_4$ higher than 4.0 mM the formation of the 450-nm takes place promptly within the laser pulse. At lower acid concentrations (0.1 - 3.0 mM) a time-resolved growth of the 450-nm transient can be observed, Figure 3.23a. Over this range of concentrations, the rate constants for the growth of **3c** increase in a linear manner with increasing acid concentration, Figure 3.23b. Linear least-squares analysis gives a slope of $(3.5 \pm 0.2) \times 10^9$ M^{-1} s^{-1} and an intercept of $(4.2 \pm 0.2) \times 10^6$ s^{-1}.

The maximum ΔO.D. values at 450 nm measured as a function of acid content are shown in Figure 3.24. The shape of this plot is similar to that for the other two enol radical cations previously described, with low absorption values at low acid concentration, followed by a region where the absorption increases with increasing acid content and finally leveling off in more acidic solutions.

In the 400-500 nm region, the absorption spectrum of the enol radical cation **3c** in Figure 3.21 is very similar to that for the enol radical cation **2c**. The main difference in this region is a small shift in the absorption maximum to 450 nm for **3c** compared to 460 nm for **2c**. On the other hand, the enol radical cation **3c** does not contain absorption at longer wavelengths between 600 and 800 nm. Since stilbene radical cations in general, and the enol radical cation **2c** in particular, have absorption in this region, the absence of the long-wavelength band raises some doubt concerning the identification of the 450 nm band as the enol radical cation **3c**.

In an effort to obtain more evidence to support the identification of the 450-nm band as the radical cation **3c**, the corresponding enol ether radical cation **7b** was generated, Scheme 3.30. The generation of **7b** was carried out by photoinduced electron transfer using the sensitizer DCA and biphenyl as cosensitizer, Figure 3.25. While the transient absorptions are weak, the biphenyl radical cation characterized by absorption bands at 380 and 670 nm can be observed immediately after the laser pulse. This radical cation is short-lived in presence of the enol ether **7a** (1.8×10^{-4} M), and as it decays gives rise to a new absorption band centered at 480 nm. These observations are consistent with an electron transfer reaction between the biphenyl radical cation and **7a**, and it is reasonable to conclude that the 480-nm transient formed upon decay of the biphenyl radical cation is the enol ether radical cation **7b**. Note that the transient spectrum of the enol ether radical cation **7b** does not have any absorption band between 600 and 800 nm. Instead, it only consists of one absorption band centered at 480 nm. This observation shows that absorption in the 600 to 800 nm is not always present for these kinds of radical cations, and supports the assignment of the transient generated upon irradiation of **3a** in acidic acetonitrile as the enol radical cation **3c**.

The absorption of the enol radical cation **3c** and the radical cation of the enol ether **7a** in the 400 to 500 nm region are not identical. The enol radical cation **3c** has a maximum at 460 nm and a weaker band at 480, while the enol ether radical cation has a maximum near 480 nm. While no explanation for this difference is available, it suggests that replacing the OH group of an enol radical cation with the OCH_3 group of an enol ether radical cation may cause slight differences in the location of their absorption maxima in the low wavelength region.

Scheme 3.30

7a R = Me
8a R = H

7b R = Me
8b R = H
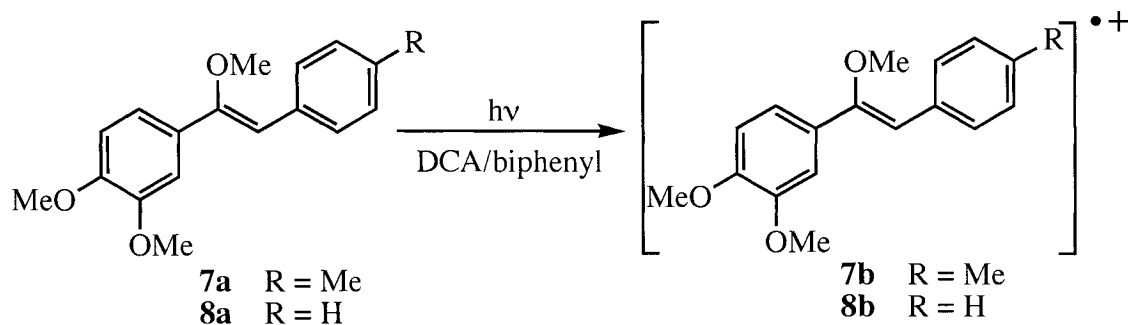
3.2.1.4 1-(3,4-Dimethoxyphenyl)-2-phenylethenol and 1-(3,4-Dimethoxyphenyl)-2-(4-fluorophenyl)ethenol Radical Cations

Figures 3.26 and 3.27 show the transient spectra obtained upon 308-nm laser irradiation of 2-bromo-1-(3,4-dimethoxyphenyl)-2-phenylethanone (**4a**) and 2-bromo-1-(3,4-dimethoxyphenyl)-2-(4-fluorophenyl)ethanone (**5a**), respectively. Both spectra consist of strong absorption bands centered around 360 nm, that decay in a second-order manner over 200 μs. The decay of these bands is accelerated in the presence of O_2, Figures 3.26 and 3.27 (insets), but it is not affected by the presence of anionic species. Based on these observations and the similarity between the transient spectra and those observed for **1b-3b**, these absorption bands have been attributed to the 1-(3,4-dimethoxyphenyl)-2-phenyl-2-oxoethyl radical (**4b**) and 1-(3,4-dimethoxyphenyl)-2-(4-fluorophenyl)-2-oxoethyl radical (**5b**).

Under acidic conditions, $[HClO_4]$ = 10 mM, absorption due to the radical **4b** is still observed, but is now accompanied by an absorption band at 420 nm and a shoulder at 470 nm, Figure 3.28a. At this concentration of acid, both bands appear promptly after the laser pulse; however, at lower concentrations, $[HClO_4]$ = 2.0 mM, the 420 nm band grows in as the radical band at 360 nm decays, Figure 3.28b.

Figure 3.29 shows the spectrum at even higher concentrations of acid, 0.10 M. Under these conditions, the absorption band corresponding to the radical **4b** is difficult to resolve, with the broad absorption between 400 and 490 nm being the dominant feature.

The transient with absorption at 420 nm showed many of the same characteristics as the enol radical cations **1c** to **3c** described above. The decay of this transient increased upon addition of Br^- and Cl^-, Figure 3.30. In addition, as shown in the inset of Figure 3.28 for decay traces obtained in the presence of 2.0 mM $HClO_4$, the observed rate constant for the growth of the 420 nm band ($k_{obs} = 1.7 \times 10^7$ s^{-1}) matchs that for the decay of the radical at 360 nm ($k_{obs} = 1.5 \times 10^7$ s^{-1}). Furthermore, the rate constants for the growth of the 420 nm band increased in a linear manner with respect to acid concentrations between 0.1 and 2.0 mM, Figure 3.31. Linear least squares analysis of the plot gives a slope of $(3.7 \pm 0.2) \times 10^9$ M^{-1} s^{-1} and an intercept of $(9.4 \pm 0.9) \times 10^6$ s^{-1}. Thus, on the basis of these results, it is reasonable to assign the transient at 420 nm as the enol radical cation **4c** generated by protonation of the radical **4b**.

It is recognized that the absorption maximum at 420 nm for the enol radical cation **4c** is considerably lower than the maxima for the other enol radical cations described above, which range from 460 nm for **3c** to 480 nm for **2c**. To determine if the same shift is observed for an enol ether radical, the enol ether 1-(3,4-dimethoxyphenyl)-2-phenyl-1-methoxyethene **8a**, was oxidized to its radical cation by photoinduced electron transfer using the dicyanoanthracene/biphenyl cosensitization method. The spectrum for the radical cation **8b** obtained after the biphenyl radical cation was completely quenched by **8a** is shown in Figure 3.32. The spectrum shows that the enol ether radical cation **8b** has

an absorption maximum at 470 nm, with a distinct shoulder at 450 nm. This maximum is shifted to lower wavelengths compared to the enol ether radical cation **7b**, which has a maximum at 490 nm, indicating that a shift to lower wavelengths is expected as the electron-donating ability of the groups on the aromatic ring is weakened. However, at the present time, it is difficult to rationalize why the absorption shift for the enol radical cation **4c** is so much greater than for the enol ether radical cation **8b**.

Laser irradiation of the 4-fluoro derivative **5a** in acidic acetonitrile gave results similar to those for **4a**. In the presence of 0.01 M $HClO_4$, the absorption spectrum shows the presence of transient at 440 nm in addition to the radical **5b** at 360 nm, Figure 3.33. At this acid concentration, the transient at 440 nm is formed promptly within the laser pulse, but at lower acid concentrations between 0.1 and 2.0 mM $HClO_4$, a time-resolved growth can be observed, Figure 3.34a. These growths were very rapid, ranging over this concentration range from 7.5×10^7 s^{-1} to ca 1×10^8 s^{-1}, and are barely within the time-resolution of the laser system. A reasonably linear relationship is seen between the observed rate constants for these growths and the concentration of acid, which provides confidence that the measured growths do represent chemical events, rather than being growths that are limited by the time-resolution of the laser system. Linear least-squares analysis of the plot in Figure 3.34b gives a slope of $(6.0 \pm 0.9) \times 10^9$ M^{-1} s^{-1} and an intercept of $(8.4 \pm 0.4) \times 10^7$ s^{-1}.

For the other enol radical cations described above, a good correspondence between the decay of radical and the growth of the radical cation was always observed at suitable acid concentrations. However, the decay of the radical **5b** generated upon irradiation of **5a** in acidic acetonitrile could not be resolved. Luminescence from the laser pulse and/or

162

from the substrate in the sample is typically stronger at 360 nm than at wavelengths greater 400 nm. Given the rapid growth of the transient at 440 nm, it is likely that the decay of the radical **5b** was obscured by the stronger luminescence.
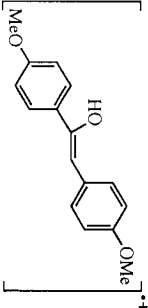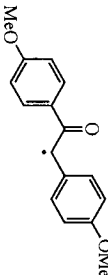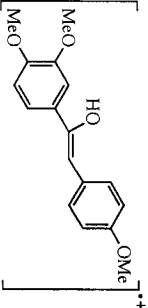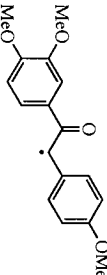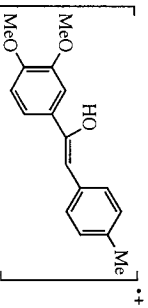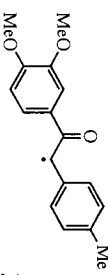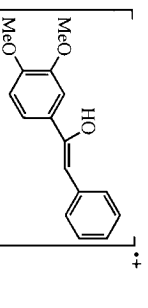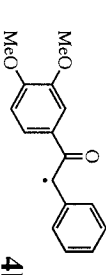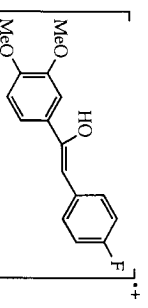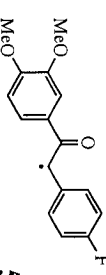
The transient at 440 nm shows some sensitivity towards the nucleophiles Br^- and Cl^-. These observations, together with the behaviour of the transient in acidic acetonitrile, are consistent with identification of the transient as the enol radical cation, **5c**.

Radical cations **4c** and **5c** are relatively long-lived in N_2-acetonitrile containing 0.02 M $HClO_4$. Under these conditions both radical cations decay in an approximately second-order manner over 200 μs. The second-order rate constant measured for the decay of **4c** is $\varepsilon(2.2 \times 10^5)$ $cm.s^{-1}$, where ε is the extinction coefficient of 4c at 420 nm. The second-order rate constant obtained for the decay of **5c** is $\varepsilon(1.1 \times 10^6)$ $cm.s^{-1}$, where ε is the extinction coefficient of **5c** at 440 nm. The decay of both species, **4c** and **5c**, is slightly accelerated in O_2-saturated acetonitrile containing 0.02 M $HClO_4$. Both species decay in a first-order manner under these conditions, with rate constants of 2.7×10^5 s^{-1} for **4c** and 3.8×10^5 s^{-1} for **5c**.

The effect of acid content on the magnitude of the maximum absorption at 420 for **4c** and at 440 nm for **5c** is shown in Figures 3.35a and 3.35b. The absorption values are small at low concentrations of acid, followed by an increase in absorption and then a leveling off as the acid concentration continues to increase. The overall shapes of these plots are similar to those for enol radical cation **1c - 3c**.

Table 3.2 summarizes the wavelengths corresponding to the maximum absorption bands for the enol radical cations **1c - 5c** as well as the α-keto radicals **1b - 5b**.

Table 3.2 Maximum absorption bands characterizing enol radical cations and the corresponding radical species. Pseudo first order rate constant observed for the decay of these in O_2-saturated conditions. ([O_2] ≈ 9.0 mM)[59]

Enol Radical Cation	λ_{max} (nm) HClO$_4$/MeCN	k_{obs} / s^{-1} enol radical cation + O_2 [HClO$_4$] = 0.02 M	α-ketoradical	λ_{max} (nm) in MeCN	k_{obs} / s^{-1} radical + O_2
1c	440, 480 and 730	2.1 x 10^5	**1b**	380	7.5 x 10^5
2c	460, 500 and 800	9.4 x 10^4	**2b**	390	6.5 x 10^5
3c	450	2.0 x 10^5	**3b**	370	7.7 x 10^5
4c	420	2.7 x 10^5	**4b**	370	5.9 x 10^4
5c	440	3.8 x 10^5	**5b**	360	5.6 x 10^5

164

3.2.2 Geometry Optimization of Enol Radical Cations.

The geometries of the enols radical cations **1c-5c** in gas phase were optimized using the Gaussian 98 program. The optimization calculation provides information concerning the charge distribution in the radical cation as well as structural parameters like bond angles, dihedral angles and bond distances. Table 3.3 shows the distribution of Mulliken charges as well as the dihedral angle specified in the table for the enol radical cations. Surprisingly, the structures of the enol radical cations are not planar but distorted, Figure 3.36, with twisting angles of ca 25 °.

The computational study also gives the energy of the optimized structure. Thus, the adiabatic ionization potentials of the neutral enols can be calculated in vacuum as the difference between electronic energies of the enol radical cation and the electronic energies corresponding to the neutral enol.[114] Table 3.3 also lists the values of the calculated ionization potentials in vacuum for the neutral enols.

Table 3.3 Quantum chemical data of the enol radical cations in gas phase.
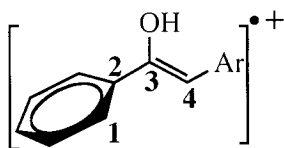
Enol Radical cation	Dihedral Angle $D_{1,2,3,4}$	Ionization Potentials [kJ/mole]	Charge Distribution
1c	-26.7 °	585.25	
2c	-26.5 °	575.50	
3c	-25.8 °	595.25	
4c	-25.5 °	607.25	
5c	-25.5 °	610.75	

3.3 Discussion

3.3.1 Identification of Enol Radical Cations

Transient species observed upon laser irradiation of α-bromoketones **1a** to **5a** in acidic N_2-saturated acetonitrile were identified as enol radical cations **1c-5c** for several reasons. First, in every case, the transients identified as the enol radical cations were only observed in acidic solution. This is consistent with identification as the enol radical cations, which can only be generated from the precursor ketones by protonation of the intermediate α-keto radicals **1b** to **5b**. Furthermore, in every case except the enol radical cation with the 4-fluoro substituent, **5c**, there was a close correspondence between the growth of the transient identified as the enol radical cation and the decay of the radical. This behavior is again consistent with formation of the enol radical cations by protonation of the radicals.

The transients identified as the enol radical cations also showed reactivity towards nucleophiles Br⁻ and Cl⁻. As described in the results section, this reactivity was complicated by several factors, including the likelihood that addition of the nucleophiles will be at least partially reversible, and that the high acidity of the solutions may result in partial protonation of the added nucleophiles. Despite these problems, the observation of sensitivity towards nucleophiles is consistent with the formation of the enol radical cations.

The absorption spectra of the transients identified as the enol radical cations **1c** to **3c** also reinforce those identifications. In particular, enol radical cations **1c** and **2c** have absorption spectra that match closely those of most other stilbene radical cations, and the absorption spectrum of enol radical cation **1c** is closely similar to the enol ether radical

167

cation **6b** generated in the present work. The enol radical cation **3c** lacks absorption at long wavelengths typically observed for stilbene radical cations. However, the corresponding enol ether radical cation **7b** also lacks absorption at long wavelengths, which shows that absorption in this region is not always observed for these kinds of radical cations.

The greatest lack of agreement between observed absorption spectrum and expectation based on the typical absorption spectra of stilbene-like radical cations is found in the results for the enol radical cation **4c**. In this case, the absorption maximum is at 420 nm. This is a considerably shorter wavelength than for most stilbene radical cations, and is also considerably shorter than for the corresponding enol ether radical cation **8b**.

Some stilbene radical cations do have absorption maxima at unusually short wavelengths. For example, the radical cation of *trans*-3,5-dimethoxystilbene has an absorption maximum at 460 nm,[27] which is considerably shorter than maximum near 500 nm observed for most stilbene radical cations. Furthermore, electron-donating groups like a methyl group directly attached to the central alkene segment of stilbene radical cations are known to have a substantial effect on the absorption maxima of these radical cations. For example, while the radical cation of 4-methoxystilbene has absorption bands at 470 and 500 nm, the radical cation of 1-methyl-1-(4-methoxyphenyl)-2-phenylethene has bands at somewhat shorter wavelengths of 440 and 490 nm.[32] The effect of substitution directly on the alkene segment of stilbene radical cations can also be demonstrated by the comparing the absorption spectra of the three stilbene radical cations shown in Scheme 3.31.

Scheme 3.31

4,4'dimethoxy-stilbene radical cation	(6b)	(1c)
540 (maximum)	480 (maximum)	480 (maximum)
480 (shoulder)	460 (shoulder)	440 (shoulder)

$$\frac{\epsilon(540)}{\epsilon(480)} = \frac{2.3}{1}$$

$$\frac{\epsilon(480)}{\epsilon(440)} = \frac{1.2}{1}$$
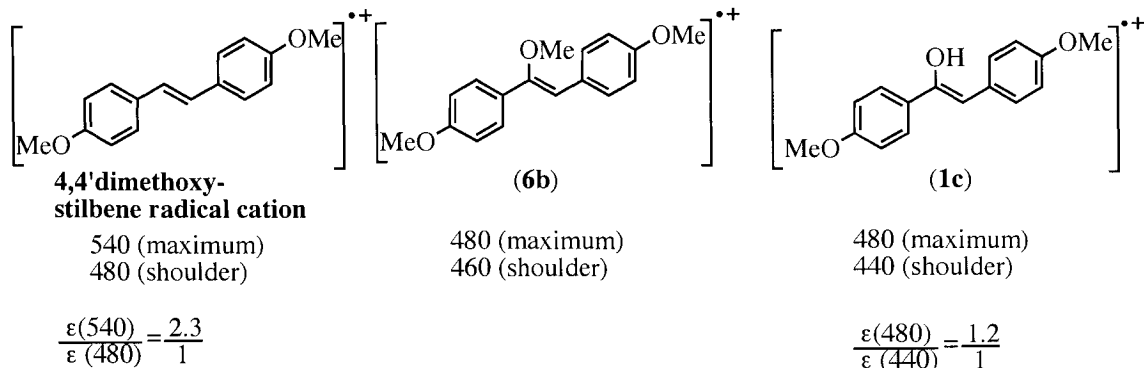
As can be seen, there is a substantial shift of almost 60 nm to shorter wavelengths in the absorption maxima of the enol ether radical cation **6b** and the enol radical cation **1c** compared to the absorption maximum of the 4,4-dimethoxystilbene radical cation. In addition, the distinct shoulder observed for the enol radical cation **1c** is shifted 40 nm to shorter wavelengths than the shoulder observed for the 4,4-dimethoxystilbene radical cation, and 20 nm compared to the shoulder for the enol radical cation **6b**. Furthermore, the short wavelength shoulder for the enol radical cation **1c** is considerably more distinct than the short wavelength shoulder for the substituted stilbene radical cation. These comparisons suggest that strong electron-donating groups shift the absorption maxima of stilbene radical cations to shorter wavelengths, and also increase the intensity of the short wavelength shoulder. The shift of the absorption maxima to shorter wavelength might also be due to steric factors. As shown by Gaussian calculations, described in section 3.2.2, the enol radical cations are not planar but are considerably twisted. Presumably, the OH group interacts with the aromatic ring forcing the molecule to adopt the twisted conformation. The deviation from a planar structure limits the conjugation along the molecular orbitals, and this might contribute to a shift to shorter wavelengths in the

169

transient spectra of the enol radical cation **1c** compared to the 4,4'-dimethoxystilbene radical cation series.

Overall, the data presented above clearly show that substitution on the stilbene framework does affect the absorption spectra of stilbene radical cations and electron-donating groups attached directly to the carbon-carbon double bond appear to shift absorption bands of stilbene radical cation to shorter wavelengths. These trends are all consistent with a shift to shorter wavelengths for the enol radical cation **4c**. However, the shift still remains larger than expected based on the trends described above, and a complete rationalization of the low wavelength absorption band is currently not available.

While generation of the enol radical cation requires protonation of the oxygen of the α-carbonyl radical, other sites of protonation are also available to the radical. One alternative site is protonation at carbon to generate the keto form of the radical cation, Scheme 3.32.

Scheme 3.32
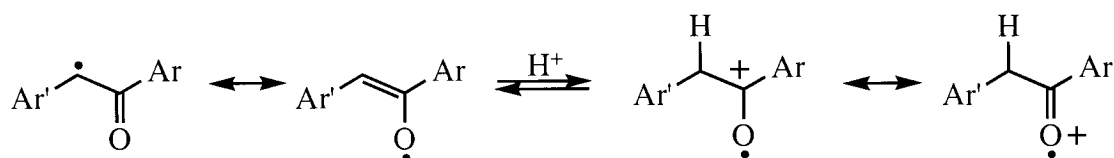
Extensive results from previous studies clearly show that the keto form of the radical cation is less stable than the enol form.[92] As a result, it is unlikely that protonation at carbon to generate the unstable keto radical cation will take place instead of protonation at oxygen. Furthermore, while spectral information for the keto radical cations is not available, there is in general a close correspondence between the spectra observed in the present work and the spectra of stilbene and enol ether radical cations.

The possibility that protonation initially occurs at carbon to generate the keto radical cation, followed by rapid tautomerization to the observed enol form, was also considered, Scheme 3.33. However, tautomerization would likely involve initial deprotonation of the keto form to regenerate the α-carbonyl radical, followed by protonation at oxygen to give the enol radical cation.

Scheme 3.33
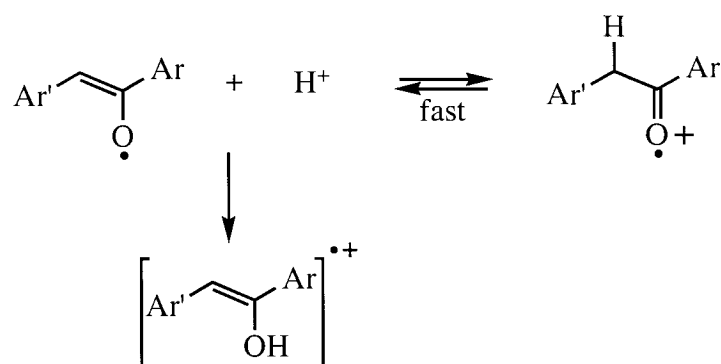
Thus, the enol radical according to this mechanism would still be generated by protonation of the oxygen of the radical, with the keto radical cation being a short-lived, unobserved transient. An alternative mechanism for tautomerization taking place by initial protonation at oxygen of the keto radical cation followed by deprotonation to the enol radical cation is unlikely due to formation of an intermediate with a +2 charge, Scheme 3.34.

Scheme 3.34
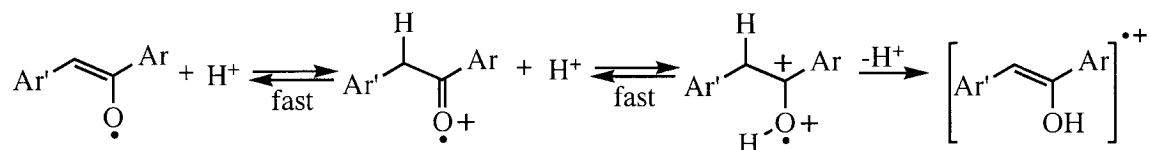
The second possible site of protonation of the radical is on one of the aromatic rings, Scheme 3.35. However, this process should be kinetically and thermodynamically

disfavored as it involves the loss of aromaticity on the aromatic ring containing the carbon being protonated.

Scheme 3.35
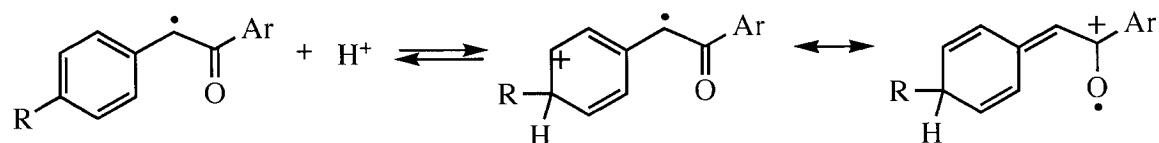
Overall, based on the kinetic and spectral data obtained in this work, it is reasonable to conclude that in acidic conditions the α-keto radicals are protonated at the oxygen of the carbonyl group and that protonation of the α-keto radicals leads to the formation of enol radical cations, Scheme 3.36.

Scheme 3.36
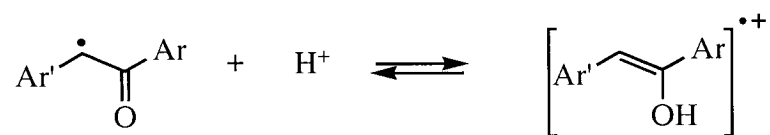
3.3.2 Reactivity of 1,2-Diaryl Enol Radical Cations

Enol radical cations **1c-5c** are all quite long-lived in N_2-saturated acetonitrile containing 0.02 M perchloric acid. Under these conditions, the decay of these species take place over 200 μs in an approximately second-order manner. These relatively long lifetimes are not completely unexpected. As mentioned in the introduction of this chapter, the major reaction pathway for the decay of enol radical cations is the deprotonation of these species. However, under the acidic conditions ($[H^+] \sim 0.01$ - 0.02 M) used in this work, deprotonation is not a reaction pathway that leads to rapid consumption of the enol radical cations.

172

Most previously studied styrene and stilbene radical cations decay in a first-order manner in solvents like acetonitrile and dichloromethane. In general these radical cations are generated from their neutral precursors, and the first-order decay represents a pseudo-first order reaction between the radical cation and its neutral precursor. When this addition reaction is not available or is very slow, the radical cations typically decay in a second-order manner. For example, the anethole radical cation in acetonitrile reacts only very slowly with anethole in acetonitrile, and when generated in laser flash photolysis experiments decays in a second-order manner over ca. 300 μs.[23] In the present work, it is unlikely that the enol radical cations will undergo an addition reaction with their neutral precursors; thus, the observed second-order rate decay over 200 μs is in agreement with results obtained with the anethole radical cation. The nature of the second-order reaction for the enol radical cations or other radical cations like the anethole radical cation is unknown.

The decay of the enol radical cations in O_2-saturated acidic acetonitrile is slightly faster than under N_2-saturated conditions. Generally, radical cations are largely unreactive towards oxygen. For example substituted styrene radical cations do not show any reactivity towards oxygen.[24, 25, 33, 68, 71] Similarly, the decay rate of stilbene radical cation in dichloroethane (DCE) is not affected by the concentration of oxygen. However, Majima et al.[115] have reported that 4-methoxy-substituted stilbene radical cations do react with oxygen in DCE. For example, the radical cation of trans-4-methoxystilbene reacts with oxygen in DCE with a second-order rate constant of 1.3 x 10^7 M^{-1} s^{-1}.[115, 116] Thus, in O_2-saturated DCE ([O_2] = 1.3 x 10^{-2} M)[115] this radical cation decays with a pseudo first-order rate constant of 1.7 x 10^5 s^{-1}, which is of the same order of magnitude as those

observed for the decay of the enol radical cations studied in this work in O_2-saturated

MeCN. According to Majima *et al.*,[115] the unusual reactivity of 4-methoxy-substituted

stilbene radical cations towards oxygen is due to a charge-spin separation induced by the

resonance interaction between the methoxy groups and the positive charge of the radical

cations, Scheme 3.37.

Scheme 3.37

(charge-spin separation)
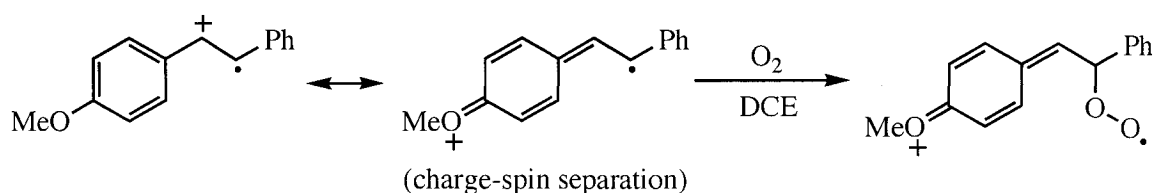
Another possible explanation for the observed reactivity of the enol radical cations

towards oxygen involves the reaction of the α-keto radical with oxygen. Since both

species, the radical cation and the radical, are in equilibrium, the reaction of the α-keto

radical with oxygen will result in the consumption of the radical species. In order to

maintain the equilibrium, the radical cation will also be consumed by rapid deprotonation

to α-keto radical, Scheme 3.38.

Scheme 3.38
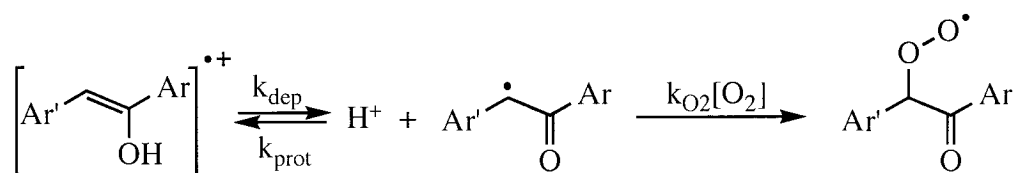
3.3.3 Acidity of Enol Radical Cations

The sensitivity of the maximum absorption of the transients **1c-5c** to the

concentration of perchloric acid supports the identification of these species as enol radical

cations, whose equilibrium concentrations should be affected by the acid content. That

is, at high concentration of acid, the equilibrium between the enol radical cation and its conjugated base is shifted to the side of the radical cation. Consequently, the equilibrium concentration of the enol radical cation is increased and the intensity of the absorption due to these species is maximized. At lower concentrations of acid the conjugated base, the α-carbonyl radical, becomes the dominant species and the absorption due to the enol radical cation is reduced.

The changes in the relative yield of the enol radical cation (**1c**), measured by its absorption at 440 and 480 nm, as a function of the concentration of perchloric acid were used to estimate the acid dissociation constant as defined by Eq. 3.1.

$$\left[Ar\overset{Ar}{\underset{OH}{=}} \right]^{\bullet+} \underset{k_{prot}}{\overset{k_{dep}}{\rightleftharpoons}} Ar\overset{\bullet}{\underset{O}{\diagup}}Ar + H^+; \quad K_a = \frac{[H^+]\left[Ar\overset{\bullet}{\underset{O}{\diagup}}Ar \right]}{\left[Ar\overset{Ar}{\underset{OH}{=}} \right]^{\bullet+}} \qquad \text{(Eq. 3.1)}$$
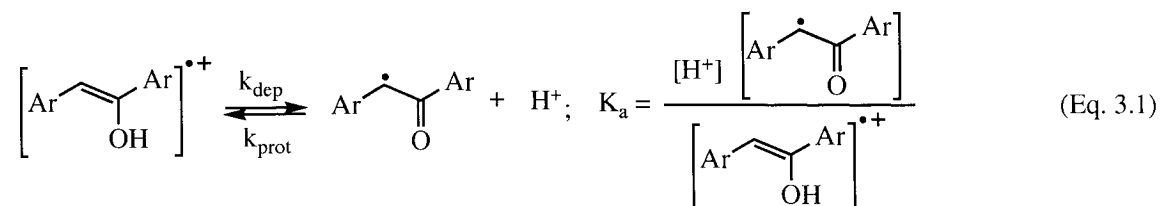
Assuming that the equilibrium is completely shifted to the side of the radical cation in 0.1 M HClO$_4$ N$_2$-saturated acetonitrile, then absorption measurements made at 480 and 440 nm (Abs^{eq}) as a function of the acid concentration can be analyzed using Eq. 3.2 to determine the acid constant, K$_a$, for the equilibrium showed above.

$$Abs^{eq} = Abs^{\infty}\left(\frac{[H^+]+\dfrac{\varepsilon_R K_a}{\varepsilon_{RC}}}{[H^+]+K_a} \right) \qquad \text{(Eq 3.2)}$$

Details concerning the derivation of Eq. 3.2 are given in Appendix B. In this equation Abs$^{\infty}$ is the absorption at high concentration acid (0.1 M HClO$_4$), Abs^{eq} is the absorption when equilibrium between the radical and the radical cation is reached, ε_R and ε_{RC} are the extinction coefficients of the radical species and the radical cation at the

175

wavelength the experiment was carried out, and [H$^+$] is the concentration of added perchloric acid.

As shown in Figure 3.8, the data for the increase in absorption at 480 and 440 nm as the concentration of acid increases fit well to Eq. 3.2. The data obtained at 440 nm gives an acid dissociation constant of 3.5 x 10^{-4} M, almost identical to the K_a of 3.7 x 10^{-4} M measured at 480 nm. Thus, the acid dissociation constant for enol radical cation **1c** is K_a = (3.6 ± 0.5) x 10^{-4} M, corresponding to a pK_a = (3.44 ± 0.06).

The K_a values corresponding to the acid/base equilibriums of radical cations **2c**, **3c**, **4c** and **5c** with their corresponding radicals were also estimated by the approach described above. Table 3.4 lists the equilibrium constants estimated for each one of the enol radical cations.

The acid dissociation constants for the acid/base equilibrium between enol radical cations and the corresponding α-keto radicals were also determined from the relationship between the observed rate constant for the formation of the enol radical cation and the concentration of acid. Given that the formation of the enol radical cation represents the formation of the enol radical cation/α-carbonyl radical equilibrium state, the rate constant observed for the growth of the enol radical cation is the sum of the rate constant for the deprotonation of the enol radical cation, k_{dep}, and the rate constant for the protonation of the radical species multiplied by the concentration of acid, k_{prot}[HClO$_4$] (Eq. 3.3).

$$k_{obs} = k_{dep} + k_{prot}[HClO_4] \hspace{2cm} \text{(Eq. 3.3)}$$

Therefore the value of the acid dissociation constant can be determined by the ratio, $K_a = k_{dep} / k_{prot}$. The value of k_{dep} is obtained from the intercept of the plots shown in Figure 3.7b, 3.16b, 3.23b, 3.31b and 3.34b (for **1c-5c**), while k_{prot} corresponds to the slope

of those plots. The K_a as well as the k_{dep} and k_{prot} values estimated from this approach are given in Table 3.5. Note that Eq. 3.3 is only valid if the enol radical cation and the α-carbonyl radicals do not participate in any other reaction, besides protonation and deprotonation, while the equilibrium state is established (refer to Appendix C).

Table 3.4 Values of K_a estimated from Equation 3.2.
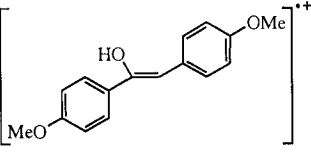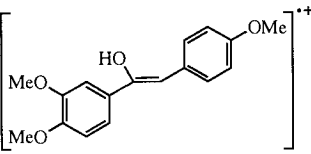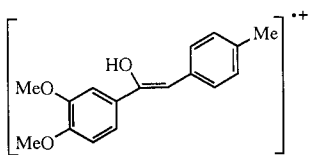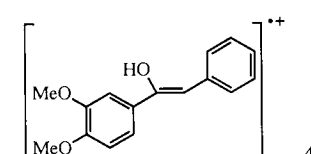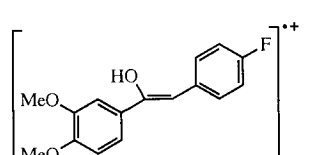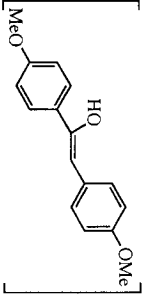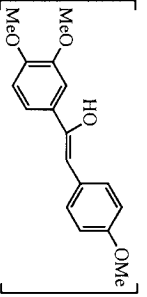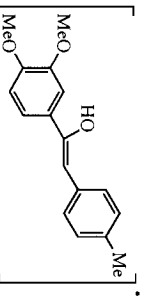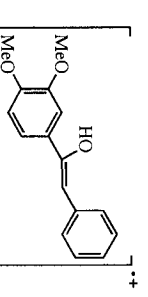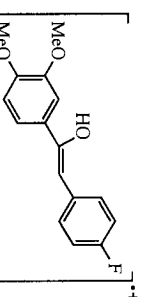
Enol Radical Cation	K_a / M	pK_a
1c	$(3.6 \pm 0.5) \times 10^{-4}$	(3.44 ± 0.06)
2c	$(1.3 \pm 0.3) \times 10^{-4}$	(3.9 ± 0.1)
3c	$(7.2 \pm 0.8) \times 10^{-4}$	(3.14 ± 0.05)
4c	$(1.0 \pm 0.3) \times 10^{-3}$	(3.0 ± 0.1)
5c	$(1.3 \pm 0.5) \times 10^{-2}$	(1.9 ± 0.2)

177

Table 3.5 Values of rate constants k_{prot}, k_{dep} and K_a, obtained from relationship between observed rate constant for the formation of the enol radical cations and the concentration of added $HClO_4$.

Enol Radical Cation	k_{dep} / s^{-1}	k_{prot} / $M^{-1} s^{-1}$	K_a / M	pK_a
1c	$(2.5 \pm 0.3) \times 10^6$	$(4.5 \pm 0.1) \times 10^9$	$(5.6 \pm 0.7) \times 10^{-4}$	(3.25 ± 0.05)
2c	$(5.0 \pm 0.9) \times 10^5$	$(6.6 \pm 0.3) \times 10^9$	$(8 \pm 2) \times 10^{-5}$	(4.1 ± 0.1)
3c	$(4.2 \pm 0.2) \times 10^6$	$(3.5 \pm 0.2) \times 10^9$	$(1.2 \pm 0.1) \times 10^{-3}$	(2.92 ± 0.04)
4c	$(9.4 \pm 0.9) \times 10^6$	$(3.7 \pm 0.2) \times 10^9$	$(2.5 \pm 0.3) \times 10^{-3}$	(2.6 ± 0.4)
5c	$(8.4 \pm 0.4) \times 10^7$	$(6.0 \pm 0.9) \times 10^9$	$(1.4 \pm 0.2) \times 10^{-2}$	(1.85 ± 0.06)

178

As shown in Table 3.5, the rate constants measured for the protonation of the α-keto radicals are basically unaffected by the nature of the substituents. On the other hand, the rate constants for deprotonation change considerably, and range from 5×10^5 s^{-1} for the most stabilized enol radical cation **2c** to 8.4×10^7 s^{-1} for enol radical cation **5c** containing the 4-F group. As a result, the acid dissociation constants are essentially determined by the values of the rate constants for the deprotonation of the enol radical cations. The pK_a values obtained from the ratio k_{dep}/k_{prot}, Table 3.5, are slightly different to the values derived from Eq. 3.2, Table 3.4, presumably due to systematic errors in the two methods used to determine the acid dissociation constants.

As illustrated in Table 3.1, the pK_a values reported for stable enol radical cations in acetonitrile range between 1 and 6. For example, the pK_a of the 1,1-dimesitylprop-1-en-2-ol radical cation is 5.6, while that of the 1,2-dimesitylprop-1-en-1-ol radical cation is 1.3.[92] The pK_a values measured for the enol radical cations (**1c-5c**) studied in the present work vary from 1.8 to 4.1. These values lies in the range of acidity reported for other enol radical cations in acetonitrile, which is consistent with the conclusion that the processes responsible for the effects of acid concentration on the transient yields are related to the enol radical cation/α-keto radical equilibrium.

The deprotonation rate constants measured for **1c-5c** are also consistent with the values reported for other enol radical cations. The values determined for enol radical cations **1c-5c** are of the same order of magnitude as that reported for the deprotonation of the radical cation of the enol of 4-methoxyphenyl acetone ($k_{dep} = 3.9 \times 10^6$ s^{-1}) in acetonitrile.[105]

3.3.3.1 Influence of Substituents on Acidity of Enol Radical Cations

As expected, the values of K_a and k_{dep} are affected by the nature of the substituents on the aryl groups of the enol radical cations. For instance, the rate constant for the deprotonation of the enol radical cations increases almost 100-fold upon substitution of a 4-methoxy group (**2c**) for a 4-fluoro group (**5c**). In order to obtain a more quantitative measure of the influence of electronic substituents effects on the acidity of the enol radical cations, the values of pK_a and log k_{dep} were correlated with the corresponding Hammett substituent constants (σ).

The σ_m values for –OMe ($\sigma_m= 0.10$) reported elsewhere,[81] implies that this substituent in the *meta* position is electron withdrawing and will destabilize a stilbene radical cation with respect to H. However, this is not necessarily true, especially when the methoxy group in *meta* position is accompanied by another MeO group in the corresponding *para* position, i.e. 3,4-dimethoxyphenyl moiety. In fact stilbene enol radical cations with F or H groups at the *para* position of the benzene ring attached to C2 of the carbon-carbon double bond ($R_1 = H$ or F) could not be observed[117] if the other ring attached to C2 contained only a methoxy group on the para position ($R_2 = H$), Scheme 3.39, while the corresponding enol radical cations are observed if the ring attached to C2 contained a second methoxy group at the *meta* position. Thus, the additional 3-methoxy group clearly provides additional stabilization to the radical cation.

Scheme 3.39

$R_2 = H$, $R_1 = F$ or H - enol radical cations could not be observed

$R_2 = OMe$, $R_1 = F$ or H - enol radical cations are observed
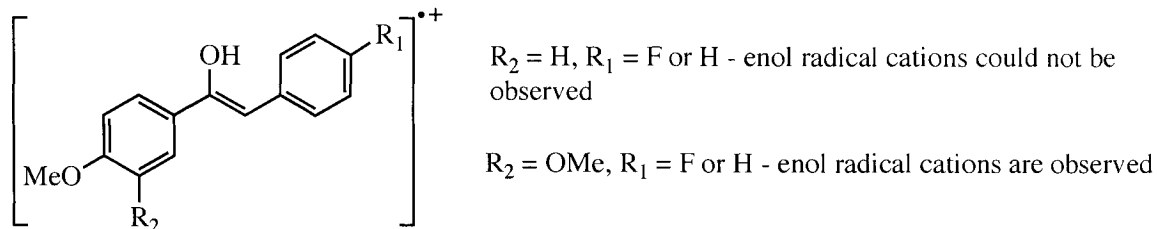
Further evidence supporting the stabilizing character of the MeO group in the *meta* position with respect to H is the fact that the oxidation potential reported for *trans*-3,4-dimethoxystilbene in acetonitrile ($E^{ox} = 0.72$ V *vs* Ag/AgNO$_3$) is considerably smaller than that reported for *trans*-4-methoxystilbene ($E^{ox} = 0.82$ V *vs* Ag/AgNO$_3$) in the same solvent,[115] indicating that the radical cation of the for *trans*-3,4-dimethoxystilbene is slightly more stable than the mono *para* substituted for *trans*-4-methoxystilbene, Scheme 3.40. An identical result is observed for the corresponding *cis* isomers also in acetonitrile, with the *cis*-3,4-dimethoxystilbene having an oxidation potential of 0.87 V *vs* Ag/AgNO$_3$ and *cis*-4-methoxystilbene having an $E^{ox} = 0.94$ V *vs* Ag/AgNO$_3$.[115]

Scheme 3.40

$E^{ox} = 0.72$ V vs Ag/AgNO$_3$ in MeCN

$E^{ox} = 0.82$ V vs Ag/AgNO$_3$ in MeCN
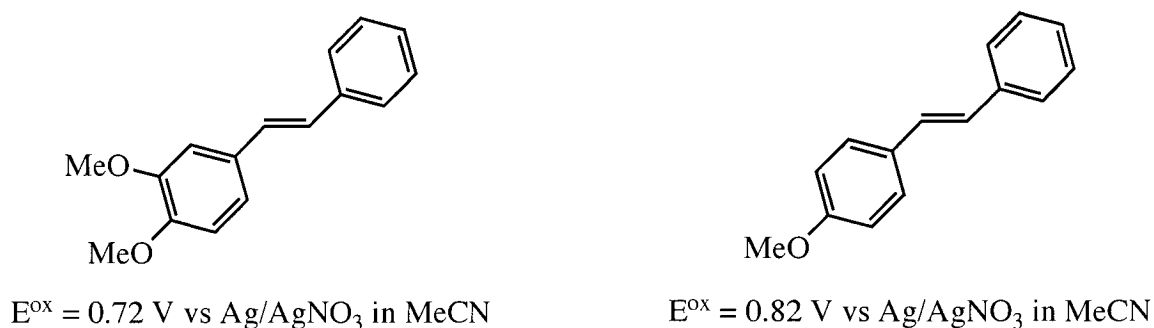
The sigma scales developed by Hammett assumes the interaction of the substituent with charge or electron density located on the α-carbon of a substituted aromatic ring (refer to Scheme 3.41). Thus, a methoxy group in the meta position is supposed to destabilize a positive charge in the α position because the magnitude of the electron

181

withdrawing inductive effect associated with this 3-MeO group is felt more strongly at the α-carbon than the electron-donating resonance effect of a MeO group. However, in the case of radical cations the positive charge can be located on the α-carbon and on the β-carbon. Therefore, the 3-MeO group will destabilize the positive charge located on the α-carbon but it will donate electron density, by resonance, to the β-carbon, Scheme 3.41. Presumably, this is the reason for the extra stabilization provided by a meta-methoxy group, compared to H, to stilbene radical cations.

Scheme 3.41

electron withdrawing
inductive effect

electron donor - resonane effect
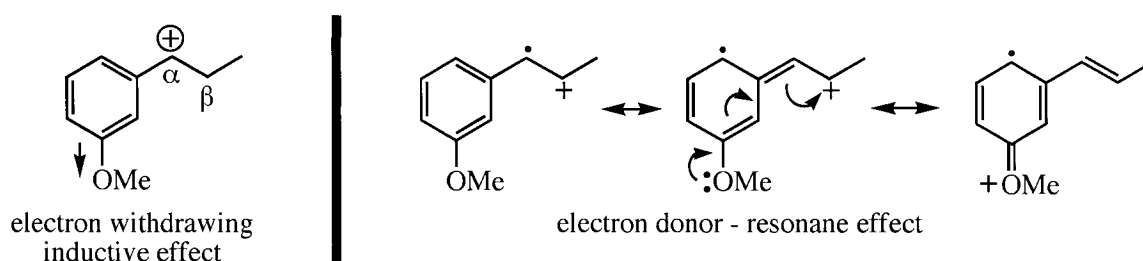
Given the lack of an appropriate value of σ_m for the MeO group, the values of $[\sigma_m + \sigma_p]$ and $[\sigma_m + \sigma_p]^+$ used in this work were estimated simply by plotting the E^{ox} reported[115] for stilbene, 4-methoxystilbene, 4,4'-dimethoxystilbene and 4-methylstilbene versus the sum of the corresponding σ_p or σ_p^+, Figure 3.37. The lines-of-best-fit for these plots were obtained by linear-least square analysis. Then, the values of $[\sigma_m + \sigma_p] = -0.4$ and $|\sigma_m + \sigma_p]^+ = -1.1$ were extrapolated from the E^{ox} reported for 3,4-dimethoxystilbene. Table 3.6 lists the values of sigma and sigma plus constants used in this work. The sigma values for individual substituents were added in order to obtain the sigma values used to create the Hammett plots. For instance, the reported σ_p^+ for MeO groups is -0.78,[81] thus the sigma plus value used for compound 1c was $-0.78 + -0.78 = -1.56$.

182

Table 3.6 Sigma and sigma plus values used in this work to obtain the Hammett plots.
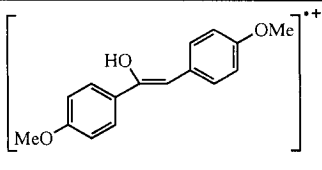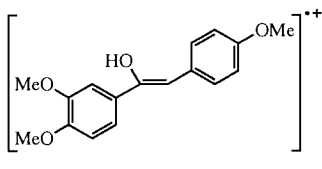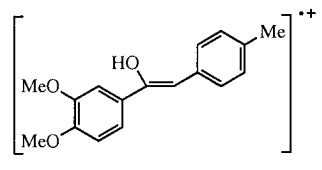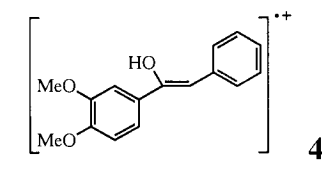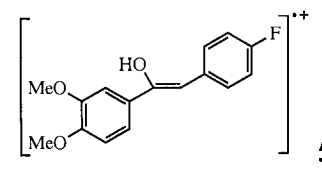
Enol Radical Cation	$\Sigma[\sigma]$	$\Sigma[\sigma^+]$
1c	-0.56	-1.56
2c	-0.65	-1.84
3c	-0.51	-1.37
4c	-0.37	-1.06
5c	-0.22	-1.13

Figure 3.38, shows the Hammett plots correlating pK_a and $\log[k_{dep}]$ with the corresponding σ^+ values. As can be seen, the trend is consistent with the fact that electron donating groups stabilize the enol radical cations. Therefore, the better the electron donating properties of the substituents, the smaller the deprotonation rate constant for the enol radical cation and the larger the pK_a. In other words, the radical cation becomes more acidic as the electron donor properties of the substituents decrease. The coefficient for the deprotonation reaction ($\rho^+ = 1.9$) obtained from the slope of the

plot of $\log[k_{dep}]$ versus σ^+ is almost similar to the coefficient obtained from the plot of pK_a vs σ^+ ($\rho^+ = 2.2$). It should be noticed however that the correlation observed in these plots is poor, $R^2 \sim 0.816$ and 0.828. Specifically, the correlation is poor due to the enol radical cation **5c** with the F group in *para* position.

A much better correlation is obtained when the pK_a ($R^2 = 0.969$) and $\log[k_{dep}]$ ($R^2 = 0.985$) are plotted against the corresponding σ values, Figure 3.39. The trend is again consistent with the stabilization of the enol radical cations by electron donor substituents. That is, as the electron donating properties of the substituents are increased, the σ value becomes more negative, and the stability of the radical cation is increased. This is reflected in a decrease in the deprotonation rate constant and a decrease in the acid dissociation constant. The coefficient factor or reaction constant (ρ) obtained from the slope of the plot of $\log[k_{dep}]$ vs $\Sigma\sigma$ values ($\rho = 4.3$) is almost identical to that obtained from the plot of pK_a vs $\Sigma\sigma$ ($\rho = 4.6$), which is consistent with the lack of influence of the substituents on the rate constants for the protonation of the α-keto radicals, Table 3.5. Since the acid dissociation constant is equal to the ratio k_{dep}/k_{prot}, the changes in values of k_{dep} are directly reflected on the values of K_a.

The value of the reaction constant $\rho \sim 4.4$ is relatively high, and indicates that the deprotonation reaction is quite sensitive to substituents effects. That is, the deprotonation of the enol radical cations is four times more sensitive to the nature of the substituents than the deprotonation of benzoic acid. Typically, a large sensitivity to electronic substituents effects for a given reaction indicates that the reactants and the transition state are very different in terms of charge development.

184

Since enol radical cations are positively charged species, the deprotonation of these species does not involve charge development but a reduction of the positive charge. The transition state for the deprotonation should possess little charge compared to the enol radical cation. The large electronic substituent effects are due to stabilization or destabilization of the radical cation, no the transition state structure. These results are consistent with a late transition state, *i.e.* a transition state that appears late along the reaction pathway, Scheme 3.42. In this late transition state, the proton-oxygen bond is substantially weakened and the interaction of the substituents with the positive charge is considerably weakened. The weak interaction between the substituents and the positive charge in the transition state is consistent with the absence of substituent effects on the rate constants for the protonation of the α-keto radicals.

Scheme 3.42

reaction coordinate
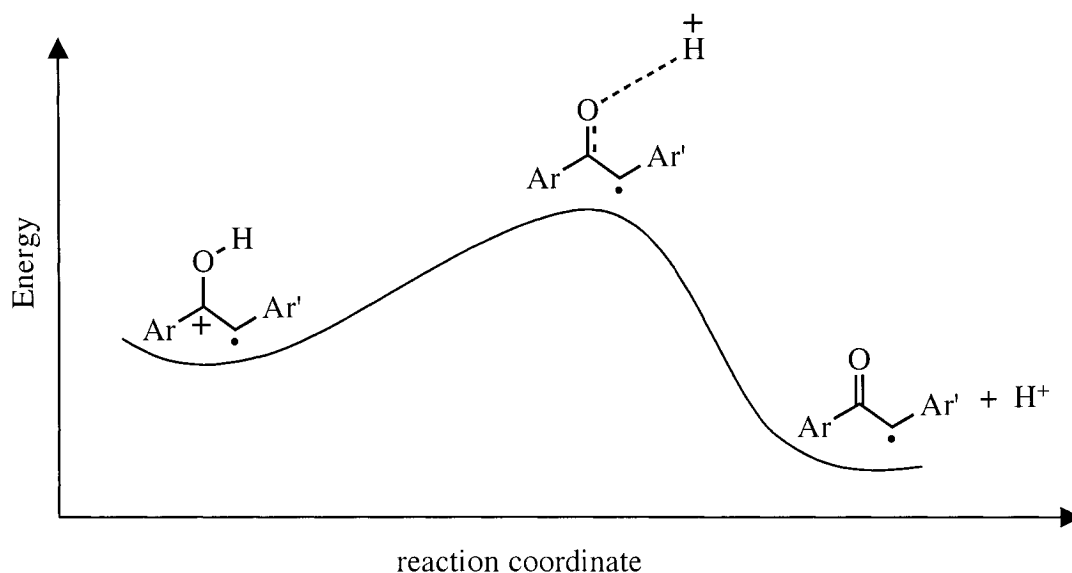
3.3.3.2 Gaussian Calculations

Given that compounds **1c-5c** are positively charged species containing substituents in the *para* position that are able to donate electronic density by direct resonance with the positive charge, Scheme 3.43, it was expected to obtain better Hammett plots using σ^+ than σ values. As explained above the results indicate exactly the opposite; thus Gaussian calculations were performed in order to understand this contradictory behavior.

Scheme 3.43
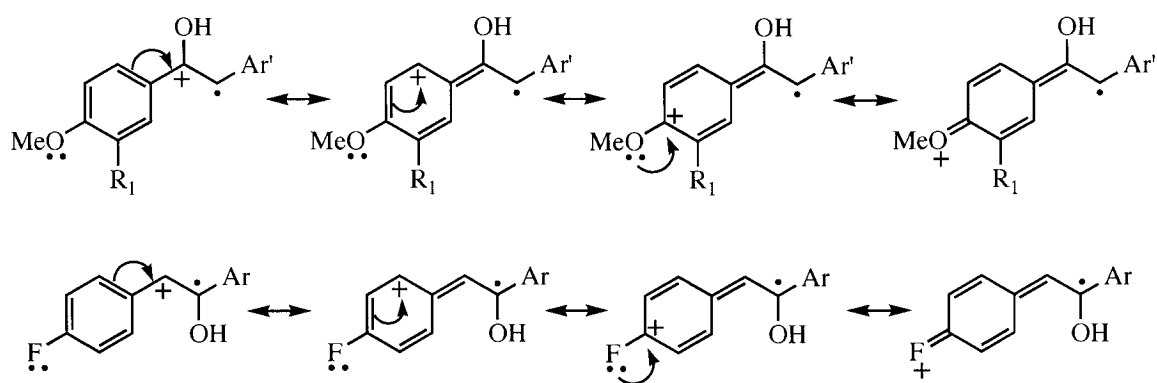
According to the theoretical calculations, the geometries of **1c-5c** are not planar. As shown in Figure 3.36, the aromatic ring bonded to the carbon containing the hydroxyl group is twisted ca. 25° with respect to the rest of the molecule. Clearly, this distortion will limit the conjugation of the -OMe group in the *para* position with the positive charge located on the carbon bonded to the OH group. Therefore, the twisted geometry could be the cause for the better correlation between pK_a and $\log k_{dep}$ with σ rather than σ^+ for the substituents on the ring bonded to the carbon bearing the OH group.

On the other hand, the twisted geometry does not exclude a direct conjugation between the positive charge and the substituent in the *para* position on the aromatic ring farthest away from the OH group. However, a comparison of the Mulliken charges

186

located on the carbons 3 and 4 (refer to Table 3.3) indicates that most of the positive charge is located on the carbon bearing the OH group, and carbon 4 is slightly negatively charged. Therefore the *para* substituent on the ring farthest from the OH group will not be in direct resonance with the positive charge. This justifies why the σ factor provides a better description for the substituent effects than σ^+.

According to the thermodynamic cycle represented in Scheme 3.44, the energy associated with the ionization of the neutral enols is proportional to the stability of the resulting enol radical cation. Therefore we should expect a good correlation between the ionization potential and the pK_a or the k_{dep} measured for the radical cations. Indeed these parameters are well correlated as can be observed in Figure 3.40. As anticipated, the larger the ionization energy, the smaller the stability of the enol radical cation.

Scheme 3.44
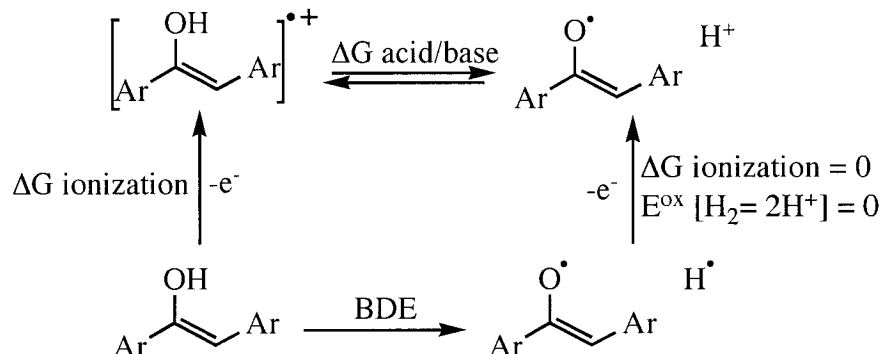
$$\Delta G \ (acid/base) \ \alpha \ pK_a = BDE - \Delta G \ (ionization)$$

3.4 Experimental Section

Materials. Perchloric acid (60 % w/w) was purchased from Fisher Scientific Company. Acetonitrile used for laser flash photolysis experiments was spectroscopic grade supplied

by Omnisolv, BDH. All the other chemicals used were purchased from Aldrich Chemical Co. and used as received. Hexanes, ethylacetate and dichloromethane were distilled prior to use.

α-bromoketones (**1a-5a**) were prepared by treating the corresponding ketones with bromine in presence of $AlCl_3$. 1,2-bis(4-methoxyphenyl)ethanone (deoxyanisoin) was purchased from Aldrich and used as received. The rest of the ketones were prepared following the procedure reported in the literature for the synthesis of deoxyanisoin.[118]

General Procedures. NMR spectra were recorded on a Brucker AV-500 spectrometer at the Atlantic Region Magnetic Resonance Centre at Dalhousie University. The data were processed with Brucker Xwin-NMR software. Chloroform-d ($CDCl_3$, 0.05 % TMS) was the solvent employed for NMR experiments. Proton chemical shifts were calculated relative to trimethylsilane (TMS) and ^{13}C chemical shifts were determined using the central peak of the $CDCl_3$ carbon signal ($\delta = 77.16$ ppm) as reference. Melting points were measured on a Fisher-Johns apparatus. High resolution mass spectroscopy (HRMS) was performed using a CEC 21-110B mass spectrometer. Spectra were obtained using electron ionization at 70 Volts and a source temperature of 160 °C. Absorption spectra of solutions prior to irradiation, and measurement of the absorption of solutions at the appropriate excitation wavelengths were determine using a Cary 100 Bio UV-Visible spectrometer. Table 3.7 lists maximum absorption wavelengths and the extinction coefficients of the α-bromoketones (**1a-5a**) used to generate the enol radical cations.

Computations were performed with the Gaussian 98 series of programs. The geometries of the enol radical cations and the corresponding neutral enols were fully optimized using the B3LYP correlation functional in conjunction with the 6-31G(d) basis set. The

optimized species were determined to be either minima or saddle points by frequency calculations.

Table 3.7   Maximum absorption wavelengths and extinction coefficients of α-bromoketones measured in acetonitrile.

α-bromoketone	λ_{max} (nm)	ε (M^{-1} cm^{-1})
1a	286	18900
2a	279	9200
	310	7430
3a	282	10440
	315	10000
4a	283	9370
	315	9190
5a	284	8800
	316	8900

Laser experiments. The nanosecond laser system used for laser flash photolysis experiments is thoroughly described on Chapter 4. A Lambda Physiks excimer laser (308 nm, XeCl, 10 ns/pulse, < 100 mJ/pulse) was used for experiments involving direct irradiation of the α-bromoketones. In experiments involving photoinduced electron transfer, a Spectra Physics Quanta Ray INDI-40-10 Nd:YAG laser (355 nm, < 8 ns/pulse, 100 mJ/pulse) was used as the excitation source.

Samples for kinetic experiments were placed in 7 x 7 mm laser cells made out of Suprasil quartz tubing. Solutions were prepared by the addition of small aliquots (~5 μL) of stock solutions of the appropriate α-bromoketones to 1.0 mL of acetonitrile contained in the laser cells. The absorption of the α-bromoketones in the laser cells was approximately 0.4 at 308 nm, corresponding to concentrations of ca. 1 x 10^{-4} M. Solutions for

experiments carried out under acidic conditions were prepared by making a stock solution ($[HClO_4]$ = 0.10 M) of perchoric acid in acetonitrile, and then making the appropriate dilutions with acetonitrile. In order to minimize the possibility of acid-catalyzed decomposition of the α-bromoketones, these substrates were added to the acidic solution just prior to performing the laser experiments. For instance, the observed rate constants for the growth of the radical cation **1b** at increasing acid concentration were obtained by adding 1.0 μL of a 0.10 M solution of perchloric acid to a laser cell containing 1.0 mL of acetonitrile containing 6.0 x 10^{-5} M of deoxyanisoin (**1a**). The resulting solution was irradiated with a laser pulse at 308 nm and the growth of the radical cation was monitored at 480 nm. A second solution was then prepared by adding 2.0 μL of a 0.10 M solution of perchloric acid containing 6.0 x 10^{-5} M of deoxyanisoin (**1a**), and the growth of the radical cation was measured again. The procedure was repeated until the growth of the radical cation was measured at five to ten different concentrations. A new cell was prepared for each concentration of perchloric acid in order to avoid decomposition of the starting material. Measurements at each concentration was repeated three times. In photoinduced electron transfer experiments, acetonitrile solutions of the sensitizer were prepared so that the absorption of sensitizer at 355 nm was 0.4. Appropriate amounts of stock solutions with known concentrations of the α-bromoketones were then added. Absorption spectra were measured using a flow cell system to ensure that only fresh solution was subjected to each laser pulse. Most laser experiments were carried out using nitrogen-saturated conditions, which was achieved by bubbling the samples with a slow stream of dry nitrogen for 20 min prior to laser irradiation. All laser experiments were carried out at room temperature (22 ± 1 °C).

Synthesis

Procedure for the preparation of 1,2-diarylethanones

The appropriate 4-substituted phenylacetyl chloride (10 mmol) was added to a mixture of AlCl₃ (1.900 g; 14.35 mmol) and 3,4-dimethoxybenzene (1.584 g, 1.459 mL, 11.45 mmol) in 15 mL of 1,2-dichloroethane under cooling (ice bath). After refluxing for 2 hours the mixture was added over 50 mL of water, the organic layer was separated and dried over MgSO₄. The solvent was then removed yielding a brown oil, which was re-crystallized from diethylether.

1-(3,4-Dimethoxyphenyl)-2-(4-methoxyphenyl)ethanone: yellowish solid, 63 % yield. mp: 104-106°C. (lit.[119] mp 115 °C, lit.[120] mp 107 °C). ^{1}H NMR(CDCl₃-500 MHz): δ 7.64 (dd, 1H, J = 8.0, 2.0 Hz), 7.54 (d, 1H, J = 2.0 Hz), 7.18 (d, 2H, J = 8.5 Hz), 6.87-6.84 (m, 3H), 4.17 (s, 2H), 3.92 (s, 3H), 3.90 (s, 3H), 3.76 (s, 3H) ppm. ^{13}C NMR(CDCl₃-125.8 MHz): δ 1.96.7, 158.6, 153.4, 149.1, 130.4, 129.9, 127.1, 123.47, 114.2, 110.8, 110.1, 56.1, 56.0, 55.3, 44.4 ppm.

1-(3,4-Dimethoxyphenyl)-2-tolylethanone: yellowish solid, 57 % yield.

mp: 95-97°C. ^{1}H NMR(CDCl₃-500 MHz): δ 7.64 (dd, 1H, J = 8.5, 2.0 Hz), 7.46 (d, 1H, J = 2.0 Hz), 7.16 (d, 2H, J = 8.0 Hz), 7.11 (d, 2H, J = 8.0 Hz), 6.86 (d, 1H, J = 8.5 Hz), 4.18 (s, 2H), 3.91 (s, 3H), 3.89 (s, 3H), 2.30 (s, 3H) ppm. ^{13}C NMR(CDCl₃-125.8 MHz): δ 196.6, 153.4, 149.1, 136.4, 132.1, 129.9, 129.4, 129.2, 123.5, 110.8, 110.1, 56.1, 56.0, 44.9, 21.1 ppm.

1-(3,4-Dimethoxyphenyl)-2-phenylethanone: colorless solid, 78 % yield.

mp: 79-80°C (lit.[121] mp 101-103°C, lit.[120] mp 82 °C). ^{1}H NMR(CDCl₃-500 MHz): δ 7.65 (dd, 1H, J = 8.5, 2.0 Hz), 7.55 (d, 1H, J = 2.0 Hz), 7.33 - 7.23 (m, 4H), 6.87 (d, 2H, J =

8.5 Hz), 4.23 (s, 2H), 3.93 (s, 3H), 3.90 (s, 3H) ppm. ^{13}C NMR(CDCl$_3$-125.8 MHz): δ

196.4, 153.5, 149.2, 135.2, 129.9, 129.9, 129.4, 128.8, 126.9, 123.6, 110.9, 110.2, 56.2,

56.1, 45.3 ppm.

1-(3,4-Dimethoxyphenyl)-2-(4-fluorophenyl)ethanone: colorless solid, 95 % yield.

mp: 100-102 °C (lit.[121] mp 102-103 °C). ^{1}H NMR(CDCl$_3$-500 MHz): δ 7.64 (dd, 1H, J =

8.5, 2.0 Hz), 7.46 (d, 1H, J = 2.0 Hz), 7.22 (dd, 2H, J = 8.0, 5.5 Hz), 7.00 (t, 2H, J = 8.0

Hz), 6.89 (d, 1H, J = 8.5 Hz), 4.21 (s, 2H), 3.94 (s, 3H), 3.91 (s, 3H) ppm. ^{13}C

NMR(CDCl$_3$-125.8 MHz): δ 196.2, 163.0, 161.0, 153.7, 149.4, 131.4, 131.0, 130.8,

129.8, 123.5, 115.5, 110.9, 110.2, 56.2, 56.1, 44.3 ppm.

Procedure for synthesis of α-bromoketones (1a-5a).

The α-bromoketones according to the method reported by Moreno *et al*.[122] Bromine (4.0

mmol) was added to a solution of 1,2-diarylethanone (1.0 mmol) in THF (30mL)

containing 20 mg of AlCl$_3$. The mixture was stirred for three hours and then the solvent

was evaporated under vacuum. The resultant brown oil was extracted with

water/dichloromethane, the organic fractions were dried over MgSO$_4$, filtered and

evaporated under vacuum. The crude product was then purified through silica gel

column using ethyl acetate/hexanes as solvent system.

2-bromo-1,2-bis(4-methoxyphenyl)ethanone (1a): yellowish solid, 85 % yield. mp:

101-103°C. (lit.[123] mp 103-105 °C) The NMR data is consistent with that reported in the

literature.[123] ^{1}H NMR(CDCl$_3$-500 MHz): δ 7.96 (d, 2H, J = 9.0 Hz), 7.75 (d, 1H, J = 2.0

Hz), 7.54 (dd, 1H, J = 8.5, 2.0 Hz), 6.91 (d, 2H, J = 9.0 Hz), 6.85 (d, 2H, J = 8.5 Hz),

6.29 (s, 1H), 3.86 (s, 3H), 3.84 (s, 3H) ppm. ^{13}C NMR(CDCl$_3$-125.8 MHz): δ 189.6,

164.2, 156.4, 134.1, 131.6, 129.6, 126.7, 114.2, 112.0, 56.4, 55.6, 49.4 ppm. HRMS (M$^+$) calcd for C$_{16}$H$_{15}$BrO$_3$, 334.0205; found 334.0201.

2-Bromo-1-(3,4-dimethoxyphenyl)-2-(4-methoxyphenyl)ethanone (2a): Yellowish oil, 89 % yield. ^{1}H NMR(CDCl$_3$-500 MHz): δ 7.55 (dd, 1H, J = 8.5, 2.0 Hz), 7.53 (d, 1H, J = 2.0 Hz), 7.40 (d, 2H, J = 8.5 Hz), 6.88 (d, 2H, J = 8.5 Hz), 6.83 (d, 1H, J = 8.5 Hz), 6.30 (s, 1H), 3.91 (s, 3H), 3.89 (s, 3H), 3.78 (s, 3H) ppm. ^{13}C NMR(CDCl$_3$-125.8 MHz): δ 190.2, 160.3, 153.9, 149.4, 129.9, 128.5, 127.5, 123.8, 114.7, 111.6, 110.3, 62.0, 56.2, 56.1, 55.4 ppm. HRMS (M$^+$) calcd for C$_{17}$H$_{17}$BrO4, 364.0310; found 364.0315

2-Bromo-1-(3,4-dimethoxyphenyl)-2-tolylethanone (3a): Yellowish oil, 90 % yield. ^{1}H NMR(CDCl$_3$-500 MHz): δ 7.59 (dd, 1H, J = 8.5, 2.0 Hz), 7.55 (d, 1H, J = 2.0 Hz), 7.42 (d, 2H, J = 8.0 Hz), 7.16 (d, 2H, J = 8.0 Hz), 6.84 (d, 2H, J = 8.5 Hz), 6.38 (s, 1H), 3.92 (s, 3H), 3.90 (s, 3H), 2.32 (s, 3H) ppm. ^{13}C NMR(CDCl$_3$-125.8 MHz): δ 189.9, 153.9, 149.4, 139.2, 133.6, 129.8, 129.0, 127.2, 123.8, 111.6, 110.2, 56.2, 56.1, 51.4, 21.3 ppm. HRMS (M$^+$) calcd for C$_{17}$H$_{17}$BrO$_3$, 348.0361; found 348.0357

2-Bromo-1-(3,4-dimethoxyphenyl)-2-phenylethanone (4a): Yellowish oil, 86 % yield. ^{1}H NMR and ^{13}C NMR spectra in CDCl$_3$ are identical to those reported in the literature.[122] ^{1}H NMR(CDCl$_3$-500 MHz): δ 7.61 (dd, 1H, J = 8.5, 2.0 Hz), 7.56-7.53 (m, 3H), 7.37-7.30 (m, 3H), 6.85 (d, 1H, J = 8.5 Hz), 6.39 (s, 1H), 3.920 (s, 3H), 3.90 (s, 3H) ppm. ^{13}C NMR(CDCl$_3$-125.8 MHz): δ 189.8, 153.9, 149.4, 136.5, 129.1, 129.1, 129.06, 127.2, 126.9, 123.8, 111.6, 110.2, 56.2, 56.1, 51.1 ppm. HRMS (M$^+$) calcd for C$_{16}$H$_{15}$BrO$_3$, 334.0205; found 334.0199.

2-Bromo-1-(3,4-dimethoxyphenyl)-2-(4-fluorophenyl)ethanone (5a): Yellowish oil, 88 % yield. ^{1}H NMR(CDCl$_3$-500 MHz): δ 7.61 (dd, 1H, J = 8.5, 2.0 Hz), 7.56-7.52 (m,

3H), 7.05 (t, 2H, J = 8.5 Hz), 6.87 (d, 1H, J = 8.5 Hz), 6.35 (s, 1H), 3.93 (s, 3H), 3.91 (s,

3H) ppm. ^{13}C NMR(CDCl$_3$-125.8 MHz): δ 189.7, 164.0, 162.0, 154.1, 149.5, 132.3,

132.3, 131.2, 131.1, 127.0, 123.8, 116.1, 115.9, 111.5, 110.3, 62.1, 56.2, 56.1 ppm.

HRMS (M$^+$) calcd for C$_{16}$H$_{14}$BrFO$_3$, 352.0110; found 352.0107.

Procedure for preparation of enol methyl ethers:

(E)-1-Methoxy-1,2-bis(4-methoxyphenyl)ethene (6a): Prepared according to procedure

reported by Krow et al.[124] A solution of 1,2-bis(4-methoxyphenyl)ethanone (508 mg;

1.97 mmol) in 20 mL of hexamethylphosphoric triamide was cooled to 5°C. Potassium

tert-butoxide (850 mg; 7.1 mmol) was added to the solution and the mixture was stirred

for 4 minutes. Then methyl fluorosulfonate (900 mg; 688 μL; 6.5 mmol) was added and

the mixture was stirred for 3 minutes. The reaction was quenched by pouring into 50 mL

of water. The crude product was extracted with diethyl ether. The combined organic

fractions were dried over Na$_2$SO$_4$ and evaporated under vacuum to yield a yellowish oil.

Further purification by column chromatography (Silica; CH$_2$Cl$_2$/MeOH (1%)) afforded

the desired product as colorless crystals, 30% yield.

mp: 112-114 °C (lit.[124] mp 114-115 °C). ^{1}H NMR(CDCl$_3$-500 MHz): δ 7.63 (d, 2H, J =

8.5 Hz), 7.47 (d, 2H, J = 8.5 Hz), 6.92 (d, 2H, J = 9.0 Hz), 6.88 (d, 2H, J = 9.0 Hz), 5.98

(s, 1H), 3.84 (s, 3H), 3.82 (s, 3H), 3.61 (s, 3H) ppm. ^{13}C NMR(CDCl$_3$-125.8 MHz): δ

159.8, 158.2, 154.6, 129.8, 129.2, 129.1, 127.8, 114.0, 114.0, 111.1, 57.9, 55.5, 55.4

ppm. HRMS (M$^+$) calcd for C$_{17}$H$_{18}$O$_3$, 270.1256; found 270.1255

1-Methoxy-1-(3,4-dimethoxyphenyl)-2-(4-methylphenyl)ethene (7a):

This product was obtained as yellowish crystals in 36 % yield by following the same

procedure used to prepare **6a**.

194

mp: 98-100°C. ^{1}H NMR(CDCl$_3$-500 MHz): δ 7.58 (d, 2H, J = 8.1 Hz), 7.16-7.13 (m, 3H), 7.07 (d, 1H, J = 1.9 Hz), 6.89 (d, 1H, J = 8.3 Hz), 6.02 (s, 1H), 3.93 (s, 3H), 3.91 (s, 3H), 3.63 (s, 3H), 2.35 (s, 3H) ppm. ^{13}C NMR(CDCl$_3$-125.8 MHz): δ 155.6, 149.4, 149.1, 136.3, 133.3, 129.6, 129.2, 128.5, 119.4, 111.8, 111.2, 109.7, 58.0, 56.1, 21.4 ppm. HRMS (M$^+$) calcd for C$_{18}$H$_{20}$O$_3$, 284.1412; found 284.1413.

1-Methoxy-1-(3,4-dimethoxyphenyl)-2-phenylethene (8a): This product was obtained as a colorless oil in 34 % yield by following the same procedure used to prepare **6a**

^{1}H NMR(CDCl$_3$-500 MHz): δ 7.69 (d, 2H, J = 7.6 Hz), 7.33 (t, 2H, J = 7.6 Hz), 7.19 (t, 1H, J = 7.4 Hz), 7.14 (dd, 1H, J = 8.3; 2.0 Hz), 7.07 (d, 1H, J = 2.0 Hz), 6.88 (d, 1H, J = 8.3 Hz), 6.02 (s, 1H), 3.92 (s, 3H), 3.91 (s, 3H), 3.64 (s, 3H) ppm. ^{13}C NMR(CDCl$_3$-125.8 MHz): δ 156.3, 149.5, 149.0, 136.1, 129.4, 128.6, 128.5, 126.5, 119.6, 111.7, 111.2, 109.8, 58.0, 56.1 ppm. HRMS (M$^+$) calcd for C$_{17}$H$_{18}$O$_3$, 270.1256; found 270.1253.

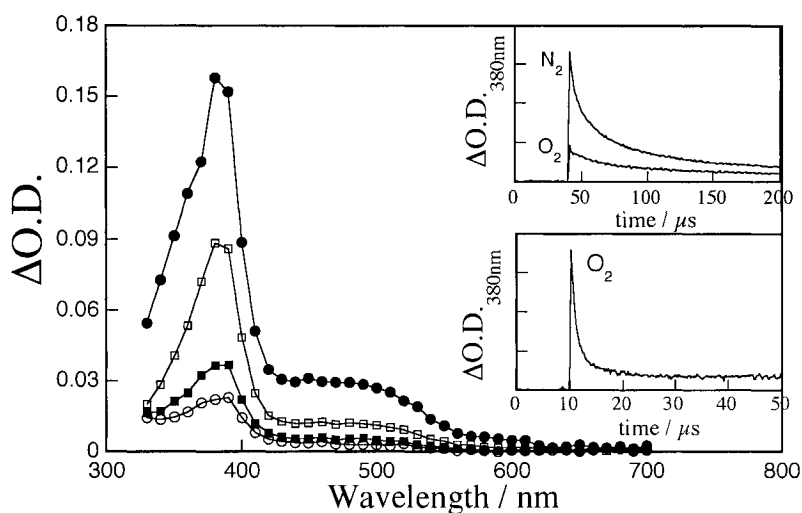**Figure 3.2** Transient spectra obtained (●) 1.60 μs, (□) 10.8μs, (■) 61.2μs and (○) 128 μs after 308-nm laser irradiation of α-bromodeoxyanisoin (**1a**) in N$_2$-saturated acetonitrile. Insets show time-resolved absorption changes at 380 nm upon 308-nm laser irradiation of α-bromodeoxyanisoin (**1a**) in N$_2$ and O$_2$-saturated acetonitrile.

Figure 3.3 Transient spectra obtained (●) 1.40 μs, (□) 6.12 μs and (■) 12.8 μs after 308-nm laser irradiation of deoxyanisoin in N$_2$-saturated acetonitrile. Insets show time-resolved absorption changes at 390 nm upon 308-nm laser irradiation of deoxyanisoin in (□) N$_2$ and (●) O$_2$-saturated acetonitrile.
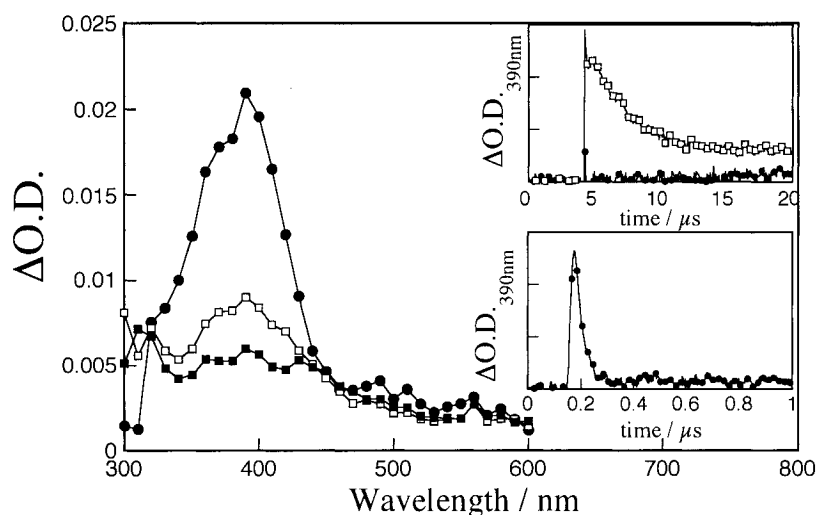
196
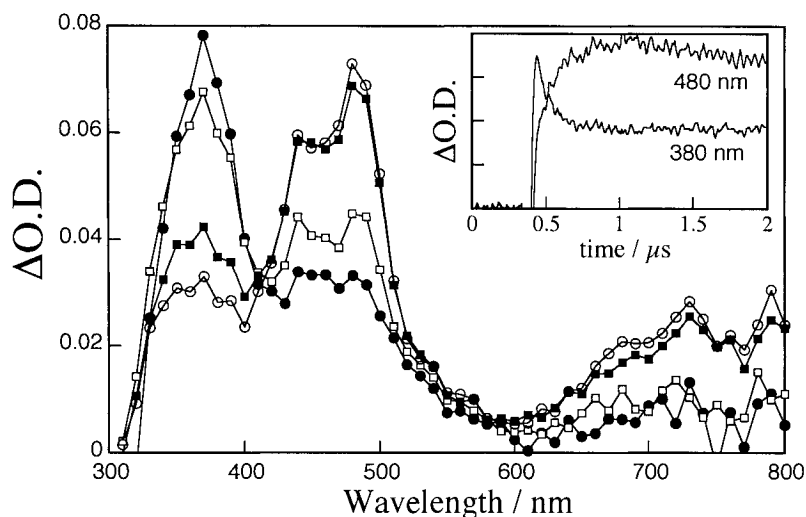
Figure 3.4 Transient spectra obtained (●) 0.052 μs, (□) 0.148 μs, (■) 0.62 μs and (○) 1.29 μs after 266-nm laser irradiation of α-bromodeoxyanisoin (**1a**) in N_2-saturated acetonitrile containing 0.005 M $HClO_4$. Inset shows time-resolved absorption changes at 480 and 380 nm upon 266-nm laser irradiation of **1a** in N_2-saturated acetonitrile containing 0.001 M $HClO_4$.
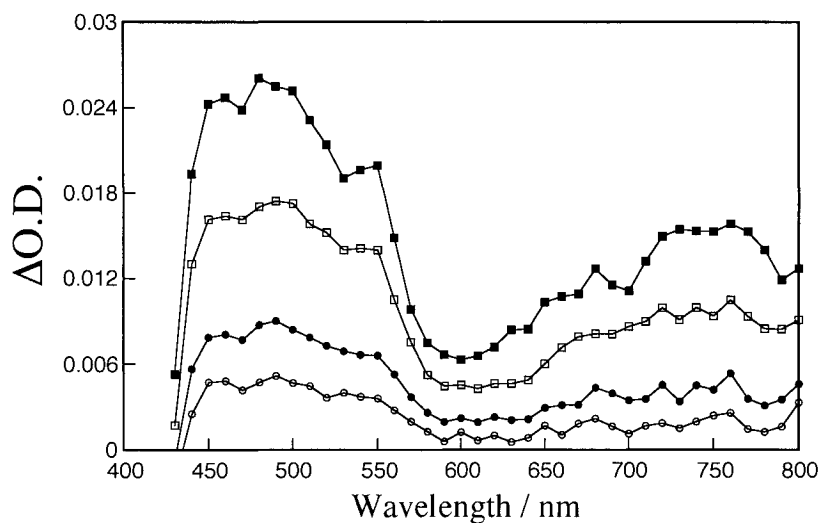
Figure 3.5 Transient spectra obtained (■) 7.0 μs, (□) 37 μs, (●) 145 μs and (○) 320 μs after 355-nm laser irradiation of triphenylpyrilium tetraborate (1.18 x 10-5 M) in N_2-saturated acetonitrile containing 1 mM of 1-methoxy-1,2-di-(4-methoxyphenyl)ethene (**6a**).

197
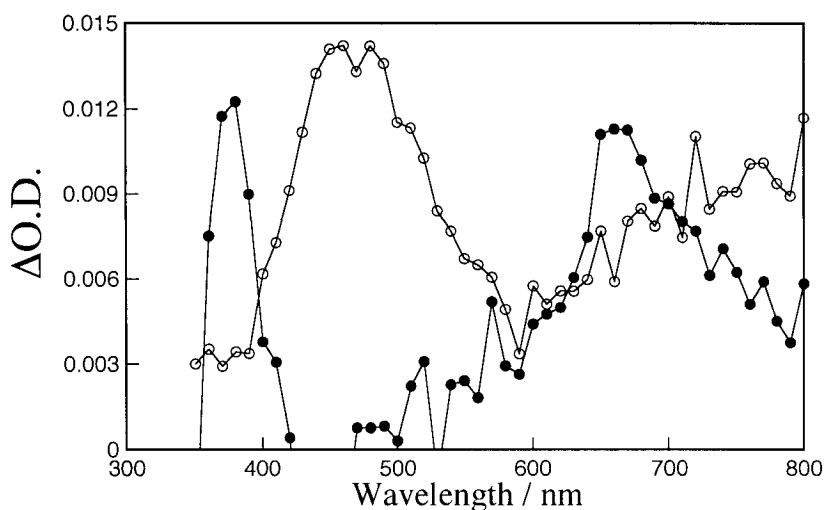
Figure 3.6 Transient spectra obtained (●) 3.20 μs after 355-nm laser irradiation of 9,10-dicyanoanthracene (1.18 x 10^{-5} M) in O$_2$-saturated acetonitrile containing 0.15 M of biphenyl and 1.8 x 10^{-4} M of 1-methoxy-1,2-di-(4-methoxyphenyl)ethene (**6a**).
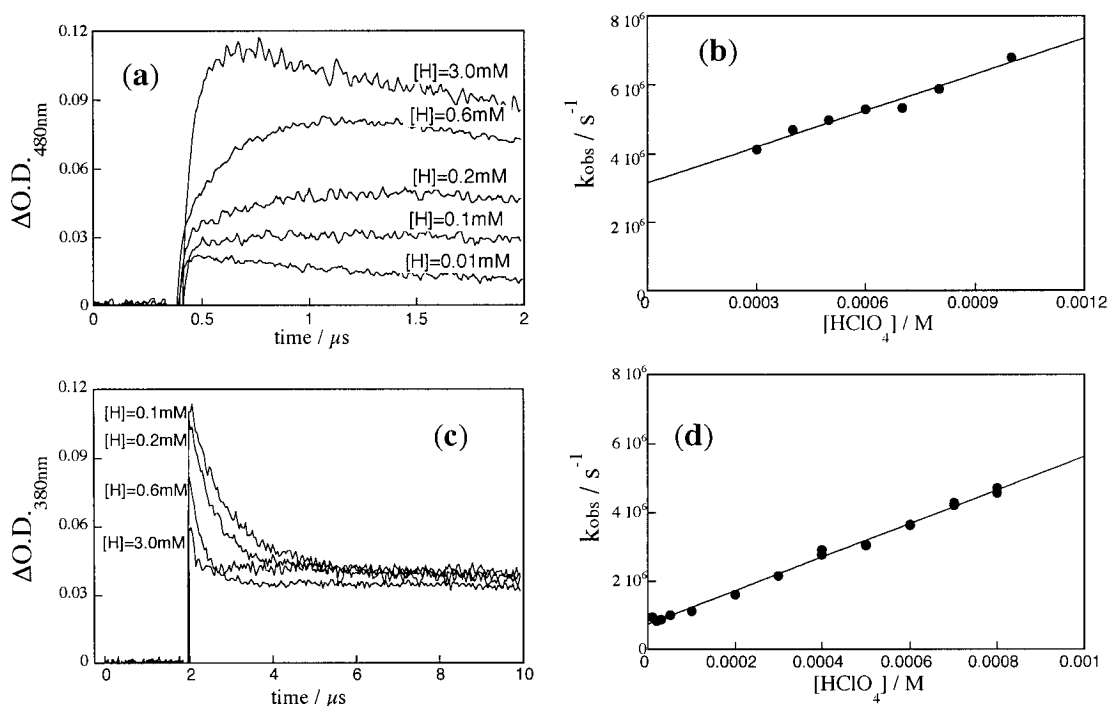
Figure 3.7 Time-resolved changes at (**a**) 480 nm and (**c**) 380 nm upon 308-nm laser irradiation of α-bromodeoxyanisoin (**1a**) in N$_2$-saturated acetonitrile containing variable concentrations of HClO$_4$. (**b**) Relationship between observed rate constants for growth of the 1,2-bis(4-methoxyphenyl)ethenol radical cation (**1c**) at 480 nm and (**d**) 380 nm, and concentration of HClO$_4$ in N$_2$-saturated acetonitrile.
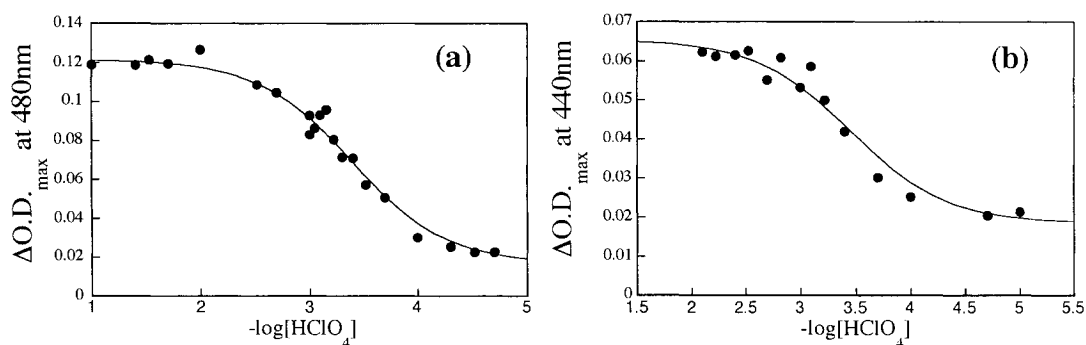
Figure 3.8 Maximum optical density at (a) 480 nm and (b) 440 nm upon 266-nm laser irradiation of α-bromodeoxyanisoin (**1a**) in N_2-saturated acetonitrile containing variable concentrations of $HClO_4$. The solid line in each graph is line-of-best-fit obtained using Eq. 3.2.
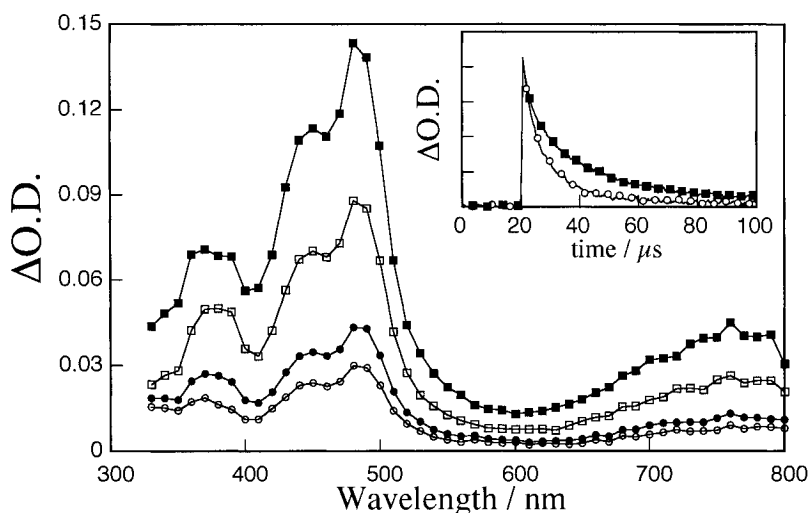
Figure 3.9 Transient spectra obtained (■) 2.40 μs, (□) 10.8μs, (●) 61.2μs and (○) 128 μs after 308-nm laser irradiation of α-bromodeoxyanisoin (**1a**) in N_2-saturated acetonitrile containing 0.01 M $HClO_4$. Inset shows time-resolved absorption changes at 480 nm upon 308-nm laser irradiation of **1a** in (■) N_2 and (○) O_2-saturated conditions.

Figure 3.10 Relationship between observed rate constant for the decay of the enol radical cation **1c**, measured at 480 nm, and concentration of tetrabutylammonium chloride in N_2-saturated acetonitrile containing 0.02 M $HClO_4$.
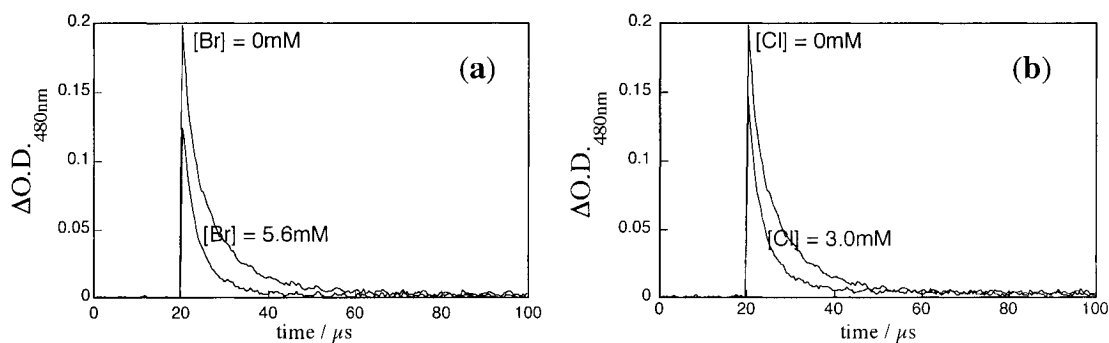
Figure 3.11 Time-resolved absorption changes at 480 nm upon 308-nm laser irradiation of α-bromodeoxyanisoin **1a** in N_2-saturated acetonitrile/$HClO_4$ (0.02 M) containing (a) bromide and (b) chloride anions.
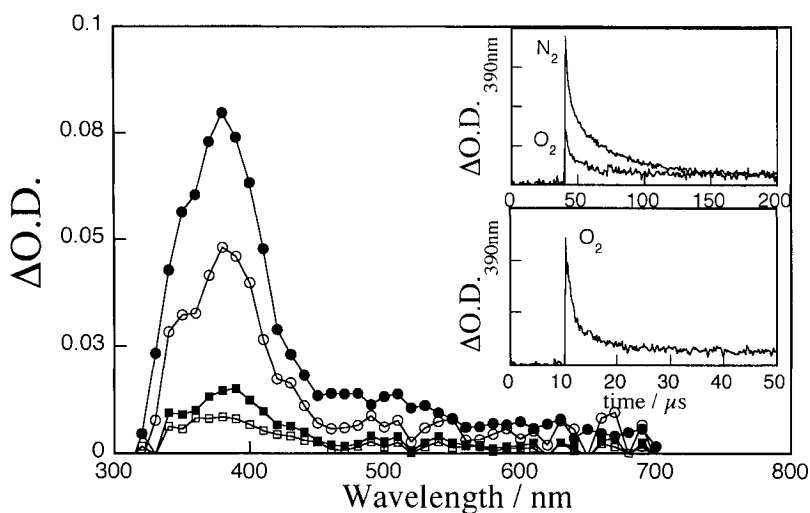
Figure 3.12 Transient spectra obtained (●) 1.8 μs, (○) 5.4 μs, (■) 31.0 μs and (□) 64.4 μs after 308-nm laser irradiation of 2-bromo-1-(3,4-dimethoxyphenyl)-2-(4-methoxyphenyl)ethanone (**2a**) in N$_2$-saturated acetonitrile. Insets show time-resolved absorption changes at 390 nm upon 308-nm laser irradiation of **2a** in N$_2$ and O$_2$-saturated acetonitrile.

Figure 3.13 Transient spectra obtained (●) 0.032 μs, (□) 0.164 μs and (■) 0.612 μs after 308-nm laser irradiation of 2-bromo-1-(3,4-dimethoxyphenyl)-2-(4-methoxyphenyl)ethanone (**2a**) in N$_2$-saturated acetonitrile containing 2.0 mM HClO$_4$. Inset shows time-resolved absorption changes at 390, 460, 500 and 800 nm upon 308-nm laser irradiation of **2a** in N$_2$-saturated acetonitrile containing 2.0 mM HClO$_4$.
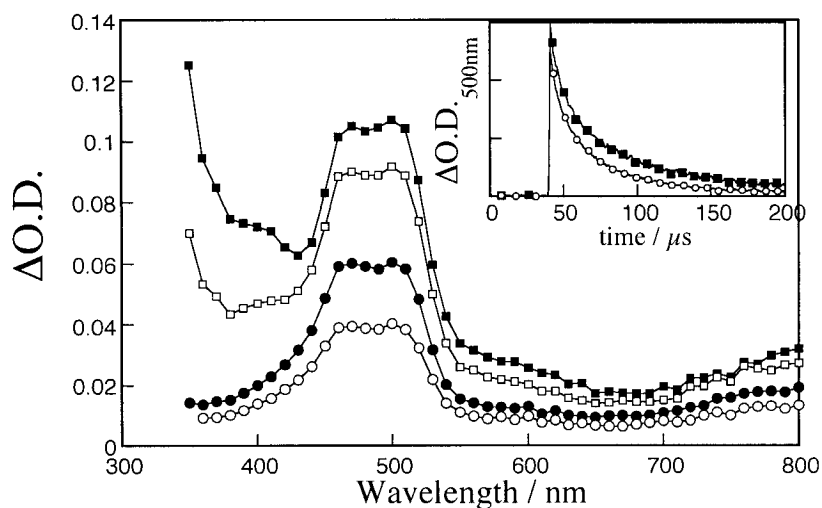
Figure 3.14 Transient spectra obtained (■) 1.6 μs, (□) 6.4 μs, (●) 42.4 μs and (○) 123 μs after 308-nm laser irradiation of 2-bromo-1-(3,4-dimethoxyphenyl)-2-(4-methoxyphenyl)ethanone (**2a**) in N_2-saturated acetonitrile containing 0.01 M $HClO_4$. Inset shows time-resolved absorption changes at 500 nm upon 308-nm laser irradiation of **2a** in (■) N_2 and (○) O_2-saturated acetonitrile containing 0.02 M $HClO_4$.
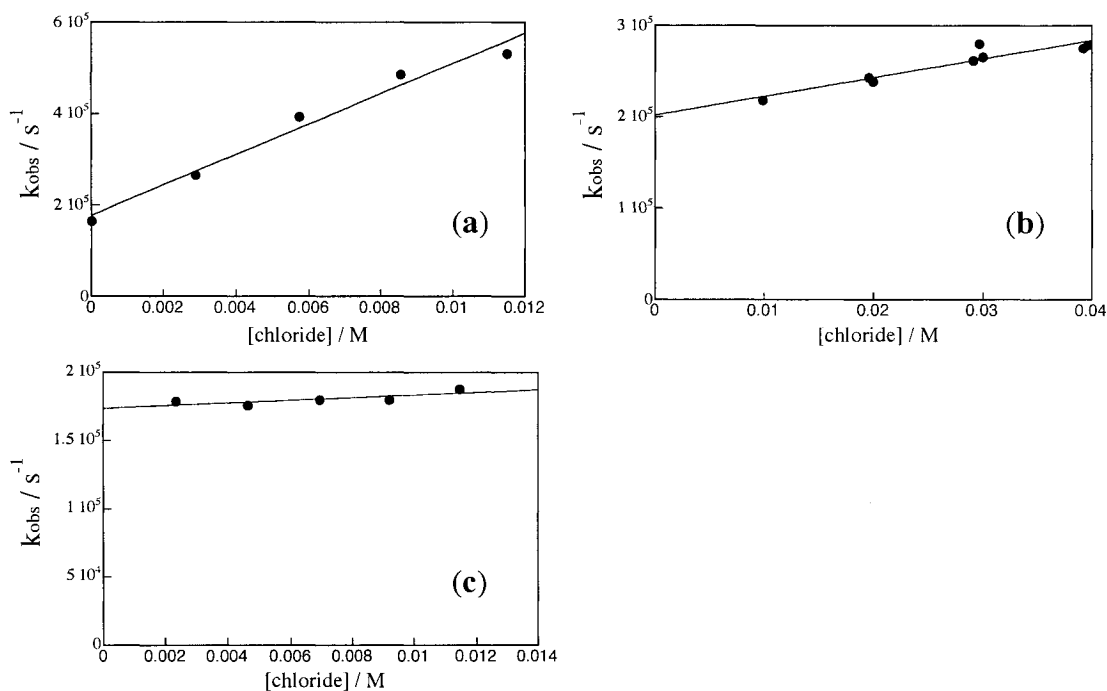

Figure 3.15 Time-resolved absorption changes at 500 nm upon 308-nm laser irradiation of 2-bromo-1-(3,4-dimethoxyphenyl)-2-(4-methoxyphenyl)ethanone (**2a**) in N_2-saturated acetonitrile/$HClO_4$ (0.02 M) containing bromide and chloride anions.
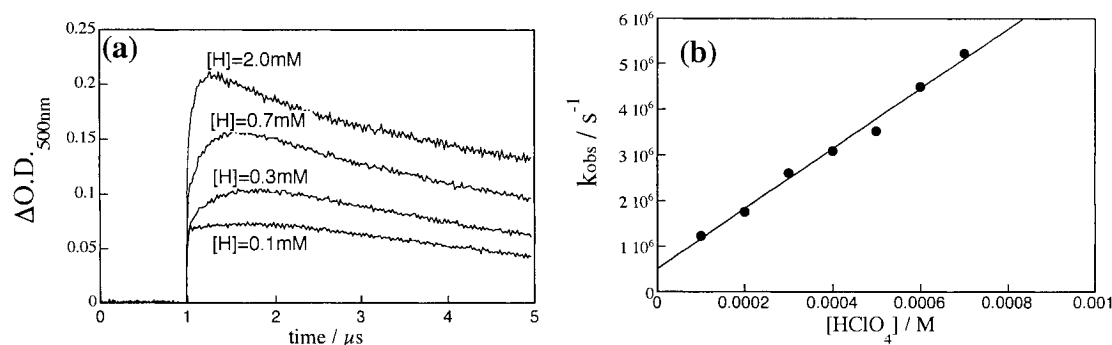
Figure 3.16 (a) Time-resolved changes at 500 nm upon 308-nm laser irradiation of 2-bromo-1-(3,4-dimethoxyphenyl)-2-(4-methoxyphenyl)ethanone (**2 a**) in N_2-saturated acetonitrile containing variable concentrations of $HClO_4$. (b) Relationship between observed rate constants for growth of 1-(3,4-dimethoxyphenyl)-2-(4-methoxyphenyl)ethenol radical cation (**2c**) at 500 nm and concentration of $HClO_4$ in N_2-saturated acetonitrile.

Figure 3.17 Maximum optical density at (a) 500 nm and (b) 460 nm measured upon 308-nm laser irradiation of 2-bromo-1-(3,4-dimethoxyphenyl)-2-(4-methoxyphenyl)ethanone (**2a**) in N_2-saturated acetonitrile containing variable concentrations of $HClO_4$. The solid line in each graph is line-of-best-fit obtained using Eq. 3.2.

203

Figure 3.18 **(a)** Time-resolved absorption changes at 350 nm upon 308-nm laser irradiation of 2-bromo-1-(3,4-dimethoxyphenyl)-2-(4-methoxyphenyl)ethanone **(2a)** in (O) N_2 and (●) O_2-saturated acetonitrile. **(b)** Time-resolved absorption changes at 350 nm upon 308-nm las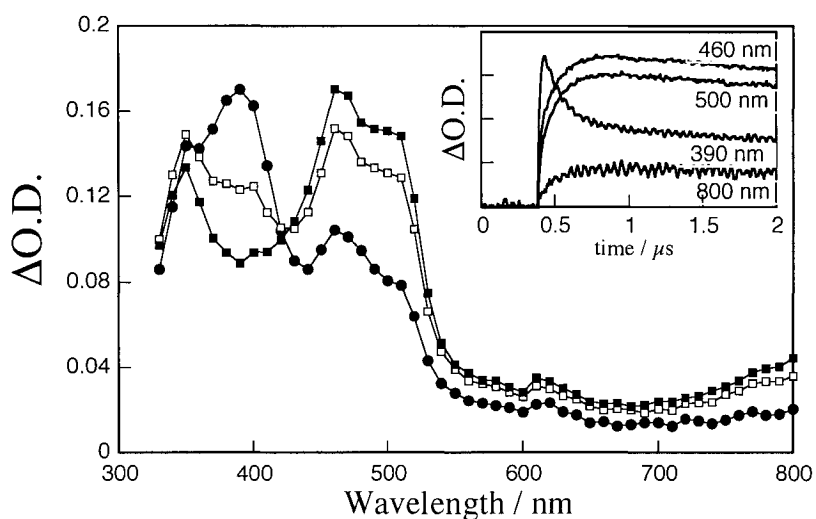er irradiation o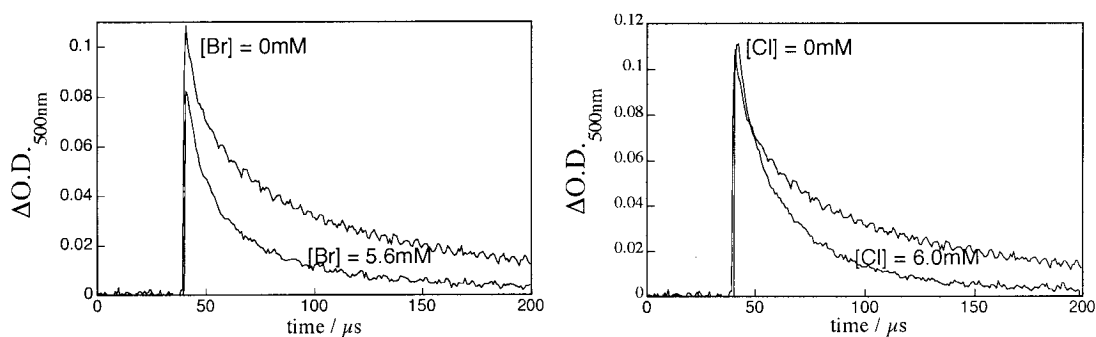f **2a** in (O) N_2-saturated acetonitrile and (●) N_2-saturated acetonitrile containing 2.9 x 10^5 M $(C_4H_9)_4NCl$. **(c)** Relationship between observed rate constant for the decay of the 350-nm transient and the concentration of $C_4H_9)_4NCl$ in N_2-saturated acetonitrile.
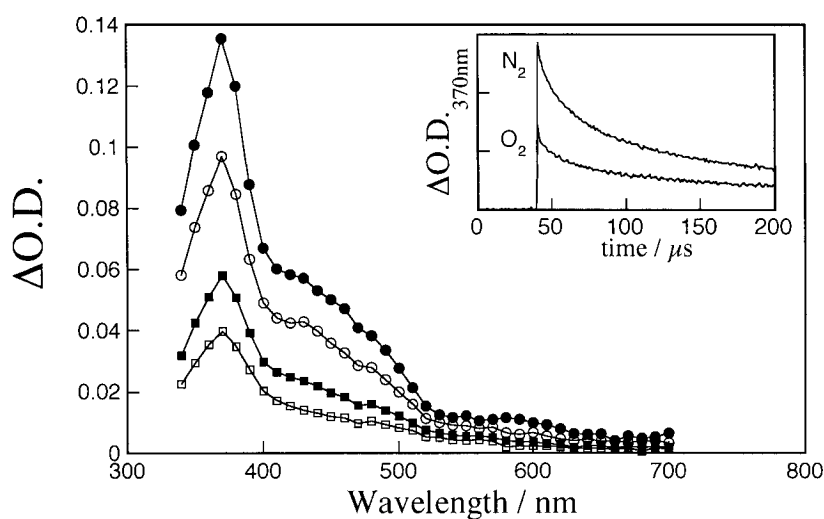
Figure 3.19 Transient spectra obtained (●) 2.0 μs, (○) 14 μs, (■) 61.2 μs and (□) 128 μs after 308-nm laser irradiation of 2-bromo-1-(3,4-dimethoxyphenyl)-2-(4-methylphenyl)ethanone (**3a**) in N_2-saturated acetonitrile. Inset shows time-resolved absorption changes at 370 nm upon 308-nm laser irradiation of **3a** in N_2 and O_2-saturated acetonitrile.

Figure 3.20 Transient spectra obtained (●) 0.048 μs, (○) 0.132 μs and (■) 0.416 μs after 308-nm laser irradiation of 2-bromo-1-(3,4-dimethoxyphenyl)-2-(4-methylphenyl)ethanone (**3a**) in N_2-saturated acetonitrile containing 2.0 mM $HClO_4$. Inset shows time-resolved absorption changes at 370 and 450 nm upon 308-nm laser irradiation of **3a** in N_2-saturated acetonitrile containing 2.0 mM $HClO_4$.
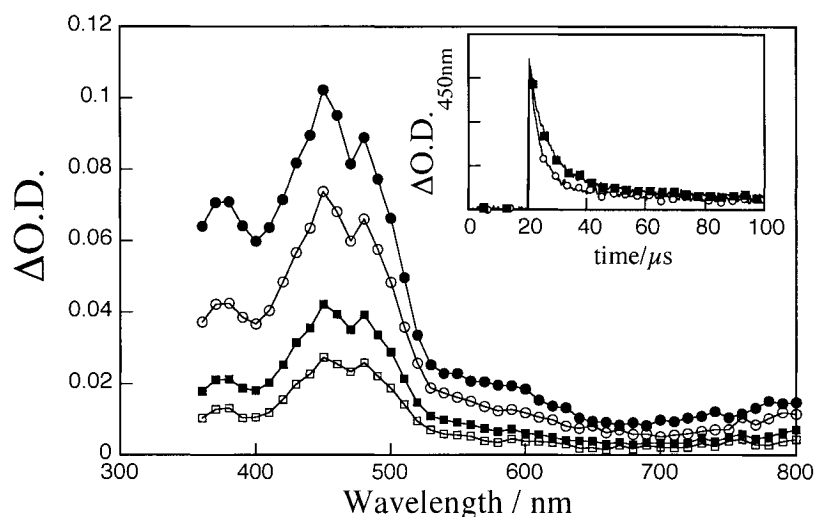
Figure 3.21 Transient spectra obtained (●) 2.0 μs, (○) 14 μs, (■) 61.2 μs and (□) 128 μs after 308-nm laser irradiation of 2-bromo-1-(3,4-dimethoxyphenyl)-2-(4-methylphenyl)ethanone (**3a**) in N_2-saturated acetonitrile containing 0.01 M $HClO_4$. Inset shows time-resolved absorption changes at 450 nm upon 308-nm laser irradiation of **3a** in (■) N_2 and (○) O_2-saturated acetonitrile containing 0.02 M $HClO_4$.
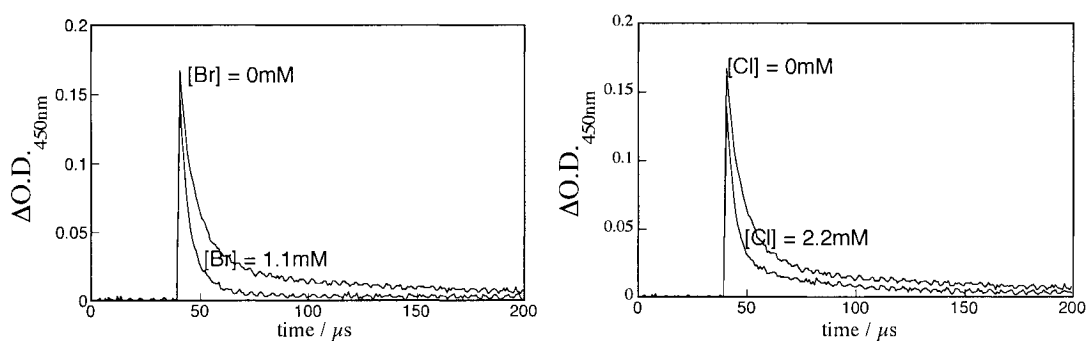
Figure 3.22 Time-resolved absorption changes at 450 nm upon 308-nm laser irradiation of 2-bromo-1-(3,4-dimethoxyphenyl)-2-(4-methylphenyl)ethanone (**3a**) in N_2-saturated acetonitrile/$HClO_4$(0.02 M) containing bromide and chloride anions.

Figure 3.23 (a) Time-resolved changes at 450 nm upon 308-nm laser irradiation of 2-bromo-1-(3,4-dimethoxyphenyl)-2-(4-methylphenyl)ethanone (**3a**) in N_2-saturated acetonitrile containing variable concentrations of $HClO_4$. (b) Relationship between observed rate constants for the growth of 1-(3,4-dimethoxyphenyl)-2-(4-methylphenyl)ethenol radical cation (**3c**) at 500 nm and the concentration of $HClO_4$ in N_2-saturated acetonitrile.
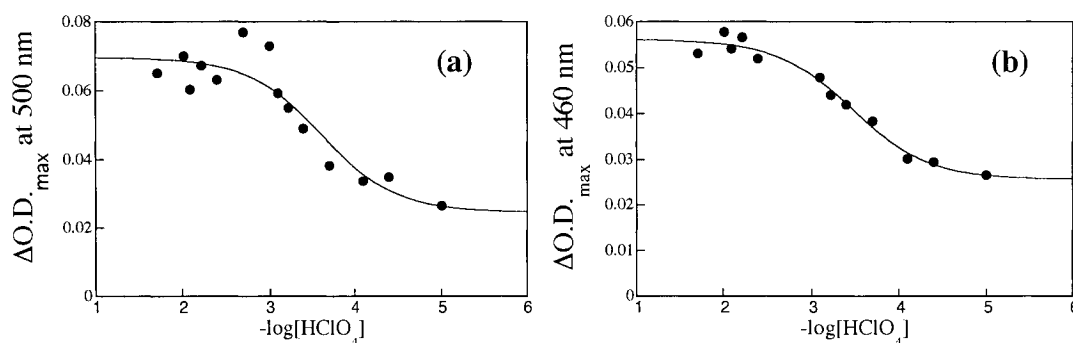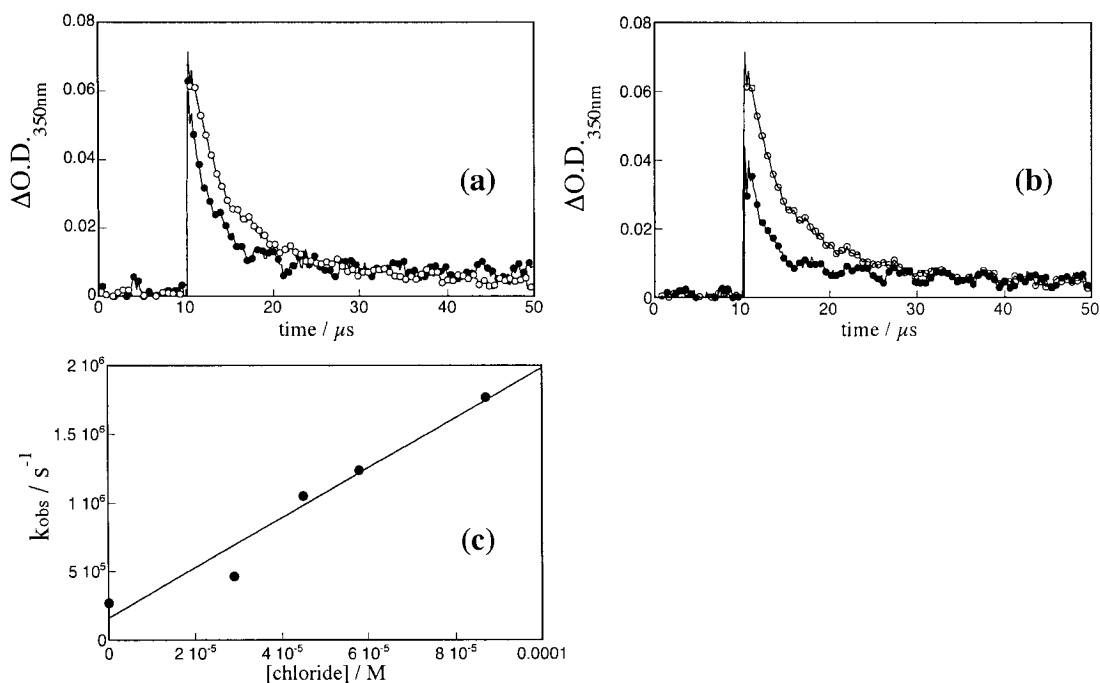

Figure 3.24 Maximum optical density at (a) 450 nm measured upon 308-nm laser irradiation of 2-bromo-1-(3,4-dimethoxyphenyl)-2-(4-methylphenyl)ethanone (**3a**) in N_2-saturated acetonitrile containing variable concentrations of $HClO_4$. The solid line is line-of-best-fit obtained using Eq. 3.2.
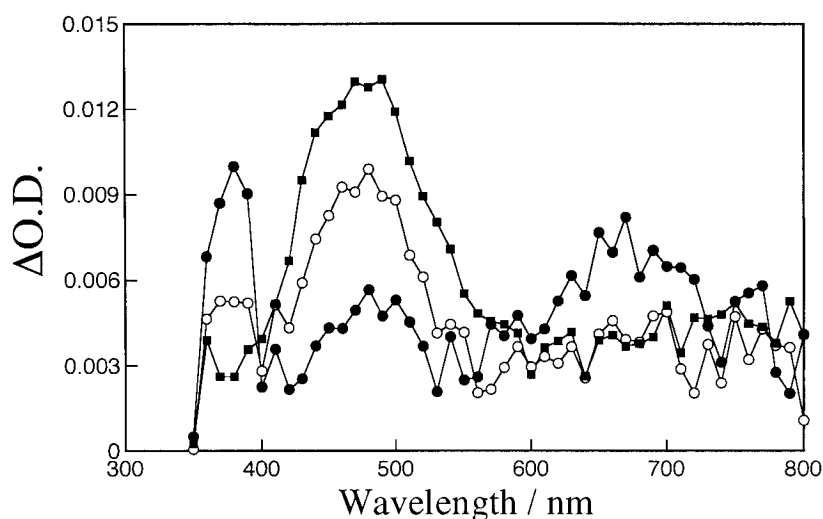
Figure 3.25 Transient spectra obtained (●) 0.11 μs, (○) 0.35 μs and (■) 3.20 μs after 355-nm laser irradiation of 9,10-dicyanoanthracene (1.18 x 10^{-5} M) in O_2-saturated acetonitrile containing 0.15 M of biphenyl and 1.8 x 10^{-4} M of 1-methoxy-1-(4-methylphenyl)-2-(3,4-dimethoxyphenyl)ethene (**7a**).

Figure 3.26 Transient spectra obtained (●) 2.8 μs, (○) 14 μs, (■) 61.2 μs and (□) 128 μs after 308-nm laser irradiation of 2-bromo-1-(3,4-dimethoxyphenyl)-2-phenylethanone (**4a**) in N_2-saturated acetonitrile. Inset shows time-resolved absorption changes at 370 nm upon 308-nm laser irradiation of **4a** in N_2 and O_2-saturated acetonitrile.
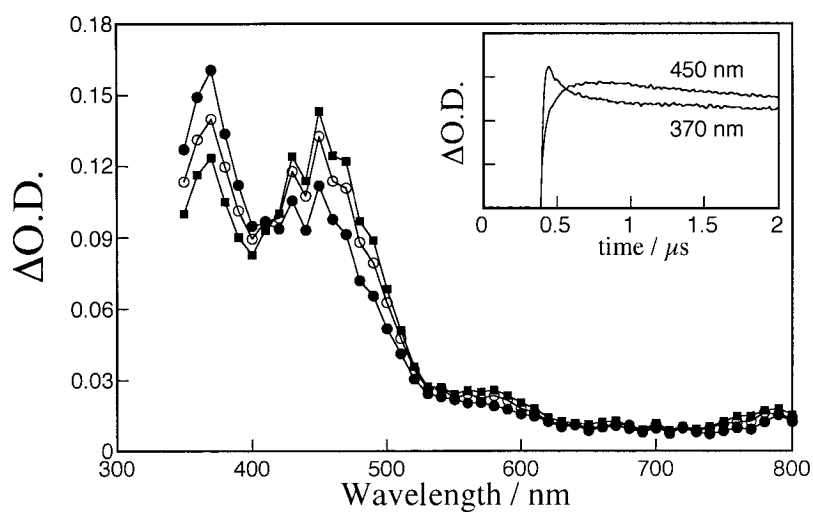
Figure 3.27 Transient spectra obtained (●) 2.8 μs, (○) 14 μs, (■) 61.2 μs and (□) 128 μs after 308-nm laser irradiation of 2-bromo-1-(3,4-dimethoxyphenyl)-2-(4-fluorophenyl)ethanone (**5a**) in N_2-saturated acetonitrile. Inset shows time-resolved absorption changes at 360 nm upon 308-nm laser irradiation of **5a** in N_2 and O_2-saturated acetonitrile.

Figure 3.28 Transient spectra obtained (●) 2.8 μs, (○) 14 μs, (■) 61.2 μs and (□) 128 μs after 308-nm laser irradiation of 2-bromo-1-(3,4-dimethoxyphenyl)-2-phenylethanone (**4a**) in N_2-saturated acetonitrile containing (**a**) 0.01 M $HClO_4$. (**b**) Transient spectra obtained (●) 0.044 μs, (○) 0.128 μs, and (■) 0.612 μs after 308-nm laser irradiation of 2-bromo-1-(3,4-dimethoxyphenyl)-2-phenylethanone (**4a**) in N_2-saturated acetonitrile containing0.001 M $HClO_4$. Inset in (**b**) shows time-resolved absorption changes at 370 and 420 nm upon 308-nm laser irradiation of **4a** in N_2-saturated acetonitrile containing 1.0 mM $HClO_4$.
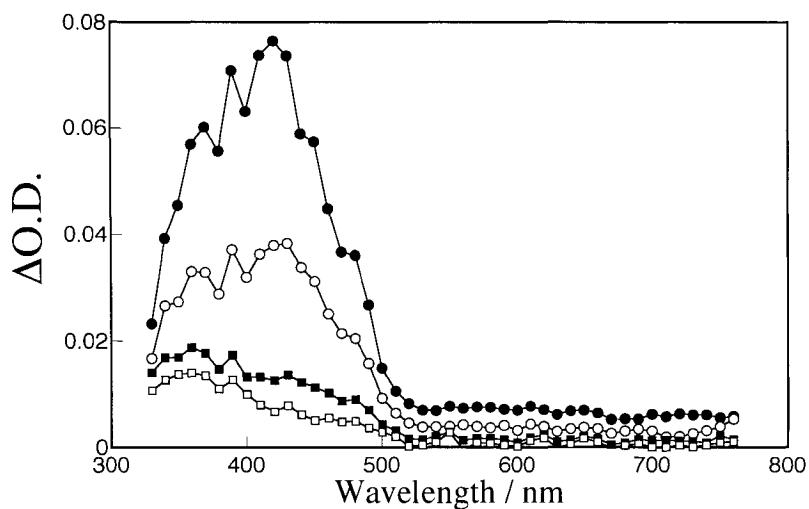
Figure 3.29 Transient spectra obtained (●) 5.0 μs, (○) 35 μs, (■) 153 μs and (□) 320 μs after 308-nm laser irradiation of 2-bromo-1-(3,4-dimethoxyphenyl)-2-phenylethanone (**4a**) in N_2-saturated acetonitrile containing (**a**) 0.1 M $HClO_4$.
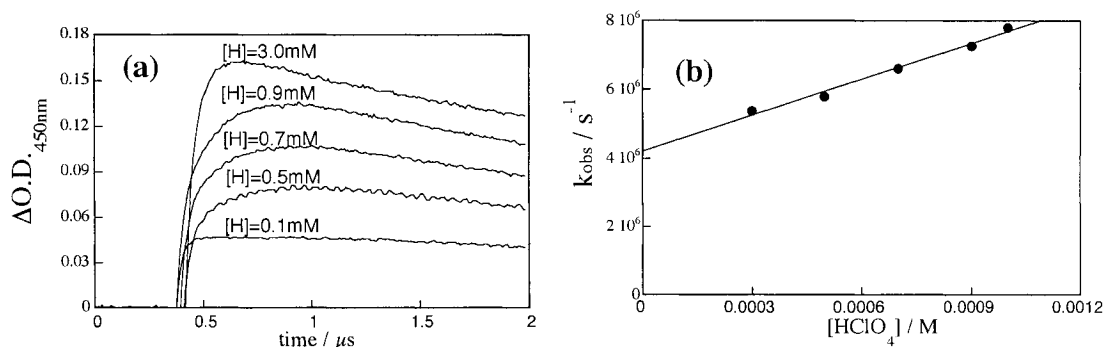

Figure 3.30 Time-resolved absorption changes at 420 nm upon 308-nm laser irradiation of 2-bromo-1-(3,4-dimethoxyphenyl)-2-phenylethanone (**4a**) in N_2-saturated acetonitrile/$HClO_4$ (0.02 M) containing (**a**) bromide and (**b**) chloride anions.

211
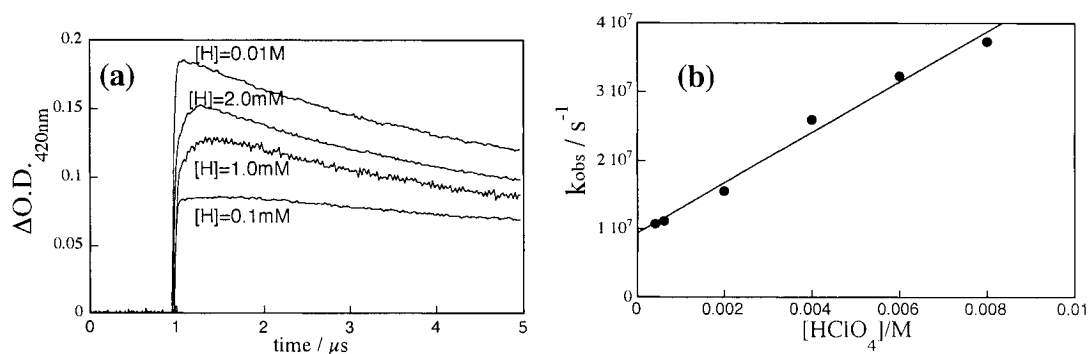
Figure 3.31 (a) Time-resolved absorption changes at 420 nm upon 308-nm laser irradiation of 2-bromo-1-(3,4-dimethoxyphenyl)-2-phenylethanone (**4a**) in N_2-saturated acetonitrile containing variable concentrations of $HClO_4$. (b) Relationship between observed rate constant for the growth of 1-(3,4-dimethoxyphenyl)-2-phenylethenol (**4c**) at 420nm and the concentration of $HClO_4$ in N_2-saturated acetonitrile.
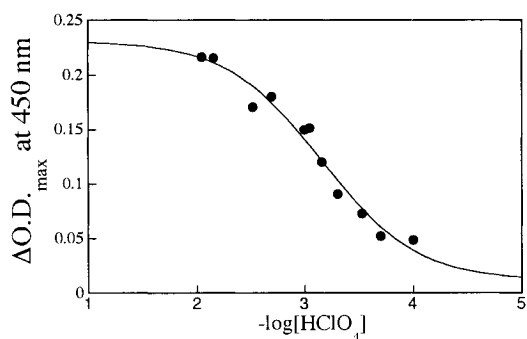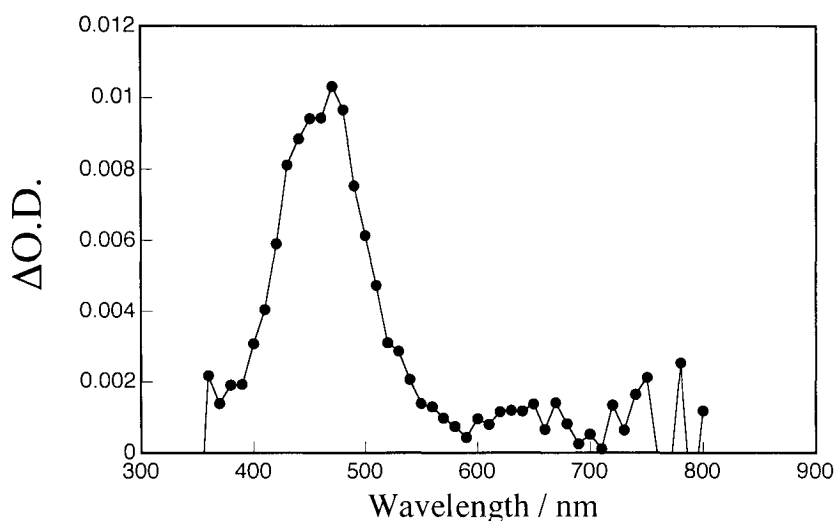

Figure 3.32 Transient spectra obtained (●) 3.20 μs after 355-nm laser irradiation of 9,10-dicyanoanthracene (1.18 x 10^{-5} M) in O_2-saturated acetonitrile containing 0.15 M of biphenyl and 1.8 x 10^{-4} M of 1-methoxy-1-(3,4-dimethoxyphenyl)-2-phenylethene (**8a**).
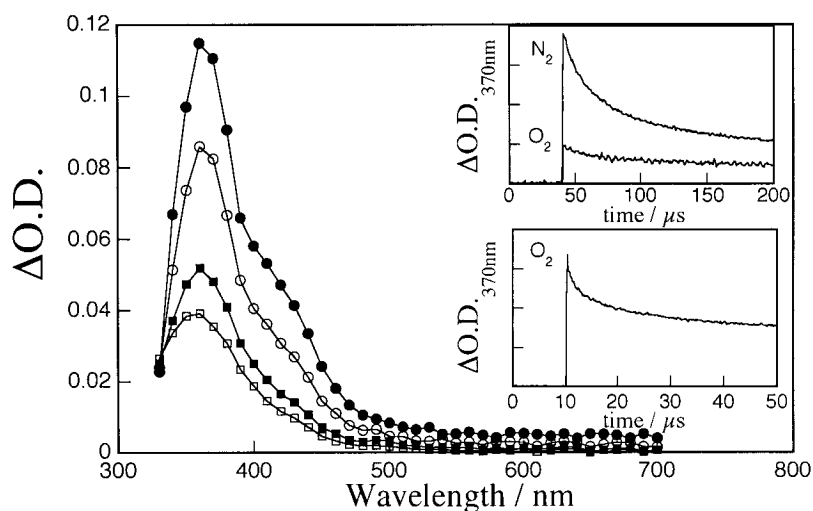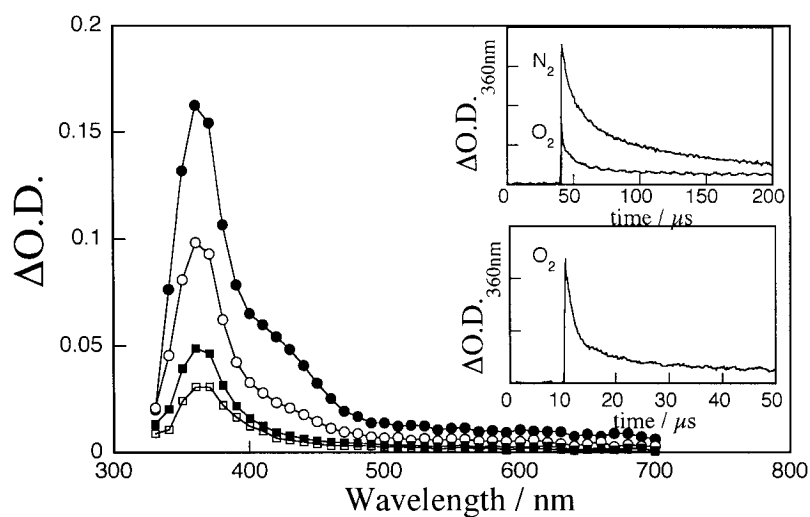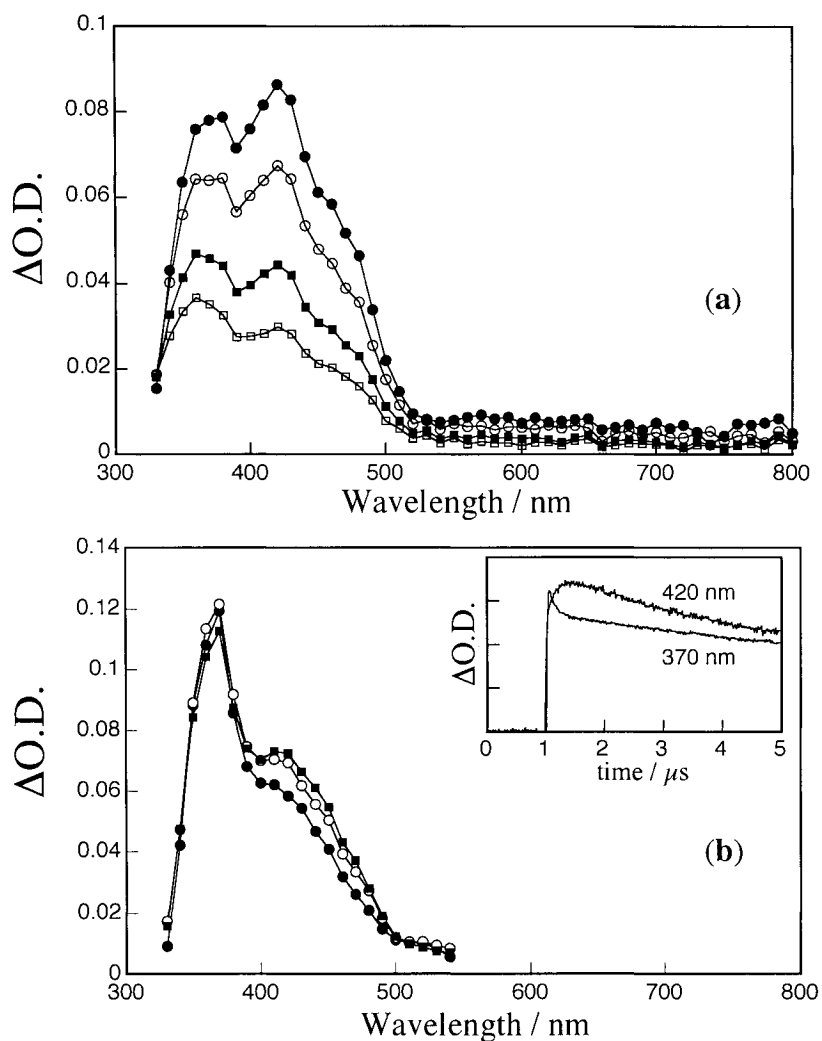
212
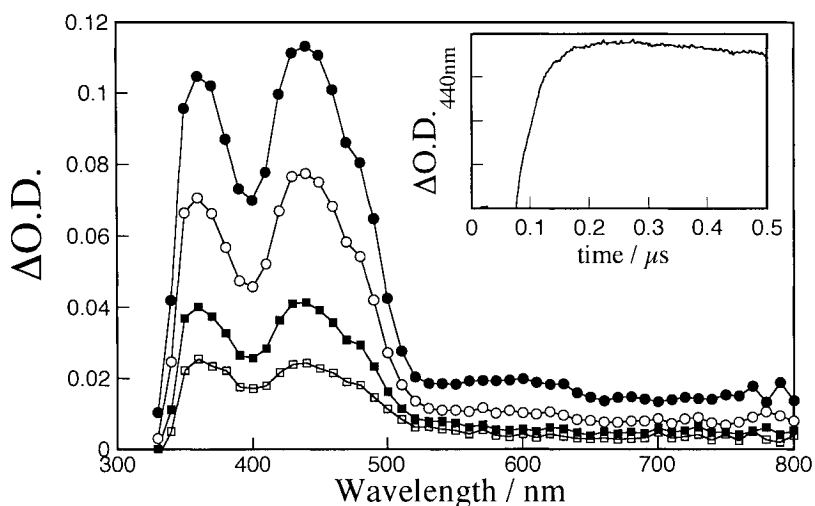
Figure 3.33 Transient spectra obtained (●) 2.8 μs, (○) 14 μs, (■) 61.2 μs and (□) 128 μs after 308-nm laser irradiation of 2-bromo-1-(3,4-dimethoxyphenyl)-2-(4-fluorophenyl)ethanone (**5a**) in N_2-saturated acetonitrile containing 0.01 M $HClO_4$. Inset shows time-resolved absorption changes at 440 nm upon 308-nm laser irradiation of **5a** in N_2-saturated acetonitrile containing 1.0 mM $HClO_4$.
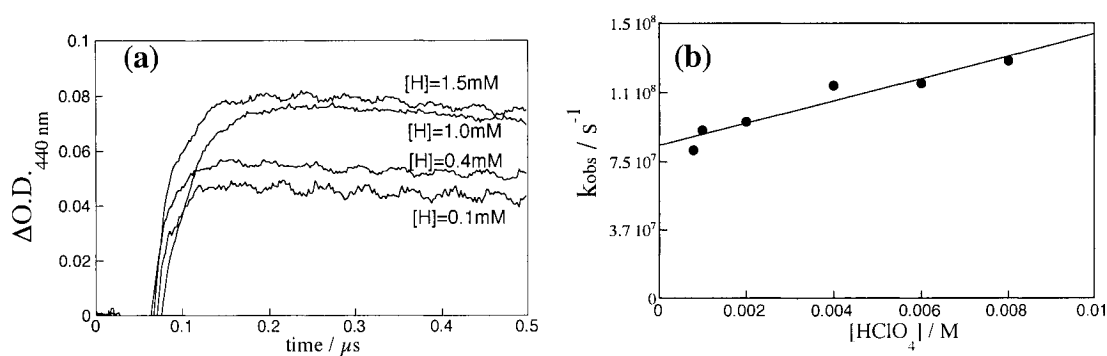
Figure 3.34 (a) Time-resolved absorption changes at 440 nm upon 308-nm laser irradiation of 2-bromo-1-(3,4-dimethoxyphenyl)-2-(4-fluorophenyl)ethanone **5a** in N_2-saturated acetonitrile containing variable concentrations of $HClO_4$. (b) Relationship between observed rate constant for the growth of 1-(3,4-dimethoxyphenyl)-2-(4-fluorophenyl)ethenol (**5c**) at 440 nm and the concentration of $HClO_4$ in N_2-saturated acetonitrile.
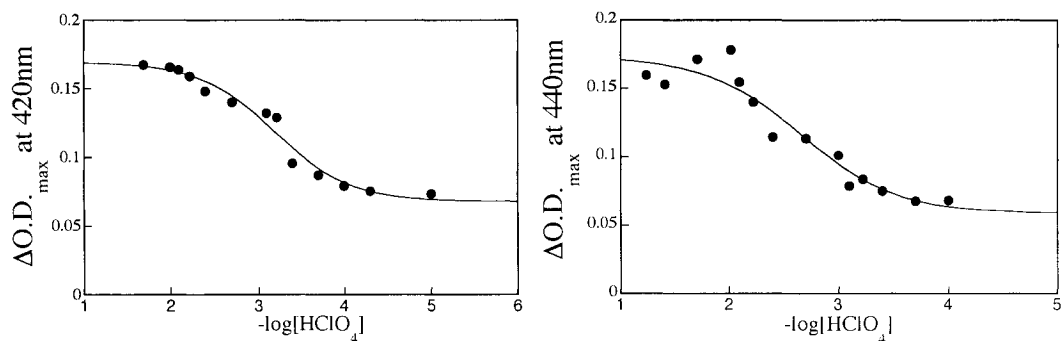
Figure 3.35 (a) Maximum optical density at 420 nm measured upon 308-nm laser irradiation of 2-bromo-1-(3,4-dimethoxyphenyl)-2-phenylethanone (**4a**) in N_2-saturated acetonitrile containing variable concentrations of $HClO_4$. (b) Maximum optical density at 420 nm measured upon 308-nm laser irradiation of 2-bromo-1-(3,4-dimethoxyphenyl)-2-(4-fluorophenyl)ethanone (**5a**) in $N_2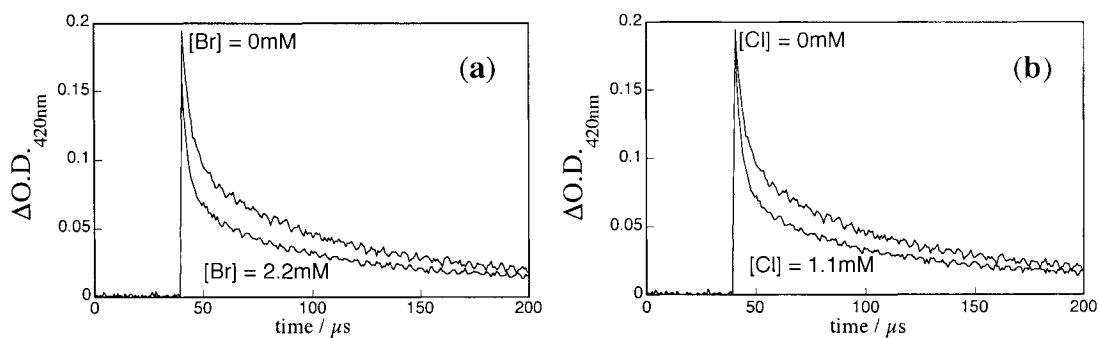$-saturated acetonitrile containing variable concentrations of $HClO_4$. The solid line is line-of-best-fit obtained using Eq. 3.2.
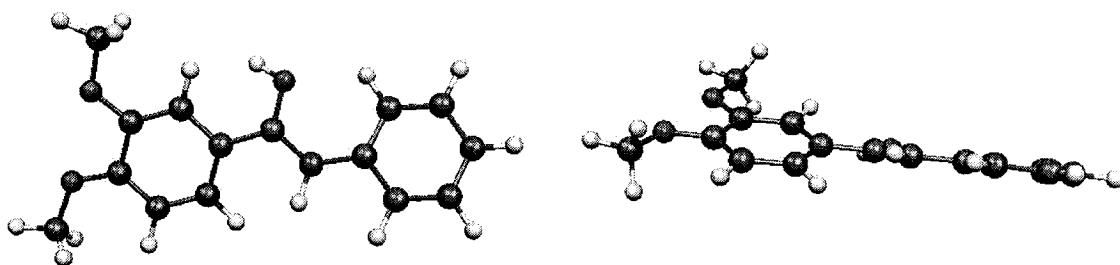
Figure 3.36 Frontal and side views of the geometry of **4c** optimized at the B3LYP/6-31G(d) level of theory.
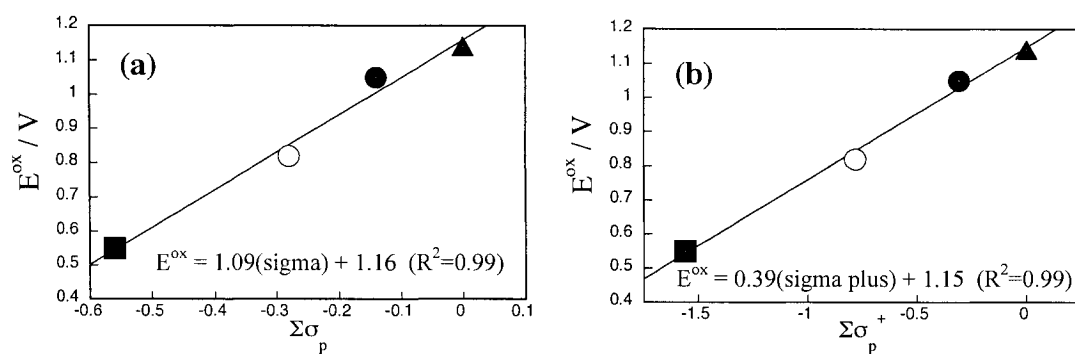
Figure 3.37 Relationship between oxidation potential measured for substituted *trans*-stilbenes in acetonitrile and the sum of (a) sigma values, and (b) sigma plus values reported in the literature. The equation inside each graph represents the line-of-best-fit obtained by linear-least square analysis. (●) *trans*-4-methylstilbene; (▲) *trans*-stilbene; (■) *trans*-4,4'-dimethoxystilbene; (○) *trans*-4-methoxystilbene
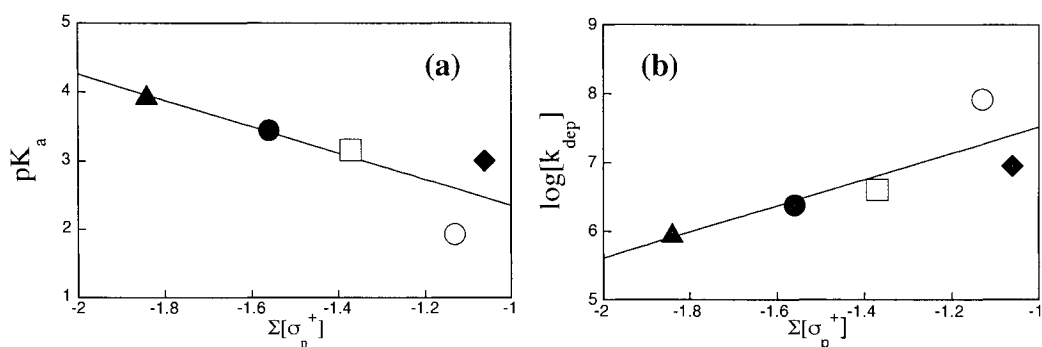
Figure 3.38 Relationship between (a) pK_a, (b) $logk_{dep}$ and sigma plus values. (●) **1c**; (▲) **2c**; (□) **3c**; (◆) **4c**; (○) **5c**.
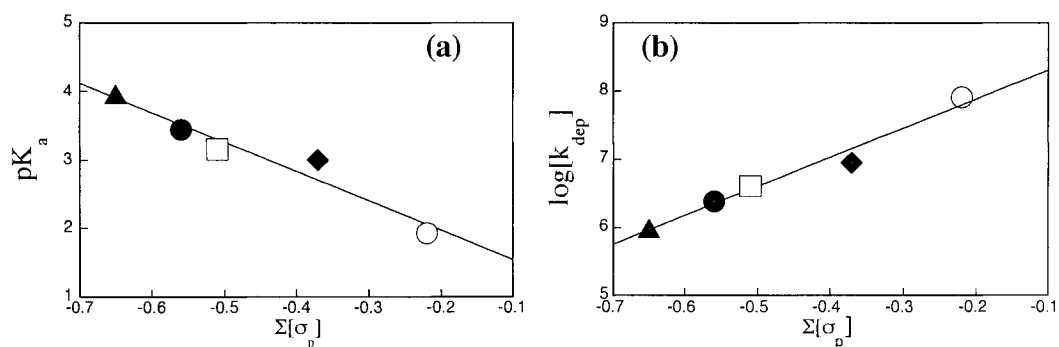
Figure 3.39 Relationship between (a) pK_a, (b) $logk_{dep}$ and sigma values. (●) **1c**; (▲) **2c**; (□) **3c**; (◆) **4c**; (○) **5c**.

215
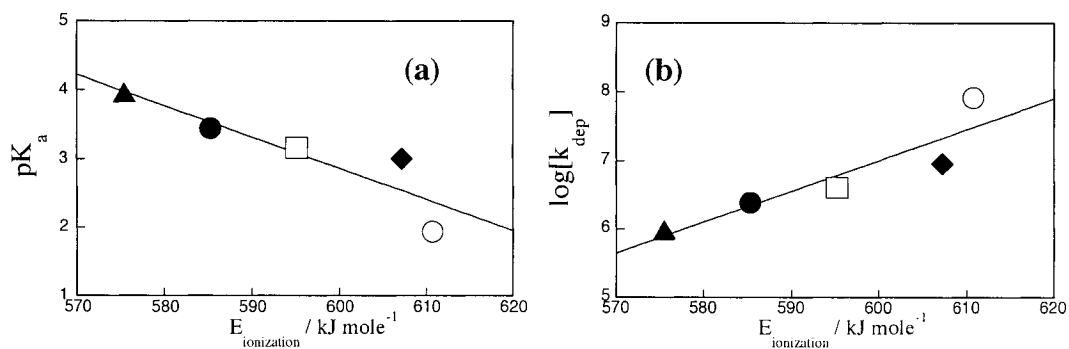
Figure 3.40 Relationship between (a) pK$_a$ and (b) logk$_{dep}$, and the adiabatic ionization potentials determined as the difference between electronic energies in vacuum of enol radical cation and corresponding neutral enol. (●) **1c**; (▲) **2c**; (□) **3c**; (◆) **4c**; (○) **5c**.

Chapter IV. Laser System

4.1 Nanosecond Laser Flash Photolysis

Nanosecond laser flash photolysis was used to generate and detect the short-lived species investigated in this work. The transient species were generated by a short intense light pulse originated from either a Lambda-Physik excimer laser filled with Xe/HCl/He mixture (308 nm, <120 mJ/pulse, < 10 ns/pulse), a Continuum Nd:YAG NY-61 laser (third and second harmonic, 355 nm, <35 mJ/pulse, < 8 ns/pulse) or a Spectra Physics Quanta Ray INDI-40-10 Nd:YAG laser (355 nm, < 8 ns/pulse, 100 mJ/pulse). Transient species generated upon laser excitation were detected by a time-resolved absorption spectrophotometer arranged perpendicular to the laser beam. Figure 4.1 illustrates the experimental set-up employed for this technique.
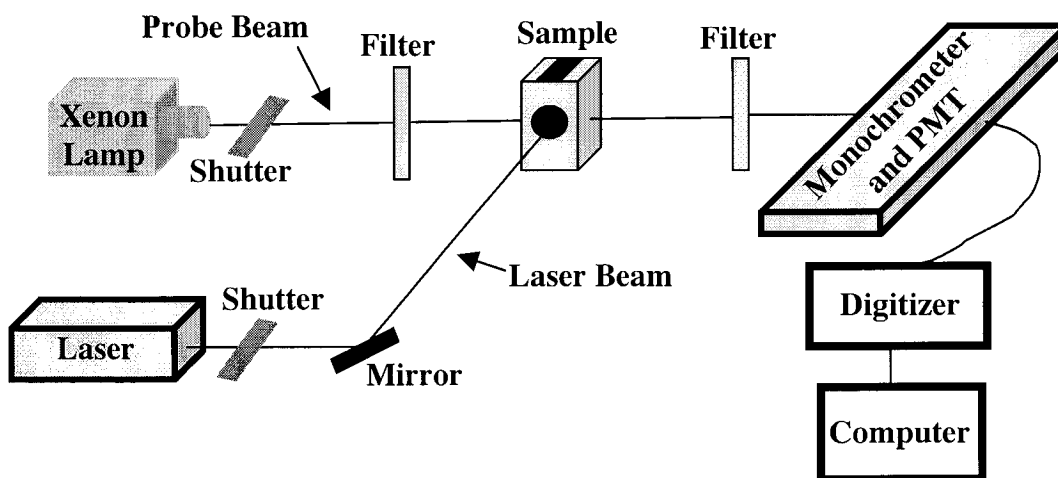
Figure 4.1 Schematic representation of the nanosecond laser flash photolysis system used for the acquisition of kinetic traces and transient absorption spectra.

The sample is exposed to the laser pulse, which generates the transient species, and the monitoring or probe beam which forms the background for the time dependant absorption measurement. The monitoring beam, provided by a pulsed 150 Watt xenon arc lamp, is passed through the sample and then directed into a monochrometer coupled to a photomultiplier tube (PMT). This device converts the light intensity into voltage signals which are captured by a Tektronix 620A digitizing oscilloscope and then sent to a computer used for processing and storage. The sample is protected from unnecessary irradiation by shutters which control the monitoring and laser beams prior to entering the sample.

The laser flash photolysis system is completely controlled through a customized operational program written in LabView (National Instruments), which allows the user to select all the experimental variables like monitoring wavelength, oscilloscope voltage scale and detection timescales.

4.2 Acquisition and Analysis of Kinetic Traces

Kinetic traces represent the changes in absorbance as a function of time at a specific wavelength. The change in absorbance, or change in optical density (ΔO.D.), at a given wavelength is given by Eq. 4.1.

$$\Delta A = \Delta O.D. = -\log\frac{I_t}{I_o} \tag{Eq. 4.1}$$

In this equation I_o is the intensity of the light transmitted in the absence of transient species, that is before the laser pulse, and I_t represents the intensity of the light transmitted in presence of transient species, that is, after the laser pulse.

Kinetic traces were processed using KaleidaGraph (Synergy Software). Each kinetic trace collected during the laser flash photolysis experiments has 250 data points, with 50-55 of these points located in the pre-trigger region, that is prior to the laser pulse, Figure 4.2. The pre-trigger points were manually removed in KaleidaGraph and the start of the remaining data points was reassigned as time zero, Figure 4.2. In most of the cases the data was analyzed using the first-order rate law given in Eq. 4.2, where A_t is the absorbance at time t, A_o is the transient absorbance at time zero (right after the laser pulse), and A_∞ is the residual absorbance due to photoproducts.

$$A_t = A_\infty + (A_o - A_\infty)e^{-kt}$$ (Eq 4.2)

For the calculation of the rate constant (k), initial estimates of k, A_∞ and A_o were provided to the program, which calculated the best fit for the data using an iterative method based on the Levenberg-Marguardt algorithm.

Sequential first-order decays were calculated using Eq. 4.3, where A_t, A_∞ and A_o represent the same as above while A_1 represents the absorbance at the time point where the first process ends and the second process starts. k_1 and k_2 are the rate constants for each one of the processes.

$$A_t = A_\infty + (A_o - A_1)e^{-k_1 t} + (A_1 - A_\infty)e^{-k_2 t}$$ (Eq 4.3)

In cases where the transient species decay with second-order rate law, Eq. 4.4 was used to calculate the bimolecular rate constant k_{bim}. As in the previous cases A_o is the absorption at right after the laser pulse, and A_∞ represents the residual absorbance due to photoproducts. Note that the bimolecular rate constant calculate from equation 4.4 is a function of the extinction coefficient of the species decaying in a second-order manner. Thus the true second-order rate constant (k) is equal to: $k = \varepsilon k_{bim}/2$, where ε is the

extinction coefficient of the transient species (A) decaying by reaction with itself:

A+A→Product.
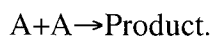
$$A_t = A_\infty + \left\{ k_{bim}t + \frac{1}{(A_o - A_\infty)} \right\}^{-1}$$ (Eq 4.4)
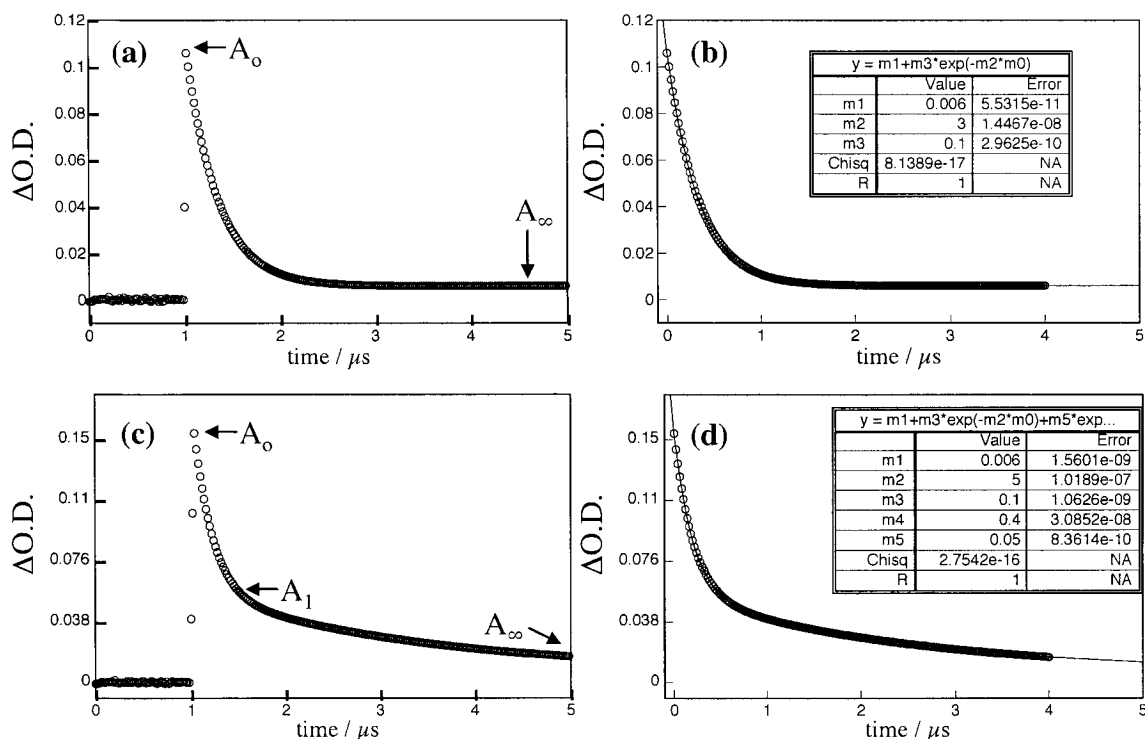
Figure 4.2 Simulated time-resolved kinetic traces showing (a) a first-order decay along with the pre-trigger data points; (b) the same decay without the pre-trigger region and analyzed with equation 6.2 (k = 3.0 x 10^6 s^{-1}); (c) a two sequential monoexponential decays including pre-trigger region; and (d) the same biphasic process without the pre-trigger region and analyzed with equation 6.3, (k_1= 5.0 x 10^6 s^{-1} and k_2 = 4.0 x 10^5s^{-1})

4.3 Acquisition of Spectral Data

While kinetic traces show time-resolved changes in absorbance at a specific wavelength, transient spectrum provides information regarding the changes in absorption as a function of the wavelength at a specific time.

Spectral data is obtained from individual kinetic traces acquired at different wavelengths. For most of the spectra measured in this work, wavelengths range from 300 to 700 nm with data points acquired every 10 nm. Therefore, each one of these spectra required the collection of 21 kinetic traces. Transient spectra were collected at four different time intervals by selecting four time windows, Figure 4.3a from the kinetic traces. The absorbance of the data points contained in each of the time windows were averaged and plotted versus the wavelength, Figure 4.3b, to generate the time-resolved absorption spectra.
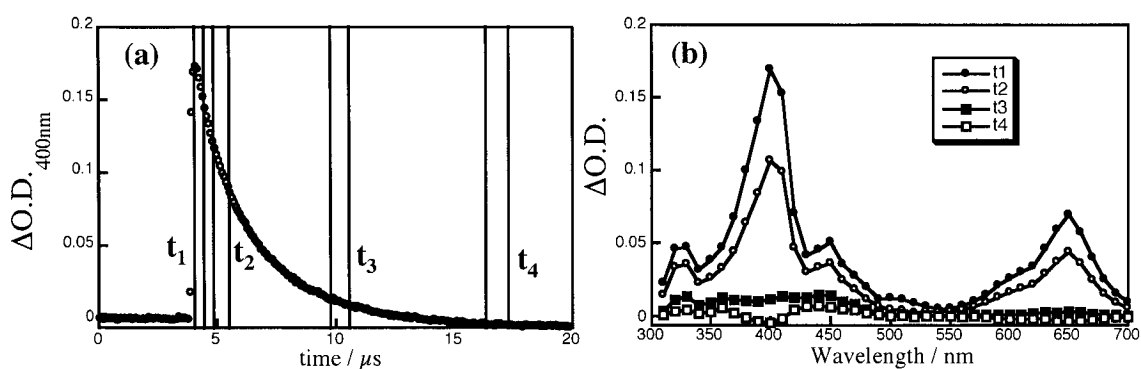
Figure 4.3 (a) Sample kinetic trace, corresponding to a decay at 400 nm, illustrating four time windows used to obtain the transient absorption spectra shown in (b).

Chapter V. Conclusions

The results presented in this thesis demonstrate that direct photoionization of substituted 4-vinylphenol substrates leads to the formation of the corresponding radical cations, characterized by absorption bands centered around 360-380 and 560-580 nm. The major reaction pathway for the decay of these species is the loss of a proton, leading to the formation of 4-vinylphenoxyl radicals. As shown with isoeugenol radical cation, the deprotonation reaction is reversible and can be manipulated by changing the concentration of acid present in the reaction media. In fact, the isoeugenol radical cation can be generated by protonation of the corresponding 4-vinylphenoxyl radical.

The 4-vinylphenol radical cations behave as acids towards hydroxylic and anionic species. The reactions with hydroxylic systems take place with second-order rate constants of $ca.$ 10^7 M^{-1} s^{-1}, while the reactions towards anionic systems occur with diffusion-controlled second-order rate constants. Surprisingly, no spectroscopic evidence was found indicating that nucleophilic addition of anionic species was taking place along with the deprotonation of the radical cations.

The radical cations of isoeugenol and coniferyl alcohol do not show any observable reactivity towards their precursors or other substitutes styenes. These observations are consistent with the low reactivity reported for other β-alkyl substituted styrene radical cations. On the other hand, the 2-methoxy-4-vinylphenol radical cation does react with its neutral parent as well as with other styrenes. The rate constants measured for these reactions are comparable to those reported for the reactions of 4-methoxystyrene radical cation with its precursor and with substituted styrenes.

Short-lived 1,2-diarylenol radical cations can be generated in solution by protonation of the corresponding α-carbonylradicals initially formed by photohomolysis of α-bromoketones. To our knowledge, the present work constitutes the first study reporting the generation of a family of short-lived enol radical cations in solution.

The enol radical cations studied in this work are characterized by a strong absorption band centered between 420 and 500 nm. A second absorption band between 730 and 800 nm is observed for two of the radical cations. These observations are consistent with the transient spectra measured for methyl enol ethers radical cations with similar structures that the enol radical cations.

The acid dissociation constants as well as the deprotonation rate constants obtained for the 1,2-diarylenol radical cations are very sensitive to the nature of the substituents on the aromatic rings. The values of pK_a and $logk_{dep}$ correlate well with Hammett σ values; in contrast, the correlation between pK_a and $logk_{dep}$ and σ^+ values is poor. These observations indicate that there is limited conjugation between the positive charge of the enol radical cations and the substituents in the *para* positions of the aromatic rings. Computational studies indeed demonstrate that the geometries of the radical cations are not planar but twisted, which is consistent with a poor conjugation along the structure. In addition, the distribution of Mulliken charges indicates that the major density of positive charge is located on the carbon bearing the enol OH group, therefore limiting the conjugation between the charge and the substituents on the aromatic ring linked to the α-carbon of the enol radical cation.

APPENDIX A

Derivation of Equation 2.13

The equilibrium constant (K_a) for the equilibrium between the isoeugenol radical cation (RC) with its conjugate base (R), is:

$$K_a = \frac{[R]_{eq}[H^+]_{eq}}{[RC]_{eq}} \tag{A1}$$

where $[RC]_{eq}$, $[R]_{eq}$, and $[H^+]_{eq}$ are the concentrations of the radical cation, the 4-vinylphenoxyl radical and hydrogen protons in the equilibrium state. Assuming that the 4-vinylphenoxyl radical are only formed by deprotonation of the the radical cation; *i.e.*, the initial concentration of phenoxyl radical is zero, then the equilibrium concentration of this species is given by:

$$[R]_{eq} = [RC]_o - [RC]_{eq} \tag{A2}$$

where $[RC]_o$ is the initial concentration of isoeugenol radical cation, i.e. the concentration of the radical cation formed immediately after the laser pulse. Therefore, the acid equilibrium constant can be expressed as:

$$K_a = \frac{\{[RC]_o - [RC]_{eq}\}[H^+]_{eq}}{[RC]_{eq}} = \frac{[RC]_o[H^+]_{eq} - [RC]_{eq}[H^+]_{eq}}{[RC]_{eq}} \tag{A3}$$

Rearranging the terms, the equation can be written as:

$$K_a = \frac{[RC]_o[H^+]_{eq}}{[RC]_{eq}} - \frac{[RC]_{eq}[H^+]_{eq}}{[RC]_{eq}} = \frac{[RC]_o[H^+]_{eq}}{[RC]_{eq}} - [H^+]_{eq} \tag{A4}$$

Therefore,

$$K_a + [H^+]_{eq} = \frac{[RC]_o[H^+]_{eq}}{[RC]_{eq}} , \tag{A5}$$

dividing both terms by $[H^+]_{eq}$ leads to:

$$\frac{K_a + [H^+]_{eq}}{[H^+]_{eq}} = \frac{[RC]_o}{[RC]_{eq}} \tag{A6}$$

The inverse of the equation gives:

$$\frac{[RC]_{eq}}{[RC]_o} = \frac{[H^+]_{eq}}{[H^+]_{eq} + K_a} \tag{A7}$$

Given that the ratio $[RC]_{eq}/[RC]_o$ relates concentrations of the same species, that is the extinction coefficient is the same, the ratio of concentrations is equal to the ratio of absorptions A_{eq}/A_o. Finally, considering that the concentration of protons in the equilibrium state is equal to the concentration of added acid, the equation A7 can be expressed as:

$$\frac{A_{eq}}{A_o} = \frac{[H^+]}{[H^+] + K_a} \tag{Eq. 2.13}$$

Derivation of equation 3.2.

In experiments carried out with compound **1a** in acidic acetonitrile, the absorption measured at 440 nm once the equilibrium state is reached is given by equation B1.

$$Abs_{440}^{eq} = \varepsilon_{440}^{RC}[RC]_{eq} + \varepsilon_{440}^{R}[R]_{eq} \tag{B1}$$

In this equation, $[RC]_{eq}$ and $[R]_{eq}$ represent the equilibrium concentrations of the radical cation (RC) and the radical R species, while ε represent the extinction coefficients of the radical cation and the radical at 440 nm.

The equilibrium concentration of the radical is defined from the acid dissociation constant of the radical cation, equation (B2)

$$K_a = \frac{[H^+]_{eq}[R]_{eq}}{[RC]_{eq}} ; [R]_{eq} = \frac{K_a[RC]_{eq}}{[H^+]_{eq}} \tag{B2}$$

Thus, equation B1 can be expressed as follows:

$$Abs_{440}^{eq} = \varepsilon_{440}^{RC}[RC]_{eq} + \varepsilon_{440}^{R}\frac{K_a[RC]_{eq}}{[H^+]_{eq}} \tag{B3}$$

Factoring out $[RC]_{eq}$, equation B3 is transformed into equation B4.

$$Abs_{440}^{eq} = \left(\varepsilon_{440}^{RC} + \varepsilon_{440}^{R}\frac{K_a}{[H^+]_{eq}}\right)[RC]_{eq} = \left(\frac{\varepsilon_{440}^{RC}[H^+] + \varepsilon_{440}^{R}K_a}{[H^+]_{eq}}\right)[RC]_{eq} \tag{B4}$$

Since, $[RC]_{eq} + [R]_{eq} = [RC]_\infty$, where $[RC]_\infty$ is the concentration of the radical cation at high acid concentration, then:

$$[RC]_{eq} + \frac{K_a[RC]_{eq}}{[H^+]_{eq}} = [RC]_\infty \qquad \text{or}$$

$$\frac{[RC]_{eq}[H^+] + K_a[RC]_{eq}}{[H^+]_{eq}} = [RC]_\infty \tag{B5}$$

Assuming that at high acid concentration $[R]_{eq} = 0$, then:

$$Abs_{440}^{\infty} = \varepsilon_{440}^{RC}[RC]_{\infty} = \frac{\varepsilon_{440}^{RC}\left([H^+] + K_a\right)[RC]_{eq}}{[H^+]_{eq}} \tag{B6}$$

Dividing B4 by B5 gives

$$\frac{Abs_{440}^{eq}}{Abs_{440}^{\infty}} = \frac{\left(\dfrac{\varepsilon_{440}^{RC}[H^+] + \varepsilon_{440}^{R}K_a}{[H^+]_{eq}}\right)[RC]_{eq}}{\dfrac{\varepsilon_{440}^{RC}\left([H^+] + K_a\right)[RC]_{eq}}{[H^+]_{eq}}} = \frac{\varepsilon_{440}^{RC}[H^+] + \varepsilon_{440}^{R}K_a}{\varepsilon_{440}^{RC}\left([H^+] + K_a\right)} = \frac{[H^+] + \dfrac{\varepsilon_{440}^{R}}{\varepsilon_{440}^{RC}}K_a}{[H^+] + K_a} \tag{B7}$$

Multiplying both terms by Abs_{440}^{∞} finally gives equation 3.2.

$$Abs_{440}^{eq} = \left(\frac{[H^+] + \dfrac{\varepsilon_{440}^{R}}{\varepsilon_{440}^{RC}}K_a}{[H^+] + K_a}\right) Abs_{440}^{\infty} \tag{Eq 3.2}$$

227

Derivation of equation 3.3. Note that equation 3.3 is the same as equation 2.18, therefore the same reasoning is valid to derive equation 2.18.

The formation of the equilibrium state between the α-ketoradicals (A) and the enol radical cations (AH) in acidic acetonitrile can be expressed as follows:

$$\underset{(A)}{Ar'\overset{\bullet}{\underset{O}{\diagup}}Ar} \ + \ H^+ \ \underset{k_{dep}}{\overset{k_{prot}}{\rightleftharpoons}} \ \underset{(AH)}{\left[Ar'\diagup\overset{Ar}{\underset{OH}{\diagup}}\right]^{\bullet+}} \qquad (C1)$$
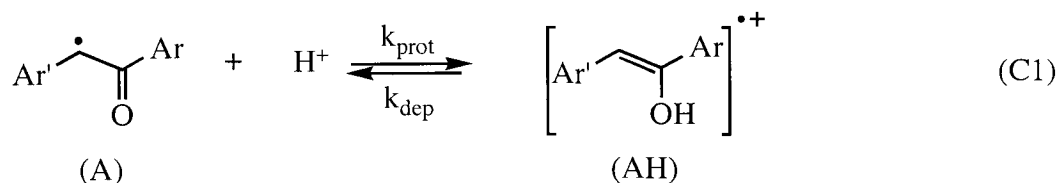
During the reaction the concentrations of A, H^+ and HA are converging towards the final equilibrium concentrations $[A]_{eq}$, $[H]_{eq}$ and $[HA]_{eq}$. The equilibrium constant K will determine the ration of the equilibrium concentrations according to equation C2.

$$K_a = \frac{[A]_{eq}[H]_{eq}}{[AH]_{eq}} \qquad (C2)$$

Since the total mass of the system cannot be changed, the sum of the concentrations at any time (t_0, t, t_{eq}) must be constant (C3).

$$[A]_0+[AH]_0+[H]_0 = [A]+[AH]+[H] = [A]_{eq}+[AH]_{eq}+[H]_{eq} \qquad (C3)$$

The rate for the growth of the enol radical cation (AH) is given by equation C4.

$$\frac{d[AH]}{dt} = k_{prot}[A][H]-k_{dep}[AH] \qquad (C4)$$

According to the mass balance (C3), the concentration of the α-ketoradical [A] can be expressed as:

$$[A] = [A]_0+[AH]_0+[H]_0-[AH]-[H] , \qquad (C5)$$

Thus, the rate expression for the growth of the enol radical cation can be transformed into equation C6.

228

$$\frac{d[AH]}{dt} = k_{prot}[H]\{[A]_0 + [AH]_0 + [H]_0 - [HA] - [H]\} - k_{dep}[AH] \qquad \text{or}$$

$$\frac{d[AH]}{dt} = k_{prot}[H]\{[A]_0 + [AH]_0 + [H]_0 - [H]\} - \left(k_{prot}[H] + k_{dep}\right)[AH] \qquad (C6)$$

Factoring out $(k_{prot}[H]+k_{dep})$ leads to equation C7.

$$\frac{d[AH]}{dt} = \left(k_{prot}[H] + k_{dep}\right)\left(\frac{k_{prot}[H]}{k_{prot}[H] + k_{dep}}\{[A]_0 + [AH]_0 + [H]_0 - [H]\} - [HA]\right) \quad (C7)$$

The fist term multiplied by $(k_{prot}[H]+k_{dep})$ can be transformed as follows:

$$\frac{k_{prot}[H]}{k_{prot}[H] + k_{dep}}\{[A]_0 + [AH]_0 + [H]_0 - [H]\} = \frac{1}{1 + \dfrac{k_{dep}}{k_{prot}[H]}}\{[A]_0 + [AH]_0 + [H]_0 - [H]\} \quad (C8)$$

Since the ratio k_{dep}/k_{prot} is equal to the acid dissociation constant defined in equation C2, equation B8 can be expressed as:

$$\frac{1}{1 + \dfrac{[A]_{eq}[H]_{eq}}{[AH]_{eq}[H]}}\{[A]_0 + [AH]_0 + [H]_0 - [H]\} \qquad (C9)$$

Considering that the concentration of added acid in much higher than the concentrations of the transients generated in laser experiments, i.e. the α-ketoradical and the enol radical cation, it is reasonable to assume that the concentration of acid is not affected by the protonation of the radical species. That is, the concentration of acid will remain contain in time. Thus, $[H]_0 = [H] = [H]_{eq}$, and equation C9 will be equal to:

$$\frac{1}{1 + \dfrac{[A]_{eq}}{[AH]_{eq}}}\{[A]_0 + [AH]_0\} = \left\{\frac{[A]_0 + [AH]_0}{[AH]_{eq} + [A]_{eq}}\right\}[AH]_{eq} \qquad (C10)$$

According to the mass balance the sum of concentrations of A and HA most be constant (C3). Thus, the numerator and denominator in equation C10 are the same, and the term

will be simply $[AH]_{eq}$. Substituting in equation C7 leads to the final differential rate

equation for the growth of the enol radical cation (HA).

$$\frac{d[AH]}{dt} = \left(k_{prot}[H] + k_{dep}\right)\left\{[HA]_{eq} - [HA]\right\}$$ (C11)

As can be inferred from this rate equation, the observed rate constant for the growth of

the enol radical cations will be given by equation 3.3.

$$k_{obs} = k_{prot}[H] + k_{dep}$$ (Eq. 3.3)

REFERENCES

(1) Roth, H. D., *Top. Curr. Chem.* **1992,** *163*, 133.

(2) Todres, Z. V., *Organic Ion Radicals: Chemistry and Applications.* Marcel Dekker, Inc.: New York, 2003; p 352.

(3) Schmittel, M.; Burghart, A., *Angew. Chem. Int. Ed.* **1997,** *36*, 2550.

(4) Bauld, N. L., *Radicals, Ion Radicals, and Triplets: The Spin-Bearing Intermediates of Organic Chemistry.* Wiley-VCH: New York, 1997; p 141.

(5) Roth, H. D., *Reactive Intermediate Chemistry.* Wiley & Sons, Inc: New York, 2004; p 209.

(6) Reynolds, D. W.; Lorenz, K. T.; Chiou, H.; Bellville, D. J.; Pabon, R. A.; Bauld, N. L., *J. Am. Chem. Soc.* **1987,** *109*, 4960.

(7) Andrulis, P. J.; Dewar, M. J. S.; Dietz, R.; Hunt, R., L., *J. Am. Chem. Soc.* **1966,** *88*, 5473.

(8) Richardson, T. J.; Tanzella, F. L.; Bartlett, N., *J. Am. Chem. Soc.* **1986,** *108*, 4937.

(9) Ramamurthy, V.; Caspar, J. V.; Corbin, D. R., *J. Am. Chem. Soc.* **1991,** *113*, 594.

(10) Bauld, N. L.; Roh, Y., *Curr. Org. Chem.* **2002,** *6*, 647.

(11) Bauld, N. L. R., Y., *Tetrahedron Lett.* **2001,** *42*, 1437.

(12) Bauld, N. L.; Yang, J., *Tetrahedron Lett.* **1999,** *40*, 8519.

(13) Bauld, N. L.; Gao, D., *J. Chem. Soc. Perkin Trans 2* **2000,** 931.

(14) Matsunaga, I.; Shiro, Y., *Curr. Op. Chem. Biol.* **2004,** *8*, 127.

(15) Poulos, T. L.; Kraut, J., *J. Biol. Chem.* **1980,** *255*, 8199.

(16) Bruck, T. B.; Gerini, M. F.; Baciocchi, E.; Harvey, P. J., *Biochem. J.* **2003,** *374*, 761.

(17) Baciocchi, E.; Fabbri, C.; Lanzalunga, O., *J. Org. Chem.* **2003,** *68*, 9061.

(18) Kersten, P. J.; Tien, M.; Kalyanaraman, B.; Kirk, T. K., *J. Biol. Chem.* **1985,** *260*, 2609.

(19) Gould, I. R.; Ege, D.; Mattes, S. L.; Farid, S., *J. Am. Chem. Soc.* **1987,** *109*, 3794.

(20) Gould, I. R.; Ege, D.; Moser, J. E.; Farid, S., *J. Am. Chem. Soc.* **1990,** *112*, 4290.

(21) Lewis, F. D.; Bedell, A. M.; Dykstra, R. E.; Elbert, J. E.; Gould, I. R.; Farid, S., *J. Am. Chem. Soc.* **1990**, *112*, 8055.

(22) Trampe, G.; Mattay, J.; Steenken, S., *J. Chem. Phys.* **1989**, *93*, 7157.

(23) Johnston, L. J.; Schepp, N. P., *J. Am. Chem. Soc.* **1993**, *115*, 6564.

(24) Schepp, N. P.; Johnston, L. J., *J. Am. Chem. Soc.* **1994**, *116*, 6895.

(25) Schepp, N. P.; Johnston, L. J., *J. Am. Chem. Soc.* **1996**, *118*, 2872.

(26) Brede, O.; David, F.; Steenken, S., *J. Chem. Soc. Perkin Trans 2* **1995**, 23.

(27) Hara, M.; Tojo, S.; Majima, T., *J. Photochem. Photobiol. A: Chem.* **2004**, *162*, 121.

(28) Neunteufel, R. A.; Arnold, D. R., *J. Am. Chem. Soc.* **1973**, *95*, 4080.

(29) Dinnocenzo, J. P.; Conlon, D. A., *J. Am. Chem. Soc.* **1988**, *110*, 2324.

(30) Maslak, P.; Narvaez, J. N., *Angew. Chem. Int. Ed.* **1990**, *29*, 283.

(31) Bauld, N. L., *Tetrahedron* **1989**, *45*, 5307.

(32) Shida, T., *Electronic Absorption Spectra of Radical Cations*. Elsevier: Amsterdam-Oxford-New York-Tokio, 1988; p 111.

(33) Johnston, L. J.; Schepp, N. P., *Advances in Electron Transfer* **1996**, *5*, 41.

(34) Boerjan, W.; Ralph, J.; Baucher, M., *Annu. Rev. Plant Biol.* **2003**, *54*, 519.

(35) De Angelis, F.; Nicoletti, R.; Spreti, N.; Veri, F., *Angew. Chem. Int. Ed.* **1999**, *38*, 1283.

(36) Khopde, S. M.; Indira-Priyadarsini, K., *Biophysical Chem.* **2000**, *88*, 103.

(37) Bassoli, A.; Di Gregorio, G.; Rindone, B.; Tollari, S.; Chioccara, F.; Salmona, M., *Gazzetta Chimica Italiana* **1988**, *118*, 763.

(38) Miller, I.; Smith, G. J., *Tetrahedron Lett.* **1973**, *25*, 2277.

(39) Leary, G., *Chem. Comm.* **1971**, 688.

(40) Leary, G., *J. Chem. Soc. Perkin II* **1972**, 640.

(41) Wilson, R. M.; Dietz, J. G.; Shepherd, T. A.; Ho, D. M.; Schnapp, K. A.; Elder, R. C.; Watkins, J. M.; Geraci, L. S.; Campana, C. F., *J. Am. Chem. Soc.* **1989**, *111*, 1749.

(42) Freudenberg, K., *Science* **1965**, *148*, 595.

(43) Fournand, D.; Lapierre, C., *J. Agric. Food Chem.* **2001**, *49*, 5727.

(44) Whiting, D. A., *Nat. Prod. Report* **2001**, *18*, 583.

(45) Whiting, D. A., *Nat. Prod. Report* **1985**, 191.

(46) Dewick, P. M., *Medicinal Natural Products: A Biosynthetic Approach.* John Wiley & Sons Ltd: Chichester, 1997; p 121.

(47) Davin, L. B.; Wang, H.; Cowell, A. L.; Bedgar, D. L.; Martin, D. M.; Sarkanen, S.; Lewis, N. G., *Science* **1997**, *275*, 362.

(48) Ward, R. S., *Nat. Prod. Report* **1999**, *16*, 75.

(49) Ralph, J.; Peng, J. P.; Lu, F. C.; Hatfield, R. D.; Helm, R. F., *J. Agric. Food Chem.* **1999**, *47*, 2991.

(50) Meyersman, H.; Morreel, K.; Lapierre, C.; Pollet, B.; De Bruyn, A.; Busson, R.; Herdewijn, B.; Devreese, B.; Van Beeumen, J.; Marita, J. M.; Ralph, J.; Chen, C.; Burggraeve, B.; Van Montagu, M.; Messens, E.; Boerjan, W., *J. Biol. Chem.* **2000**, *275*, 36899.

(51) Onnerud, H.; Zhang, L.; Gellerstedt, G.; Henriksson, G., *The Plant Cell* **2002**, *14*, 1953.

(52) Freudenberg, K.; Dietrich, H., *Chem. Ber.* **1953**, *86*, 1157.

(53) Miller, I.; Smith, G. J., *Aus. J. Chem* **1975**, *28*, 825.

(54) Miller, I.; Smith, G. J., *Aus. J. Chem* **1975**, *28*, 193.

(55) Jaeger, C.; Nourmamode, A.; Catellan, A., *Holzforschung* **1993**, *47*, 375.

(56) Leary, G., *Aus. J. Chem* **1977**, *30*, 1133.

(57) Radotic, K.; Zakrezewska, J.; Sladic, D.; Jeremic, M., *Photochem. Photobiol.* **1997**, *65*, 284.

(58) Lowry, T. H.; Richardson, K. S., *Mechanism and Theory in Organic Chemistry.* Harper & Row: New York, 1987; p 229.

(59) Murov, S. L.; Carmichael, I.; Hug, G. L., *Handbook of Photochemistry.* New York, 1993; p.

(60) Workentin, M. S.; Schepp, N. P.; Johnston, L. J.; Wayner, D. D. M., *J. Am. Chem. Soc.* **1994**, *116*, 1141.

(61) Crellin, R. A.; Lambert, M. C.; Ledwith, A., *J. Chem. Soc. Chem. Commun.* **1970**, 682.

(62) Lewis, F. D.; Kojima, M., *J. Am. Chem. Soc.* **1988**, *110*, 8664.

(63) Mattes, S. L.; Farid, S., *J. Am. Chem. Soc.* **1983**, *105*, 1386.

(64) Mattes, S. L.; Farid, S., *J. Am. Chem. Soc.* **1986**, *108*, 7356.

(65) Bauld, N. L.; Pabon, R., *J. Am. Chem. Soc.* **1983**, *105*, 633.

(66) Bauld, N. L.; Bellville, D. J.; Pabon, R.; Chelsky, R.; Green, G., *J. Am. Chem. Soc.* **1983**, *105*, 2378.

(67) Tojo, S.; Toki, S.; Takamuku, S., *J. Am. Chem. Soc.* **1991**, *56*, 6240.

(68) Schepp, N. P.; Shukla, D.; Sarker, H.; Bauld, N. L.; Johnston, L. J., *J. Am. Chem. Soc.* **1997**, *119*, 10325.

(69) Ganapathu, M. R.; Naumov, S.; Hermann, R.; Brede, O., *Chem. Phys. Letters* **2001**, *337*, 335.

(70) Bordwell, F. G.; Cheng, J. P., *J. Am. Chem. Soc.* **1989**, *111*, 1792.

(71) Schepp, N. P.; Rodriguez-Evora, Y., *Can. J. Chem.* **2003**, *81*, 799.

(72) Andre, J. J.; Weill, G., *Mol. Phys.* **1968**, *15*, 97.

(73) Oxidation potential measured as irreversible peak in acetonitrile containing 0.1M tetraethylammonium perchlorate.

(74) Gadosy, T. A.; Shukla, D.; Johnston, L. J., *J. Chem. Phys. A* **1999**, *103*, 8834.

(75) Das, P. K.; Encinas, M. V.; Steenken, S.; Scaiano, J. C., *J. Am. Chem. Soc.* **1981**, *103*, 4162.

(76) Rodriguez-Evora, Y.; Schepp, N. P., *Org. Biomolec. Chem.* **2005**, *3*, 4444.

(77) Eskins, K.; Glass, C.; Rohwedder, W.; Kleiman, R.; Sloneker, J., *Tetrahedron Lett.* **1972**, *9*, 961.

(78) Kuo, Y. H.; Lin, S. T., *Experientia* **1983**, *39*, 991.

(79) Gassman, P. G.; Singleton, D. A., *J. Am. Chem. Soc.* **1984**, *106*, 7993.

(80) Land, E.; G., P., *Trans. Faraday Soc.* **1963**, *59*, 2016.

(81) Ruff, F.; Csizmadia, I. G., *Organic Reactions. Equilibria, Kinetics and Mechanism.* Elsevier: Amsterdam, 1994; p 365.

(82) Kolthoff, I. M.; Bruckenstein, S.; Chantooni, M. K. J., *J. Am. Chem. Soc.* **1961**, *83*, 3927.

(83) Nerbonne, J. M.; Weiss, R. G., *J. Am. Chem. Soc.* **1978,** *100,* 5954.

(84) Evans, C.; Scaiano, J. C.; Ingold, K. U., *J. Am. Chem. Soc.* **1992,** *114,* 4589.

(85) Augustin-Nowacka, D.; Makowski, M.; Chmurzynski, L., *Anal. Chim. Acta* **2000,** *418,* 233.

(86) Bordwell, F. G.; Cheng, J.-P., *J. Am. Chem. Soc.* **1991,** *113,* 1736.

(87) Pan, H.-L.; Cole, C. A.; Fletcher, T. L., *Synthesis* **1980,** 813.

(88) Shiba, T.; Xiao, L.; Miyakoshi, T.; Chen, C.-L., *J. Mol. Cat B: Enzymatic* **2000,** *10,* 605.

(89) Leopold, B., *Acta Chem. Scand.* **1950,** *4,* 1523.

(90) Mourgues, P.; Denhez, J. P.; Audier, H. E., *Org. Mass Spect.* **1993,** *28,* 193.

(91) Turecek, F., *The Chemistry of Enols.* John Wiley & Sons: Chichester, 1990; p 95.

(92) Schmittel, M., *Top. Curr. Chem.* **1994,** *169,* 183.

(93) Heinrich, N.; Wolfram, K.; Gernot, F.; Schwarz, H., *J. Am. Chem. Soc.* **1986,** *108,* 593.

(94) Stubbe, J. A., *Annu. Rev. Biochem.* **1989,** *58,* 257.

(95) Frey, P. A., *The Chemical Record* **2001,** *1,* 277.

(96) Magnusson, O. T.; Frey, P. A., *Biochem.* **2002,** *41,* 1695.

(97) Smith, D. M.; Golding, B. T.; Radom, L., *J. Am. Chem. Soc.* **2000,** *123,* 1664.

(98) Heinrich, N.; Louage, F.; Lifshitz, C.; Schwarz, H., *J. Am. Chem. Soc.* **1988,** *110,* 8183.

(99) Green, M. M.; Mayotte, G. J.; Meites, L.; Forsyth, D., *J. Am. Chem. Soc.* **1980,** *102,* 1464.

(100) Marcinek, A.; Michalak, J.; Rogowski, J.; Tang, W.; Bally, T., *J. Chem. Soc. Perkin II* **1992,** 1353.

(101) Orliac-Le Moing, M. A.; Le Guillanton, G.; Simonet, J., *Electrochim. Acta* **1982,** *27,* 1775.

(102) Fuson, R.; Rabjohn, N.; Byers, D. J., *J. Am. Chem. Soc.* **1944,** *66,* 1272.

(103) Hart, H.; Rappoport, Z.; Biali, S. E., *The Chemistry of Enols.* John Wiley & Sons Ltd: Chichester, 1990; p 481.

(104) Gilbert, B. C.; Whitwood, A. D., *J. Chem. Soc. Perkin II* **1989**, 1921.

(105) Schepp, N. P., *J. Org. Chem.* **2004**, *69*, 4931.

(106) Purohit, P. C.; Sonawane, H. R., *Tetrahedron* **1981**, *37*, 873.

(107) Strachan, A. N.; Blacet, F. E., *J. Am. Chem. Soc.* **1955**, *77*, 5254.

(108) Barltrop, J. A.; Thomson, A., *J. Chem. Soc. (C)* **1968**, 155.

(109) Bejan, E. V.; Font-Sanchis, E.; Scaiano, J. C., *Org. Lett.* **2001**, *3*, 4059.

(110) Kaplan, B. E.; Hartwig, A. L., *Tetrahedron Lett.* **1970**, 4855.

(111) Givens, R. S.; Strekowski, L., *J. Am. Chem. Soc.* **1975**, *97*, 5867.

(112) Miranda, M. A.; Garcia, H., *Chem. Rev.* **1994**, *94*, 1063.

(113) Cozens, F. L.; O'Neill, M.; Bogdanova, R.; Schepp, N. P., *J. Am. Chem. Soc.* **1997**, *119*, 10652.

(114) Ganapathi, M. R.; Naumov, S.; Hermann, R.; Brede, O., *Chem. Phys. Lett.* **2000**, *337*, 335.

(115) Majima, T.; Tojo, S.; Ishida, A.; Takamuku, S., *J. Org. Chem.* **1996**, *61*, 7793.

(116) Hara, M.; Samori, S.; Xichen, C.; Fujitsuka, M.; Majima, T., *J. Org. Chem.* **2005**, *70*, 4370.

(117) Rodriguez-Evora, Y., *Unpublished Results*.

(118) Lubczyk, V.; Bachmann, H.; Gust, R., *J. Med. Chem.* **2003**, *46*, 1484.

(119) Napolitano, E.; Giannone, E.; Fiaschi, R.; Marsili, A., *J. Org. Chem.* **1983**, *48*, 3653.

(120) Dyke, S. F.; Tiley, E. P.; White, W. C.; Gale, D. P., *Tetrahedron* **1975**, *31*, 1219.

(121) Churruca, F.; SanMartin, R.; Carril, M.; Tellitu, I.; Dominguez, E., *Tetrahedron* **2004**, *60*, 2393.

(122) Moreno, I.; Tellitu, I.; Dominguez, E.; SanMartin, R., *Eur. J. Org. Chem.* **2002**, 2126.

(123) Mortensen, D. S.; Rodriguez, A. L.; Carlson, K. E.; Sun, J.; Katzenellebogen, B. S.; Katzenellebogen, J. A., *J. Med. Chem.* **2001**, *44*, 3838.

(124) Krow, G. R.; Michener, E., *Synthesis* **1974**, 572.